

Dissertation

Zur Erlangung des Grades eines Doktors der Naturwissenschaften

(Dr. rer. nat.)

Viologen Stars and Rods: Synthesis, electrochemical Investigations and Polymerization

**Fachbereich Biologie/Chemie
Institut für Chemie**

von Veronica-Alina Constantin

aus Tulcea (Rumänien)

Osnabrück 2012

Die vorliegende Arbeit wurde in der Zeit von Februar 2007 bis Februar 2012 am Institut für Chemie, Fachbereich Biologie/Chemie der Universität Osnabrück unter Anleitung von Prof. Dr. Lorenz Walder ausgeführt.

Hauptberichterstatter: Prof. Dr. Lorenz Walder, Universität Osnabrück

Zweitberichterstatter: apl. Prof. Dr. Helmut Rosemeyer, Universität Osnabrück

weitere Mitglieder: Prof. Dr. Martin Steinhart, Universität Osnabrück

Dr. Kasten Kömpe, Universität Osnabrück

Aknowledgements

First of all, I would like to thank to my supervisor, Prof. Dr. Lorenz Walder for the chance he had given to me to come to Germany and work in his group, for his interesting discussions and good tips that have been helpful in my research.

I owe my deepest gratitude to apl. Prof. Dr. Helmut Rosemeyer for agreeing to be my co-adviser, for giving me good ideas and suggestions regarding my work and providing valuable comments for my thesis.

I am pleased to thank Prof. Dr. Martin Steinhart and Dr. Kasten Kömpe for accepting to be examiners of my PhD thesis defense, as well as for their useful discussions and comments about my work. Thanks also to Johannes Ludden for the synthesis of the viologen dimers and for the nice collaboration we had during his master's thesis.

This is a great opportunity to express my gratitude to Prof. Uwe Beginn for many stimulating discussions during my PhD. I am indebted to all participants to the Monday morning literature seminar for the nice scientific moments we had together.

I would like to show my gratitude to my former and present colleges: Dereje Taffa, Kathiresan Murugawel, Ina Rianasari, Dirk Bongard, Holger Oelrich, Liangcheng Cao and Shamaila Sadaf for the interesting scientific and non scientific conversations, for the encouragements during my PhD and for their contribution in creating a friendly and positive working atmosphere in the laboratory. I am also grateful to Christine Schulz-Kölbel and Simona Webersinn for their assistance during my experiments and for creating a family-like atmosphere in the laboratory. I would like to thank to Simona

Webersinn for providing me STM images of the rod-like molecules and to Marianne Gather for introducing me to NMR measuring technique and for her assistance during my first NMR experiments. Thanks to Shamaila Sadaf for the STM measurements on polymer-CNT composites.

I owe my deepest gratitude to Prof. Prof. h. c. Dr. Dr. h. c. Manfred Neumann and his PhD student Christine Derks for the XPS measurements on the modified electrodes.

I would like to thank to Dr. Rajesh Komban, Shamaila Sadaf and Anna Hodge for reading the manuscript of the thesis and checking for language errors. Special thanks to my friend Dr. Diana Ster for the fruitful discussions and for sharing with me her experience as PhD. I also want to thank the Romanian researchers from our institute: Dr. Simona Asaftei, Ana-Maria Lepădatu and Marius Ciobanu for their advice and support.

I would like to express my thanks to our institute and department secretaries, Claudia Ratermann, Monika Dubiel and Anne Hodge for their kind help throughout my research work.

I would like to express my sincere thank to my sister Mihaela-Anca Constantin for her encouragement and advice. I will never forget the nice conversations that we had on telephone while taking our morning coffee or before going to sleep. She spends hours listening about my stories from the lab and sharing some of her own about her scientific work. My dear Ulrich Jens Färber, I would like to thank for being there for me and for his patience and understanding during writing of this dissertation.

Finally, I would like to thank my parents, aunt and uncle, for putting me through school, for all their encouragement and support.

Table of contents

1 Introduction and aim of the thesis	1
1.2 General methods for the preparation of oligomers	3
1.3 Applications of rigid rod-like oligomers	4
1.3.1 Molecular rods as “light pipes”	5
1.3.2 Rod-like oligomers in biomembrane models	7
1.3.3 Rod-like molecules as liquid crystals for OLEDs	8
1.4 From oligomers to star-like molecules	9
1.5 Applications of star-like molecules	10
1.6 Aim of the thesis	11
1.7 Synthetic strategies for synthesis of viologens with bonded π - conjugation	13
2 Synthesis and characterization of rigid viologen stars and dendrimers	17
2.1 Introduction	17
2.2 Results and discussions	19
2.2.1 Synthesis	19
2.2.2 Cyclic voltammetry of 1 , 2 , 3 , 4 , 5 and 7	22
2.2.3 Spectroelectrochemical investigation of 4 and 5	25
2.2.4 Redox orbital sequence from PM6 semiempirical calculations	30
2.2.5 Electrochemical polymerization of viologen stars 4 and 7	32
2.2.6 UV-Vis characterization of Poly-4 thin film on ITO electrode	36
2.2.7 STM investigation of Poly-4 on ITO	38
2.2.8 Ion transfer across the Poly-4 film on ITO	40

2.2.9 STM investigation of chemically synthesized Poly-4	44
2.2.10 Preparation and characterization of polyviologen-carbon nanotubes composites (Poly-4-CNTs)	47
2.2.11 Electrochemical and spectroelectrochemical characterization of viologen dendrimer 14	53
2.3 Conclusions	54
2.4 Experimental part	57
2.4.1 Cyclic voltammetry measurements	57
2.4.2 Spectroelectrochemistry of 4 , 5 and 14 in solution	58
2.4.3 Electropolymerization of 4 and 7	58
2.4.4 Spectroelectrochemistry at modified electrode (Poly-4 on ITO) ...	59
2.4.5 PM6 modeling	60
2.4.6 STM measurements on modified electrodes (Poly-4 on ITO and HOPG and Poly-4-CNTs on ITO)	60
2.4.7 Ion transfer studies	61
2.4.8 FT-IR investigation of viologen star 4 and Poly-4	61
2.4.9 Detailed synthetic procedure	62
2.4.9.1 Materials and devices	62
2.4.9.2 Synthesis description	62
3 Synthesis and characterization of π-conjugated rod-like viologens ..	72
3.1 Introduction	72
3.2 Results and discussion	75
3.2.1 Synthesis	75
3.2.2 Electrochemical investigation of 18a-b , 20a-b and 23a-b	82
3.2.3 Diffusion coefficient investigation of methoxy-rods series	85

3.2.4 Spectroelectrochemical investigation of π -conjugated rod-like viologens	89
3.3 Conclusions	93
3.4 Experimental part	95
3.4.1 Cyclic voltammetric measurements	95
3.4.2 Diffusion coefficient studies	96
3.4.3 Spectroelectrochemical measurements	96
3.4.4 Detailed synthetic procedure	96
3.4.4.1 Materials and devices	96
3.4.4.2 Synthesis description	97
4 Electropolymerization of the viologen rods (18a, 20a and 23a) on conductive substrates	113
4.1 Introduction	113
4.2 Results and discussion	115
4.2.1 Reaction of diazotation and coupling	115
4.2.2 Electrochemical characterization of the modified electrodes with the rod-like viologen polymers (Poly-18a , Poly-20a and Poly-23a)	117
4.2.3 FT-IR and XPS characterization of the modified electrodes (Poly-18a-ITO and Poly-20a-ITO)	119
4.2.4 Spectroelectrochemical characterization of Poly-18a and Poly-23a on ITO	121
4.2.5 STM investigation of Poly-18a , Poly-20a and Poly-23a on ITO	122
4.3 Conclusions	124
4.4 Experimental part	124
4.4.1 Materials	124

4.4.2 General procedure of diazotization	125
4.4.3 Cleaning procedure	125
4.4.4 Electropolymerization (grafting)	125
4.4.5 Spectroelectrochemistry of Poly-18a and Poly-23a at ITO electrode	126
4.4.6 FT-IR investigation of 18a , D18a and Poly-18a on ITO.....	126
4.4.7 STM investigation of ITO-modified with Poly-18a , Poly-20a and Poly-23a	126
5 Conjugated viologen rods with amide and ester linkage	127
5.1 Introduction	127
5.2 Results and discussion	128
5.2.1 Synthesis	128
5.2.3 Cyclic voltammetric characterization of 30 and 38	133
5.3 Conclusions	134
5.4 Experimental part	135
5.4.1 Materials and devices	135
5.4.2 Cyclic voltammetric investigation of compounds 30 and 38	136
5.4.3 Detailed synthetic procedure	137
6 Summary and outlook.....	146
References	149
Appendix	170
A.1 Cyclic voltammetry of 4	170
A.2 Electropolymerization of 4 and 7 at GC, Au and ITO electrodes	170
A.3 FT-IR characterization of Poly-4 (chemical polymerization)	172
List of abbreviations	173

Curriculum Vitae.....	176
------------------------------	------------

List of figures

Figure 1.1 Examples of rigid rod-like non conjugated oligomers: a) oligo (cubyls); ⁹ b) oligo(staffanes) ¹⁰ ; c) oligo(ladderanes) ¹¹ and d) oligo(piperidines). ¹²	2
Figure 1.2 Examples of molecular wires based on conjugated molecules: a) oligo(p-phenylene), b) oligo(phenylene-ethynylene), c) pyridinium oligomer, d) carbon nanotube, e) oligo(thiophene) and f) oligo(phenylenevinylene)	6
Figure 1.3 Electron transfer from excited donor (at one end of the rod) to the acceptor (at the other end of the rod) ³⁹	7
Figure 1.4 The orientation of the rod-like molecule guest within lipid bilayers of the host biomembrane, adapted from literature ⁴⁰	7
Figure 1.5 Liquid-crystal phase (smectic) of a rod-like molecule. ⁵²	8
Figure 1.6 From localized to extended π -conjugation in viologen oligomers: a) viologen dendrimer type I (average-extension: 2 aromats), b) viologen dendrimer type II (average-extension: 3 aromats), c) viologen star (average-extension: 4 aromats), d) viologen rod (average-extension: ∞ aromats (depending on rod length); highlighted red: interruption of π -system by -CH ₂ ; red circle at periphery: polymerizable end groups	12
Figure 2.1 CV of the monomeric phenyl viologens 1 (A)) and 2 (B)) at ca. millimolar concentration in MeCN/Bu ₄ NPF ₆ , $v = 100 \text{ mVs}^{-1}$ at GC (0.07 cm ²)	23
Figure 2.2 Single scan voltammograms of dibenzyl viologen (BnV , $c = 1.6 \text{ mM}$, blue), diphenyl viologen (PhV , $c = 1.7 \text{ mM}$, red) and 4 (0.5 mM black; blue	

and red indicating BnV and PhV subunits) in DMF/0.1M n-Bu₄NPF₆, $\nu = 100$ mVs⁻¹ at GC. All viologen stars show pronounced adsorption behavior 24

Figure 2.3 UV-Vis spectra of PhV²⁺ and BnV²⁺ in DMF and 0.1M n-Bu₄NPF₆ ...
..... 26

Figure 2.4 Potential dependent UV-Vis spectra of **4** in DMF and 0.1M n-Bu₄NPF₆. The 4th transition states are illustrated as circles in the color of the redox species in solution: I→II (green), II→III (blue), III→IV (olive), IV→V (yellow). The periphery and the core are represented as two circles: one of the circles (the core) lies inside the other (the periphery) 27

Figure 2.5 Potential dependent UV-Vis spectra of **5** in DMF and 0.1M n-Bu₄NPF₆. The 4th transition states are illustrated as circles in the color of the redox species in solution: I→II (green), II→III (blue), III→IV (olive), IV→V (yellow). The periphery and the core are represented as two circles: one of the circles (the core) lies inside the other (the periphery) 28

Figure 2.6 Spectroelectrochemical titration of **4** (at $\lambda = 399$ nm) in DMF and 0.1M n-Bu₄NPF₆. The 4th transition states are illustrated as circles in the color of the redox species in solution: I→II (green), II→III (blue), III→IV (olive), IV→V (yellow). The periphery and the core are represented as two circles: one of the circles (the core) lies inside the other (the periphery) 29

Figure 2.7 Spectroelectrochemical titration of **5** at ($\lambda = 404$ nm) in DMF and 0.1M n-Bu₄NPF₆. The 4th transition states are illustrated as circles in the color of the redox species in solution: I→II (green), II→III (blue), III→IV (olive), IV→V (yellow). The periphery and the core are represented as two circles: one of the circles (the core) lies inside the other (the periphery) 30

Figure 2.8 HOMO (= redox-orbital), LUMO and spin density localization on a single branch of 5 (including from left to right: phenylviologen (PhV), benzyl viologen (BnV) and central benzene subunits) as a function of electron occupancy calculated with PM6; charge on system refers to the calculated single branch, roman numbers refer to the corresponding species in eq. a)-d) and in Scheme 2.3; broken arrows show the sequential PhV-BnV-PhV-BnV LUMO and BnV-PhV-BnV-PhV HOMO (redox orbital) localization	31
Figure 2.9 Electropolymerization of 4 ($c = 4.9 \cdot 10^{-4}$ M) (A)) and 7 ($1.8 \cdot 10^{-4}$ M) (B)) on GC in DMF/Bu ₄ NPF ₆ during the first 60 scans, $v = 100$ mVs ⁻¹ ; response of Poly-4 (C) ($\Gamma_4 = 3 \cdot 10^{-9}$ or $\Gamma_{\text{subunits}} = 1.8 \cdot 10^{-8}$ mol/cm ²) and Poly-7 (D) ($\Gamma_7 = 2.8 \cdot 10^{-10}$ or $\Gamma_{\text{subunits}} = 3.3 \cdot 10^{-9}$ mol/cm ²) on GC in pure DMF/Bu ₄ NPF ₆ at $v = 100$ mVs ⁻¹	32
Figure 2.10 CVs on GC of A) 1 ($1.55 \cdot 10^{-3}$ M, 5 scans) and B) 5 ($3.42 \cdot 10^{-4}$ M, 60 scans).....	33
Figure 2.11 Eleven overlaid CVs of 4 ($c=4.9 \cdot 10^{-4}$ M) on GC registered after equilibration at -0.3, -0.4, -0.5 -1.2, -1.3 V for 30 s, $v= 100$ mVs ⁻¹ (lower panel) and plot of the neg. absolute cathodic current ($-i_{\text{abs}(-0.43\text{V})}$) measured at -0.43 V (red vert. line) vs. the equilibration potential (upper panel); interpretation of $-i_{\text{abs}(-0.43\text{V})}$ as rel. polymerization efficiency (crucial involvement of 4 th reduction wave)	35
Figure 2.12 UV-Vis absorption spectra of an ITO electrode coated with 4 (Γ ca. $0.37 \cdot 10^{-10}$ mol•cm ⁻²) at 0 V, -0.39 V, -0.51 V, -0.69 V and -0.99 V in 0.1M KCl	37
Figure 2.13 STM images ($V_b = 0.050$ V, $I_t = 1.001$ nA) of bare ITO (A-C) and Poly-4	38

Figure 2.14 MM+MD calculations of 4 and 7 with and without PF_6^- counter ions, double arrows indicate the center-triangle corner distance	40
Figure 2.15 CVs of Fc in DMF-0.1M n-Bu ₄ NPF ₆ at a bare ITO electrode A) and at Poly-4 /ITO modified electrode (area= 0.78 cm ²) (red line) B). The CV response of Poly-4 /ITO is shown as black line	42
Figure 2.16 CVs of $[\text{Fe}(\text{CN})_6]^{3-}$ in 0.1M KCl at a bare ITO electrode A) and at Poly-4 /ITO modified electrode (area= 0.78 cm ²) (red line) B). Graph showing the CV response of Poly-4 /ITO (black line) and Poly-4 /ITO + $[\text{Fe}(\text{CN})_6]^{3-}$ after washing with H ₂ O (blue line)	42
Figure 2.17 CVs of MeV in 0.1M KCl at a bare ITO electrode A) and at Poly-4 /ITO modified electrode (area= 0.72 cm ²) (red line) B). Graph showing the CV response of Poly-4 /ITO (black line) and Poly-4 /ITO + MeV after washing with H ₂ O (blue line)	43
Figure 2.18 CVs of HEV in 0.1M KCl at a bare ITO electrode A) and at Poly-4 /ITO modified electrode (area= 0.72 cm ²) (red line) B). Graph showing the CV response of Poly-4 /ITO (black line) and Poly-4 /ITO + HEV after washing with H ₂ O (blue line)	43
Figure 2.19 CVs of Ru(bpy) ₃ in DMF-0.1M n-Bu ₄ NPF ₆ at a bare ITO electrode A) and at Poly-4 /ITO modified electrode (area= 0.78 cm ²) (red line) B). Graph showing the CV response of Poly-4 /ITO (black line) and Poly-4 /ITO + Ru(bpy) ₃ after washing with acetone (blue line)	44
Figure 2.20 STM images ($V_b = 0.05$ V, $I_t = 1$ nA) of Poly-4 (chemical preparation) on graphite (A-D): A) 335 x 335 nm, Z range 12.5 nm; B) 141 x 141 nm, Z range 12.5 nm; C) 90 x 90 nm, Z range 12.5 nm; D) 72 x 72 nm, Z range 6.25 nm	45

Figure 2.21 a) Polymer strands assembled in helical structure; b) topographic profile along the green line in the polymer strand in a)	45
Figure 2.22 MM+ optimized geometry ¹¹² of 6-mer (oligo-4) arranged in helical structure. The distance between the branches oriented upwards and downwards is ca. 6-7 nm and the double helix is 7-8 nm width.....	47
Figure 2.23 Solvated structures of two polymer strands (each consisting of 6 monomers (4)) arranged in helix. The molecule is twisted by 90 degree.....	47
Figure 2.24 Electropolymerization of 4 ($c = 4.9 \cdot 10^{-4}$ M) + CNTs ($c = 0.2$ M) (A) on GC in DMF/ Bu_4NPF_6 during the first 60 scans, $v = 100 \text{ mVs}^{-1}$; response of Poly-4-CNTs (B) ($\Gamma_4 = 2.73 \cdot 10^{-9}$ or $\Gamma_{\text{subunits}} = 1.63 \cdot 10^{-8} \text{ mol/cm}^2$) on GC in pure DMF/0.1M- Bu_4NPF_6 at $v = 100 \text{ mVs}^{-1}$	49
Figure 2.25 XPS spectra of ITO-Poly-4-CNT composite film. Wide scan A) and core level: B) C1s and C) N1s	49
Figure 2.26 STM images ($V_b = 0.2 \text{ V}$, $I_t = 0.4 \text{ nA}$) of Poly-4-CNT ($\Gamma_{4+\text{CNTs}} = 1.36 \cdot 10^{-9} \text{ mol/cm}^2$) on ITO (A-D): A) 596 x 596 nm, Z range 25 nm; B) 260 x 260 nm, Z range 25 nm; C) 178 x 178 nm, Z range 12.5 nm; D) 38 x 38 nm, Z range 3.13 nm; E) 22 x 22 nm, Z range 50 nm; F) 11 x 11 nm, Z range 1.56 nm	50
Figure 2.27 STM images ($V_b = 0.05 \text{ V}$, $I_t = 1 \text{ nA}$) of Poly-4-CNT (chemical preparation) spread on graphite (A-F): A) 596 x 596 nm, Z range 50 nm; B) 191 x 191 nm, Z range 12.5 nm; C) 106 x 106 nm, Z range 6.25 nm; D) 36 x 36 nm, Z range 3.13 nm; E) 21 x 21 nm, Z range 3.13 nm; F) 19 x 19 nm, Z range 1.56 nm	52
Figure 2.28 Poly-4-CNT composites as cast film on GC electrode. CV recorded in DMF + 0.1M n- Bu_4NPF_6 at scan rate 50 mVs^{-1}	52

Figure 2.29 A) CV of 1.35×10^{-4} M of 14 in DMF + 0.1M n-Bu ₄ NPF ₆ at gold electrode, scan rate 100 mVs ⁻¹ ; B) Rotating disk voltammetry of 14 (7.18×10^{-5} M) at a GC RDE and different rotation speeds: 52.33, 104.66, 157, 209.33, 261.66 and 314 rads ⁻¹	53
Figure 2.30 Potential dependent UV-Vis spectra of 7.2×10^{-5} M of 14 in DMF and 0.1M n-Bu ₄ NPF ₆	54
Figure 3.1 Conjugated viologen-analog oligomers and polymers from literature	73
Figure 3.2 Chemical structures of the rod-like viologenmonomers, oligomers and polymers discussed in this work	75
Figure 3.3 ¹ H-NMR of 18a•2PF₆ measured in MeCN -d ₃	81
Figure 3.4 CVs of: a) methoxy substituted-rods (6.75×10^{-7} mol/ml); b) butoxy substituted-rods (2.61×10^{-7} mol/ml) in DMF solution containing 0.1M n-Bu ₄ NPF ₆ at GC and sweep rate of 50 mVs ⁻¹	83
Figure 3.5 a) Plot of the $E_{1/2}^{\text{red } 1}$ of the methoxy-rod series versus 1/N; b) Plot of the band gap of the methoxy-rod series versus 1/N. The band gap was calculated with eq. 3.1 and 3.2 and N is equal to the number of viologen units in the oligomers	84
Figure 3.6 Current-potential curves for the reduction of 18a•2PF₆ , 20a•4PF₆ and 23a•6PF₆ with the rotating disk electrode at 314 rad/sec	86
Figure 3.7 a) Slope-concentration dependence of 23a•6PF₆ and b) Diffusion coefficient-concentration dependence of 23a•6PF₆ in DMF-0.1M n-Bu ₄ NPF ₆	87
Figure 3.8 Wavelength-dependent extinction coefficients of the 18a-b•2PF₆ , 20a-c•4PF₆ , 21a•4PF₆ , and 23a-b•6PF₆ oligomers at 0.0 V	90

Figure 3.9 Wavelength-dependent extinction coefficients of 18a-b•2PF₆ , 20a-c•4PF₆ , 21a•4PF₆ and 23a-b•6PF₆ oligomers at -0.4 V	92
Figure 3.10 Wavelength-dependent extinction coefficients of 18a-b•2PF₆ , 20a-c•4PF₆ , 21a•4PF₆ and 23a-b•6PF₆ at -0.68 V.....	92
Figure 3.11 Dependence of ϵ (at λ_{\max}) on N (number of viologen subunits) for methoxy substituted viologen-oligomers in oxidized form.....	93
Figure 4.1 CVs of 18a•2Cl ($2.4 \cdot 10^{-3}$ mM) in 0.5M HCl on: a) Au and b) ITO electrode (black line). Reduction of in situ formed diazonium salt: 1 st cycle red line; 2 nd cycle blue line; 10 th cycle green line. Scan rate 0.1 V/s.....	116
Figure 4.2 CVs of 20a•2Cl ($9 \cdot 10^{-4}$ mM) in 0.5M HCl on: a) GC and b) Au electrodes (black lines). Reduction of in situ-formed diazonium salt: 1 st cycle red line; 2 nd cycle blue line; 10 th cycle green line. Scan rate 0.1 V/s	117
Figure 4.3 CVs of a) Au- Poly-18a ($\Gamma = 1.71 \cdot 10^{-9}$ mol/cm ²) and b) ITO- Poly-18a ($\Gamma = 4.45 \cdot 10^{-9}$ mol/cm ²) in 0.1M aq. KCl after derivatization in CV mode, scan rate 0.1V/s	117
Figure 4.4 CVs of a) GC- Poly-20a ($\Gamma = 4.63 \cdot 10^{-9}$ mol/cm ²) and b) Au- Poly-20a ($\Gamma = 9.13 \cdot 10^{-9}$ mol/cm ²) in 0.1M aq. KCl after derivatization in CV mode, scan rate 50 mV/s	118
Figure 4.5 CVs of a) ITO- Poly-18a electrode ($\Gamma = 5.35 \cdot 10^{-8}$ mol/cm ²) in 0.1M KCl; b) Au- Poly-23a electrode ($\Gamma = 1.50 \cdot 10^{-9}$ mol/cm ²) in 0.1M DMF- n-Bu ₄ NPF ₆ ; scan rate 50 mV/s	118
Figure 4.6 CVs (50 scans) of a) GC- Poly-20a electrode ($\Gamma = 6.28 \cdot 10^{-9}$ mol/cm ²) and (b) ITO- Poly-20a electrode ($\Gamma = 6.47 \cdot 10^{-9}$ mol/cm ²) in 0.1M aq. KCl.....	119

Figure 4.7 C1s a) and N1s b) core level spectra recorded on Poly-20-ITO modified electrode. Polymerization time 500 s; $\Gamma_{\text{Poly-20}} = 1.08 \cdot 10^{-8} \text{ mol/cm}^2$..	120
Figure 4.8 FT-IR spectra: a) 18a•2Cl ; b) D18a•2Cl ; and c) Poly-18a on ITO	121
Figure 4.9 UV-Vis spectra of: A) Poly-18a and B) Poly-23a on ITO. The spectra were registered at different potential steps: 0.0 V (black lines); -0.45 V (green lines) and -1.0 V (red lines)	122
Figure 4.10 STM images ($V_b = 0.050 \text{ V}$, $I_t = 1.001 \text{ nA}$) of Poly-18a ($\Gamma_{\text{Poly-18a}} = 2 \cdot 10^{-8} \text{ mol/cm}^2$, A-C), Poly-20a ($\Gamma_{\text{Poly-20a}} = 1.08 \cdot 10^{-8} \text{ mol/cm}^2$, D-E) and Poly-23a ($\Gamma_{\text{Poly-23a}} = 2.5 \cdot 10^{-9} \text{ mol/cm}^2$, F) on ITO: A) 100 x 100 nm, Z range 12.5 nm; B) 45 x 45 nm, Z range 6.25 nm; C) 25 x 25 nm, Z range 3.13 nm; D) 214 x 214 nm, Z range 25 nm; E) 27 x 27 nm Z range 3.13 nm; F) 72 x 72 nm, Z range 25 nm	122
Figure 4.11 STM images ($V_b = 0.050 \text{ V}$, $I_t = 1.001 \text{ nA}$) and topographic profiles of Poly-18a (A) and Poly-20a (B): A) 25 x 25 nm, Z range 3.13 nm; B) 27 x 27 nm, Z range 3.13 nm; C) topographic profile along the blue line in A) and D) topographic profile along the blue line in B)	123
Figure 5.1 Cyclic voltammograms of 30 ($0.86 \cdot 10^{-3} \text{ M}$) in DMSO 0.1M n-Bu ₄ NPF ₆ at a sweep rate of 100 mVs ⁻¹ . The potential was swept from: A) +1.2 V and -2.2 V and B) 0.1 V and -0.7 V	133
Figure 5.2 Cyclic voltammograms of 38 ($1.9 \cdot 10^{-3} \text{ M}$) in DMF-0.1M n-Bu ₄ NCl at the scan rate 100 mVs ⁻¹ . The potential was cycled between: a) +1.0 V and -1.2 V and b) 0.1 V and -0.5 V	134
Figure 6.1 Nanometer-sized viologen stars and viologen rods exemplified by compounds 4 and 23a	146

Figure 6.2 STM images ($V_b = 0.050$, $I_t = 1.001$) of polyviologen star (Poly-4) and polyviologen rod (Poly-23a) on ITO: A) 13.6 x 13.6 nm, Z range 0.781nm and B) 72 x 72 nm, Z range 25 nm	147
Figure 6.3 Representation of a CNTs-based field effect transistor doped with the rod-like viologen	148
A.1 Linear dependence of the peak current (i_p) on the square root of the scan rate (V)	170
A.2 A) The electropolymerization of 4 ($4.9 \times 10^{-4}M$). B) CVs of Poly-4 on Au. CVs were measured in 0.1M n-Bu ₄ NPF ₆ at a scan rate of 100mV/s.....	171
A.3 A) The electropolymerization of 4 ($4.9 \times 10^{-4}M$). B) CVs of Poly-4 on ITO. CVs were measured in 0.1M n-Bu ₄ NPF ₆ at a scan rate of 100mV/s	171
A.4 CVs of Poly-4 on GC in 0.1M n-Bu ₄ NPF ₆ and scan rate 100mVs ⁻¹ : A) potential range 0.2→ -0.4V and B) potential range 0.2→ -0.6V. GC was modified from $4.9 \times 10^{-4}M$ of 4 during 20 scans at $U = 100 \text{ mVs}^{-1}$ and potential range: 0.2 V→1.2 V	171
A.5 A) The electropolymerization on ITO of 7 ($1.76 \times 10^{-4}M$). B) CVs of Poly-7 on ITO. CVs were measured in 0.1M n-Bu ₄ NPF ₆ at a scan rate of 100mV/s	172
A.6 FT-IR spectra of 4 (a) and Poly-4 (b)	172

List of schemes

Scheme 1.1 Principle of the iterative divergent/convergent approach. ¹⁷	3
Scheme 1.2 Divergent (A) and convergent (B) approaches for the synthesis of star-shaped oligomers	9
Scheme 1.3 Approach to the synthesis of star-shaped viologens	13
Scheme 1.4 Approach to the synthesis of a rigid viologen-dendrimer	14
Scheme 1.5 Approach to the synthesis of rod-like viologen-based oligomers	15
Scheme 2.1 The synthesis of viologen stars	20
Scheme 2.2 Synthetic route to ellipsoidal dendritic viologens.....	21
Scheme 2.3 Structure of 4 representing the four possible transitions states generated electrochemically (top left side) and spectroelectrochemically (bottom). The 4 th transition states are illustrated as circles and arrows in the color of the redox species in solution: I→II (green), II→III (blue), III→IV (olive), IV→V (yellow). The periphery and the core are represented as two circles: one of the circles (the core) lies inside the other (the periphery)	26
Scheme 2.4 Interactions of Poly-4-ITO with anionic and cationic guests	40
Scheme 2.5 Formation of a double-helix structure of polyviologen (Poly-4)	46
Scheme 2.6 Preparative methods of Poly4-CNT composites	48
Scheme 3.1 Synthesis of rod-like 4,4'-bipyridinium monomers and their building blocks: a) DMF/K ₂ CO ₃ /90°C/3 days; b) benzene/Zn/NaOH 50 %/70°C/14 h; c) HCl 20 %; d) (CH ₃) ₂ CO/Zn/NaOH/reflux/24 h; e) EtOAc/Zn/NaOH/reflux/12 h; f) CH ₃ CN /reflux/72 h; g) MeOH/ reflux/20 h	76

Scheme 3.2 Synthesis of rod-like 4,4'-bipyridinium dimers and their building blocks: a) MeOH/reflux/48 h; b) MeOH/reflux/4 days; c) CH ₃ CN/reflux/48 h; d) MeOH/ reflux/3 days	77
Scheme 3.3 Synthesis of rod-like 4,4'-bipyridinium trimers and their building blocks: a) MeOH/reflux/3 days; b) MeOH/reflux/4 days; c) CH ₃ CN/reflux/48 h	78
Scheme 3.4 Reduction of 2-alkoxybenzene to 1,2-bis(2-alkoxyphenyl) hydrazine in the presence of Zn and NaOH	79
Scheme 3.5 Side products of acid-catalyzed benzidine rearrangement	80
Scheme 4.1 The electropolymerization of viologen oligomers on electrode surface.....	113
Scheme 4.2 a) Chemical structure of a diazonium molecule A; b) The two possible couplings of diazonium: route 1 (C-C bounds formation) or route 2 (azo-bridges formation). The scheme was adapted from the literature ²¹⁴	114
Scheme 4.3 Synthesis of rod-like viologen diazonium salts.....	115
Scheme 5.1 Proposed synthetic route to π -conjugated oligoviologens.....	129
Scheme 5.2 Synthesis of bis-1,1'-[N ¹ , N ⁴ bis(4-(amino-phenyl)phenyl)benzene-1,4-dicarboxylate]-4,4'-bipyridinium hexafluorophosphate (30)	130
Scheme 5.3 Synthesis of bis-1,1'-[(4,4'-(amino-phenyl)phenyl)benzene-1,4-dicarboxylate]-4,4'-bipyridinium hexafluorophosphate (33)	130
Scheme 5.4 Synthesis of bis-1,1'-[4,4'-(amino-phenyl)phenyl]thiophene-2,5-dicarboxylate]-4,4'-bipyridinium hexafluorophosphate (37)	132
Scheme 5.5 Synthesis of bis-1,1'-bis(4-methyl-benzoate)-4,4'-bipyridinium bis (hexafluorophosphate) (38).....	132

Scheme 5.6 Electrochemical reduction of the benzoate ester at GC electrode	
.....	134

List of tables

Table 2.1 Compilation of the electrochemical data of the monomers	24
Table 2.2 Surface concentrations (Γ) of Poly-4 and Poly-7 polymerized on GC, gold and ITO	34
Table 2.3 Intermolecular interactions between Poly-4 (on ITO) and anionic or cationic guests.....	41
Table 3.1 Integration of ^1H -NMR spectra of viologen oligomers with amine end-groups measured at 300 K	81
Table 3.2 Electrochemical properties and energy levels of viologen-oligomers	83
Table 3.3 Number of exchanged electrons per molecule measured by preparative electrolysis coulometry	85
Table 3.4 Diffusion coefficient values of 23a•6PF₆ at different concentrations	88
Table 3.5 Diffusion coefficients (D) of 18a•2PF₆ , 20a•4PF₆ and 23a•6PF₆ ...	88
Table 3.6 Extinction coefficient of oligomeric viologen-radical cations.*	91

Abstract

This doctoral thesis focuses on synthesis of rigid star-shaped and rod-like viologen oligomers. The work is divided in two parts: (1) synthesis, characterization and electropolymerization of star-shaped and (2) rod-like viologens oligomers. In the first part the preparation of viologen stars consisting of a phenyl core with triple 1,3,5-branching, each branch consisting of a linear alternating series of diphenyl (PhV^{++}) and dibenzyl (BnV^{++}) viologens and a variety of peripheral groups $-\text{X}$ (Br, OH), is presented. A new electrochemical method of electrode modification (Gold, GC, ITO and CNTs) with viologen derivatives based on a benzyl radical coupling mechanism is described. The radicals are excessively generated at the star periphery resulting in a highly cross-linked polyviologen film with persisting star subunits. It was characterized by CV, STM and UV-Vis methods. Redox-titration experiments monitored by UV-Vis reveals that the reduction of the viologen stars begins at the periphery with the formation of PhV^{+} , continues with generation of BnV^{+} and ends with the reduction of the radical cations in the same sequence. Thus, viologen stars combine the unique redox and electrochromic property of isolated phenyl and benzyl viologen in one molecule.

The second part of the thesis focuses on the step-wise synthesis of a library of rigid rod-like conjugated difunctional viologen/diphenyl oligomers with varying chain lengths including different side chain substitution. All oligomers are soluble in DMSO or MeOH depending on the counter anion (PF_6^- or Cl^-). In order to tune the solubility of the oligomers, the side chains were varied from methoxy to butoxy and oligo(ethylene oxide). The most solubilizing side-chains are of the oligo(ethylene oxide) type. All viologen

oligomers were characterized by means of ^1H -NMR, ^{13}C -NMR, elemental analysis, optical spectroscopy and cyclic voltammetry. A simple surface functionalization and grafting technique has been developed for covalent binding of the viologen oligomers onto various conductive substrates e.g.: Au, GC and ITO. These modified electrodes are suitable for potential applications in designing field-effect transistors, sensors and supercapacitors. The polymer layers were characterized by means of FT-IR, STM, XPS and CV.

The combined results presented in thesis represent a major advance in electrode functionalization by n-dopable viologen polymers and herald a variety of potential applications that make use of n-type semiconductors.

1 Introduction and aim of the thesis

The way nature organizes macromolecules in cells influences their morphology and functions. Even the simplest organism such as the rod-shaped tobacco mosaic virus has a well-defined form, because structure and function are related to each other. The nature achieved a perfect fit of rigid and flexible molecules into organisms. We can consider molecules inside of an organism as “molecular construction kit”, analogous to the children’s Tinkertoy construction set, which are used to build complicated objects from a limited set of rods, connectors and other simple building elements. The organism is built following a simple and logical concept: the rigid rod-like molecules form the skeleton and allow the organism to build and hold its shape, which in turn is obtained by the connection of flexible molecules to the rigid ones. Thus, there is a connection between the molecular structure of a molecule and its function. But, to obtain the perfect form, nature uses in its constructive process semi-rigid rod-like molecules that interact easier with other flexible molecules than the rigid one, and build macromolecules by non-covalent interactions. So, several supramolecular architectures are created in organisms such as spherical micelles, vesicles, fibers, supramolecular helices or nanotubes. Each supramolecular system is different, but they are mutually dependent on each other. Together they make life possible.

This fact can also be a guide for organic synthesis, as some functions can only be realized if the structure of a molecule is stable. The synthesis of large molecules having a defined form is a big challenge for organic chemists.

In chemistry the term “molecular rod” refers to long molecules showing a relatively rigid conformation. Their synthesis and characterization is an

important task and opens new possibilities in various fields of research: chemistry, material science and biochemistry.

Based on their unique properties, three applications for rod molecules are evident; i.e. building blocks in supramolecular assemblies, in investigation of long-range interactions (charge and energy transfer) and model systems for polymers with special optical and electronic properties.

A variety of rod-like oligomers have been designed and synthesized over the past century. Based on the C-C bonds type (single, double, triple) present in the molecule they are divided in saturated and π -conjugated rods. Most rod-like oligomers have extended π -system and consist of unsaturated repetitive subunits such as oligo(phenylenes) (OP),¹ oligo(thiophenes),¹ oligo(phenylenevinylenes) (OPVs),^{2,3} oligo(p-phenyleneethylenes) (OPEs),⁴ oligo(p-benzamides),⁵ oligodienes 1-3,⁶ carbon-rich metal-containing complexes,^{7,8} etc.

Only a few examples for molecular rods with a saturated backbone are known (Fig.1.1).

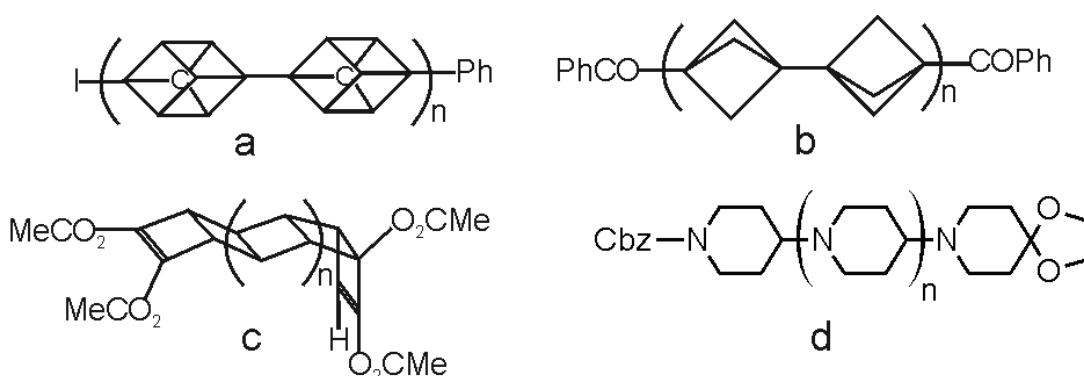


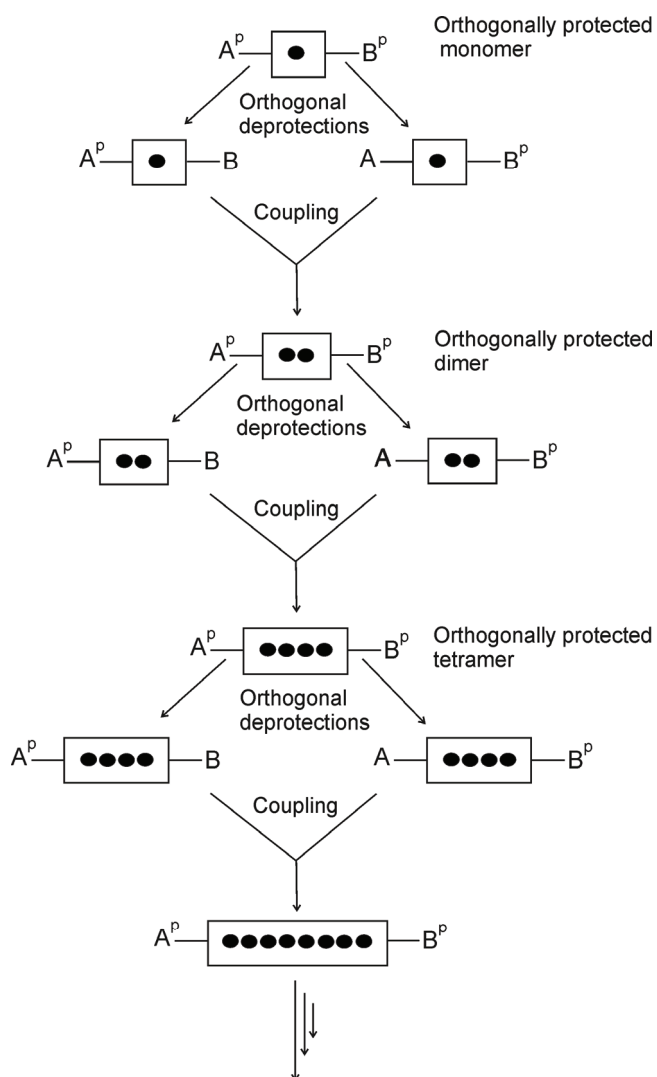
Figure 1.1 Examples of rigid rod-like non conjugated oligomers: a) oligo(cubyls);⁹ b) oligo(staffanes);¹⁰ c) oligo(ladderanes)¹¹ and d) oligo(piperidines).¹²

Their architecture was achieved by three different approaches concerning

the connection of the building blocks: a) the building blocks are connected by one bond (staffanes);^{13,14} b) by two or more bonds¹⁵ and c) the building blocks are connected by a spiroatom as for example in the case of oligospiranes.

1.2 General methods for the preparation of oligomers

Well defined oligomers have several advantages over polymers. It is thoroughly understood that the well-defined architecture of oligomers facilitate the investigation of structure-property relationship within an oligomeric series, and thus they serve as model system for polymers.



Scheme 1.1 Principle of the iterative divergent/convergent approach.¹⁶

Experimental tests of current theories for the correlation of molecular architecture and physical properties require model molecules with precisely defined structures. Unfortunately, oligomer synthesis is limited by their poor solubility, difficult separation, and demanding characterization.

Generally oligomers are prepared following two stepwise approaches (without and with activation of monomers end groups). In the first approach, the elongation of the oligomer chain is achieved by stepwise addition of an excess amount of monofunctional monomer to the active end of a growing chain. In the next step, the end groups of the oligomeric chain are converted into active groups that make them easier to react with monomers, and, therefore, enabling the oligomer to extend its molecular length.

Well defined oligomers with different end groups are synthesized by following the iterative divergent/convergent approach (Scheme 1.1).¹⁶⁻¹⁸ The monomer with inactive end groups is introduced into the reaction after the selective activation of one of the end groups. This approach is attractive because the molecular length of oligomers grows rapidly, and, therefore, the purification of the products is relatively easy.¹⁹

1.3 Applications of rigid rod-like oligomers

The application of molecular rods depends on their nature of backbone (saturated or π -conjugated) and its side chain functionality.

Based on their functional side chain they can manage catalysis, selective chiral interactions, light emission, cross-linking, hydrogen-bonding and to form an assembly, in consideration of their simple rod shape.

1.3.1 Molecular rods as “light pipes”

The nanotechnology works with materials having very specific electronic and mechanical properties suited for many applications. Synthetic chemists are encouraged to design well-defined compounds which meet these requirements. They have developed the ability to control the structure and properties of the building blocks.

Due to their rigid character with the high shape-persistence the conjugated rigid rod-like oligomers can be regarded as ideal candidates for molecular wires. Their purpose is to provide efficient electron transfer through the molecular backbone. One can expect that in assembling molecular circuits in a bottom-up fashion, instead of building assembling components in a top down fashion on a chip, a last step of device miniaturization will be achieved.

Several rigid rod-like disperse oligomers have been investigated as potential materials for wires in electronic applications. The most investigated molecular wires belong to oligo(p-phenylenes),²⁰ oligo(phenylenevinylene),^{2,3} oligo(phenylene-ethynylene),^{21,22} oligo(thiophene),²³ oligo (thiopheneethynylene),^{24,25} carbon nanotubes,²⁶ organometallic molecular wires,^{27,28} oligoporphyrines,^{27,28} etc. Some representative structures are shown in Fig. 1.2.

Carbon nanotubes have been used as molecular wires in electronics²⁹ but they are difficult to handle due to their insolubility in most organic solvents³⁰ and also due to the loss of electrical properties after functionalization.^{31,32}

Pyridine based oligomers^{33,34} are a special class of molecular wires. They have attracted enormous interest due to the ability to form coordination compounds with metals since they are easily converted to salts which affords

oligomers soluble in water or organic solvents and also due to their redox properties.

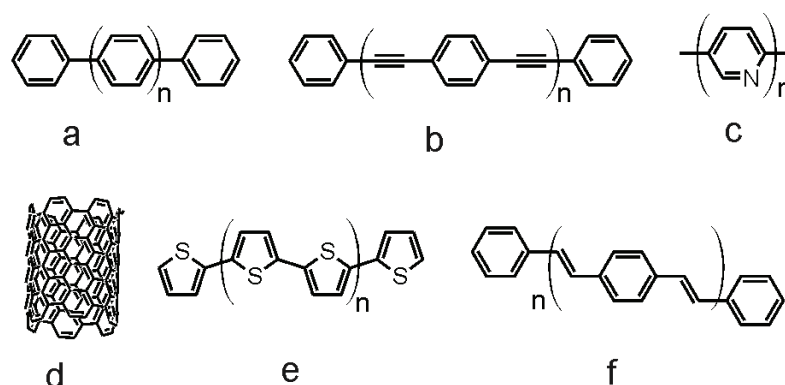


Figure 1.2 Examples of molecular wires based on conjugated molecules: a) oligo(p-phenylene), b) oligo(phenylene-ethynylene), c) pyridinium oligomer, d) carbon nanotube, e) oligo(thiophene) and f) oligo(phenylenevinylene).

Extended viologens³⁵ or viologen analogues³⁶ should be also mentioned. The rigid structure and the fully conjugated backbones make them candidates for molecular wires. The synthesis of discrete viologen oligomers may be crucial due to their unique redox and electrochromic properties: they not only serve as model compounds for understanding the fundamental properties of π -conjugated viologen-based polymers derived from their oligomers, but also due their natural electron affinity, which makes them candidates for n-type semiconductors. Their synthesis will be discussed in more detail in Chapter 3.

Metal alkynyls molecular rods⁸ have been shown to be ideal building blocks for luminescent molecular rods, in which the luminescence can be tuned by changing the alkynyl ligands. Much interest exists in preparing rod-like conjugated systems that capable of absorbing light at one end and emitting light at the other end.³⁷ The excitation of the donor at one end of the rod leads to energy transfer to the acceptor at the other end of the rod, Fig. 1.3. These types of molecular rods tend to form columnar stacks due to the π -

π interactions between donor and acceptor and are used in the construction of solar cells. The advantage in such solar cells is that the photogenerated exciton split off at the place where is formed.

Nanofibres were grown from oligothiophene or oligophenylene on silicate sheet substrate by Hot-Wall Epitaxy (HWE).³⁸ The formed nanofibre show highly polarized emission which make them useful in several applications like waveguides, frequency doublers and lasers.

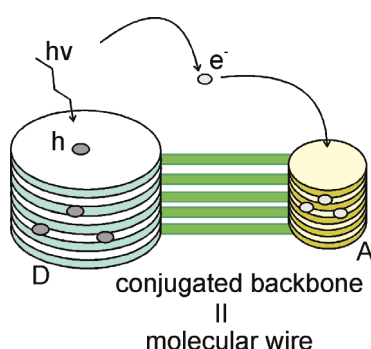


Figure 1.3 Electron transfer from excited donor (at one end of the rod) to the acceptor (at the other end of the rod).³⁹

1.3.2 Rod-like oligomers in biomembrane models

Highly hydrophobic rigid rod-like molecules labeled with fluorophores can be assembled within the hydrophobic core of membranes in order to fulfill many functions of some proteins found throughout the cell membrane .

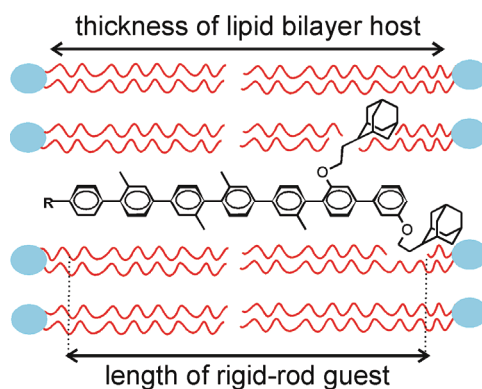


Figure 1.4 Orientation of the rod-like molecule guest within lipid bilayers of the host biomembrane, adapted from literature.⁴⁰

It has been shown that the oligo(p-phenylenes) can be tuned to recognize the lipid bilayer membranes (Fig.1.4) either by their thickness or polarization^{40,41} due to the interactions between the rod (guest) and the lipid bilayer (host).⁴² Artificial ion channels based on oligo(p-phenylene) were also designed to investigate the selectivity mechanism of ion transport across bilayer membranes.^{43,44}

1.3.3 Rod-like molecules as liquid crystals for OLEDs

Rod-like monodisperse oligomers with luminiscent properties have been investigated to use in emissive electronic and photonic organic devices, such as light-emitting diodes (OLEDs)⁴⁵⁻⁴⁷ and organic lasers.⁴⁸ A large group of rod-like oligomers, e.g.: oligo(p-phenylene),⁴⁹ oligo(thiophene),⁵⁰ oligo(p-benzamides),⁵ oligo(p-phenylene-vinylene),⁵¹ etc. have a liquid crystalline (LC) state. In conventional LC, rod-like oligomers are mostly formed by rod-like molecules that have flexible chains attached to rigid cores (Fig. 1.5). Usually, rod-like molecules arrange themselves into layers (known as smectic LC phase).⁵²

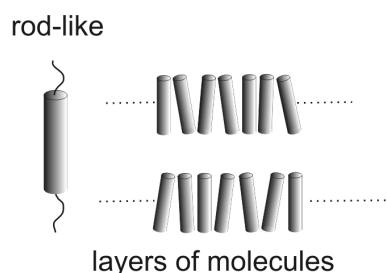
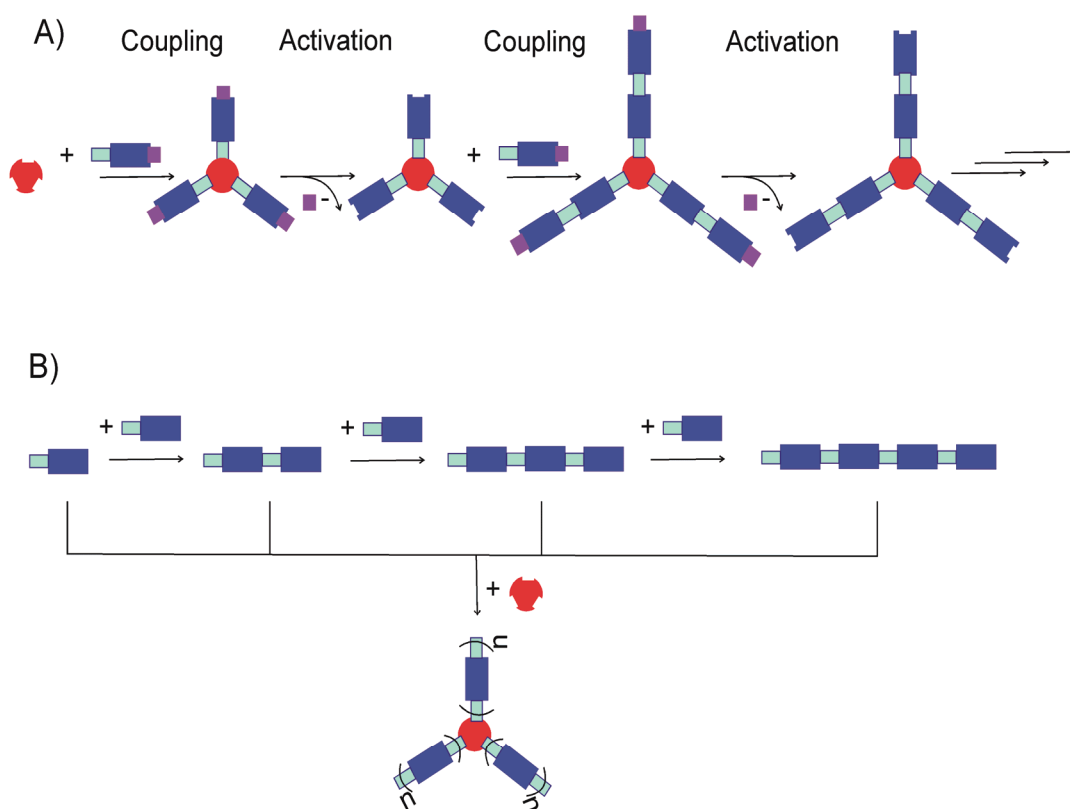


Figure 1.5 Liquid-crystal phase (smectic) of a rod-like molecule⁵².

The main interest in these type of compounds is that they exhibit high charge-carrier mobility, polarized emission and that they can be aligned by an external electric field.

1.4 From oligomers to star-like molecules

The linear oligomers that are connected through a central structure (core) will give a star-shaped molecule. Two basic synthetic strategies, divergent and convergent approaches, have been used to design well defined star-shaped systems (Scheme 1.2).



Scheme 1.2 Divergent (A) and convergent (B) approaches for the synthesis of star-shaped oligomers.

In the divergent approach, the star-shaped molecule grows in repetitive steps outwards from the core diverging into space. A schematic representation is shown in Scheme 1.2-A. Starting from a reactive core, the star-shaped molecule is grown by joining with the monomer (Step 1). Then the end functionality of the arms are activated for the reaction with another molecule monomer (Step 2). The steps 1-2 can be repeated until the high molecular

structure is achieved. The divergent approach has the advantage of using a simple monomer building block at every coupling stage. However, the difficulty of separating the product from partially reacted star-shaped precursor or unreacted monomer, remains a drawback of this strategy.

The convergent approach (Scheme 1.2-B) results in a star-shaped system within one synthetic step by attaching the prepared oligomeric arms to the core unit. This approach is the most adopted method to prepare star-shaped molecules.

Combining different viologen subunits in star-shaped architectures is advantageous because it allows for the inclusion of their inherent properties, such as well-defined redox potentials and electrochromic properties. A well-defined combined oligo-phenylviologen/benzylviologen star-like supramolecule might also be interesting, because it combines the properties of two type of viologen in an unpredictable way.

1.5 Applications of star-like molecules

Star-like molecules have attracted interest for applications in electroluminescence (EL) devices,⁵³ because they exhibit an amorphous state and strong luminescence,⁵⁴ which is an important factor for the operation of devices based on organic materials.

Amphiphilic star-like macromolecules were used as drug delivery system.⁵⁵ Their amphiphilic character and nanosize dimensions were used to promote interactions with cell membranes and related biological systems. The star-shaped systems containing a targeting molecule (antibody) in the centre and a hydrophilic polymer bearing drug molecules in the shell of the supramolecule were prepared for studies in cancer therapy. The results of the

flow cytometric analysis showed that the star-shaped conjugates are more effective for targeted drug delivery and cancer treatment than the classic linear antibody-targeted polymers.⁵⁶

1.6 Aim of the thesis

Among the reported viologen-based molecular architectures (as dendrimers,⁵⁷⁻⁵⁹ linear molecules for rotaxanes,^{60,61} organic/inorganic composites⁶² etc.), rigid star-shaped and rod-like structures are rare, but especially desirable because of their fixed geometric shape, stability and their electronic and electrochemical properties. A thorough literature research revealed that the star-shaped or the rod-like viologes have been not described yet.

One of the motivation of the work described in the thesis is the synthesis of π -conjugated viologens that can be reduced to radical cations which are delocalized over very large distances. Fig. 1.6 shows the evolution of the degree of conjugation in a series of known and hypothetical structures that are compared to known flexible viologen dendrimer (a), where the π -conjugation is interrupted by methylene spacers separating each 4,4'-bipyridinium unit from its neighbours.

The planned compounds b) to d) have increasing π -conjugation. From compounds a) to d) the average number of conjugated 6 membered rings follows the sequence $1.5 \rightarrow 3 \rightarrow 4 \rightarrow \infty$. The later infinite conjugation is of course only correct for very long rods, however, it demonstrates the fact that the rods have no built-in "conjugation break". With increasing conjugation the number of methylenes groups decreases gradually. This affects additionally the stiffness of the resulting macromolecules, as each methylenic center is a

source of conformational freedom. Increased π -conjugation or even infinite π -conjugation is a prerequisite for electronic conductivity in oligomers as: oligo(p-phenylene), polyacetylene, polythiophene, etc. Thus, an intriguing question would be, if compounds such as viologen rods are electronically conductive or not.

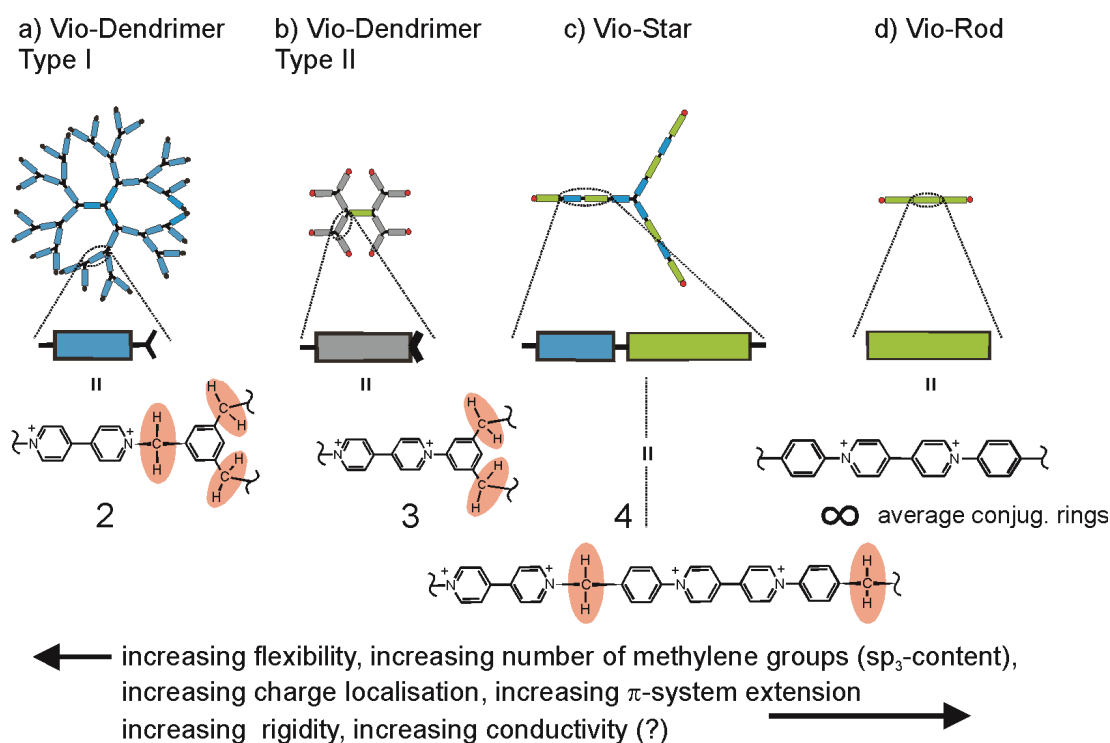


Figure 1.6 From localized to extended π -conjugation in viologen oligomers: a) viologen dendrimer type I (average-extension: 2 aromats), b) viologen dendrimer type II (average-extension: 3 aromats), c) viologen star (average-extension: 4 aromats), d) viologen rod (average-extension: ∞ aromats (depending on rod length); highlighted red: interruption of π -system by $-CH_2-$; red circle at periphery: polymerizable end groups.

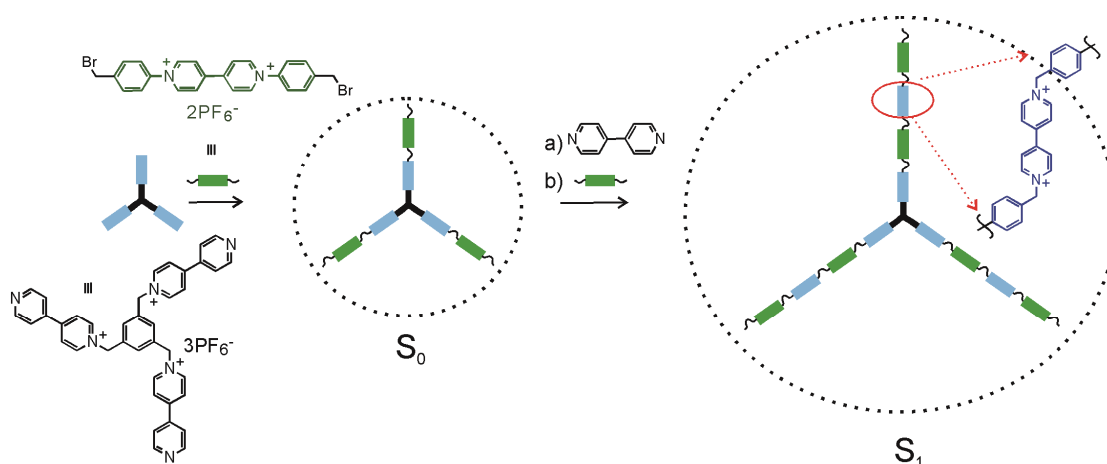
Since molecular electronics is a flourishing current field of research, a viologen rod such as in d) may be a candidate for applications as interconnectors, transistors or photovoltaics. However, the experimental setup for such measurements is highly sophisticated (nano-electronics) but many phenomena can also be studied on the micrometer scale. For such purposes I

would like to introduce further polymerizable functions at the periphery of structures b-d) and polymerize these molecules into thin films which can be studied by conventional technologies.

During my PhD work, I was guided by macromolecules with molecular architectures of type b), c), d) in Fig. 1.6. In addition, I planned to introduce peripheral groups which undergo electrochemical polymerization upon reduction. Two mechanisms were in discussion a) a new electrochemically triggered benzyl-benzyl radical coupling for star-shaped viologens and a well-known aryl-aryl coupling triggered electrochemically by reduction of the corresponding diazonium salts in case of the viologen-rods.

1.7 Synthetic strategies for synthesis of viologens with extended π -conjugation

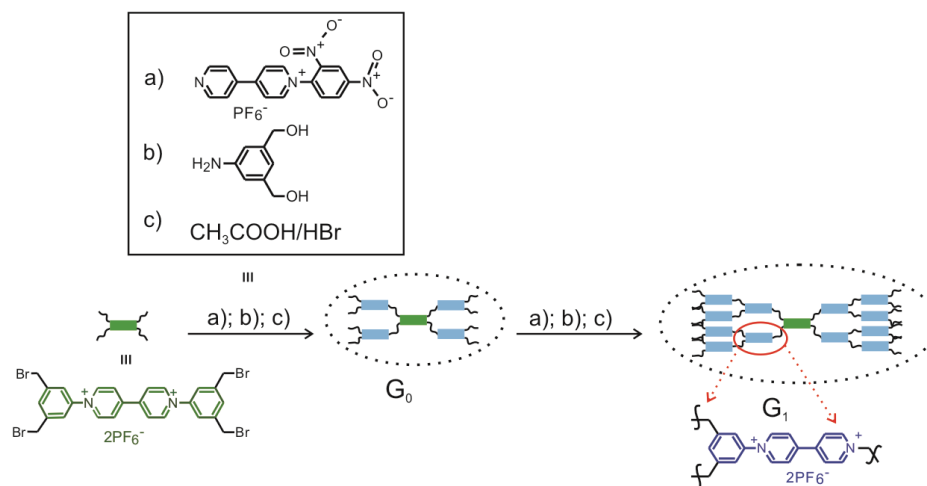
The synthesis of the star-shaped viologens involves growing of the arms (a linear alternating series of diphenyl and dibenzyl viologens) from the core (1,3,5-trisubstituted benzene) (Scheme 1.3). It involves the solution of two problems: the complete alkylation of viologen star (1,3,5-tris((4,4'-bipyridinium)-methyl)benzene) and cross-linking which takes place during alkylation.



Scheme 1.3 Approach to the synthesis of star-shaped viologens.

The selectivity during alkylation is based on the addition of the viologen star into a solution containing excess of bromide. Several precipitations were conducted to afford counter-ion pure products, either upon precipitations from methanol/ether or under anion exchange conditions.

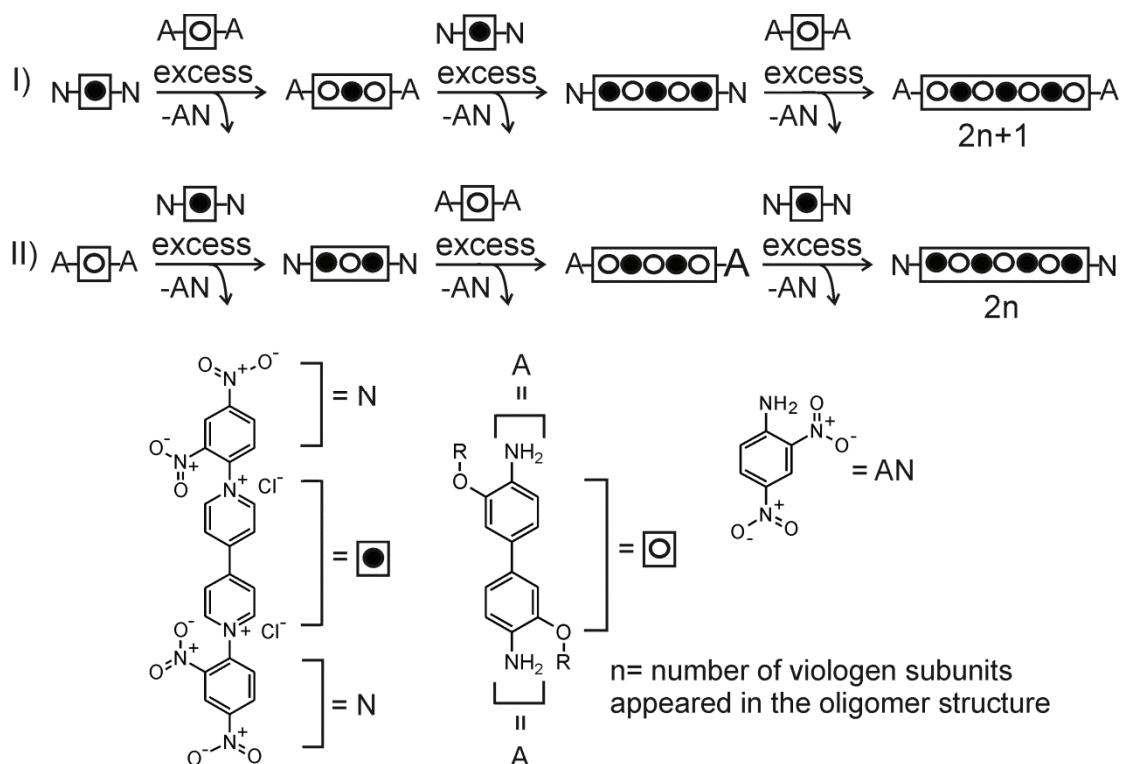
The synthetic strategies towards rigid viologen dendrimers (G_0 and G_1) involves three successive reactions: N-alkylation, N-arylation and activation of the functional end groups (Scheme 1.4). From the core 1,1'-bis(3,5-bromomethyl-phenyl)-4,4'-bipyridinium) hexafluorophosphate the branches are build up by N-alkylation with 1-(2,4-dinitrophenyl)-4-pyridin-4-ylpyridinium and further by N-arylation with 3,5-bis(hydroxymethyl)aniline. Bromination of the hydroxyl end groups, allows further N-alkylation/N-arylation and thereby growth of the molecule. Steps b) \rightarrow c) corresponds to the typical transformation of a latent electrophile into its active state.



Scheme 1.4 Approach to the synthesis of a rigid viologen-dendrimer.

Discrete π -conjugated viologen oligomers are pure materials with defined structure. Two 4,4'-bipyridine molecules could be conveniently linked in a π -conjugated system via N-arylation or by Zincke reaction. Direct N-arylation is not suitable for chain elongation because it requires that the aryl halide

electrophile is activated by electron withdrawing groups.⁶³ In contrast, the Zincke reaction tolerates a wide variety of π -conjugated amines as nucleophiles, resulting in a versatile route to N-aryl pyridinium salts.



Scheme 1.5 Approach to the synthesis of rod-like viologen-based oligomers.

The synthesis of the viologen/alkoxy diphenyl co-oligomers was achieved by successive Zincke reactions between two monofunctional co-monomers: bis-[1,1'-(2,4-dinitropheny-4,4'-bipyridinium)] dichloride (viologen= acceptor) and 3,3'-alkoxy-benzidine (donor) (Scheme 1.5). The selectivity is controlled by an excess of co-monomers used for chain elongation. In a first approach ((I) in Scheme 1.5), the viologen monomer reacts with an excess of 3,3'-alkoxy-benzidine and forms an oligomer containing NH_2 end groups. Furthermore, the chain elongation can be achieved by successive addition of an excess of monomers (acceptor/donor) to obtain the oligomeric series

expressed as $(2n+1)$, where n represents the number of viologen subunits in the oligomer. In a second approach ((II) in Scheme 1.5), 3,3'-alkoxy-benzidine reacts with an excess of viologen monomer and forms an oligomer containing 2,4-dinitrophenyl groups. The elongation is achieved as described in the first approach, with the difference that monomers are added in succession donor/acceptor and leads to a $2n$ oligomeric series.

2 Synthesis and characterization of rigid viologen stars and dendrimers

2.1 Introduction

Viologens (N,N'-disubstituted 4,4'-bipyridinium salts) have been extensively used as electron acceptors in molecular devices, such as photovoltaic cells,^{64,65} sensors,^{66,67} electrochromics^{68,69} and field-effect transistors.^{64,70} They can undergo two one electron-transfer reactions to form first a stable radical cation (violet/blue/green) and second, at a more negative potential, a neutral quinoidal species (yellowish), which is prone to electrophilic attack. The type of R groups (alkyl, benzyl, phenyl) at the pyridinium nitrogen strongly influences their reduction potentials and spectral properties, reflected by the synthetic efforts concerning new electrochromic viologens with symmetrical or mixed alkyl, benzyl or phenyl substitution patterns, or asymmetric combinations thereof.⁷¹

For many devices viologen-modified electrode surfaces are needed. Polyviologens can be coated onto the electrode surface by graft copolymerization. Efforts have been made to fabricate modified electrodes based on viologen films⁷² or by cation-anion interaction of the polyviologens with a negatively charged electrode surface.⁷³ Electropolymerization is another possibility to fabricate such interfaces and, as electropolymerization proceeds only at the electrode surfaces, it is a particularly suitable method for the modification of area-defined electrodes. Electrochemically induced electrode modifications involves "electrochemically assisted adsorption" of a poly-viologen⁷⁴ or cross linking of a polymer with viologen oligomers.⁷⁵

The polyviologen-modified electrodes were successfully prepared from pyrrole⁷⁶⁻⁷⁹, vinyl⁷⁸ or thiophene⁸⁰ functionalized viologen monomers. The electropolymerization of a branched cyanopyridinium monomer to highly cross-linked polyviologen is also described.^{81,82} Beside their electrochromic and sensing properties, viologens may be interesting candidates as n-dopable semiconducting materials.⁸³

Various families of large molecules with viologen or pyridinium subunits have been synthesized over the years. These supramolecules combine unique geometric and electronic features. For example, π -conjugated viologen oligomers or viologen analogs⁸⁴⁻⁸⁷ were intended to be used as molecular wires in organic electronics or the viologen⁵⁹/pyridinium⁸⁸ dendrimers with interrupted conjugation were used to trap molecules or counter ions. Rotaxanes/pseudorotaxane^{89,90} with viologen subunits were used as electrochemical switches. Rigid star-shaped pyridinium molecules were synthesized in order to improve the e-transfer efficiency along the branches as compared to flexible dendrimers with interrupted conjugation.⁹¹

In this chapter I will discuss the synthesis of three-armed viologen stars consisting of a regularly alternating arrangement of dibenzyl viologen/diphenyl viologen with up to 5.8 nm branch length and exhibiting a combined phenyl and benzyl viologen electroactivity.

Recently, it has been shown that benzyl bromide can be electropolymerized on HOPG (highly ordered pyrolytic graphite) probably via radical intermediates.⁹² In the present work this principle was applied for the electropolymerization of viologen stars. It includes monomeric viologens, as well as the star structures consisting of three, six and twelve viologen subunits

and all of them showing efficient electropolymerization on ITO, gold and GC. Obviously, electropolymerization of molecules characterized by a branching structure results in cross-linked structures with increased mechanical stability as compared to linear polymer analogues. Furthermore, the overlapping benzylic and phenylic viologen reduction waves are expected to yield a broad existence region for the localized radical species which is a crucial criterion for electronic conductivity in n-dopable materials.

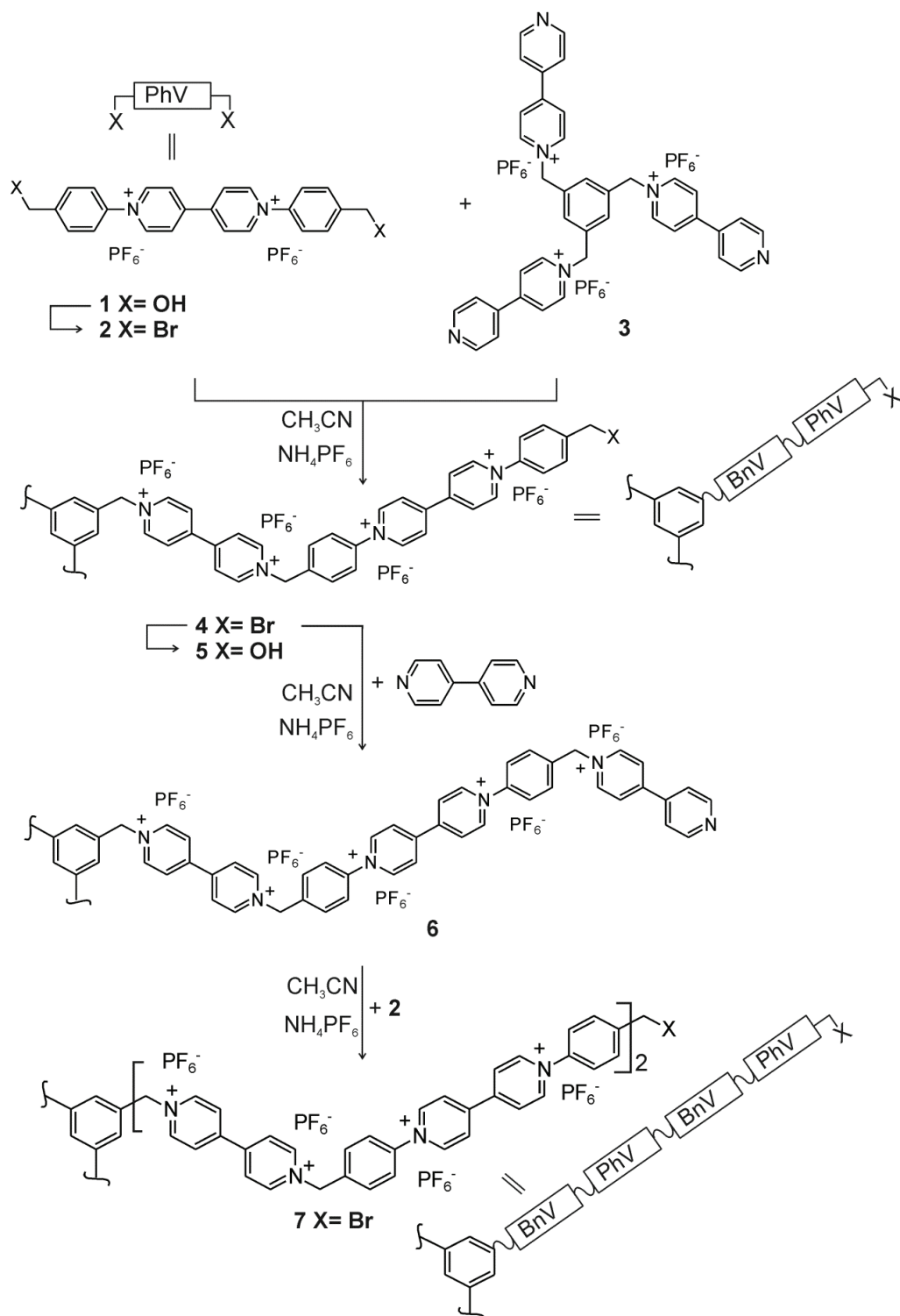
2.2 Results and discussion

2.2.1 Synthesis

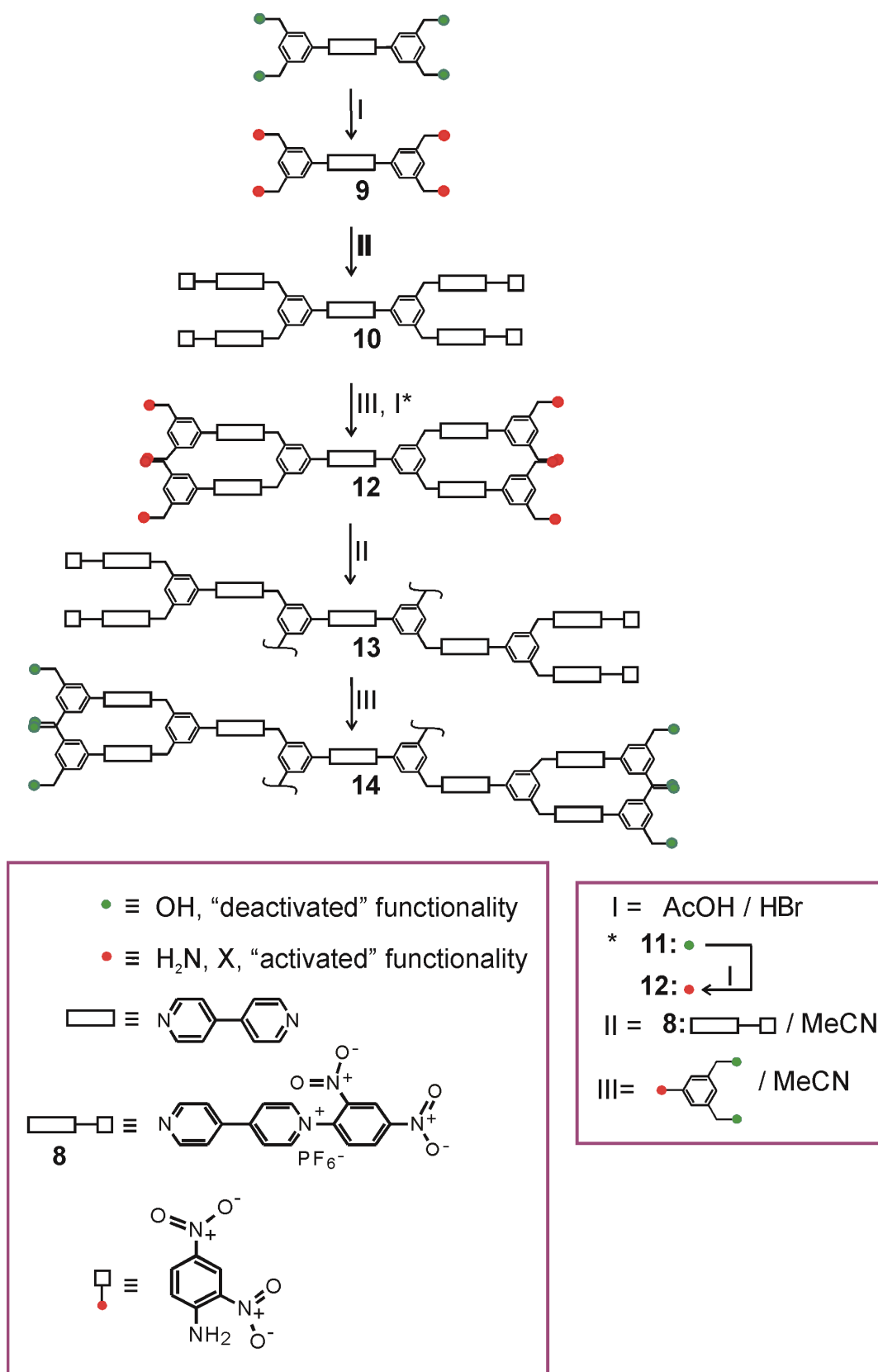
A new class of semi-flexible dendritic molecules containing viologens have been synthesized and investigated. The synthetic methods employed include a combination of Zincke reactions and alkylation of monosubstituted viologens for building up the two different classes of dendritic molecules (Scheme 2.1 and 2.2).

The synthesis of triple-branched viologen stars of generation 0 and 1 consisting of a benzene core are shown in Scheme 2.1. The diquatery salt **1** was prepared by the reaction of 1,1'-bis-(2,4-dinitrophenyl)-4,4'-bipyridinium dichloride⁹³ with an excess (2.3 eq) of 4-aminobenzylalcohol via the Zincke reaction. Methanol/water 80 % (V:V) was the preferred solvent to ensure good solubility of both starting materials. The exchange of the hydroxyl groups in **1** against bromide was achieved in HBr-acetic acid affording **2** in good yields. In addition, **2** reacts with **3** (prepared according to literature⁹⁴) in acetonitrile to yield **4**. The bromo-methyl derivative **4** was reacted with 4,4'-bipyridine in MeCN to obtain **6** (as PF₆⁻ salt), which was purified by several ion exchange

steps. Alkylation of **6** with an excess of **2** yielded **7** as PF_6^- salt after ion exchange. Hydrolysis of C-Br in **4** was performed under mild conditions (in MeCN/water) to yield **5**.



Scheme 2.1 The synthesis of viologen stars.



Scheme 2.2 Synthetic route to ellipsoidal dendritic viologens.

In most cases several precipitations were conducted to afford pure products, either upon addition of ether or under anion exchange conditions. The latter is based on the fact that the halide salts are water/methanol soluble, whereas the PF_6^- salts are insoluble in water, but soluble in MeCN.

The synthetic route for the preparation of the ellipsoidal dendritic molecule **14** containing a PhV as core and mixed PhVBn branches is depicted in Scheme 2.2. The preparation of **8** and **9** has been described.⁹⁵⁻⁹⁸ The reaction of **9** with an excess of **8** in MeCN for 72 h gave **10** in moderate yield (66.6 %). Compounds **11** and **14** were synthesized by analogous Zincke reaction with 3,5-bis(hydroxymethyl)aniline in MeCN of **10** and **13**, respectively. Nucleophilic substitution of OH by Br in **12** was achieved in HBr/AcOH solution after 4 days (yield 72 %).

2.2.2 Cyclic voltammetry of **1**, **2**, **3**, **4**, **5** and **7**

The redox properties of **1**, **2**, **4**, **5** and **7** were investigated by means of cyclic voltammetry and spectroelectrochemistry. The CVs of **1** and **2** in DMF/0.1M $\text{n-Bu}_4\text{NPF}_6$ at a glassy carbon (GC) electrode, are shown in Fig. 2.1. Both compounds undergo two one-electron reversible redox processes as typical for phenyl viologens,⁹⁹ the bromine substituent shifts the first reduction wave ($E^0_{\text{PhV}^{++}}$) to more positive values (**1**(OH): -0.174, **2**(Br): -0.102 V). For compound **2**, an additional irreversible reduction peak is observed mainly on the first scan at ca. -1.0 V. It is attributed to the reductive cleavage of the benzylic carbon-bromine bond. The catalytic cathodic plateau current on the second reduction peak indicates electrocatalysis, i.e. intra- or inter-molecular from the two fold reduced phenyl viologen into the antibonding C-Br σ^* orbital.

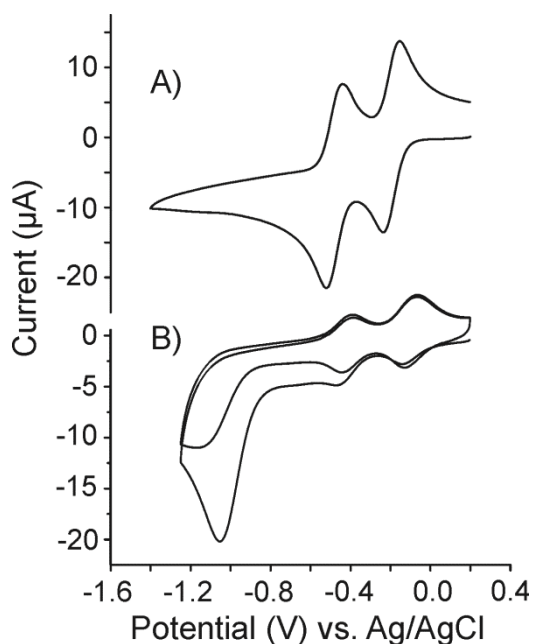


Figure 2.1 CV of the monomeric phenyl viologens **1** (A) and **2** (B)) at ca. millimolar concentration in MeCN/ Bu_4NPF_6 , $v = 100 \text{ mVs}^{-1}$ at GC (0.07 cm^2).

The single scan voltammograms of **4** together with those of benzyl viologen (BnV) and phenyl viologen (PhV) are illustrated in Fig. 2.2. Obviously the reduction/oxidation of the viologen star **4** involves three simultaneous electron transfers at the same potential. BnV and PhV represent the subunits in the viologen star **4**. The four waves of **4** can be definitively attributed to the interdigitated set of waves of the subunit, following the order $a \rightarrow b \rightarrow c \rightarrow d$ with:

- a) $\text{C}-(\text{BnV}^{++}\text{-PhV}^{++})_3 / \text{C}-(\text{BnV}^{++}\text{-PhV}^{+•})_3 = \text{I/II} \quad E_{\text{PhV}^{+•}}^{0'}$
- b) $\text{C}-(\text{BnV}^{++}\text{-PhV}^{+•})_3 / \text{C}-(\text{BnV}^{+•}\text{-PhV}^{+•})_3 = \text{II/III} \quad E_{\text{BnV}^{+•}}^{0'}$
- c) $\text{C}-(\text{BnV}^{+•}\text{-PhV}^{+•})_3 / \text{C}-(\text{BnV}^{+•}\text{-PhV}^0)_3 = \text{III/IV} \quad E_{\text{PhV}^0}^{0'}$
- d) $\text{C}-(\text{BnV}^{+•}\text{-PhV}^0)_3 / \text{C}-(\text{BnV}^0\text{-PhV}^0)_3 = \text{IV/V} \quad E_{\text{BnV}^0}^{0'}$

In case of compound **7** the same pattern is observed but involving a 6-fold one-electron transfer on each wave (see electropolymerization).

Table 2.1 Compilation of the electrochemical data of the monomers.

Compound	(E°') _{PV⁺⁺}	(E°') _{BV⁺⁺}	(E°') _{PV^{•+}}	(E°') _{BV^{•+}}	(E°') _{CH₂(-)}	Polymerizable
1	-0.174	-	-0.466	-	-	0
2	-0.102	-	-0.434	-	-1.04	0
BnV	-	-0.311	-	-0.701	-	0
4	-0.116	-0.273	-0.421	-0.696	-	x
5	-0.137	-0.267	-0.403	-0.655	-	(x)
7	-0.123	-0.282	-0.419	-0.695	-	X

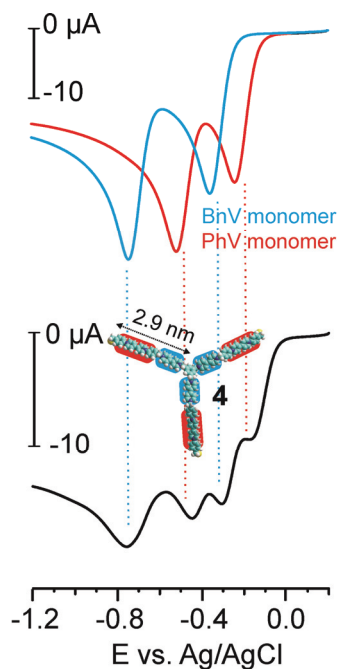


Figure 2.2 Single scan voltammograms of dibenzyl viologen (**BnV**, $c = 1.6$ mM, blue), diphenyl viologen (**PhV**, $c = 1.7$ mM, red) and **4** (0.5 mM, black; blue and red indicating BnV and PhV subunits) in DMF/0.1M $n\text{-Bu}_4\text{NPF}_6$, $v = 100$ mVs^{-1} at GC. All viologen stars show pronounced adsorption behavior.

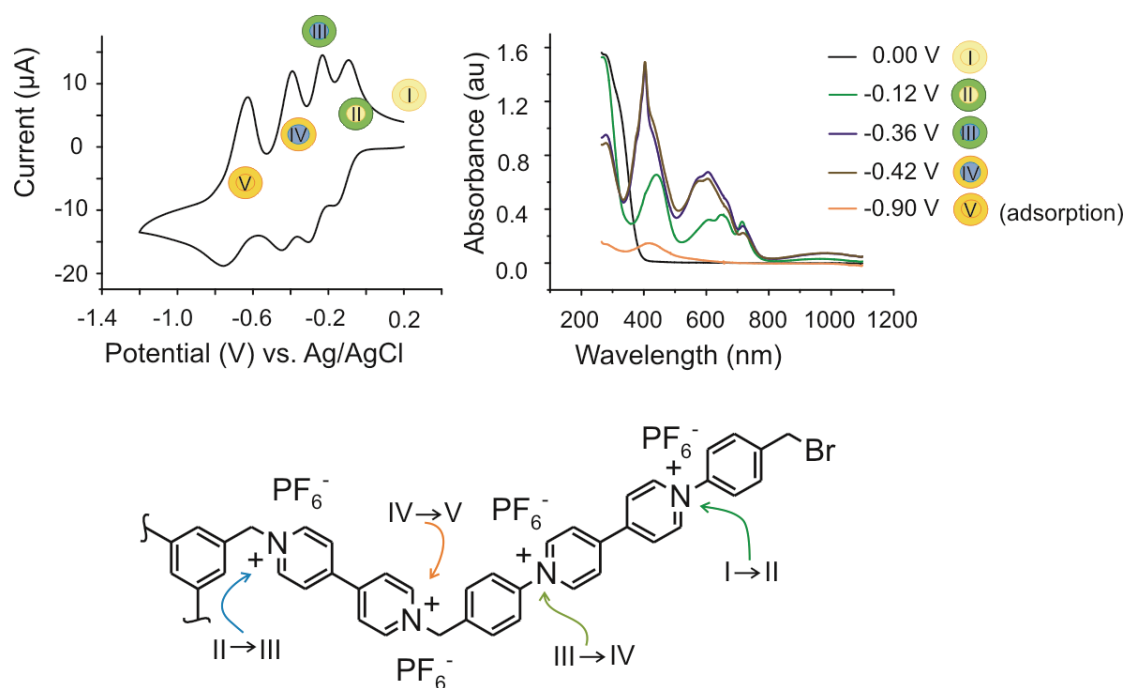
The 0th generation viologen stars, **4** and **5**, have similar size but carrying different peripheral groups, i.e. Br and OH. Their influence on $E_{\text{PhV}^{+•}}^{0'}$ is less pronounced but observable ($E_{\text{PhV}^{+•}}^{0'}$ **4** (Br): -0.116V and **5** (OH): -0.137) (table 2.1). The first benzyl viologen reduction in **4** and **5** (all $E_{\text{BnV}^{+•}}^{0'} \approx -0.27$ V) is shifted positive as compared to $E_{\text{BnV}^{+•}}^{0'}$ of the monomer BnV ($E_{\text{BnV}^{+•}}^{0'} = -0.31$ V), probably for electrostatic reasons, involving 12+ and 2+, in the stars and the monomer, respectively. The 1st generation viologen star **7** carries 24 positive charges, but no further positive shift of $E_{\text{BnV}^{+•}}^{0'}$ is observed, in contrast to viologen dendrimers.⁵⁹ This reflects one fundamental difference between viologen stars and dendrimers. The local charge density (charge per volume) is increasing in dendrimers for higher generations, but not so in molecular stars.

2.2.3 Spectroelectrochemical investigation of **4** and **5**

Scheme 2.3 show the four reversible transition states of **4** as discussed previously in Section 2.2.2. First, the phenyl viologen subunit is reduced to a radical cation, followed by 1 e⁻ reduction of benzyl viologen subunit to benzyl viologen radical cation. The evidence supporting this affirmation is provided in the redox titration of **4** and **5**.

The UV-Vis spectra of the electrochemically generated radical cations in **4** and **5** were compared with the spectrum of PhV²⁺ and BnV²⁺ (Fig. 2.4). The first transition which is the reduction of PhV subunit to PhV²⁺ was observed for both molecules (**4** and **5**) when the applied potential was sequentially increased from 0.0 V to -0.21 V (Fig. 2.4 and Fig. 2.5). The color of the solution changes from pale yellow to green. The absorbance maxima at 441 nm (431 nm for **5**) 605 nm, 648 nm and 715 nm, identified also in the spec-

trum of $\text{PhV}^{+\bullet}$ (Fig. 2.3), are known to be characteristic for viologen radical cations.^{100,101}



Scheme 2.3 Structure of **4** representing the four possible transitions states generated electrochemically (top left side) and spectroelectrochemically (bottom). The 4th transition states are illustrated as circles and arrows in the color of the redox species in solution: I→II (green), II→III (blue), III→IV (olive), IV→V (yellow). The periphery and the core are represented as two circles: one of the circles (the core) lies inside the other (the periphery).

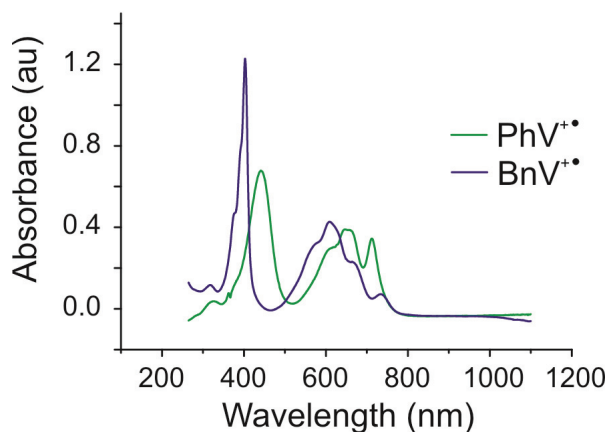


Figure 2.3 UV-Vis spectra of $\text{PhV}^{+\bullet}$ and $\text{BnV}^{+\bullet}$ in DMF and 0.1M $n\text{-Bu}_4\text{NPF}_6$.

Upon gradual reduction to more negative potentials, the bands at 431 nm and 648 nm became less intense, and a new sharp absorption band emerges at 405 nm. The last one is observed also in the spectrum of $\text{BnV}^{+•}$.

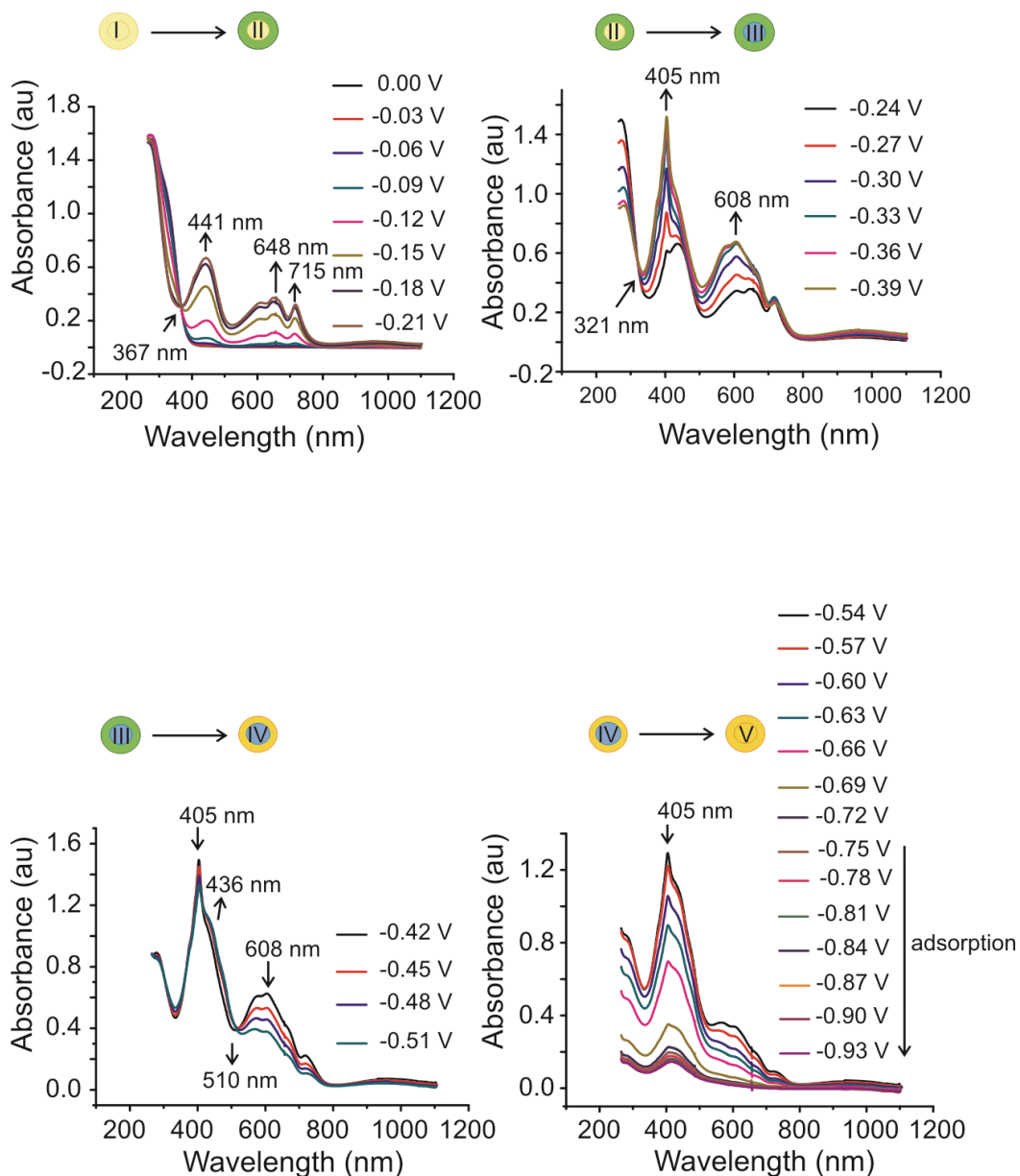


Figure 2.4 Potential dependent UV-Vis spectra of **4** in DMF and 0.1M $n\text{-Bu}_4\text{NPF}_6$. The 4th transition states are illustrated as circles in the color of the redox species in solution: I→II (green), II→III (blue), III→IV (olive), IV→V (yellow). The periphery and the core are represented as two circles: one of the circles (the core) lies inside the other (the periphery).

The color of the solution now is a mixture of green (from persistent $\text{BnV}^{+•}$ subunits) and blue (characteristic for the formed $\text{BnV}^{+•}$) (recognized as a second transition in the absorption spectrum).

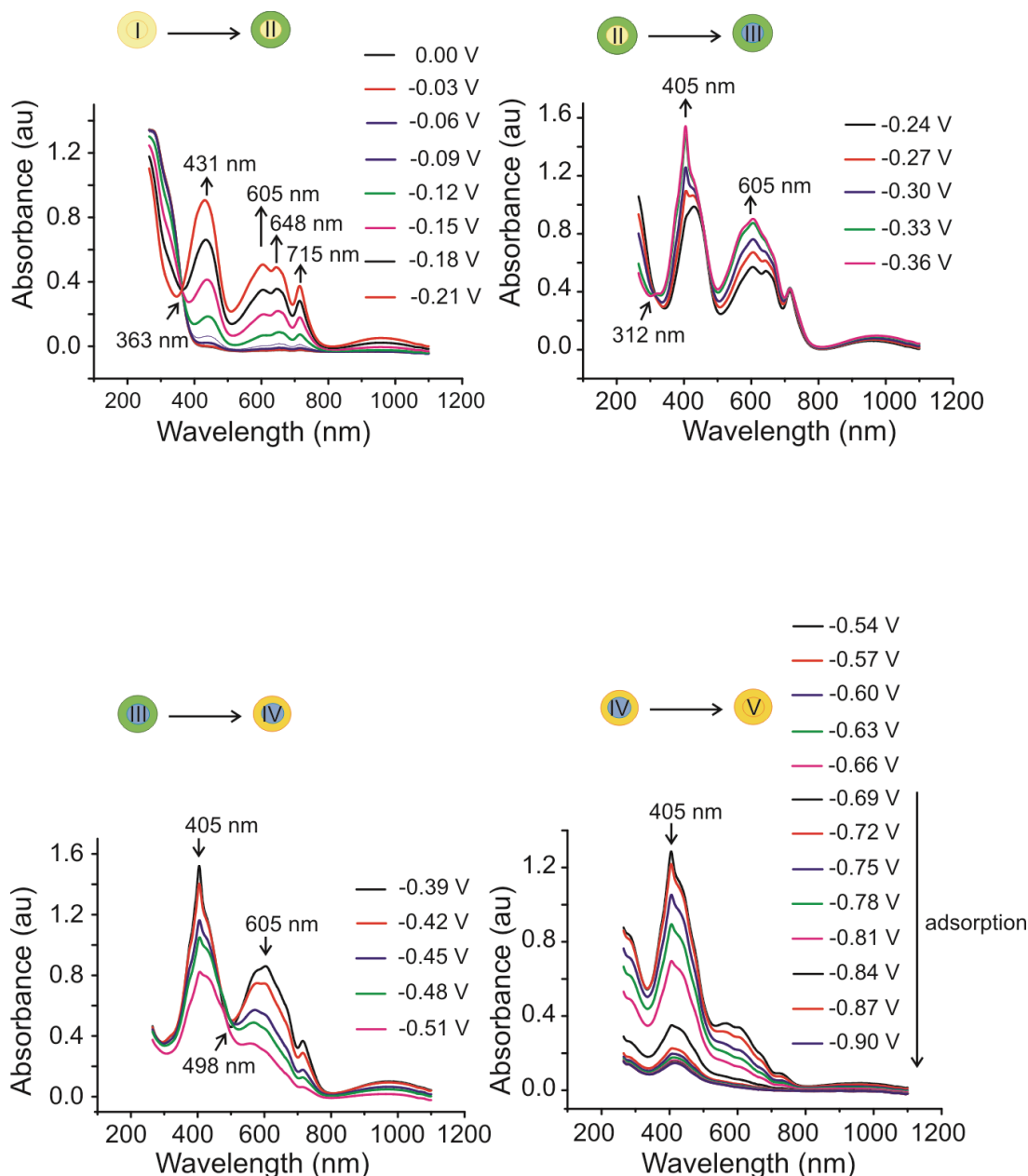


Figure 2.5 Potential dependent UV-Vis spectra of **5** in DMF and 0.1M $n\text{-Bu}_4\text{NPF}_6$. The 4th transition states are illustrated as circles in the color of the redox species in solution: I \rightarrow II (green), II \rightarrow III (blue), III \rightarrow IV (olive), IV \rightarrow V (yellow). The periphery and the core are represented as two circles: one of the circles (the core) lies inside the other (the periphery).

The third transition was observed in UV-Vis spectra of **4** and **5** when the potential was further increased in a negative potential range from -0.42 V to -0.51 V and coincides with 1 e⁻ reduction of PhV⁺⁺ subunits. The color of the solution changes to olive. A decrease in intensity of absorption bands were observed with the exception of a broad shoulder which appears at 436 nm in the spectrum of **4**. An isosbestic point was observed for **4** at 510 nm (498 nm for **5**). The broad absorption at ~1000 nm observed in the first three transitions is also specific for the viologen radical cation.^{102,103} The fourth transition is due to 1 e⁻ reduction of BnV⁺⁺ subunits (the color of the solution changes to brown). The absorbance of **4** and **5** during the fourth transition suddenly decreases at potentials more negative than about -0.66 V due to the electropolymerization or electrosorption of the neutral species at high-area carbon felt working electrode.

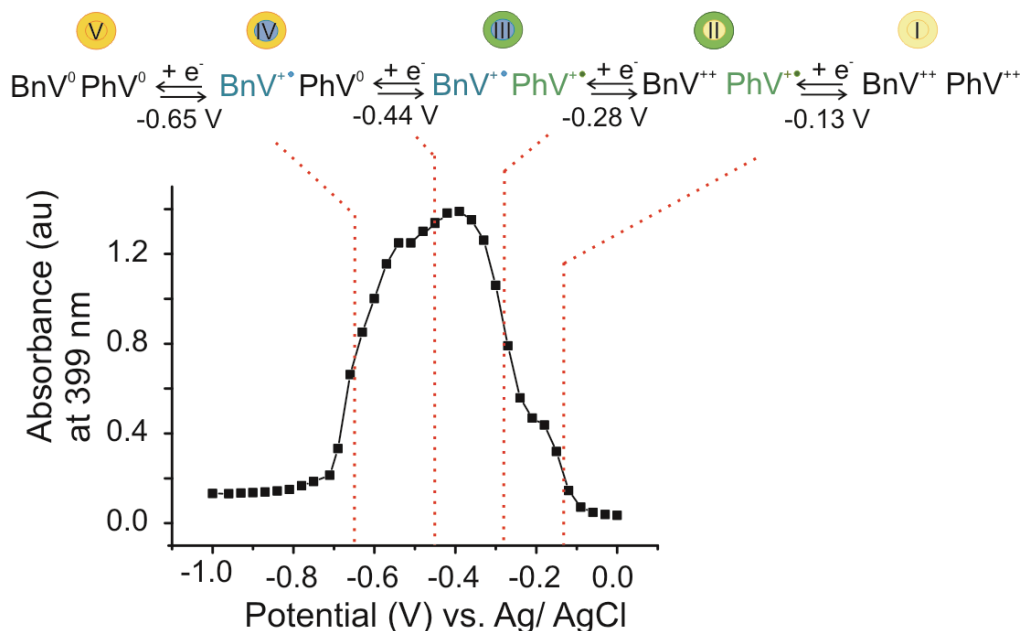


Figure 2.6 Spectroelectrochemical titration of **4** (at $\lambda = 399$ nm) in DMF and 0.1M n-Bu₄NPF₆. The 4th transition states are illustrated as circles in the color of the redox species in solution: I \rightarrow II (green), II \rightarrow III (blue), III \rightarrow IV (olive), IV \rightarrow V (yellow). The periphery and the core are represented as two circles: one of the circles (the core) lies inside the other (the periphery).

The dependence of the absorbance at a fixed wavelength on the electrode potential is depicted in Fig. 2.6 and Fig. 2.7, and spectra show four steps characteristics. The appearance of four transition steps confirms sequential reduction of the two viologen subunits (PhV and BnV).

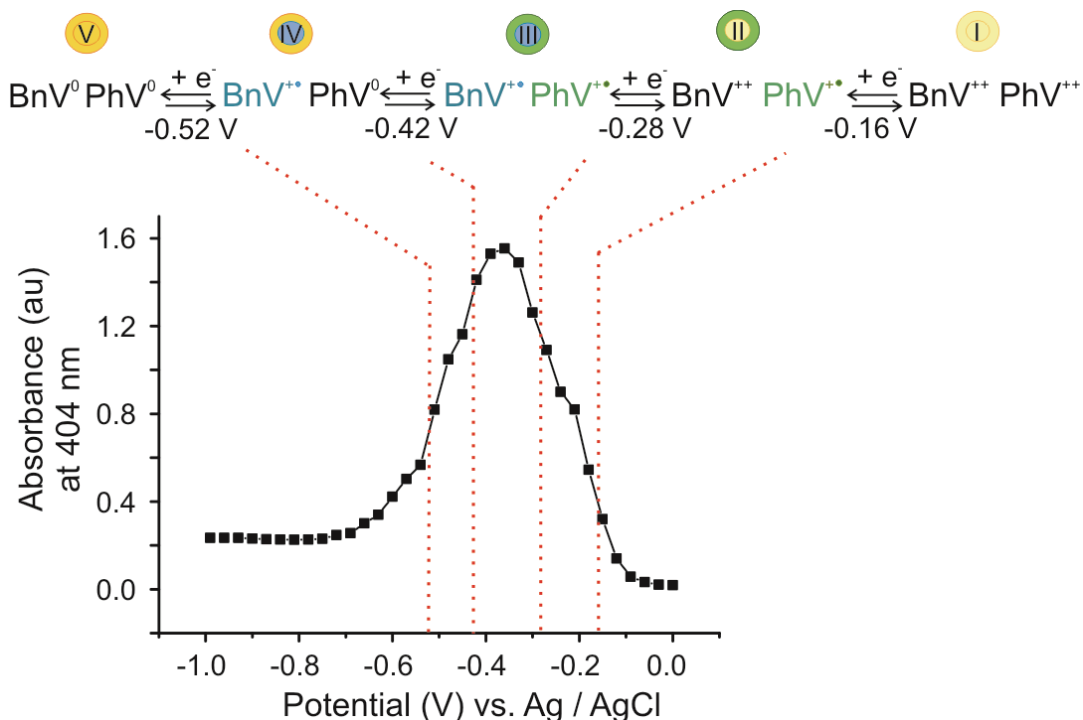


Figure 2.7 Spectroelectrochemical titration of **5** (at $\lambda = 404$ nm) in DMF and 0.1M $n\text{-Bu}_4\text{NPF}_6$. The 4th transition states are illustrated as circles in the color of the redox species in solution: I \rightarrow II (green), II \rightarrow III (blue), III \rightarrow IV (olive), IV \rightarrow V (yellow). The periphery and the core are represented as two circles: one of the circles (the core) lies inside the other (the periphery).

The spectroscopically determined potentials are close to those found by the voltammetry. As electropolymerization takes place at negative potentials, the 4th reduction potential is not reliable.

2.2.4 Redox orbital sequence from PM6 semiempirical calculations

The electronic structure of a single branch of compound **5** in its five oxidation states (charge on system 4 to 0 corresponding to redox states I to V (eq. a-d)) and Fig. 2.10-B) was calculated after geometry optimization using

the semiempirical PM6 method.¹⁰⁴ Notably, the HOMO localization switches between phenyl (PhV) and benzyl viologen (BnV) upon addition of single electron (decreasing charge on the system) following the order: 3+: PhV; 2+: BnV; 1+: PhV; 0: BnV (dotted arrows in Fig. 2.8). The same phenomenon is observed on the LUMO localization but shifted one oxidation state higher, e.g. LUMO 4+ = HOMO 3+. These results point unambiguously to the jumping redox state observed experimentally (Fig. 2.2, Scheme 2.3 and Fig.2.10-B). The calculation of the spin density reveals the following sequence of multiplicities 4+: singlet \rightarrow 3+: doublet on PhV \rightarrow 2+: triplet spread over PhV and BnV \rightarrow 1+: doublet on PhV, 0: singlet, as expected.

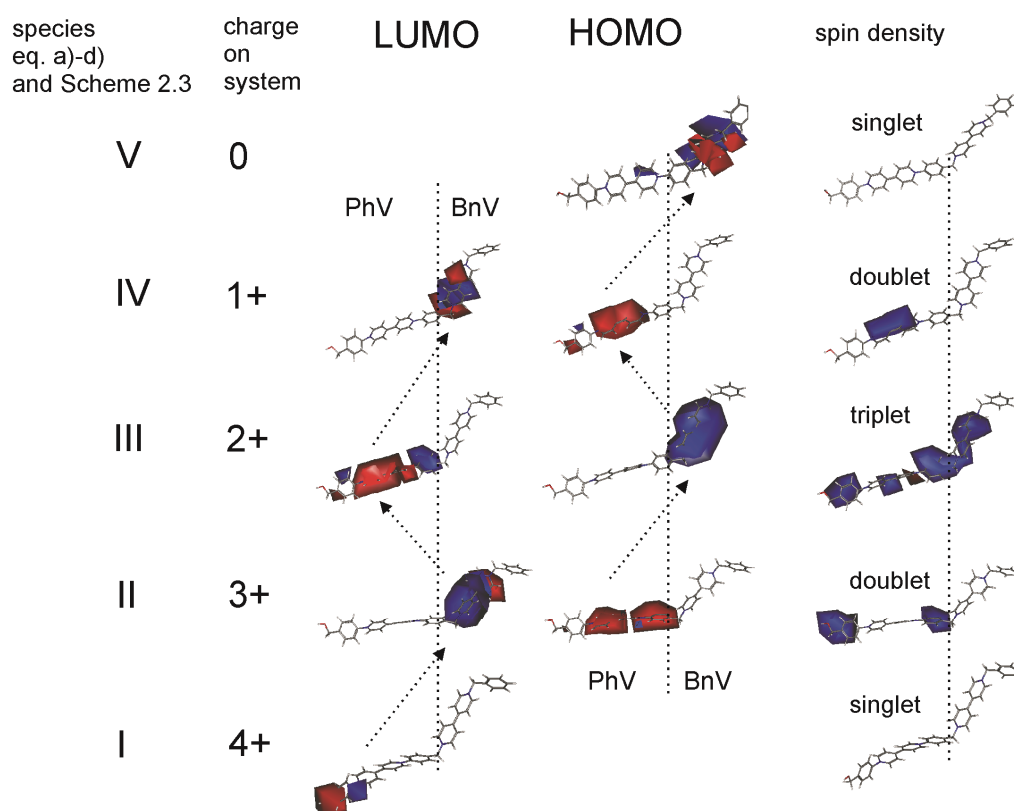


Figure 2.8 HOMO (= redox-orbital), LUMO and spin density localization on a single branch of **5** (including from left to right: phenylviologen (PhV), benzyl viologen (BnV) and central benzene subunits) as a function of electron occupancy calculated with PM6; charge on system refers to the calculated single branch, roman numbers refer to the corresponding species in eq. a)-d) and in Scheme 2.3; broken arrows show the

sequential PhV-BnV-PhV-BnV LUMO and BnV-PhV-BnV-PhV HOMO (redox orbital) localization.

2.2.5 Electrochemical polymerization of viologen stars 4 and 7

The electrochemical polymerization of trimeric viologens **4**, **5** and **7** was carried out in DMF containing 0.1M n-Bu₄NPF₆ at GC, gold and ITO electrodes by repetitive potential cycling between 0.2 and -1.2 V. Fig. 2.9 shows typical CVs for the electropolymerization of **4** and **7**. The peak currents grow steadily under these conditions on different electrode materials (GC, Au and ITO) (Fig. 2.9- A, B). The viologen stars **4** and **7** of generation 0 and 1, both carrying 3 peripheral-Br, show efficient electropolymerization.

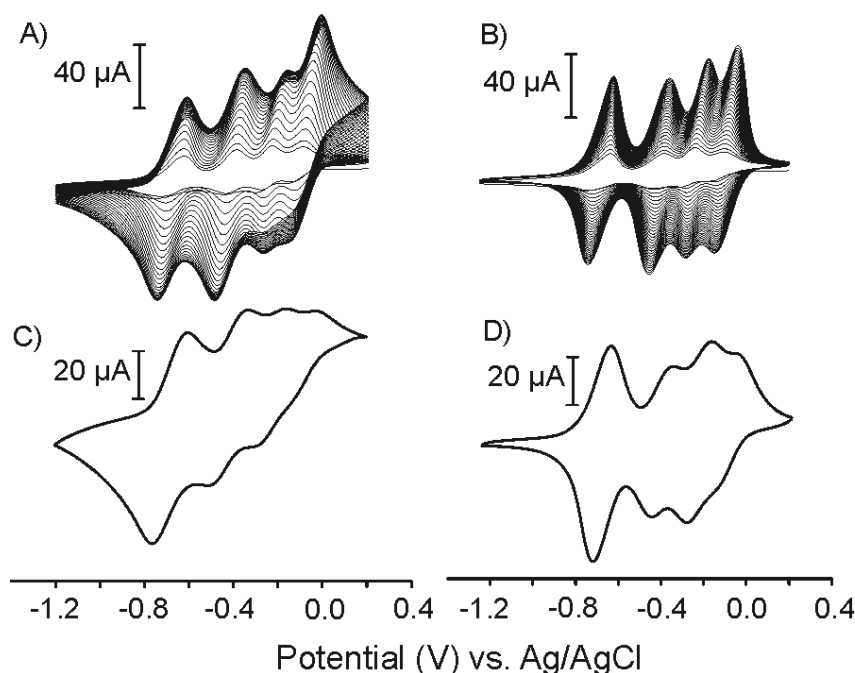


Figure 2.9 Electropolymerization of **4** ($c = 4.9 \cdot 10^{-4}$ M) (A)) and **7** ($1.8 \cdot 10^{-4}$ M) (B)) on GC in DMF/Bu₄NPF₆ during the first 60 scans, $v = 100$ mVs⁻¹; response of **Poly-4** (C) ($\Gamma_4 = 3 \cdot 10^{-9}$ or $\Gamma_{\text{subunits}} = 1.8 \cdot 10^{-8}$ mol/cm²) and **Poly-7** (D) ($\Gamma_7 = 2.8 \cdot 10^{-10}$ or $\Gamma_{\text{subunits}} = 3.3 \cdot 10^{-9}$ mol/cm²) on GC in pure DMF/Bu₄NPF₆ at $v = 100$ mVs⁻¹.

In contrast, the monomeric viologens with 2 peripheral -OH or -Br, i.e. **1** and **2**, and the viologen star **5** carrying peripheral OH did not show any ele-

ctropolymerization (Fig. 2.10). First, the increase of the peak current in Fig. 2.10-B) until the 12th cycle is due to the adsorption/precipitation of the 3 e⁻ reduction product onto the electrode surface (also shown by spectroelectrochemistry) and does not prove electropolymerization.

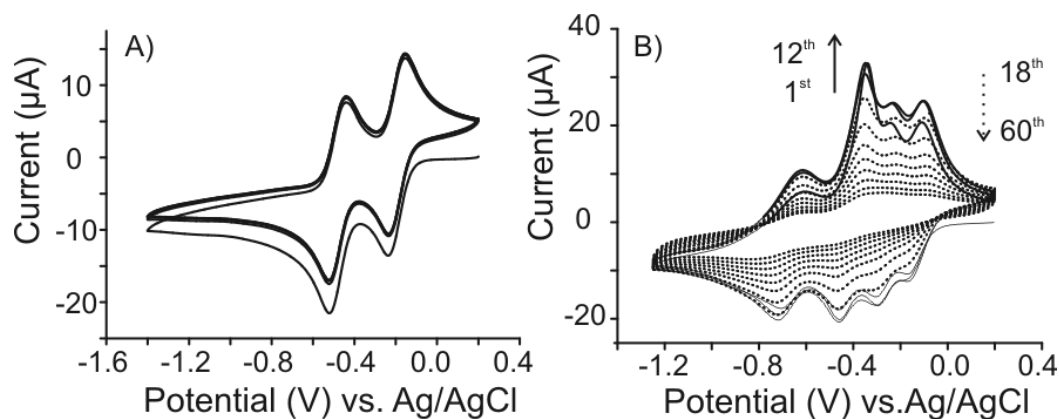


Figure 2.10 CVs on GC of A) **1** ($1.55 \cdot 10^{-3}$ M, 5 scans) and B) **5** ($3.42 \cdot 10^{-4}$ M, 60 scans).

Upon the electropolymerization of **4** and **7**, the electrodes were grafted with different amounts of polyviologen film (Table 2.2).

Thus, two prerequisites have to be met for efficient polymerization, (i) the presence of a benzylic bromide and (ii) triple branching such as present in viologen stars. Assuming benzylic radical coupling, cross-linking can only be achieved with the viologen stars. The linear smaller monomer **2** can at best lead to linear polymeric structures. In order to find the threshold electrode potential for the electropolymerization, a series of 11 voltammograms equilibrated between -0.3 and -1.3 V with a 100 mV off-set each and with a 30 second polarisation at the starting potential were recorded. The electropolymerization takes place during the equilibration time. The current observed on the scan following the equilibration is a measure for the degree of polymerization (Fig. 2.11).

Table 2.2 Surface concentrations (Γ) of **Poly-4** and **Poly-7** polymerized on GC, gold and ITO.

Viologen-Star	Modified electrode	Trimer conc. (M)	(Γ , Mol viologen subunits/cm ²)*	(Γ , Mol star-like viologen/cm ²)
4	GC	4.9×10^{-4}	1.8×10^{-8}	3×10^{-9}
4	Gold	4.9×10^{-4}	1.75×10^{-8}	2.9×10^{-9}
4	ITO	4.9×10^{-4}	1.52×10^{-8}	2.5×10^{-9}
7	GC	1.76×10^{-4}	3.3×10^{-9}	2.75×10^{-10}

* Γ from charge integration over the four reduction peaks in CV in pure electrolyte/solvent after 60 scans of electropolymerization.

$$\Gamma = Q/nFA \quad (2.1)$$

Where A is the area of electrode, n is the number of electrons involved in the redox process and F is the Faraday constant.

The absolute cathodic current at -0.43 V (red vertical line in Fig. 2.12) was plotted vs. the equilibration potential (red sigmoidal plot in Fig. 2.12). The mid potential of the sigmoidal current function is located at -0.7 V corresponds definitely to the 4th wave in the CV, earlier identified as the C-(BnV⁺-PhV⁰)₃/C-(BnV⁰-PhV⁰)₃ transition. Notably, from the CV in Fig. 2.1, it was found that the reduced phenylviologen subunit is able to catalyze the benzylbromide reduction, however, the reduced benzylviologen with its more negative E⁰ is even a better electrocatalyst. No further increase is observed upon extension of the equilibration potential into the region of direct benzyl bromide reduction.

The direct or electrocatalytic reduction of benzyl halides has been extensively investigated, and it involves a one electron-transfer to form the corresponding benzyl radical either involving a dissociative or a stepwise mechanism. In the presence of protons at large negative overpotential, the radical may be further reduced to the benzyl anion. However, this path is unlikely under the given experimental conditions.

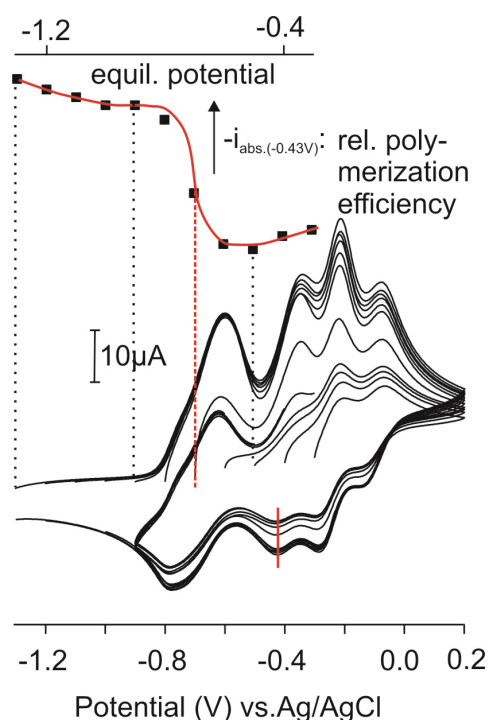
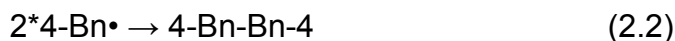


Figure 2.11 Eleven overlaid CVs of **4** ($c = 4.9 \cdot 10^{-4}$ M) on GC registered after equilibration at -0.3, -0.4, -0.5 -1.2, -1.3 V for 30 s, $v = 100 \text{ mVs}^{-1}$ (lower panel) and plot of the neg. absolute cathodic current ($-i_{\text{abs}(-0.43\text{V})}$) measured at -0.43 V (red vert. line) vs. the equilibration potential (upper panel); interpretation of $-i_{\text{abs}(-0.43\text{V})}$ as rel. polymerization efficiency (crucial involvement of 4th reduction wave).

The benzyl radical may attack carbon electrodes and form films,⁹² but for a similar reaction on gold the more reactive phenyl radical is necessary.¹⁰⁵ The observed coulometry is definitely related to much more than a monolayer. The radical may undergo further typical radical reactions, such as radical-radical coupling (eq. 2.2).¹⁰⁶



The electrochemical properties of the GC-modified electrodes were studied in monomer-free solutions. CVs of **Poly-4** and **Poly-7** are shown in Fig. 2.9, as C and D. The interdigitated structure of four waves persists nicely and yields a broad range of electroactivity which could indicate electronic conductivity in the solid state if reasonably doped with electrons. The preliminary tests on the persistence in the electron-doped state reveal that the stability depends much on the degree of doping. If the polymer **4** is cycled between the $\text{C-(BnV}^{++}\text{-PhV}^{++})_3$ and the $\text{C-(BnV}^{++}\text{-PhV}^{++})_3$ state, reasonable stability (33 % loss of electroactivity after 20 cycles) is observed. However, if scanned between $\text{C-(BnV}^{++}\text{-PhV}^{++})_3$ and -1.2, i.e. negative of $\text{C-(BnV}^0\text{-PhV}^0)_3$ a fast decay (90 % loss of electroactivity in 20 cycles) is observed. The difference in polymer stability was related to protonation of $\text{C-(BnV}^0\text{-PhV}^0)_3$ by residual water in the solvent.

The monomer **4** dissolved in DMF was also polymerized using metallic Zn powder or granulated Zn. The collected polymeric material showed loss of the benzylic bromide (disappearance of the prominent C-Br stretching mode at 552 cm^{-1} (experimental part).

2.2.6 UV-Vis characterization of Poly-4 thin film on ITO electrode

The spectroelectrochemical studies were carried out to confirm whether the 4 transition states observed for compound **4** in solution are also electrochemically induced in the polymer film. Depending on the applied potential the film shows four different colors as demonstrated by the absorption spectra in Fig. 2.12. The film colors are homogeneously distributed

across the electrode surface, and the color changes are easily detected by naked eye. In the oxidized form at 0 V, the absorption maximum of the film is located in a UV range at ca. 300 nm. In the polymer backbone, the viologen subunits are covalently bonded, and thus the charge transport through the film can be considered to occur via an electron-hopping process^{107,108} between the viologen subunits. The transitions $\text{PhV}^{++} \rightarrow \text{PhV}^{+}$ and $\text{BnV}^{++} \rightarrow \text{BnV}^{+}$ have absorptions similar to that observed for the molecule **4** in solution, with an absorption maximum around 414 nm (green PhVs^{+} , -0.39 V) and 407 nm (blue BnVs^{+} , -0.51 V).

Transitions specific for viologen radical cations were observed also at 631 nm, 622 nm and ~ 1000 nm, respectively. After application of a sufficiently negative potential (-0.69 V) to reduce all of the PhVs^{+} to PhVs^0 , the absorption band at ~ 622 nm disappeared confirming the existence of a third transition. When the potential was more than -0.69 V, a broad absorption between 300 nm and 500 nm was observed. The result indicates that the BnVs^{+} began to form neutral species (fourth transition).¹⁰³

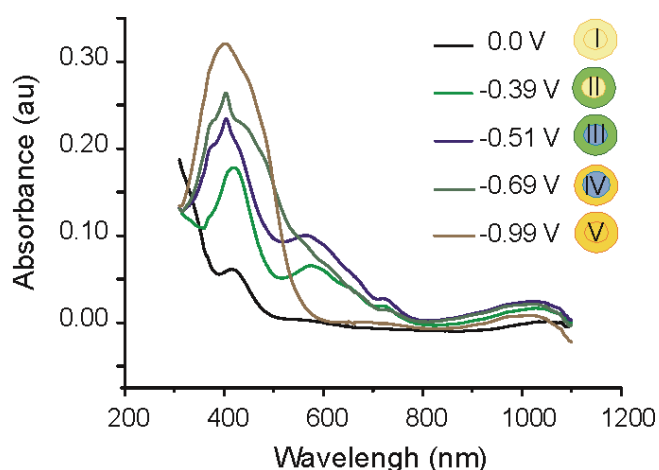


Figure 2.12 UV-Vis absorption spectra of an ITO electrode coated with **4** (Γ ca. $0.37 \times 10^{-10} \text{ mol} \cdot \text{cm}^{-2}$) at 0 V, -0.39 V, -0.51 V, -0.69 V and -0.99 V in 0.1M KCl.

2.2.7 STM investigation of Poly-4 on ITO

Poly-4 on ITO was imaged with STM under ambient conditions. The surface structure of the supporting naked ITO has been described in many studies as granular with an average grain size of 50-100 nm, exhibiting no edges and a smooth surface.^{109,110} The STM measurement on bare ITO (Fig. 2.13, A, B, C) confirms the granular structure, but additional structuring below 10 nm is observed (Fig. 2.13 C). The **Poly-4**-modified electrodes reveal that the ITO grains and the inter-grain valleys are completely covered with **Poly-4**. The average film thickness is approx. 60 nm as calculated from the density ($d_4 = 0.95 \text{ g/cm}^3$) and its electrochemically accessible surface concentration ($\Gamma_4 = 1.53 \cdot 10^{-9} \text{ mol/cm}^2$). For visual comparison the viologen star **4** has been modeled with MM+ in Hyperchem (Fig. 2.14).¹¹¹ A closer view (Fig. 2.13 E-F) reveals structures which could be related to benzyl-benzyl coupled monomers (tri-fold branching centers).

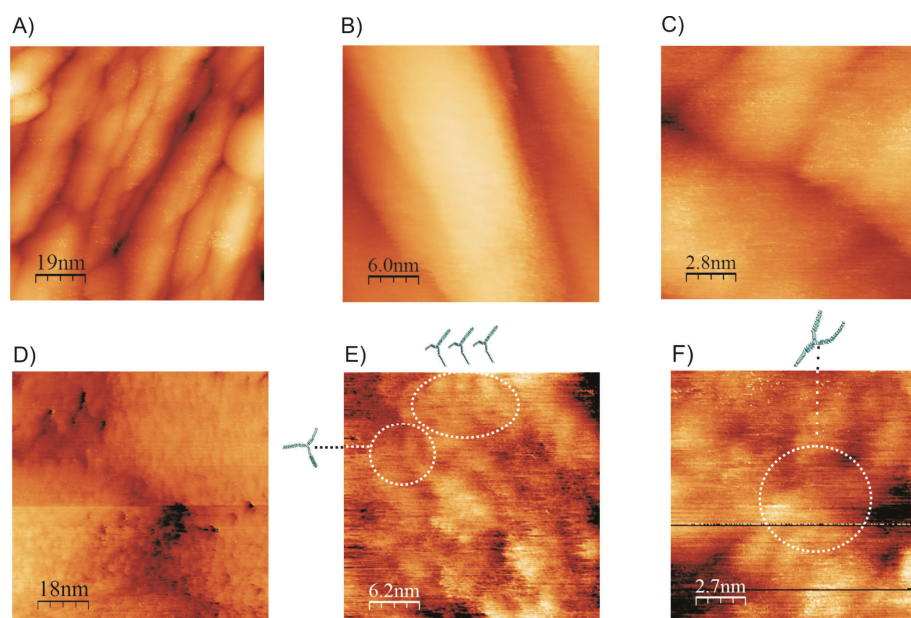


Figure 2.13 STM images ($V_b = 0.050 \text{ V}$, $I_t = 1.001 \text{ nA}$) of bare ITO (A-C) and **Poly-4** ($\Gamma_4 = 1.53 \cdot 10^{-9} \text{ mol/cm}^2$) on ITO (D-F): A) $93 \times 93 \text{ nm}$, Z range 12.5 nm ; B) $30 \times 30 \text{ nm}$, Z range 6.25 nm ; C) $14 \times 14 \text{ nm}$, Z range 3.13 nm ; D) $88.5 \times 88.5 \text{ nm}$, Z range

12.5 nm; E) 31x 31nm, Z range 6.25 nm and F) 13.6 x 13.6 nm, Z range 0.781 nm; MM⁺ optimized **4** monomer structures are plotted at the same scale for comparison.

Notably, at 60 nm average film thickness such structures are detected on the polymer surface exposed to the air which indicates reasonable electrical conductivity of the polymer underneath. The gap voltage was not critical in resolving molecular sub-subunits (0.1 to 1 V). This is in contrast to published results on molecular STM-imaging of viologens which is restricted so far to adsorbed molecular monolayers on Cu,^{112,113} ITO,¹¹⁴ and Au⁸⁰.

The compounds **4•12PF₆**, **4¹²⁺**, **7•24PF₆**, and **7²⁴⁺**, i.e. with counter-balanced charge and with fully developed cationic charge, were geometry optimized with molecular dynamics using the MM+ force field (implemented in Hyperchem)¹¹¹ using one fully localized positive charge on each pyridinium and 1/6 negative charge on each F⁻ and PF₆⁻ in the gas phase.

The MD temperature program was 273K-600K (5ps) -273K (1ps). The polycations stretch because of the repulsive charge interaction. Only a slight contraction is observed in the presence of the counter ions. **4•12PF₆** shows a volume of 6490 Å³ (calculated with QSAR in Hyperchem).¹¹¹ From M = 3574.3 g/mol and V= 6490 Å³ follows a density d = 0.92 g/ml.

This value is lower than typically for crystalline viologen (d= 1.25 g/ml for dimethylviologen dichloride), but d= 1 has been used in the literature for another viologen polymer.¹¹⁵

Polymer film thickness:

Using d= 0.92 g/ml and the coulometrically determined surface concentration $\Gamma_4 = 1.53 \cdot 10^{-9}$ mol/cm², i.e. $5.47 \cdot 10^{-6}$ g/cm², the average polymer thickness x is $5.47 \cdot 10^{-6}$ g/cm² / 0.92 g/cm³ = $5.9 \cdot 10^{-6}$ cm or 59 nm.

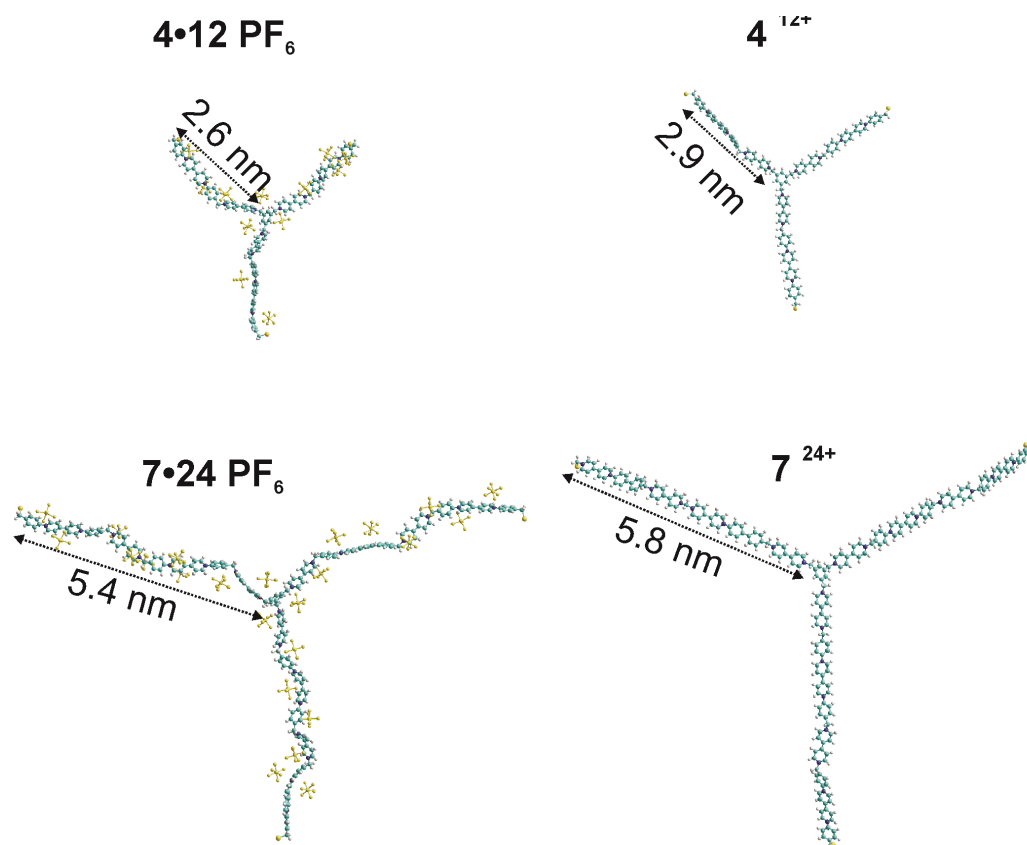
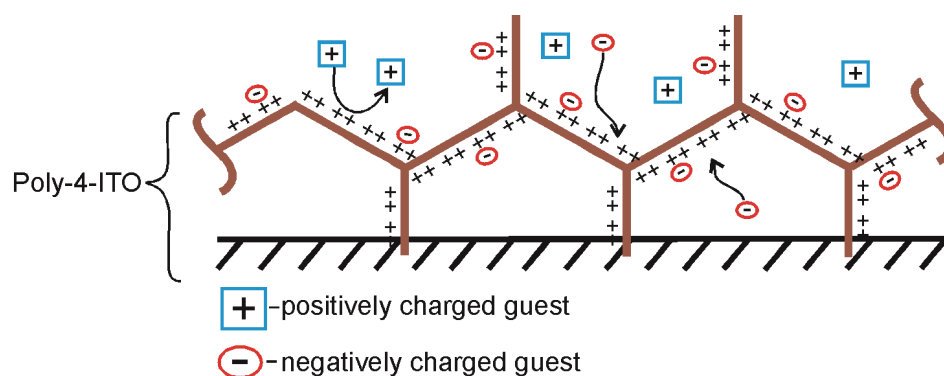


Figure 2.14 MM+MD calculations of **4** and **7** with and without PF_6^- counter ions, double arrows indicate the center-triangle corner distance.

2.2.8 Ion transfer across the Poly-4 film on ITO



Scheme 2.4 Interactions of **Poly-4-ITO** with anionic and cationic guests.

The embedding of organic molecules in a cross-linked polymer film is naturally more facile. Such polymer films are ideal as an inert matrix for

accommodating guest molecules (Scheme 2.4). In order to evaluate the permselective properties of the electro-generated **Poly-4**, a series of guests (Table 2.3) were used as interacting redox species.

Table 2.3 Intermolecular interactions between **Poly-4** (on ITO) and anionic or cationic guests.

guest molecule	ferrocene (Fc)	$K_3[Fe(CN)_6]$ $([Fe(CN)_6]^{3-})$	1,1'-bis-2-hydroxyethyl- 4,4'-bipyridinium•2Cl ⁻ (HEV)	methyl- viologen (MeV)	Ru(bpy) ₃
^{a)} Charge of the guest molecule	+0	2-/3-	2+ / +	2+ / +	3+ / 2+
Accumulation in Poly-4	0	x	0	0	0

a) the charge is considered during electrochemical oxidation/reduction ; X and 0 represents concentration and rejection of guests within **Poly-4** film, respectively.

The modification of the ITO electrode was performed in 60 cycles by cycling the potential between 0.2 and -1.2 V. After cleaning with acetone, it was immersed in a 0.1M KCl solution containing Fc (1.07×10^{-3} M), $[Fe(CN)_6]^{3-}$ (1.45×10^{-3} M), MeV (1.5×10^{-3} M), HEV (1.5×10^{-3} M) and Ru(bpy)₃ (1.5×10^{-3} M). The inclusion of organic molecules into the **Poly-4** film was studied following the effects on the charging current of polyviologen/ITO electrode.

The preconcentration of Fc within the **Poly-4** film was confirmed by the appearance of the Fc/Fc⁺ oxidation peak (in Fig. 2.15) when the potential was scanned from -1.2 to 1.4 V. Due to the electrostatic repulsion forces between positively charged molecules (host and guest) the formed Fc⁺ is ejected within and near to the polymer layer. No reduction peak of Fc⁺/Fc could be observed during the cathodic scan.

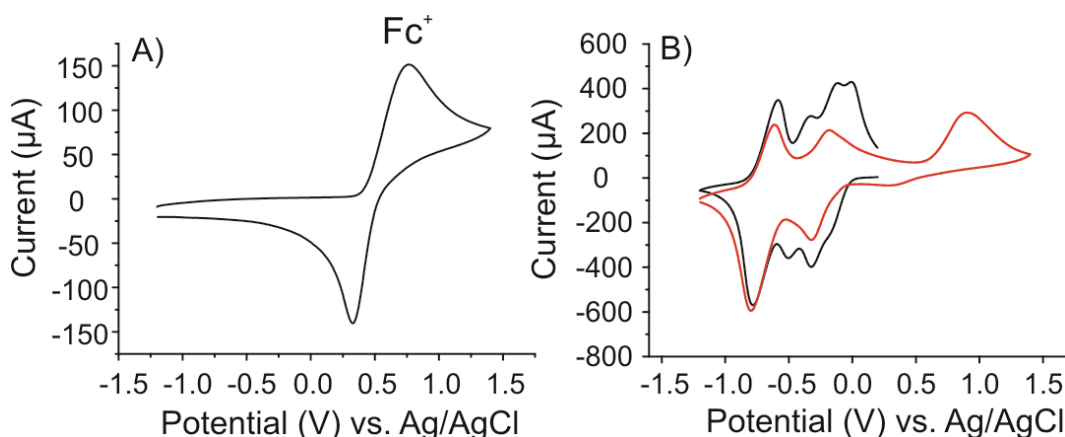


Figure 2.15 CVs of Fc in DMF-0.1M n-Bu₄NPF₆ at a bare ITO electrode A) and at **Poly-4** /ITO modified electrode (area= 0.78 cm²) (red line) B). The CV response of **Poly-4**/ITO is shown as black line.

As expected, the polycationic polymer favours the encapsulation of small anionic guests such as [Fe(CN)₆]³⁻ as shown in Fig. 2.16.

Figures 2.17, 2.18 and 2.19 shows the CVs of MeV, HEV and Ru(bpy)₃ at bare ITO (A) and at ITO modified with **Poly-4**. For the three redox species a similar behavior was observed.

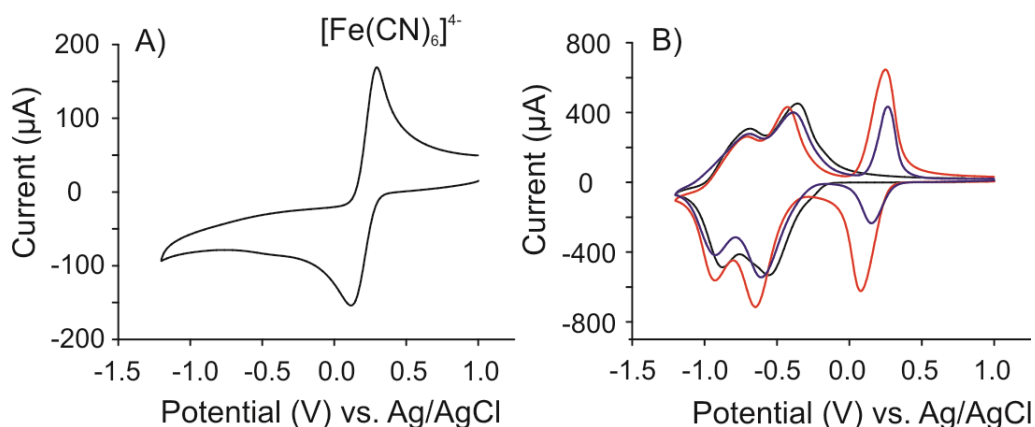


Figure 2.16 CVs of [Fe(CN)₆]³⁻ in 0.1M KCl at a bare ITO electrode A) and at **Poly-4**/ITO-modified electrode (area= 0.78 cm²) (red line) B). Graph showing the CV response of **Poly-4**/ITO (black line) and **Poly-4**/ITO + [Fe(CN)₆]³⁻ after washing with H₂O (blue line).

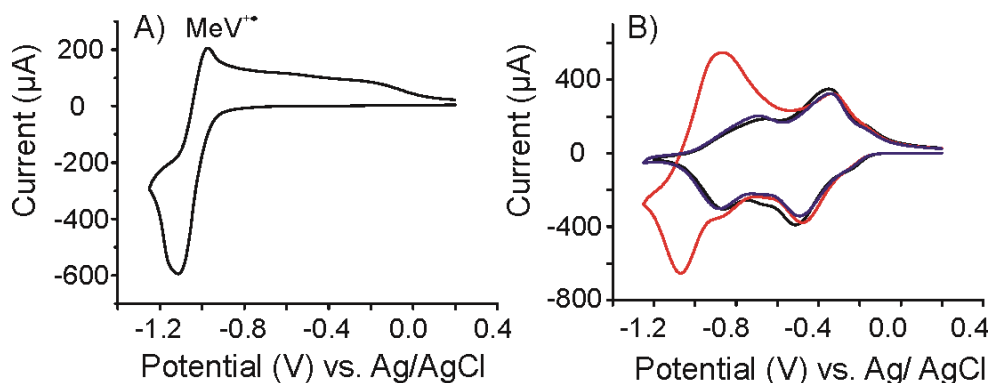


Figure 2.17 CVs of MeV in 0.1M KCl at a bare ITO electrode A) and at **Poly-4**/ITO-modified electrode (area= 0.72 cm²) (red line) B). Graph showing the CV response of **Poly-4**/ITO (black line) and **Poly-4**/ITO + MeV after washing with H₂O (blue line).

As can be seen from the CVs, an important increase in the reduction currents at the peak potentials was observed at the ITO-modified electrode which confirms the preconcentration of the positively charged molecule at **Poly-4**-solution interface. That is probably due to the π - π interactions between the 4,4'-bipyridinium guest system and the polymer. After the electrode was washed with adequate solvent (acetone or water), no preconcentration of the redox guest at the electrode surface was observed (in CV as blue line).

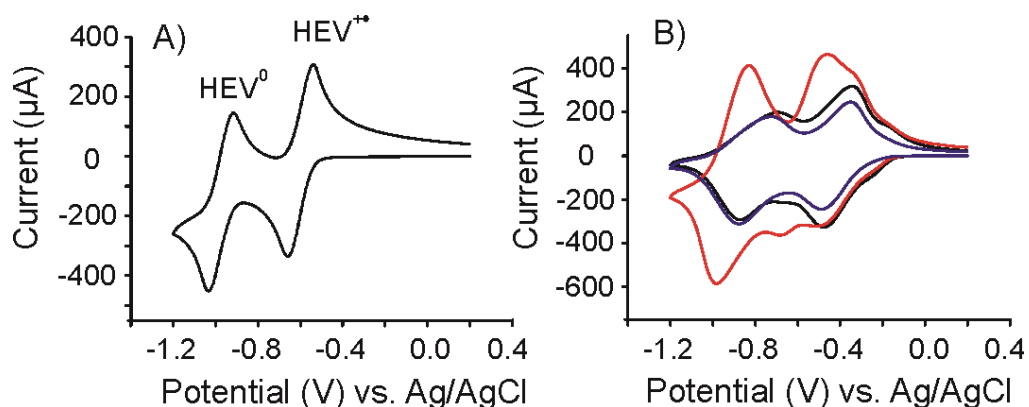


Figure 2.18 CVs of HEV in 0.1M KCl at a bare ITO electrode A) and at **Poly-4**/ITO modified electrode (area= 0.72 cm²) (red line) B). Graph showing the CV response of **Poly-4**/ITO (black line) and **Poly-4**/ITO + HEV after washing with H₂O (blue line).

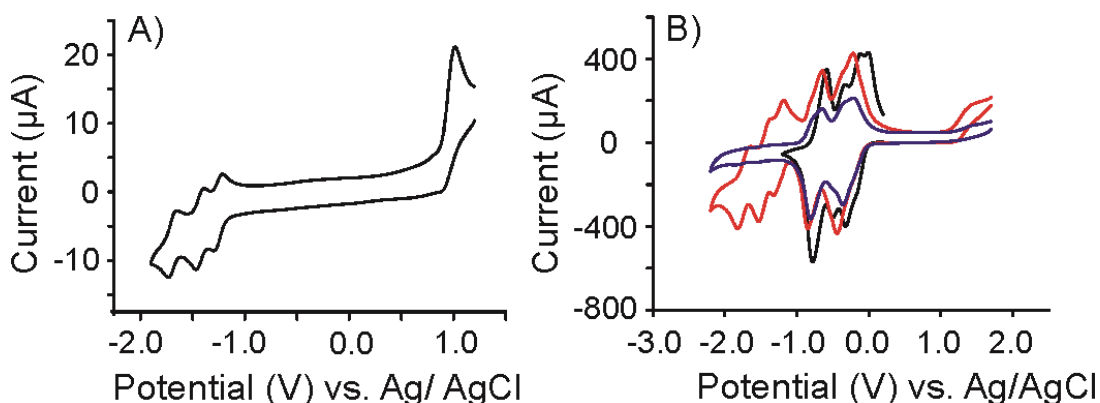


Figure 2.19 CVs of $\text{Ru}(\text{bpy})_3$ in DMF - 0.1M $\text{n-Bu}_4\text{NPF}_6$ at a bare ITO electrode A) and at **Poly-4**/ITO modified electrode (area= 0.78 cm^2) (red line) B). Graph showing the CV response of **Poly-4**/ITO (black line) and **Poly-4**/ITO + $\text{Ru}(\text{bpy})_3$ after washing with acetone (blue line).

2.2.9 STM investigation of chemically synthesized Poly-4

The viologen star **4** was polymerized by reductive coupling in the presence of Zn and its helical structure was solved by STM measurements.

Surprisingly, the **Poly-4** when re-dispersed in DMF, and spread on HOPG reveals straight nanofibres by STM. Fig. 2.20 shows STM images of **Poly-4** on HOPG. The polymer observed on HOPG shows well-defined double helical structures (Fig. 2.20-C, D). The interactions between the coils in isolated strands are probably weak,¹¹⁶ which lead to disordered structures (Fig. 2.20-B, I).

The organization of the **Poly-4** in a helical shape may be explained in terms of van der Waals¹¹⁷ and hydrophobic¹¹⁸ attractive forces between the 4,4'-ethane-1,2-diyl diphenyl moieties in a linear polymer chain, which were formed upon the reductive coupling of **4** (Scheme 2.5).

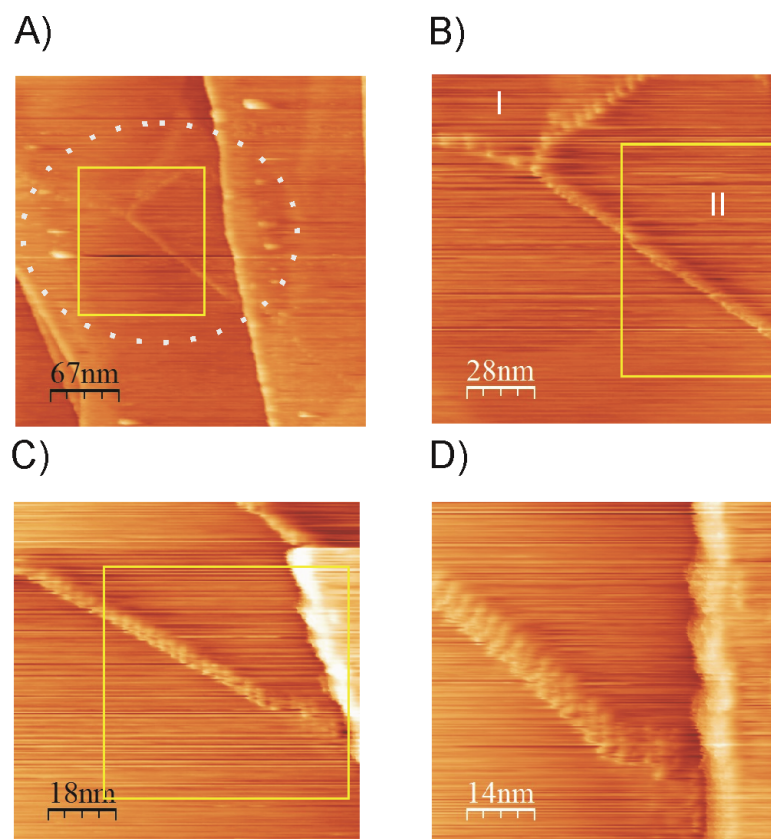


Figure 2.20 STM images ($V_b = 0.05$ V, $I_t = 1$ nA) of **Poly-4** (chemical preparation) on graphite (A-D): A) 335 x 335 nm, Z range 12.5 nm; B) 141 x 141 nm, Z range 12.5 nm; C) 90 x 90 nm, Z range 12.5 nm; D) 72 x 72 nm, Z range 6.25 nm.

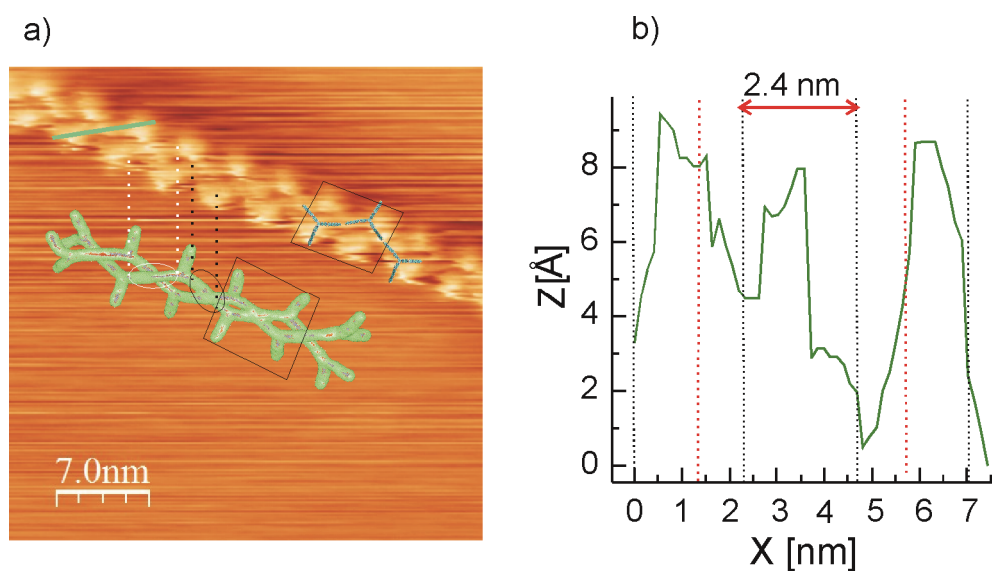
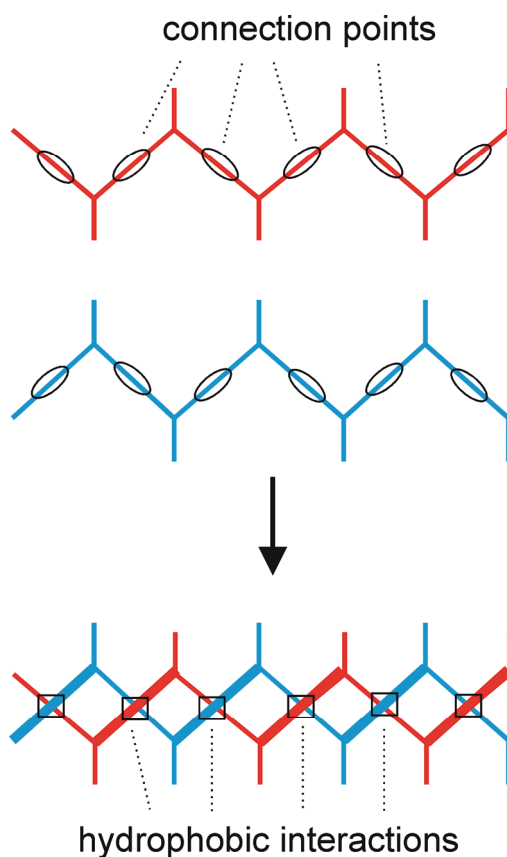


Figure 2.21 a) Polymer strands assembled in helical structure; b) topographic profile along the green line in the polymer strand in a).

The double helical structure of **Poly-4** has been modeled with MM+ in HyperChem¹¹¹ (Fig. 2.22 and 2.23) and added to the STM image (Fig. 2.21-a). The polymer strands are formed by the reaction of each monomer units in only two positions (possible are 3) as shown in Fig. 2.21 and Scheme 2.5.

The outwards oriented arms in Fig. 2.21 (green model) are probably partially visible by STM, and the connected arms appears as bright and dark areas (Fig. 2.21-b, red dotted lines). The section profile along the green line in Fig. 2.21-a spans ca. 2.4 nm bright areas (Fig. 2.21-b, black dotted lines). The central current maximum is probably related to the upwards bending of two benzyl-benzyl coupled branches. Upwards bending may be related to the blue branch sitting on top of the red branch in Scheme 2.5.



Scheme 2.5 Formation of a double-helical structure of polyviologen (**Poly-4**).

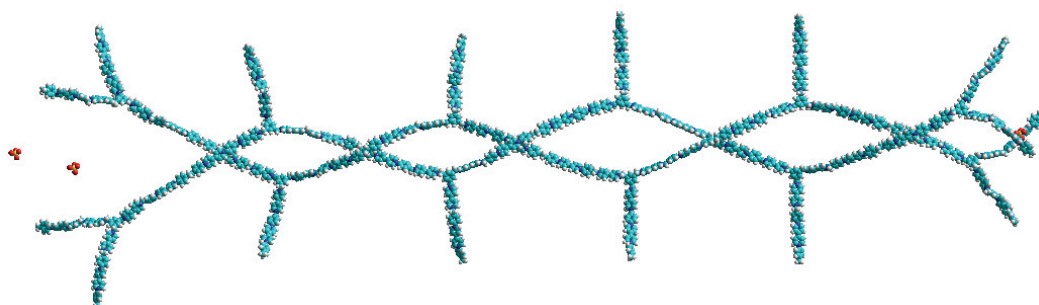


Figure 2.22 MM+ optimized geometry¹¹¹ of 6-mer (**oligo-4**) arranged in helical structure. The distance between the branches oriented upwards and downwards is ca. 6-7 nm and the double helix is 7-8 nm width.

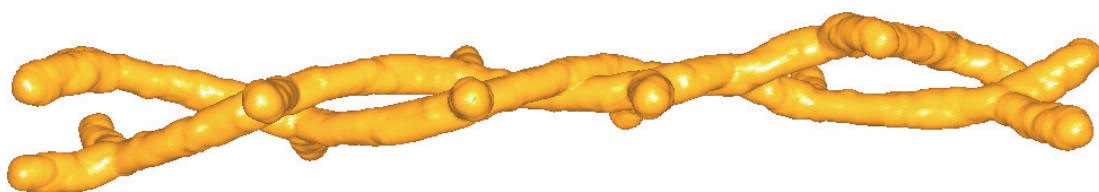


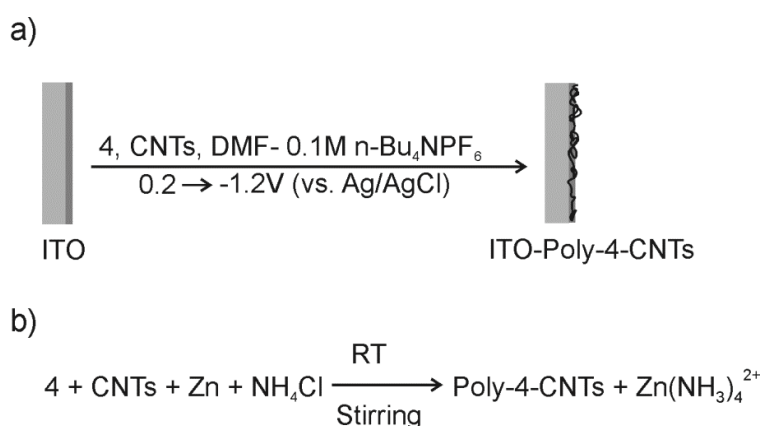
Figure 2.23 Solvated structures of two polymer strands (each consisting of 6 monomers (**4**)) arranged in helix. The molecule is twisted by 90 degree.

2.2.10 Preparation and characterization of polyviologen - carbon nano-tubes composites (Poly-4-CNTs)

In this subchapter I will discuss the preparation of polyviologen-CNTs composites by chemical and electrochemical polymerization of viologen star **4**. The **Poly4-CNT** composites were successfully obtained by copolymerization of the two components probably from a pre-organized state. It is based on the π -stating and electrostatic interactions between the positive nitrogen in and negatively charged COO^- group of CNTs. The triple branched structure of the monomer **4** is a key parameter for composite formation. It's length

correlates with the CNTs (area 4-6 nm²) and the three branches can interconnect CNTs.

The reductive coupling of the benzylic bromides in **4** occurs in the presence of CNT's either electrochemically or by Zn⁰/NH₄Cl (Scheme 2.6) and results in composite **Poly-4-CNT** polymer with **Poly-4** in tight and regular contact on the CNT's and clear CNT-interconnection chains made up of several viologen star monomer.



Scheme 2.6 Preparative methods of **Poly-4-CNT** composites.

a) Electrochemical preparation of **Poly-4-CNT** composite film

The electropolymerization of **4** in the presence of CNTs in DMF-0.1M n-Bu₄NPF₆ on ITO electrode was performed by consecutive CVs. Fig. 2.24-A shows an increase of the peak current with each scan indicating that the electropolymerization takes place. Fig. 2.24-B represents the electrochemical signal of **Poly4-CNT** composite film in bare electrolyte solution. The CV are almost indistinguishable from those obtained in Section 2.2.5, Fig. 2.9.

An XPS was carried out on the **ITO-Poly-4-CNT** composite film surface. P, C, N, O and F were detected on the surface (Fig. 2.25-A). The existence of the big O1s peak is due to the presence of COOH groups on the CNTs and possibly also due to the environmental moisture trapped in the film surface.¹¹⁹

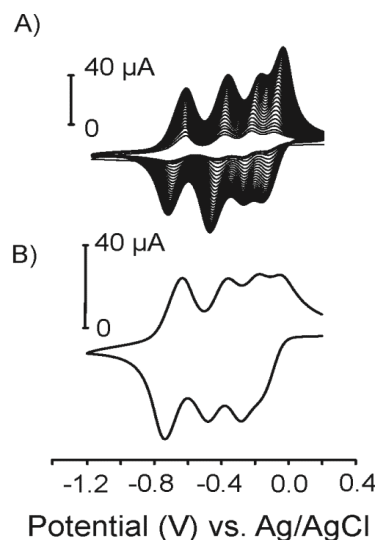


Figure 2.24 Electropolymerization of **4** ($c = 4.9 \times 10^{-4}$ M) + CNTs ($c = 0.2$ M) (A) on GC in DMF/ Bu_4NPF_6 during the first 60 scans, $v = 100 \text{ mVs}^{-1}$; response of **Poly-4-CNTs** (B) ($\Gamma_4 = 2.73 \times 10^{-9}$ or $\Gamma_{\text{subunits}} = 1.63 \times 10^{-8} \text{ mol/cm}^2$) on GC in pure DMF/0.1M- Bu_4NPF_6 at $v = 100 \text{ mVs}^{-1}$.

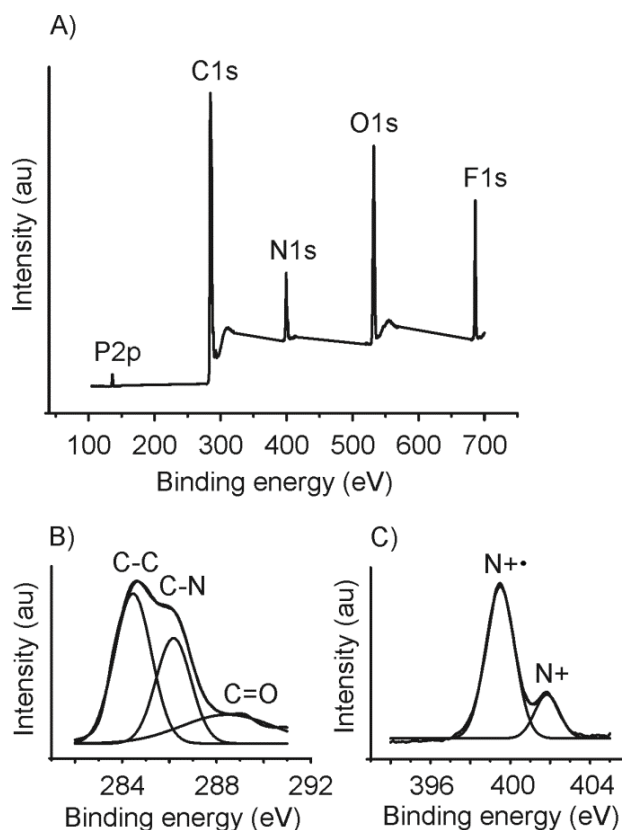


Figure 2.25 XPS spectra of ITO-Poly-4-CNT composite film. Wide scan A) and core level: B) C1s and C) N1s.

As expected, the binding energies of P2p (136 eV), C1s (284.62 eV; 286.12 eV), N1s (399.50 eV and 401.75 eV) and F1s (686 eV) are attributed to the viologen polymer.¹²⁰ No Br⁻ 3d peak was observed in the range 68-72 eV,¹²¹ confirming the reductive cleavage of C-Br bond during the electropolymerization.

Fig 2.26 shows several STM images of the **Poly-4-CNT** composites as film on ITO. Notice that in “far-view”, the polymer is hard to be recognized on ITO. CNTs appeared as “sticks” covering the granular structure of ITO. In higher magnification of a set of tubes (Fig. 2.26-B, C), it is clear that the composite film consists of short CNTs (most of the tubes are around 120 nm).

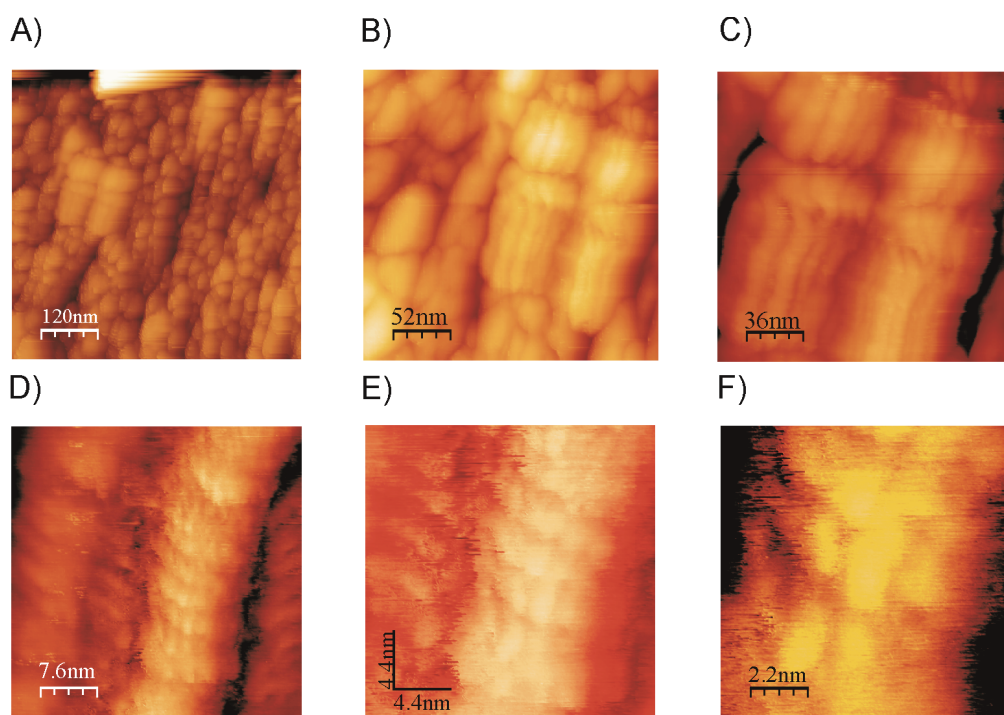


Figure 2.26 STM images ($V_b = 0.2$ V, $I_t = 0.4$ nA) of **Poly-4-CNT** ($\Gamma_{4+CNTs} = 1.36 \times 10^{-9}$ mol/cm²) on ITO (A-D): A) 596 x 596 nm, Z range 25 nm; B) 260 x 260 nm, Z range 25 nm; C) 178 x 178 nm, Z range 12.5 nm; D) 38 x 38 nm, Z range 3.13 nm; E) 22 x 22 nm, Z range 50 nm; F) 11 x 11 nm, Z range 1.56 nm.

Similar length of CNTs was earlier reported when CNTs were coated onto ITO glass.¹²² In Fig. 2.26-D can be seen a bundle of CNTs arranged in

parallel “sticks” along the vertical direction. In horizontal direction parallel linear chains can be clearly distinguishable. This is not surprising, because the STM analysis of **Poly-4** on HOPG proves his linear fiber-like structure. The polymer chains cover and join CNTs bundles by means of non-covalent and covalent wrapping. Fig. 2.26-E, F reveal regular oval-shaped patterns with a length of 2.5 nm. These structures happen to be on the same length scale as the arms of the monomer which are the repetitive units in the chain of the polymer. The regular patterns on CNTs are evidence for the non-covalent interactions between the CNTs and the polymer (monomer).

b) Chemical preparation of Poly-4-CNT composites

Fig. 2.27-A is a large STM image of **Poly-4-CNT** composites on graphite. Several nanotubes come out from the upper to the lower corner of the image. The macroscopic morphology of the tubes does not change when they are covered by the polymer. Fig. 2.27-C-D) shows **Poly-4** wrapped CNTs, where the polymer is aligned in rows on the CNTs surface. The polymer appears as a continuous film that covers the surface of the CNTs completely. Two different areas can be distinguished: i) areas of composite formed from shortened CNTs and ii) from long CNTs. This is because the CNTs break during sonification due to the input energy which is necessary to disperse them in solution.¹²³ A magnified view of the shorter tubes is shown in Fig. 2.27-E) where it can be seen that the polymer covers the tubes entirely making a connection with the other CNTs. A high degree of **Poly-4** chain organization can be seen along the tubes axis. This confirms that in monomer solution (**4**), the CNTs adsorb as many molecules of **4** as possible to reduce the interactions between tubes. Zooming in to the area where long CNTs are

included in the composite (Fig. 2.27-F), allows to observe the polymer as linear strands, without resolved molecular structure.

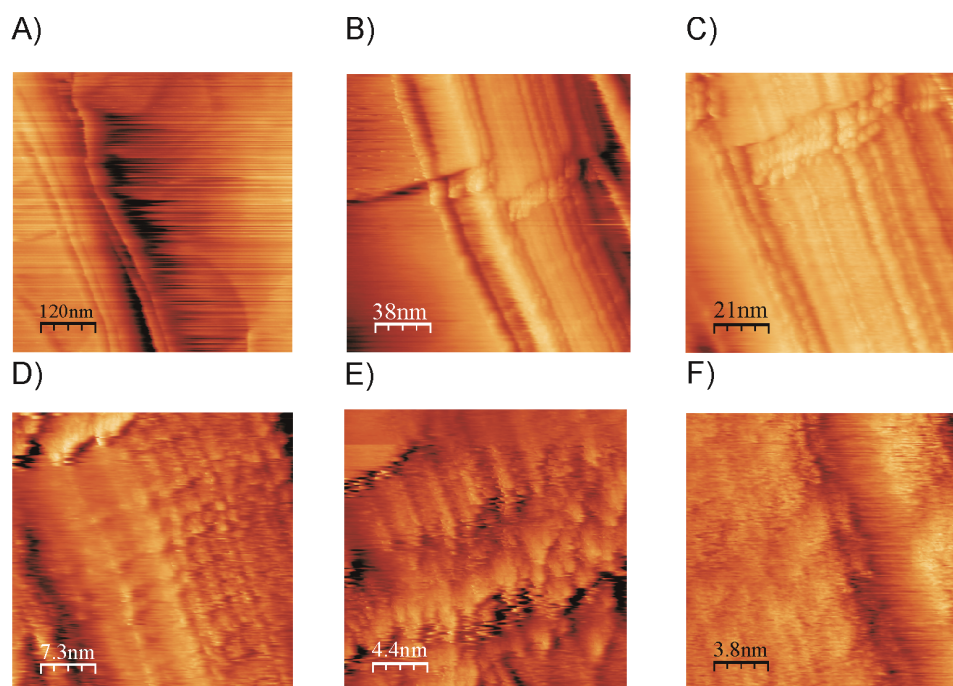


Figure 2.27 STM images ($V_b = 0.05$ V, $I_t = 1$ nA) of **Poly-4-CNT** (chemical preparation) spread on graphite (A-F): A) 596 x 596 nm, Z range 50 nm; B) 191 x 191 nm, Z range 12.5 nm; C) 106 x 106 nm, Z range 6.25 nm; D) 36 x 36 nm, Z range 3.13 nm; E) 21 x 21 nm, Z range 3.13 nm; F) 19 x 19 nm, Z range 1.56 nm.

The CV curves of **Poly-4-CNTs** (Fig. 2.28) show the persistent four-electron transfer process observed for **Poly-4** on ITO (Fig. 2.9-C).

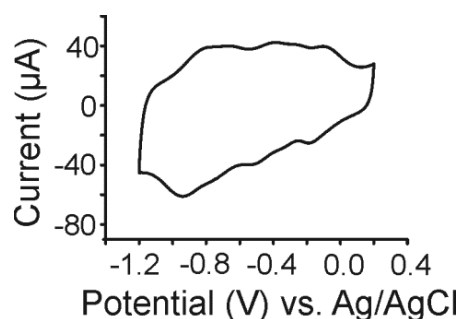


Figure 2.28 **Poly-4-CNT** composites as cast film on GC electrode. CV recorded in DMF + 0.1M n-Bu₄NPF₆ at scan rate 50 mVs⁻¹.

2.2.11 Electrochemical and spectroelectrochemical characterization of viologen dendrimer **14**

The viologen dendrimer **14** consists of benzyl/phenyl-substituted viologen subunits. As expected, **14** will have the tendency to accept e^- easier than BnV. But in the same time it is more difficult to reduce as compared with PhV (Table 2.1). The cyclic voltammogram of **14** exhibits two reversible reduction waves in negative scans (Fig. 2.29-A) assigned to $V^{+•}$ ($E^{0'} = -0.20$ V) and V^0 ($E^{0'} = -0.56$ V), respectively.

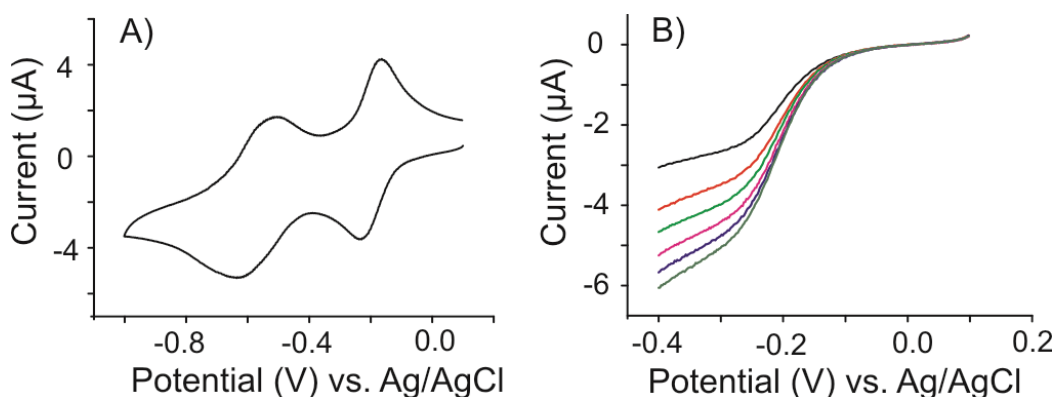


Figure 2.29 A) CV of 1.35×10^{-4} M of **14** in DMF + 0.1M $n\text{-Bu}_4\text{NPF}_6$ at gold electrode, scan rate 100 mVs^{-1} ; B) Rotating disk voltammetry of **14** (7.18×10^{-5} M) at a GC RDE and different rotation speeds: 52.33, 104.66, 157, 209.33, 261.66 and 314 rads^{-1} .

The controlled-potential electrolysis at potentials between 0 and -0.49 V gave rise to the precipitation of the reduced species on carbon felt electrode, as indicated by the strong decrease in spectral absorption at -0.49 V in Fig. 2.30.

The electronic absorption spectrum of **14** in the radical cation state, is typical of $V^{+•}$ and is characterized by a sharp band at 411 nm and additional absorptions at 602 nm, 717 nm and 957 nm (green solution).

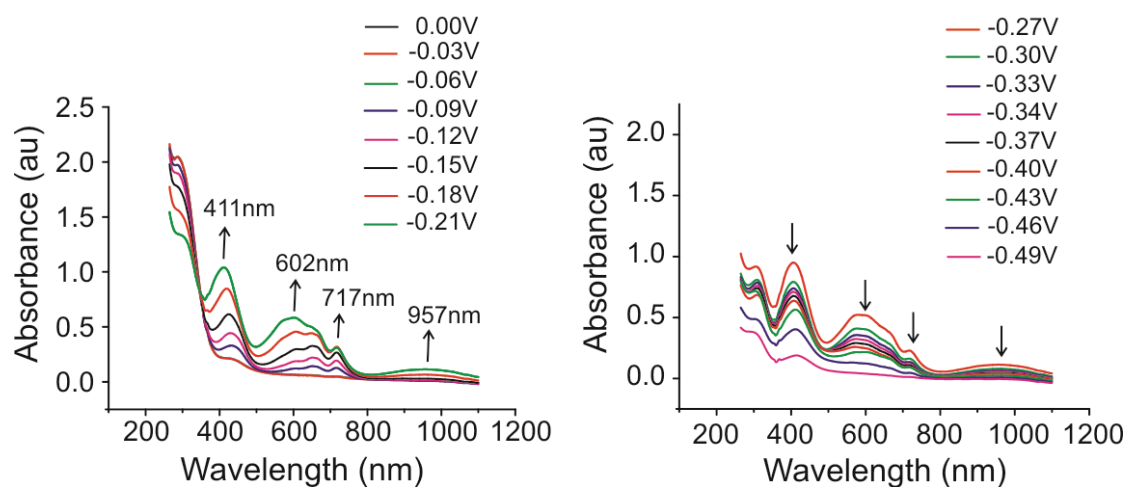


Figure 2.30 Potential-dependent UV-Vis spectra of 7.2×10^{-5} M of **14** in DMF and 0.1M $n\text{-Bu}_4\text{NPF}_6$.

The diffusion coefficient was calculated from the i_L dependence on $\omega^{1/2}$ (Fig.2.20 B)) by using the Levich equation:¹²⁴

$$I_{\text{lev}} = 0.620 n F A D^{2/3} \omega^{1/2} \nu^{-1/6} C_s \quad (2.2)$$

where n is the number of electrons transferred (13), F is the Faraday's constant (96485 C mol^{-1}), A is the area of the rotating disk electrode (0.070 cm^2), D is the solution diffusion coefficient of the electroactive species ($\text{cm}^2 \text{ s}^{-1}$), ω is the rotation speed of the RDE in $\text{rad} \cdot \text{s}^{-1}$, ν is the kinematic viscosity of the electrolyte (for DMF $9.19 \times 10^{-3} \text{ cm}^2 \text{ s}^{-1}$) and C_s is the concentration of the electroactive species in solution ($7.18 \times 10^{-8} \text{ mol/ml}$).

The diffusion coefficient (D) of **14** was found to be equal to $0.12 \times 10^{-6} \text{ cm}^2 \text{ s}^{-2}$. The value is in the same range with the one obtained by Heinen¹²⁵ for a charge trapping dendrimer with 26 bipyridinium subunits.

2.3 Conclusions

The synthesis, chemical and electrochemical characterization of two series of rigid viologens (stars and dendrimers), with branched structure and

alternating benzyl viologen/phenyl viologen subunits are discussed. These molecules were obtained by consecutive Zincke/Menshutkin reactions. The introduction of the hydroxymethyl groups at the periphery of the molecules by the Zincke reactions allows their activation and their subsequent growth. The presence of two different viologen subunits results in combined electrochemical and optical properties of the molecule.

The four reduction peaks in the CVs of **4** and **5** are clearly visible and correspond to the four consecutive monoelectronic reductions of the PhV and BnV subunits. The UV-Vis redox titration of **4** and **5** yields approximately the same E^0_s exhibiting a very similar spectrum to that of PhV and BnV.

The viologen stars **4**, **5** and **7** are monodisperse triple-branching macromolecules consisting of alternating benzyl and phenyl viologen subunits. According to MM⁺ molecular dynamics simulations (fully developed charge, gas phase) the stars adopt an open, flat or slightly convex structure with the branches pointing towards the corners of an equilateral triangle (Fig. 2.14). This conformation allows an uncomplicated direct heterogeneous electron transfer with all viologen subunits at their corresponding E^0 , in accordance with the whole set of four waves appearing in CV (Fig. 2.2) and the isosbestic spectroelectrochemistry (Fig. 2.4).

Polyviologen films (**Poly-4** and **Poly-7**) can be successfully prepared on GC, gold and ITO by cyclic voltammetry with potential ranging from 0.2 to -1.2 V at scanning rate of 100 mV/s. The electropolymerization is highly dependent on the initial viologen structure. Despite the presence of bromomethyl-phenyl on the viologen termini, only **4** and **7** formed polymers upon electroreduction.

The introduction of benzyl viologen subunit in the branches seems to be important for efficient electropolymerization. Viologen stars **4** and **7** can easily be electropolymerized via benzyl-benzyl radical coupling. The radicals are most probably generated by an intramolecular electron transfer from doubly reduced benzyl viologen into the antibonding σ^* orbital of the benzylic C-Br bond,^{126,127} as indicated by the potential-dependent polymerization efficiency (Fig. 2.11). The stars cross link to achieve a surface subunit concentration up to 2×10^{-8} subunits/cm². The persistence of the four waves is similar as earlier observed in poly-pyrrole based benzyl and phenylviologens.⁷⁸

No differences in the electrochemical and spectroelectrochemical properties of the polymers compared with the star monomers were observed.

The chemical polymerization of **4** was also successfully performed in the presence of Zn and NH₄Cl. The disappearance of C-Br stretching vibration at 552 cm⁻¹ in the FT-IR spectrum¹²⁸ of **Poly-4** proves the benzyl-benzyl radical coupling mechanism. The STM image of **Poly-4** on HOPG shows polymer fibers packed in helical structures.

A new composite material was prepared using CNTs and **4** by electrochemical and chemical polymerization. The **Poly-4-CNT** composites exhibits electrochemical behavior of **Poly-4**. The STM and XPS confirm the presence of CNTs in the polymer film.

Because the **Poly-4** film can preconcentrate anions at the electrode surface, the **Poly-4-ITO**-modified electrode could be used as sensitive and selective sensor for organic/inorganic anions.

The cyclic voltammetry and spectral changes of two e⁻ reduced species of **14** have been investigated. The CV of **14** shows that the two e⁻ reduction of

BnV core coincide with the two e^- reduction of PhVBn branches. The absorption spectra of **14** at -0.37 V is similar to that of PhV. Analysis of the diffusion coefficient was done according to Levich equation, and the value of D is in agreement with the reported value of a similar viologen derivative.

2.4 Experimental part

2.4.1 Cyclic voltammetry measurements

All solutions were de-aerated by Ar bubbling for 3 min. prior to the electrochemical experiment. CV measurements were carried out at RT, in a standard three electrode cell. The working electrodes were a gold disc (area= 0.070 cm², Methrom, 6.1204.140), a glassy carbon (GC) (area= 0.066 cm², Metrohm (6.0804.010)) and ITO glass slides ((In-doped SnO₂, 20 Ω /cm²) from BTE Bedampfungstechnik (Elsoff, Germany), and the counter electrode was a Pt wire. The reference electrode was a saturated (3M) Ag/AgCl/KCl electrode (Metrohm, 6.0724.140), separated by a salt bridge containing the same organic solvent/electrolyte as the measuring compartment. Prior to each electrochemical synthesis, the working electrode (GC or Au) was carefully polished with alumina powder on a polishing cloth and then rinsed with distilled water. ITO glasses were cleaned following conventional procedures.¹²⁹ All of these electrodes were dipped into the electrolyte solution prepared by dissolving 0.1M tetrabutylammonium hexafluorophosphate (n-Bu₄NPF₆) (Sigma-Aldrich, $\geq 99\%$) in DMF (Sigma-Aldrich, $\geq 99.9\%$). Potentiostatic control was performed by a PGSTAT 20 potentiostat from AUTOLAB, connected to the cell and controlled by a PC running under GPES for Windows, Version 4.2 (ECO Chemie 1995).

The RDE measurements performed to find D of **14** were conducted at a sweep rate of 5 mVs⁻¹. A Metrohm 663 VA stand with a GC (0.29 cm diameter) was used for rotating disk (RDE) studies. The experiments were performed for rotational speeds of 500, 1000, 1500, 2000, 2500 and 3000 rpm.

2.4.2 Spectroelectrochemistry of 4, 5 and 14 in solution

Absorption spectroscopy can be utilized for the redox titration whenever the absorption spectra of oxidized vs. reduced molecule show significant differences throughout the visible range.

The cell¹³⁰ used for the spectroelectrochemical characterization of the monomer solutions was of glass construction with a 2 mm cuvette and a Ag/AgCl electrode as reference (Metrohm, 6.0724.140) (3M KCl, aqueous solutions). The working electrode was a graphitized carbon felt GFA-5 of ca. 2 cm diameter from SGL Carbon. The cell was driven by an EG&G PAR model 173/179 potentiostat. The changes in absorbance were measured using a Hewlett-Packard 8453 spectrophotometer with a maximum time resolution of 0.5 s. After thorough de-aeration of the solution by bubbling argon, an initial reducing potential was applied in the interval from 0.0 V to -1.0 V. The potential was held constant until the solution volume was totally reduced as indicated by the stable absorption spectrum. The electrode potential was sequentially increased in 30 mV steps. The electrolyte used for the redox titrations was 0.1M n-Bu₄NPF₆ in DMF.

2.4.3 Electropolymerization of 4 and 7

Polymer films were deposited on GC, gold and ITO from monomer solutions

in 0.1M Bu₄NPF₆/DMF by scanning the potential between 0.2 V and -1.2 V vs. Ag/AgCl at 100 mVs⁻¹. The sweep was stopped after 60 cycles, and the modified electrode was rinsed with acetone prior to further experiments. The modified electrodes were investigated by repetitive cyclic voltammetry (60 scans, at 100 mVs⁻¹) to explore the polymer by CV, UV-Vis or STM.

Poly-4-CNT nanocomposites on ITO were prepared by mixing an amount of CNTs (0.25 wt %) to a solution of **4** (5*10⁻⁴ M) containing 0.1M n-Bu₄NPF₆. The solution was then homogeneously dispersed by ultrasonification for 30 minutes. It was observed that viologen-star **4**, dissolved in DMF, is a good dispersive medium for the CNTs. Once the sonification was completed, the solution was subjected to CV by scanning the potential between 0.2 V and -1.2 V vs. Ag/AgCl at a scan rate of 100 mVs⁻¹. The formed nanocomposite film was then analyzed by CV, STM and XPS.

For preparation of **GC-Poly-4-CNTs**-coated electrode, a DMF solution of **Poly-4-CNTs** (prepared according Scheme 2.6-b) was used to cover the GC electrode and then dried at 40°C for the electrochemical measurements.

2.4.4 Spectroelectrochemistry at modified electrode (Poly-4 on ITO)

A homemade spectroelectrochemical cell was constructed for the analysis of aqueous samples using a 1cm quartz cell that was attached at the bottom of a conventional three-electrode cell. The cell was mounted in the sample compartment of a Hewlett-Packard 8453 spectrophotometer, and the measurements were performed in aq. 0.1M KCl under Ar atmosphere. The working electrode was ITO glass (ca. 0.98 cm²) containing the polymer, the reference electrode was Ag/AgCl (3M KCl, aqueous solutions), and a Pt wire

was used as the counter. The cell was driven by an EG&G PAR model 173/179 potentiostat.

The ITO/film electrode was immersed in aq. 0.1M KCl solution and subjected to potential steps between 0 and -0.99 V. The spectra were recorded when absorption was constant, after 100 s.

2.4.5 PM6-modelling

A single branch of **5** (= **sb5**) was geometry optimized in the gas phase without counter ions with PM6 embedded in MOPAC2009 and using Gabedit 2.40 as the graphical interface.^{131,132} According to the electronic occupancy the multiplicity was defined as singlet (4+ and 0 charged) or doublet (3+ or 1+ charged). In the ambiguous case (2+ charged) singlet and triplet were both calculated providing a ca. 45 kcal lower energy for the triplet multiplicity.

2.4.6 STM measurements on modified electrodes (Poly-4 on ITO and HOPG and Poly-4-CNTs on ITO)

The STM imaging was carried out with an EasyScan Nanosurf (Switzerland) instrument at RT using typically 0.050 V bias voltages and 1.000 nA tunneling current. The images are raw data without any filtering. The STM tips were cut from Pt/Ir wire (0.25 mm) (Schaefer Technologie GmbH in Langen, Germany). The polymer-covered ITO glass electrodes were glued onto the magnetic support and the surface was electrically connected to the support with silver lacquer painted over the glass edge.

Poly-4-HOPG: Polymer adsorption on graphite was done from **Poly-4** solution in DMSO (ca. 1 mg/ml). A drop of the polymer solution was deposited on the freshly cleaved graphite surface and evaporated at 40 °C.

Poly-4-CNT-ITO: After preparation (electrochemical approach), the composite film was washed with acetone and dried in air before visualization by STM.

Poly-4-CNTs-HOPG: After chemical preparation, the composite were suspended in DMF and ultrasonicated for 30 minutes. A drop of the solution was adsorbed on the freshly cleaved graphite surface, evaporated within 24 hours at RT and visualized by STM.

2.4.7 Ion transfer studies

Ferrocene (Fc) (Fluka, $\geq 98\%$), tris(2,2'-bipyridyl) dichlororuthenium (II) hexahydrate ($\text{Ru}(\text{bpy})_3$) (Aldrich, 99.95 %) and potassium ferricyanide (III) ($[\text{Fe}(\text{CN})_6]^{3-}$) (Sigma-Aldrich, min. 99 %) were used as purchased. The synthesis of 1,1'-bis-2-hydroxyethyl-4,4'-bipyridinium dibromide (HEV) was performed using procedures described earlier.^{133,134} Methyl viologen hexafluorophosphate (MeV) was obtained after the ion exchange to PF_6^- following the procedure described by Xiao et al.¹³⁵ The experimental setup used in this study was described in Section 2.4.1. For this study, the ITO glass electrodes were modified as described in Section 2.4.3.

2.4.8 FT-IR investigation of viologen star 4 and Poly-4

The infrared spectroscopy (IR) measurements were performed using a Vertex 70 instrument (Bruker) with Fourier transformation (FT-IR), equipped with ATR module based on diamond crystal. The spectra were recorded over the wavenumber range of $400\text{--}4000\text{ cm}^{-1}$ for viologen star **4** and **Poly-4** obtained via chemical reductive coupling. Bands are characterized as: strong (s), medium (m), and weak (w).

2.4.9 Detailed synthetic procedure

2.4.9.1 Materials and devices

The reagents: 4,4'-bipyridine (Aldrich, 98 %), 1-chloro-2,4-dinitrobenzene (Fluka, ≥ 98 %), 4-aminobenzyl alcohol (Aldrich, 98 %), HBr (Sigma-Aldrich, ≥ 33 % in acid acetic), 1,3,5-tris(bromomethyl)benzene (Aldrich, 97 %), 5-amino-isophthalic acid dimethyl ester (Aldrich, 98 %), HBr (Sigma-Aldrich, 48 %), Single-Wall Carbon Nanotubes (99 wt %, $d = 1\text{--}2$ nm, length = $3\text{--}30$ μm , Cheap Tube Inc), tetrabutylammonium chloride (TBACl) (Fluka, ≥ 97 %), ammonium hexafluorophosphate (NH_4PF_6) (Fluorochem, ≥ 99 %) and lithium aluminium hydride (Merck, tablets) were used without further purification.

Organic solvents were purified prior to use as follows: ethyl acetate was distilled over phosphorus pentoxide (P_2O_5 , Acros Organics) and methanol was distilled over Na (Riedel de Haën, min. 99 %). All other solvents: acetonitrile (MeCN) (Sigma-Aldrich ≥ 99.9 %) and diethyl ether, (Sigma-Aldrich, ≥ 99 %) were used as received.

^1H - and ^{13}C -NMR spectra were recorded on Bruker Avance spectrometer at 250 and 63 MHz, respectively, using the solvent signal as internal standard.

Elemental analyses were performed on Elementar Vario microcube instrument.

2.4.9.2 Synthesis description

1•2PF₆ ($\text{C}_{24}\text{H}_{22}\text{F}_{12}\text{N}_2\text{O}_2\text{P}_2$): 1,1'-Bis-(4,4'-hydroxymethyl-phenyl)-4,4'-bipyridinium bis (hexafluorophosphate)

To a solution of 2 g (3.56 mmol) 1,1'-bis-(2,4-dinitrophenyl)-4,4'-bipyridinium dichloride in 560 ml MeOH/water 80 % (V/V) at reflux 1.02 g (8.28

mmol) 4-Aminobenzyl alcohol in 50 ml MeOH/water 80 % (V/V) was added and allowed to reflux for 48 h. The mixture was cooled to RT and the solvent was evaporated. The residue was dissolved in 150 ml water and filtered through a filter paper to remove the 2,4-dinitroaniline side product. The filtrate was washed three times with chloroform to remove 4-aminobenzylalcohol, the aqueous phase was evaporated, then the residue was dissolved in 80 ml MeOH, and the product was precipitated with 200 ml diethyl ether. The brown precipitate was collected by suction filtration, dissolved in 80 ml water and precipitated as PF_6^- salt by addition of 10 ml 3M aq. NH_4PF_6 . The beige precipitate was filtered, washed with water to remove excess of NH_4PF_6 and dried under high vacuum to give **1•2PF₆** (1.39 g, 59.52 %).

¹H NMR (CD₃CN, 250 MHz): 3.43 (s, OH, 2H); 4.80 (s, CH₂, 4H); 7.78 (s, CH_{arom.}, 8H); 8.67 (d, J= 7.5 Hz, Vio 4H); 9.22 (d, J= 7.5 Hz, Vio, 4H).

¹³C NMR (CD₃CN, 63 MHz): 62.95 (CH₂); 124.77; 127.69; 128.72; 141.44; 146.03; 147.30; 150.60.

Elemental analysis for C₂₄H₂₂F₁₂N₂O₂P₂•3H₂O: C40.34, H3.95, N3.92 (calc.), C40.26, H3.83, N3.87(found).

2•2PF₆ (C₂₄H₂₀Br₂F₁₂N₂P₂): 1,1'-Bis-(4,4'-bromomethyl-phenyl)-4,4'-bipyridinium bis (hexafluorophosphate)

2.5 g (3.78 mmol) 1,1'-Bis-(4,4'-hydroxymethyl-phenyl)-4,4'-bipyridinium bis (hexafluorophosphate) (**1**) in 200 ml HBr in CH₃COOH (5.7M) was stirred for 4 days at RT while protected from light. The acid was evaporated, and the residue was dissolved in methanol and then precipitated by addition of diethyl ether. The brown precipitate was filtered, dissolved in water/MeOH (8:2 V/V) and treated with 10 ml 3M aq. NH_4PF_6 . The white precipitate (PF_6^- salt) was

filtered, washed several times with water and dried under high vacuum (2.12 g, 71.55 %).

^1H NMR (CD_3CN , 250 MHz): 4.77 (s, CH_2 4H); 7.84 (dd, J = 10.0 Hz, CHarom., 8H); 8.69 (d, J = 5.0 Hz, Vio 4H); 9.23 (d, J = 5.0 Hz, Vio 4H).

^{13}C NMR (CD_3CN , 63 MHz): 31.51 (CH_2); 125.08; 127.38; 131.24; 141.86; 142.93; 145.68; 150.44.

$4 \cdot 12\text{PF}_6$ ($\text{C}_{111}\text{H}_{93}\text{Br}_3\text{F}_{72}\text{N}_{12}\text{P}_{12}$):

To a solution of 2.6 g (3.30 mmol) 1,1'-bis-(4,4'-bromomethyl-phenyl)-4,4'-bipyridinium bis (hexafluorophosphate) (**2**) in 60 ml MeCN, 0.8 g (2.06 mmol) Bu_4NPF_6 was added and then heated to 70°C. 0.38 g (0.37 mmol) of **3** (prepared according to the literature⁹⁸) in 6 ml MeCN was added in portions while stirring over a period of 8 h. The mixture was further stirred for 5 days at 70°C. After cooling to RT, the mixture was filtered. The filtrate was added to 5ml TBACl (1M solution in MeCN). The brown precipitate (Cl^- salt) was collected by filtration and washed with MeCN to remove the excess of TBACl. For further purification, the product was precipitated three times from MeOH/diethyl ether.

TLC: MeOH/HOAc/ H_2O , 10:4:1-product stay at the start line

The brown precipitate was dissolved in 100 ml water/MeOH (1:1) and mixed with 10 ml 3M aq. NH_4PF_6 . The brown precipitate formed (PF_6^- salt), was isolated, washed with water and dried under high vacuum (0.68 g, 51 %).

^1H NMR (CD_3CN , 250 MHz): 4.77 (s, CH_2 , 6H); 5.81 (s, CH_2 , 6H); 6.04 (s, CH_2 , 6H); 7.92-7.71(m, CHarom., 27H); 8.49 (bs, Vio, 12H); 8.69 (bs, Vio, 12H); 8.99 (bs, Vio, 6 H); 9.05 (bs, Vio, 6 H); 9.21 (bs, Vio, 12H).

^{13}C NMR (CD_3CN , 63 MHz): 31.51 (CH_2); 63.49 (CH_2); 63.66 (CH_2); 125.09;

125.68; 127.40; 127.49; 127.60; 127.73; 131.25; 131.43; 131.83; 134.90; 136.62; 141.87; 142.94; 143.22; 145.71; 145.89; 145.99; 150.57; 150.77.

IR: aromatic C-H (w, 3135; w, 3075), aromatic C=N⁺ (s, 1635),¹³⁶ aromatic C=C (w, 1560; s, 1494; s, 1447; s, 1422), aromatic C-H in plane bending (w, 1000-1250), aromatic C-H out of the plane (s, 810), aliphatic C-Br (s, 552).

Elemental analysis for C₁₁₁H₉₃Br₃F₇₂N₁₂P₁₂: C 37.30; H 2.62; N 4.70 (calc.), C 37.06; H 2.98; N 5.11 (found).

Chemical polymerization of **4** was performed after a modified procedure described by Malvestiti et al.¹³⁷

Poly-4: Compound **4** (0.02 g, 5.5* 10⁻⁶ mmol) dissolved in 4 ml DMF was stirred with one Zn pellet at RT and under Ar until the color of the solution turned into dark green. 0.4 ml saturated aq. NH₄Cl solution was added to the mixture at which point the anion exchange with Cl⁻ takes place and the mixture precipitated. Water (ca. 2ml) was added to obtain a clear solution. After being stirred for 5 h at RT and under Ar, the Zn pellet was removed from the mixture, then the solution was filtered and washed with water and acetone (ca. 0.012 g, 60 %).

FT-IR: aromatic C-H (w, 3117; w, 3035), aromatic C=N⁺ (s, 1632),¹³⁶ aromatic C=C (w, 1558; s, 1505; s, 1442; s, 1419), aromatic C-H in plane bending (w, 1000-1250), aromatic C-H out of the plane (s, 821).

Poly-4-CNTs composites: Compound **4** (0.02 g, 5.5*10⁻⁶ mmol), dissolved in 4 ml DMF, and 0.009 g CNTs were ultrasonicated for 10 minutes. One Zn pellet was added to the solution and the mixture stirred at RT under Ar until the color of solution turned into dark green. 0.4 ml saturated aq. NH₄Cl and 0.2 ml

water were added to the mixture and stirred for 5 h under Ar. The Zn pellet was removed from the mixture, the solution filtered and the brown powder washed with water and acetone.

5•12PF₆ (C₁₁₁H₉₆F₇₂N₁₂O₃P₁₂):

0.2 g (0.05 mmol) of **4•12PF₆** in 90 ml MeCN/water (1:1, V/V), was stirred for 72 hours at 70°C. The mixture was then allowed to cool at RT, the solvent evaporated, the residue dissolved in MeCN and added to 5 ml TBACl (1M solution in MeCN). The brown precipitate (Cl⁻ salt) was collected by filtration and washed with MeCN to remove excess of TBACl. After precipitation from MeOH/diethyl ether, the product was converted into PF₆⁻ salt, was filtered, and washed with water to remove excess of NH₄PF₆ and then dried under high vacuum (0.16 g, 84.65 %).

¹H NMR (CD₃CN, 250 MHz): 3.58 (s, OH, 3H); 4.80 (s, CH₂, 6H); 5.88 (s, CH₂, 6H); 6.04 (s, CH₂, 6H); 7.70 (bs, CH_{arom.}, 3H); 7.92-7.78 (m, CH_{arom.}, 24H); 8.49 (bs, Vio, 12H); 8.69 (bs, Vio, 12H); 8.98 (d, J= 5 Hz, Vio, 6H), 9.05 (bs, Vio, 6H); 9.22 (bs, Vio, 12H).

¹³C NMR (CD₃CN, 63 MHz): 62.55 (CH₂); 63.50 (CH₂); 63.68 (CH₂); 124.39; 125.68; 127.35; 127.46; 127.60; 127.73; 128.33; 131.44; 131.83; 134.89; 136.60; 143.23; 145.70; 145.88; 146.00; 146.92; 150.59; 150.77.

6•15PF₆ (C₁₄₁H₁₁₇F₉₀N₁₈P₁₅):

To a solution of 0.3 g (1.92 mmol) 4,4'-bipyridine dissolved in 4 ml MeCN at 70°C, 0.4 g (0.11 mmol) **4•12PF₆** dissolved in 40 ml MeCN was added in portions with stirring over a period of 6 h. The mixture was stirred further for 3 days at 70°C. It was then allowed to cool to RT. The reaction mixture was

diluted with 100 ml MeCN and then added to 10 ml 1M TBACl (solution in MeCN). The precipitated Cl^- salt was filtered, washed with MeCN to remove excess of TBACl, dried for 3 h under high vacuum and then dissolved in 100 ml water. The water phase was washed three times with 100 ml chloroform to remove an excess of 4,4'-bipyridine, and then the water evaporated. The residue was dissolved in 100 ml water and added to 10 ml 3M aq. NH_4PF_6 to convert the product into PF_6^- salt. Then, the brown precipitate was filtered, washed with water to remove excess of NH_4PF_6 and dried under high vacuum (0.3126 g, 66 %).

^1H NMR (CD_3CN , 250 MHz): 5.88 (s, CH_2 , 6H); 5.98 (s, CH_2 , 6H); 6.04 (s, CH_2 , 6H); 7.70 (s, $\text{CH}_{\text{arom.}}$, 3H); 7.87-7.92 (m, $\text{CH}_{\text{arom.}}$, 24 H); 8.47-8.49 (m, Vio, 24 H); 8.70 (d, $J = 7.5$ Hz, Vio, 12H); 8.92 (dd, $J = 5.0$ Hz, Vio, 18H); 9.06 (d, $J = 7.5$ Hz, Vio 6H); 9.21 (d, $J = 5.0$ Hz, Vio, 12H).

^{13}C NMR (CD_3CN , 63 MHz): 62.97 (CH_2); 63.50 (CH_2); 63.67 (CH_2); 122.58; 125.63; 125.68; 126.70; 127.52; 127.60; 127.73; 131.23; 131.43; 131.83; 134.89; 136.61; 137.04; 142.53; 143.12; 143.23; 145.39; 145.73; 145.87.

Elemental analysis for $\text{C}_{141}\text{H}_{117}\text{F}_{90}\text{N}_{18}\text{P}_{15} \cdot 13\text{H}_2\text{O}$: C37.86, H3.22, N5.63 (calc.), C37.56, H3.57, and N5.77 (found).

$7 \cdot 24\text{PF}_6$ ($\text{C}_{213}\text{H}_{177}\text{Br}_3\text{F}_{144}\text{N}_{24}\text{P}_{24}$):

To a solution of 0.363 g (0.46 mmol) 1,1'-bis-(4,4'-bromomethyl-phenyl)-4,4'-bipyridinium bis (hexafluorophosphate) (**2**) dissolved in 20 ml MeCN at 70°C, 0.2 g (0.055 mmol) of **6•15PF₆**, dissolved in 20 ml MeCN, was added in portions while stirring over a period of 5 h. The mixture was stirred further for 5 days at 70°C. After cooling to RT, the reaction mixture was diluted with 40 ml MeCN and then added to 10 ml 1M TBACl (solution in MeCN). The

precipitated Cl^- salt was filtered, washed with MeCN to remove an excess of TBACl, and then recrystallized from MeOH (60 ml)/diethyl ether (100 ml) mixture. The brown precipitate formed was filtered, dissolved in 50 ml water and added to 5 ml 3M aq. NH_4PF_6 . The PF_6^- salt was filtered, washed with water and dried in vacuum (0.178 g, 46.90 %).

^1H NMR (CD_3CN , 250 MHz): 4.77 (s, CH_2 , 6H); 5.74 (s, CH_2 , 6H); 6.05 (s, CH_2 , 18H); 7.90 (bs, $\text{CH}_{\text{arom.}}$, 51H); 8.50 (bs, Vio, 24H); 8.69 (bs, Vio, 24H); 8.99-9.06 (m, Vio, 24H); 9.21 (bs, Vio, 24 H).

^{13}C NMR (CD_3CN , 63 MHz): 31.51 (CH_2); 63.50 (CH_2); 63.68 (CH_2); 125.09; 125.68; 127.40; 127.52; 127.61; 127.74; 127.82; 131.25; 131.44; 131.83; 134.89; 136.64; 143.23; 145.73; 145.88; 146.00; 150.58; 150.76.

$10\cdot 10\text{PF}_6$ ($\text{C}_{90}\text{H}_{66}\text{F}_{60}\text{N}_{18}\text{O}_{16}\text{P}_{10}$):

Compound **8** (4.8 g, 10.25 mmol) was dissolved in 50 ml MeCN and stirred at 70°C. 1.9 g (1.95 mmol) of **9·2PF₆** in 20 ml MeCN were added in portions. The reaction mixture was stirred at 70°C for 72 h; 100 ml of diethyl ether was then added. The solid formed was filtered and dissolved in conc. HBr to perform anion exchange to Br^- . The excess of acid was distilled, the residue dissolved in MeOH and the product purified by several recrystallizations from MeOH/diethyl ether mixture (1:1). Finally, the brown precipitate was dissolved in MeOH/ H_2O mixture and added to 10 ml 3M aq. NH_4PF_6 . Then, the precipitated PF_6^- salt was filtered, washed with water and dried under high vacuum (4.04 g, 66.60 %).

^1H NMR (DMSO , 250 MHz): 6.16 (bs, $\text{CH}_2\text{-N}^+$, 8H); 8.25 (bs, $\text{CH}_{\text{arom.}}$, 6H); 8.39 (bs, $\text{CH}_{\text{arom.}}$, 4H); 9.05 (bs, $\text{CH}_{\text{arom.}}$ + Vio, 24H); 9.19 (bs, $\text{CH}_{\text{arom.}}$, 4H); 9.54 (bs, Vio, 4H); 9.71 (bs, Vio, 16H).

^{13}C NMR (DMSO, 63 MHz): 62.98; 122.05; 126.93; 127.32; 127.72; 130.82; 132.28; 136.68; 138.69; 143.00; 143.41; 146.20; 146.90; 147.74; 149.37; 149.88; 150.11; 151.43.

Elemental analysis for $\text{C}_{90}\text{H}_{66}\text{F}_{60}\text{N}_{18}\text{O}_{16}\text{P}_{10}$: C34.81, H2.14, N8.11 (calc.), C34.53, H2.60, N8.12 (found).

$11\cdot 10\text{PF}_6$ ($\text{C}_{98}\text{H}_{90}\text{F}_{60}\text{N}_{10}\text{O}_8\text{P}_{10}$):

2.74 g (0.88 mmol) of $10\cdot 10\text{PF}_6$ and 0.91 g (5.97 mmol) 3,5-bis(hydroxymethyl)aniline were dissolved in 300 ml MeCN and refluxed for 72 h. The purification of **11** from 3,5-bis (hydroxymethyl)-aniline and 2,4-dinitroaniline side product was achieved by several precipitations from MeOH/diethyl ether (1:2) of the corresponding Cl^- salt. Finally, the brown precipitate was dissolved in MeOH/ H_2O mixture and added to 10 ml 3M aq. NH_4PF_6 . Then, the precipitated PF_6^- salt was filtered, washed with water and dried under high vacuum (1.05 g, 40 %).

^1H NMR (CD_3CN , 250 MHz): 3.57 (bs, OH, 8H); 4.78 (s, $\text{CH}_2\text{-O}$, 16H); 6.07 (s, $\text{CH}_2\text{-N}^+$, 8H); 7.69 (d, $J = 6.75$ Hz, $\text{CH}_{\text{arom.}}$, 12H); 8.01 (s, $\text{CH}_{\text{arom.}}$, 4H); 8.08 (s, $\text{CH}_{\text{arom.}}$, 2H); 8.59 (d, $J = 4.75$ Hz, Vio, 16H); 8.71 (d, $J = 6.75$ Hz, Vio, 4H); 9.08 (d, $J = 6.75$ Hz, Vio, 8H); 9.20 (d, $J = 6.5$ Hz, Vio, 12H).

^{13}C NMR (CD_3CN , 63 MHz): 62.54 ($\text{CH}_2\text{-O}$); 63.23 ($\text{CH}_2\text{-N}^+$); 120.60; 127.13; 127.26; 127.50; 127.63; 127.73; 134.05; 136.20; 142.52; 143.41; 145.53; 145.57; 145.74; 146.13; 150.43; 150.71; 151.19.

$12\cdot 10\text{PF}_6$ ($\text{C}_{98}\text{H}_{82}\text{Br}_8\text{F}_{60}\text{N}_{10}\text{P}_{10}$):

1 g (0.33 mmol) of $11\cdot 10\text{PF}_6$ was dissolved in 100 ml HBr in AcOH (5.7M) and stirred at RT for 4 days while protected from light. The acid was

evaporated and the crude product washed with 100 ml ethyl acetate. Anion exchange was further performed by dissolving the precipitate in 150 ml MeOH/H₂O mixture (1:3) and adding it to 15 ml 3M aq. NH₄PF₆. Then, the precipitated PF₆⁻ salt was filtered, washed with water and dried under high vacuum (0.84 g, 72 %).

¹H NMR (CD₃CN, 250 MHz): 4.75 (bs, CH₂-Br, 16H); 6.09 (bs, CH₂-N⁺, 8H); 7.84 (bs, CHarom., 8H); 7.95 (bs, CHarom., 4H); 8.04 (bs, CHarom., 6H); 8.62 (bs, Vio, 16H); 8.74 (bs, Vio, 4H); 9.13 (bs, Vio, 8H); 9.21 (bs, Vio, 12H).

¹³C NMR (CD₃CN, 63 MHz): 31.01 (CH₂-Br); 63.25 (CH₂-N⁺); 124.95; 127.17; 127.36; 127.64; 127.79; 133.04; 134.11; 136.20; 141.92; 142.56; 143.41; 145.66; 145.75; 146.16; 150.59; 150.95; 151.20.

13•26PF₆ (C₂₂₆H₁₇₀F₁₅₆N₄₂O₃₂P₂₆):

0.81 g (1.74 mmol) of **8** was dissolved in 25 ml MeCN and heated at 70°C. While stirring, 0.49 g (0.14 mmol) of **12•10PF₆** dissolved in 15 ml MeCN were added to the above solution. The reaction mixture was stirred for 6 days. The formed precipitate was filtered, dissolved in conc. HBr and stirred for 10 min. The acid was distilled, and the crude product dissolved in water, and then added to 5 ml 3M aq. NH₄PF₆. Then the precipitated PF₆⁻ salt was filtered, washed with water and dried under high vacuum (0.78 g, 71.34 %).

¹H NMR (CD₃CN, 250 MHz): 6.07 (bs, CH₂-N⁺, 24H); 8.03 (bs, CHarom., 18H); 8.18 (bd, J = 8.5 Hz, CHarom., 8H); 8.58 (bs, Vio + CHarom., 28H); 8.66 (bs, Vio, 20H); 8.87 (bs, CHarom., 8H); 9.10 (bs, Vio, 32H); 9.16 (bs, Vio, 32H).

¹³C NMR (CD₃CN, 63 MHz): 63.33 (CH₂-N⁺); 122.29; 127.25; 127.49; 127.83;

128.00; 130.54; 131.60; 134.10; 136.13; 138.07; 143.30; 143.42; 145.67; 146.20; 146.80; 150.16; 150.43; 150.55; 151.19; 151.51; 152.92.

14•26PF₆ (C₂₄₂H₂₁₈F₁₅₆N₂₆O₁₆P₂₆):

0.73 g (0.094 mmol) of **13•26PF₆** in 100 ml MeCN was mixed with 0.17 g (1.14 mmol) 3,5-bis(hydroxymethyl)aniline in 30 ml MeCN and refluxed for 4 days. The solution was concentrated by evaporation (ca. 30 ml). Then, 50 ml diethyl ether was added, and the formed precipitate was filtered, washed two times with MeOH and dried under high vacuum (0.56 g, 79.61 %).

¹H NMR (DMSO, 500 MHz): 4.66 (s, CH₂-OH, 32H); 6.09 (s, CH₂-N⁺, 16H); 6.18 (s, CH₂-N⁺, 8H); 7.66 (d, J= 9 Hz, CHarom., 24H); 8.05 (t, J= 6.5 Hz, CHarom., 8H); 8.15 (d, J= 5.5 Hz, CHarom., 4H); 8.22 (t, J= 7 Hz, CHarom., 6H); 8.74 (d, J= 6 Hz, Vio, 16H); 8.77 (d, J= 7 Hz, Vio, 16H); 8.87 (d, J= 7 Hz, Vio, 16H); 9.31(d, J= 6.5 Hz, Vio, 8H); 9.38 (d, J= 6 Hz, Vio, 16H); 9.44 (d, J= 6 Hz, Vio, 8H); 9.50 (d, J= 6.5 Hz, Vio, 16H); 9.58 (d, J= 5 Hz, Vio, 4H); 9.65 (bs, Vio, 4H).

¹³C NMR (DMSO, 126 MHz): 61.98; 62.42; 122.06; 122.10; 125.44; 126.43; 126.61; 126.92; 127.10; 136.13; 142.12; 142.78; 144.87; 144.94; 145.00; 145.09; 145.44; 145.76; 146.05; 149.29; 149.52; 150.69; 150.88.

Elemental analysis for C₂₄₂H₂₁₈F₁₅₆N₂₆O₁₆P₂₆•25H₂O: C36.48, H3.39, N4.57 (calc.), C36.06, H3.48, and N4.79 (found).

3 Synthesis and characterization of π -conjugated rod-like viologens

3.1 Introduction

The optical and electrochemical properties of conjugated oligomers makes their use in construction of light-weight batteries,¹³⁸ thin-film transistors,^{139,140} light-emitting diodes¹⁴¹⁻¹⁴³ and photovoltaic cells (PV) possible.^{47,144} Organic PV devices are made by creating an interface of an electron-rich material (p-type) with an electron-poor material (n-type). Most of the known organic oligomers or polymers are hole-transporting (p-type), on the other hand n-type semiconductors (electrons carriers) are far less developed.¹⁴⁵ A variety of n-type oligomers have been designed and synthesized to control the band gap in order to achieve the desired electrical and optical properties. The majority of OTFTs (organic thin film transistors) consists of fullerene derivatives as electron acceptor which were combined with PCBM (phenyl-C61-butyric-acid-methyl-ester) to increase the absorption in the visible and near-infrared region and OTFTs mobility^{146,147} therefore, the synthesis of n-type oligomers with large absorption in the visible region is a big challenge from the point of view of technical applications.

1,1'-Disubstituted 4,4'-bipyridinium salts (viologens) are possible candidates for the design of new n-type oligomers as these species have interesting redox (they can be electrochemically reduced) and electrochromic properties.¹⁴⁸

Oligomers having 4,4'-bipyridinium moieties substituted with biphenyl groups are expected to be easily electrochemically reduced and possibly show conductivity in this potential range. Over the past two decades, a lot of

efforts have been made for developing synthesis of extended viologens or viologen-analogs.

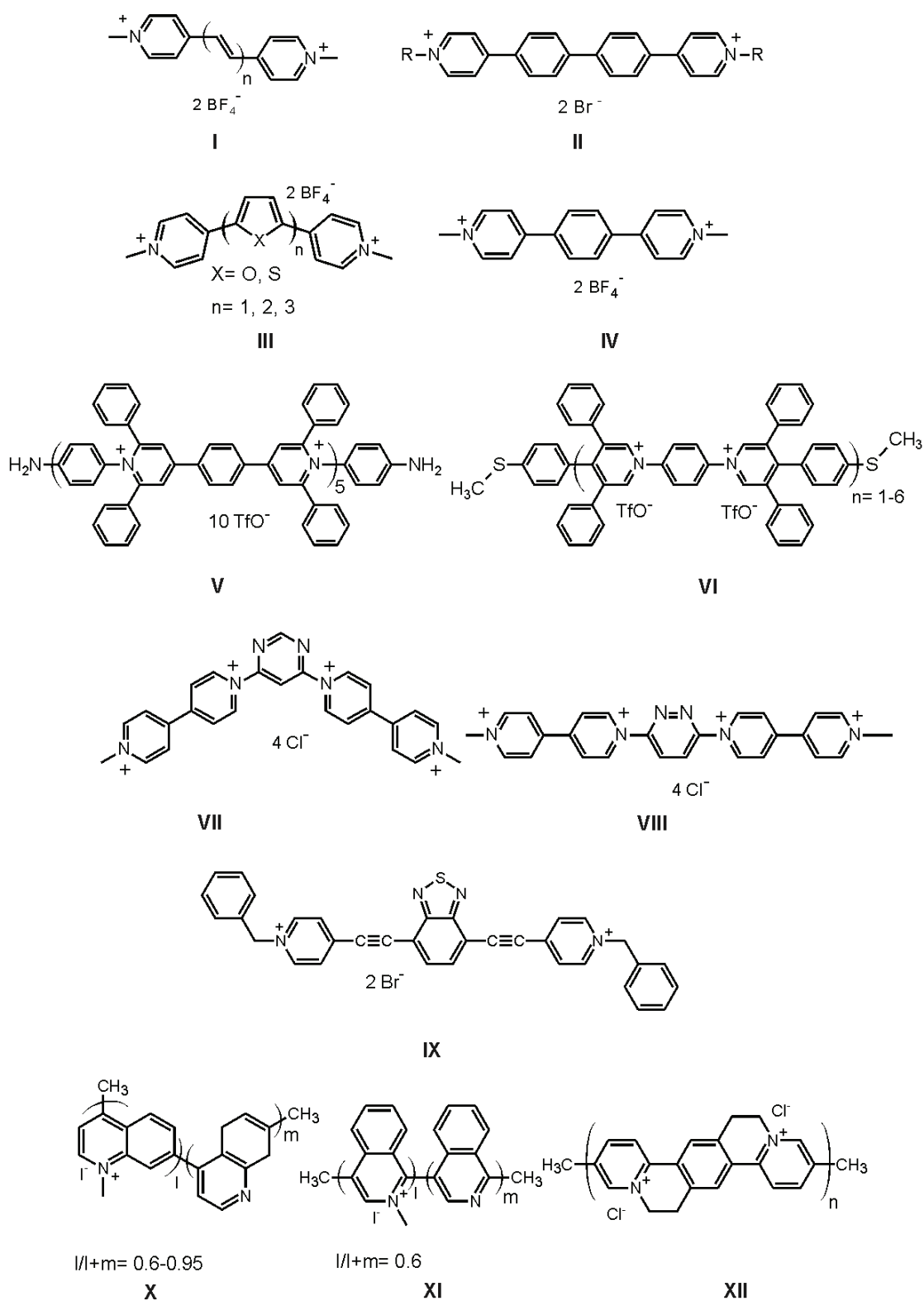


Figure 3.1 Conjugated viologen-analog monomers, oligomers and polymers from literature.

The extended viologens **III** and **IV** undergo reversible two-step one-electron reduction in the cyclic voltammetry (CV), indicating the formation of stable radical cations and neutral species.^{86,149,150} The compounds **I** and **II** undergo one-step two-electron reduction to neutral species,^{151,152} whereas compound **IX** undergo only one-electron reversible reduction.¹⁵³ M. Valášek et al. synthesized extended oligomeric viologens (**V**, **VI**) from p-connected 1,4-benzene and 1,4-pyridinium rings. They show a reversible multi-step electron transfer in the CV.^{84,154-156} Matsushita et al.^{157,158} have shown that **VII** and **VIII** are reduced by two electrons, whereas **VII** shows a biradical character according to ESR measurements. Poly(quinolinium) and poly(isoquinolinium) salts **X** and **XI**, showing viologen-like behavior, were also synthesized. Only compound **X** forms stable radical cations upon 1 e⁻ reduction (dark purple) which is further electrochemically reduced to the neutral molecule. Compound **XI** shows two irreversible 1 e⁻ reduction steps.¹⁵⁹ Izuhara et al. synthesized conjugated polymers with bipyridinium-phenylene units (**XII**) exhibiting viologen-like redox behavior and n-type conductivity.¹⁶⁰

This chapter focuses on the preparation and characterization of new π -conjugated, electroactive, cationic molecular rods. The structure can be considered as an N-analogue of oligo-p-phenylene with the nitrogen carrying positive charges. It can be also considered as an oligomeric chain of dialkoxyphenyl viologens or sequential arrangement of 3,3'-alkoxybiphenyl and 4,4'-bipyridinium units as an alternating chain of moderate electron donor and strong electron acceptor units, respectively. The most discussed oligomers are presented in Fig. 3.2.

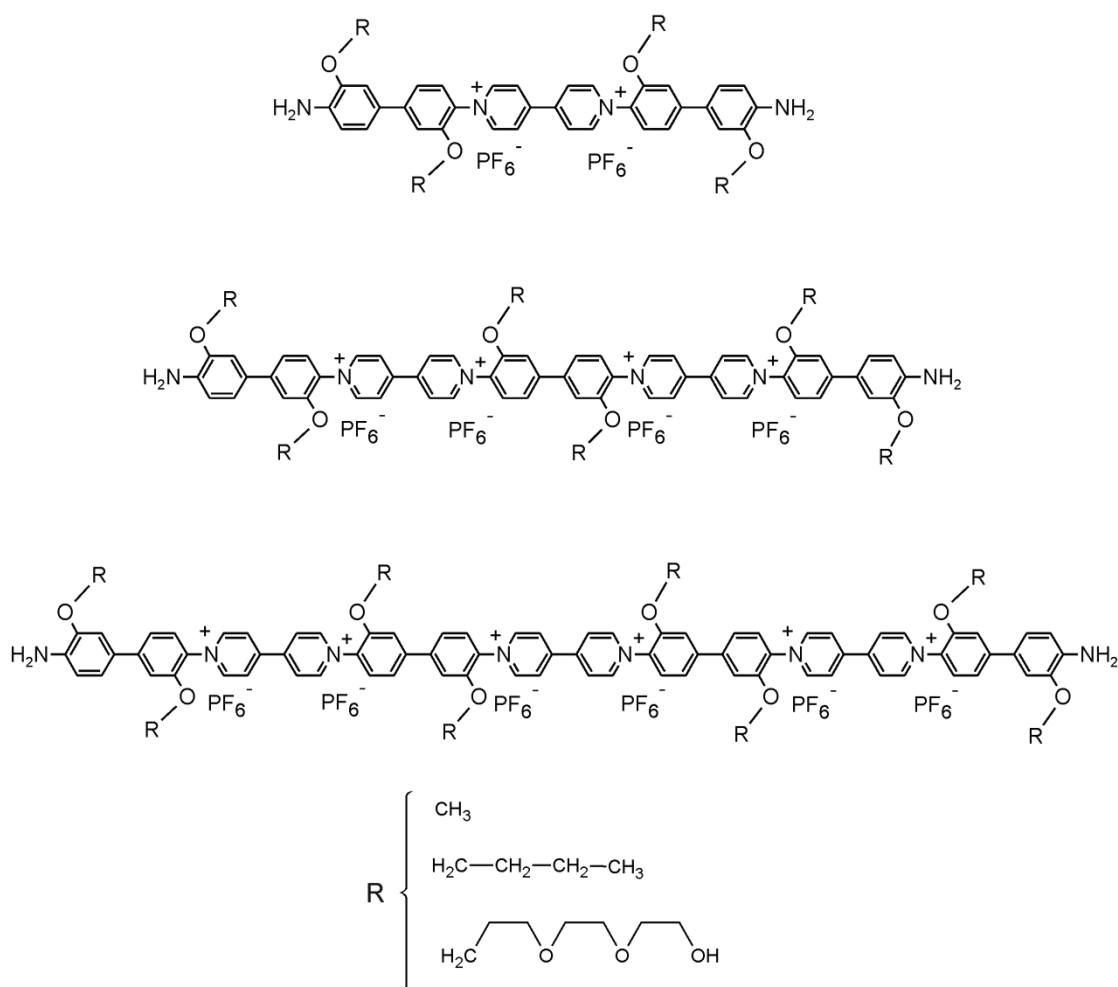


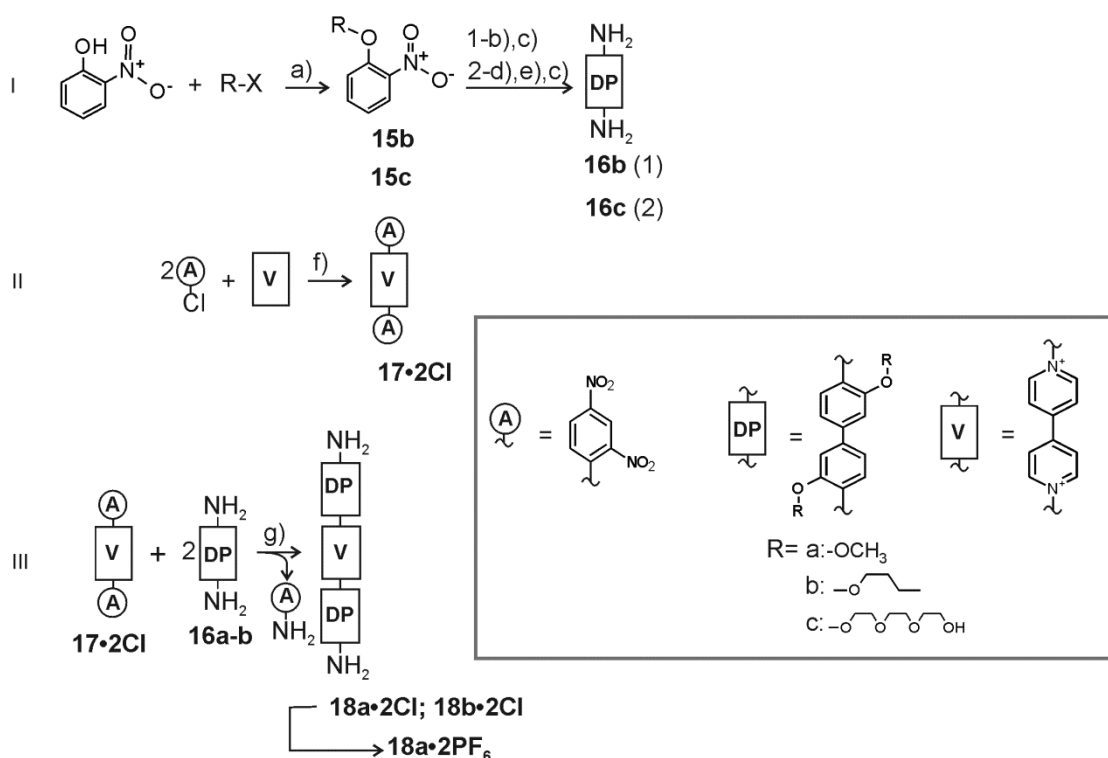
Figure 3.2 Chemical structures of the rod-like viologen oligomers discussed in this work.

3.2 Results and discussion

3.2.1 Synthesis

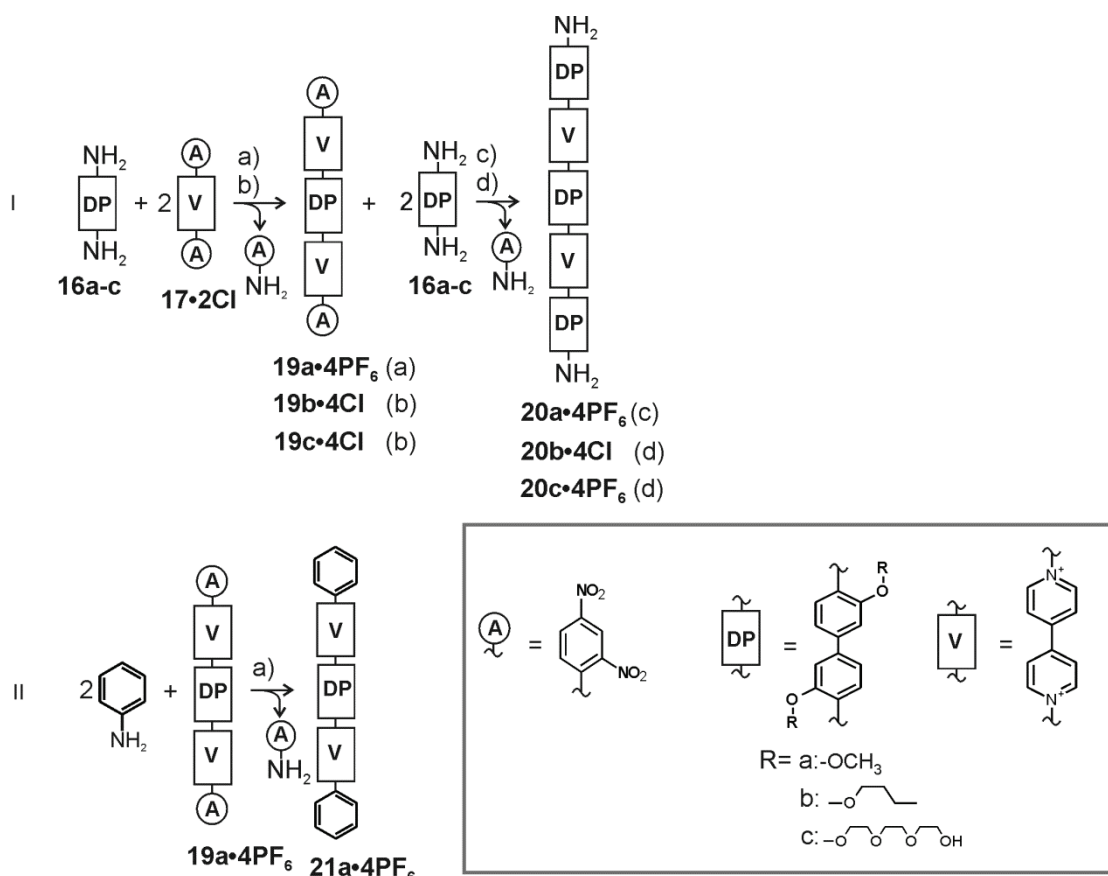
The synthesis of a series of new conjugated, electroactive rods consisting of biphenyl viologens are described in Schemes 3.1-3.3. The general strategy is based on the reaction of 1,1'-bis(2,4-dinitrophenyl)-4,4'-bipyridinium derivatives (**17**, **19a-c**, **22a-b**) with 4,4'-bis(aminobiphenyl) compounds (**16a-c** and **18a-b**) through a known reaction (the Zincke reaction).^{93,161,162} Selectivity was achieved using an excess of the additional peripheral groups.

It starts with the preparation of 1,1'-bis(2,4-dinitrophenyl)-4,4'-bipyridinium (**17•2Cl**) according to Nanasawa,⁹³ with minor modifications from 4,4'-bipyridine and an excess of 2,4-chlorobenzene (II, Scheme 3.1). It is followed by a double Zincke reaction between **17•2Cl** and two molecules of o-dianisidine (**16a**) in methanol/water to yield **18a•2Cl** containing a central dipyridinium unit (V) and two peripheral diphenyl units (DP) with two terminal –NH₂ groups in 82 % yield (abbreviated as NH₂-DP-V-DP-NH₂, III, Scheme 3.1). Notably, completeness and suppression of polymerization is solely controlled by the excess of o-dianisidine used in the reaction (1 eq. excess was sufficient). For its characterization the compound was quantitatively ion exchanged to give **18a•2PF₆**.



Scheme 3.1 Synthesis of rod-like 4,4'-bipyridinium monomers and their building blocks: a) DMF/K₂CO₃/90°C/3 days; b) benzene/Zn/NaOH 50 %/70°C/14 h; c) HCl 20 %; d) (CH₃)₂CO/Zn/NaOH/reflux/24 h; e) EtOAc/Zn/NaOH/reflux/12 h; f) CH₃CN /reflux/72 h; g) MeOH/reflux/20 h.

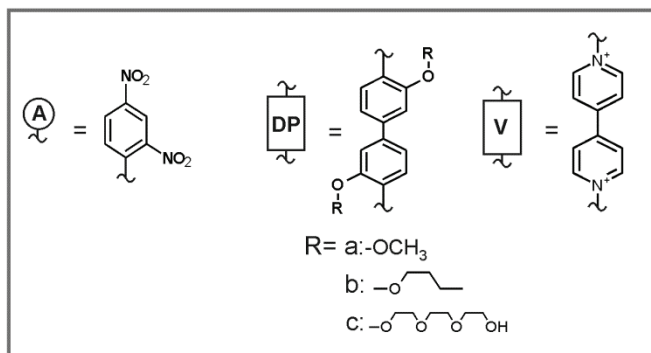
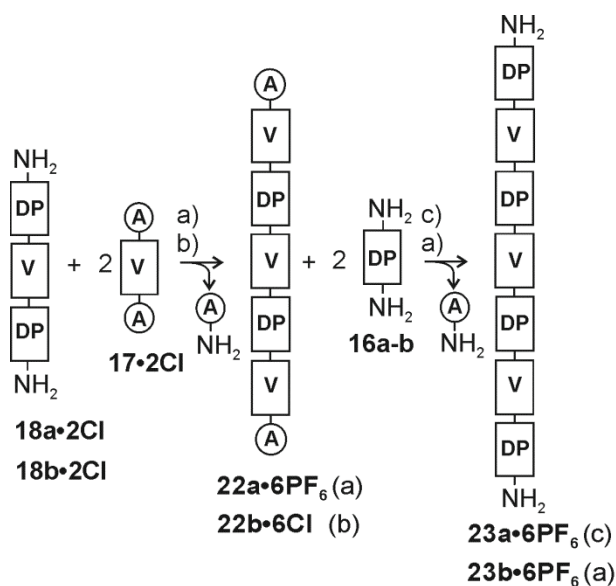
Further elongation of rod **18a•2Cl** is based on the same sequence of reactions. Treatment of **18a•2Cl** with a fourfold amount of the viologen unit **17•2Cl** yields after ion exchange **22a•6PF₆** in 86 % yield. Incorporation of the two peripheral DP-NH₂ groups was achieved by the treatment of **22a•6PF₆** with a fivefold amount of o-dianisidine to yield **23a•6PF₆** (NH₂-DP-V-DP-V-DP-V-DP-NH₂) in 93 % yield (Schemes 3.2 and 3.3).



Scheme 3.2 Synthesis of rod-like 4,4'-bipyridinium dimers and their building blocks: a) MeOH/reflux/48 h; b) MeOH/reflux/4 days; c) CH₃CN/reflux/48 h; d) MeOH/reflux/3 days.

In another series of syntheses, rods with DP as the central group (I, II, Scheme 3.2) are envisaged. Starting with o-dianisidine and a fourfold amount of **17•2Cl**, **19a•4PF₆** was obtained after ion exchange in 45 % yield. The corresponding amine-terminated rod **20a•4PF₆** (NH₂-DP-V-DP-V-DP-NH₂) was obtained in 50 % yield from treating with a fivefold excess of o-

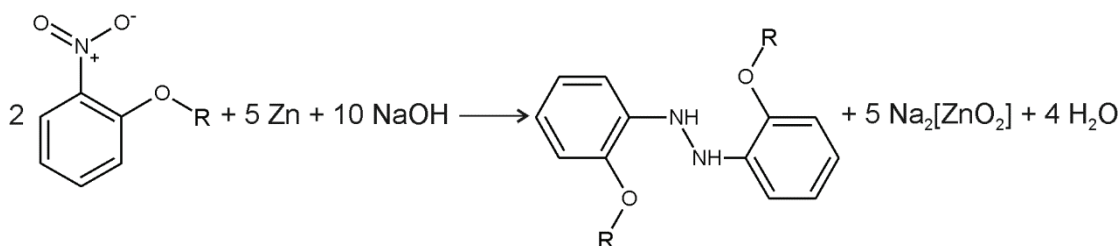
dianisidine. Compound **21a•4PF₆** was also prepared from **19a•4PF₆** but using aniline (10 eq.) instead of o-dianisidine in 74% yield.



Scheme 3.3 Synthesis of rod-like 4,4'-bipyridinium trimers and their building blocks: a) MeOH/reflux/3 days; b) MeOH/reflux/4 days; c) CH₃CN/reflux/48 h.

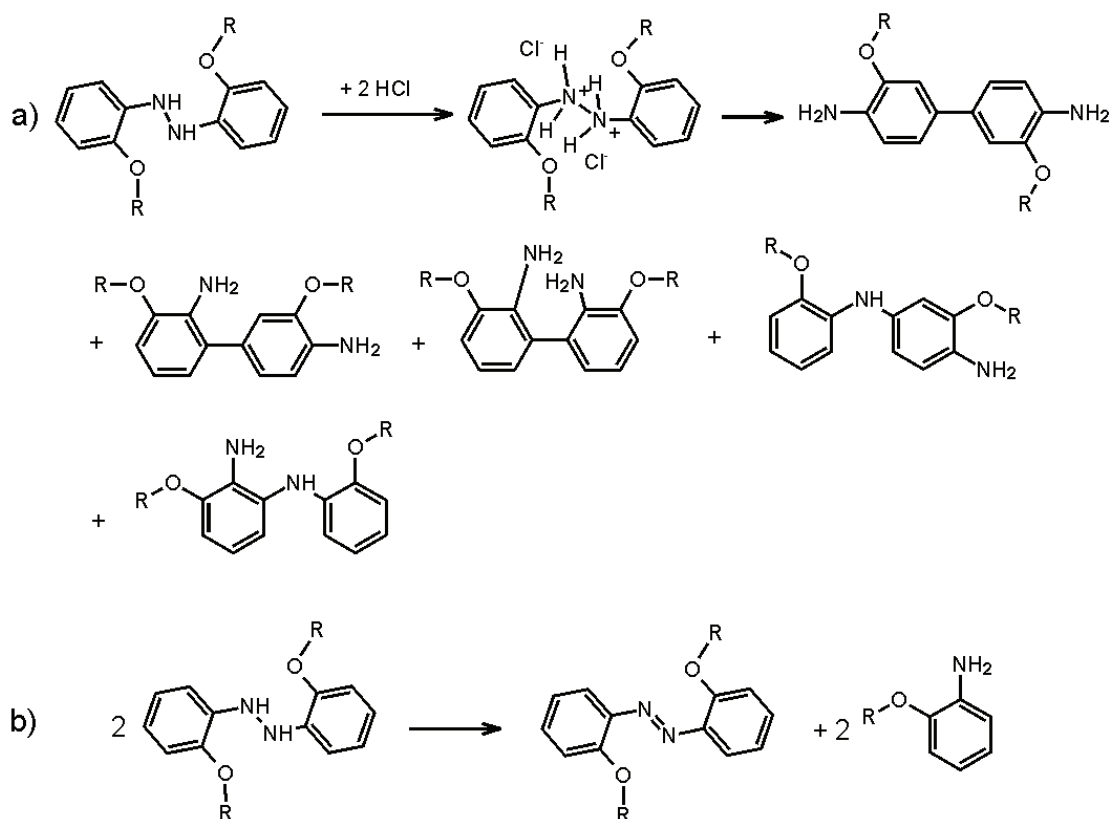
Separation of the product (**23a•6PF₆**, **22a•6PF₆**, **20a•4PF₆**, **19a•4PF₆**) from mixtures of starting material excess (**17•2Cl**) and from dinitroaniline side product was generally tedious due to their similar solubility, and purification of the product was achieved by repetitive precipitation of the salts from methanol/ethyl acetate (for Cl⁻ salts) or acetonitrile/diethyl ether (for PF₆⁻ salts). Other conjugated rods consisting of viologen and biphenyl alternating units were synthesized using the same scheme as for methoxy-biphenyl-viologen rod-like derivatives (see detailed synthetic procedure), but replacing

o-dianisidine (**16a**) with 3,3'-buthoxy-benzidine (**16b**) and 4,4'-diaminobiphenyl-3,3'-[(oxy)2-ethoxy]2-ethoxy]2-ethanol] (**16c**). The synthetic route to prepare **16b** and **16c** is shown in Scheme 3.1: I. The 2-alkoxy-nitrobenzene derivatives (**15b-c**) were first reduced with Zn and NaOH to hydrazobenzenes (Scheme. 3.4) and were further rearranged to benzidines in acidic conditions. The amount of Zn and base taken into the reaction is an important parameter for the benzidine rearrangement, due to the several parallel and consecutive reactions which may occur during the hydrogenation process.¹⁶³



Scheme 3.4 The reduction of 2-alkoxybenzene to 1,2-bis(2-alkoxyphenyl)hydrazine, in the presence of Zn and NaOH.

Compound **16c** was obtained by reduction of **15c** with Zn and NaOH in acetone and ethyl acetate, but in poor yield (22 %). Its preparation was a challenging task, due to the complicated mechanism of benzidine rearrangement which leads to a mixture of diaminobiaryls and amino-diarylamines (Scheme 3.5-a)^{164,165} and the disproportionation of hydrazoderivates which accompanies all acid-catalyzed rearrangements (Scheme 3.5-b).¹⁶⁶ However, the influence of some parameters as: solvent, Zn and base amount that may help to improve the yield of this reaction, was studied in a collaborative work with J. Ludden.¹⁶⁷



Scheme 3.5 Side products of acid-catalyzed benzidine rearrangement.

The reactivity of series b and c in the conjugated electroactive rods was reduced as compared with the 3,3'-methoxy-diphenyl homologous due to their large side chains attached to the diphenyl subunits.

Purification of compounds **19b-c**, **20b-c**, **22b**, **23b**, could not be accomplished by simple repetitive precipitation of the product from methanol/ethyl acetate (for Cl^- salts) or acetonitrile/diethyl ether (for PF_6^- salts). Repetitive column chromatography (elution with methanol) on Sephadex LH-20 was used as key purification step in case of **19b-c**, **20b-c**, **22b**, **23b**, as Cl^- salts (yield 21-33 %).

The purity control of the compounds is based on ^1H -NMR, ^{13}C -NMR, and elemental analysis after purification and drying. The same 4 groups of resonances (V, DP, NH and O- CH_2 -X) can be found for all rods **18a-b**• 2PF_6 , **20a-c**• 4PF_6 and **23a**• 6PF_6 (Fig. 3.3).

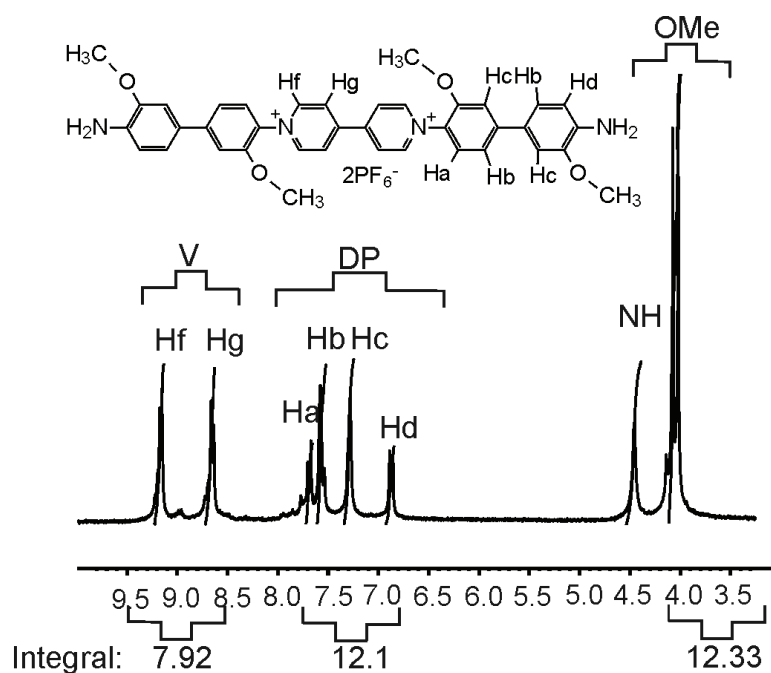


Figure 3.3 ^1H -NMR of **18a•2PF₆** measured in MeCN- d_3 .

Table 3.1 Integration of ^1H -NMR spectra of viologen oligomers with amine end-groups measured at 300 K.

Compound	experimental			theoretical		
	I_V/I_{DP}	I_A/I_{DP}	I_{O-CH_2-X}/I_{DP}	I_V/I_{DP}	I_A/I_{DP}	I_{O-CH_2-X}/I_{DP}
18a•2PF₆	0.65	0.33	1.02	0.66	0.33	1
18b•2PF₆	0.64	0.32	0.64	0.66	0.33	0.66
20a•4PF₆	0.90	0.22	1.01	0.88	0.22	1
20b•4PF₆	0.87	-	0.70	0.88	0.22	0.66
20c•4PF₆	0.87	-	0.70	0.88	0.22	0.66
23a•6PF₆	0.96	0.16	1.02	1	0.16	1

Where X is H, C₃H₇ or C₅H₁₁O₃; A is the integral of amine protons; DP is the integral of diphenyl protons; V is the integral of viologen protons; O-CH₂-X is the integral of the protons pertain to the first carbon atom in alkoxy groups.

The ratio of intensities for the four groups are specific for **18a-b•2PF₆**, **20a-c•4PF₆** and **23a•6PF₆** (Table 3.1, theoretical). The corresponding experimental values are as expected, confirming the structures unambiguously (experimental, Table 3.1.). These data, together with the elemental analyses corrected for some water content, ¹³C-NMR and the results from cyclic voltammetry indicate that a successful chain extension has occurred.

3.2.2 Electrochemical investigation of 18a-b, 20 a-b and 23a-b

To determine the electrochemical properties of these compounds and to estimate the energy levels of their highest occupied molecular orbital (HOMO) and lowest unoccupied molecular orbital (LUMO), cyclic voltammetry (CV) experiments were performed in DMF solutions containing 0.1M n-Bu₄NPF₆ using Ag/AgCl as the electrode reference at a scan rate of 50 mVs⁻¹.

As shown in Fig. 3.4, the monomeric, dimeric and trimeric viologen rods exhibit similar electroactivity. It involves two phenyl-viologen typical reversible reduction waves¹⁶⁸ and one irreversible oxidation of anilins.¹⁶⁹⁻¹⁷¹ Compounds **20a** and **23a** adsorb on the electrode surface as manifested by the sharp peaks at the second reduction potential in Fig. 3.4-a. Coulometry during bulk electrolysis indicates that the rods undergo an overall two-electron reduction for each viologen subunit present in the molecule, and the n_e (the number of exchangeable electrons) increase linearly with the number of viologen subunits (Table 3.2 and 3.3).

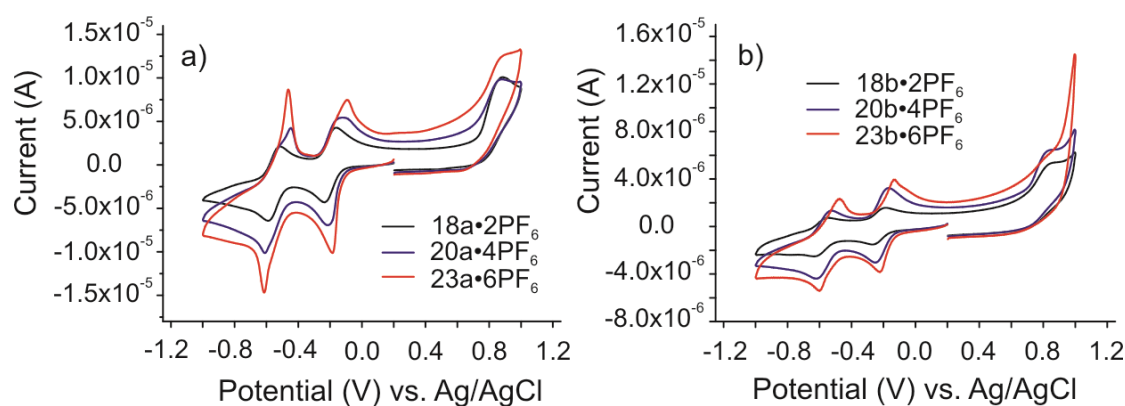


Figure 3.4 CVs of: a) methoxy substituted-rods (6.75×10^{-7} mol/ml); b) butoxy substituted-rods (2.61×10^{-7} mol/ml) in DMF solution containing 0.1M $n\text{-Bu}_4\text{NPF}_6$ at GC and a sweep rate of 50 mVs^{-1} .

As expected for the same concentration of monomer, dimer and trimer in a viologen oligomeric series, the peak current in CV increase with the number of viologen subunits of each molecule.

Table 3.2 Electrochemical properties and energy levels of viologen-oligomers.

Compound	$E_{1/2}^{\text{rd}(1)}$ (V)		n_e	$E_{1/2}^{\text{rd}(2)}$ (V)	E^{ox} (V)	Band gap (eV)
18a•2PF₆	-0.2 ^a	-0.23 ^b	0.75 ^c	-0.55 ^a	0.88 ^a	1.2
20a•4PF₆	-0.17 ^a	-0.18 ^b	1.21 ^c	-0.53 ^a	0.87 ^a	1.07
23a•6PF₆	-0.14 ^a	-0.16 ^b	1.16 ^c	-0.54 ^a	0.87 ^a	1.01
18b•2PF₆	-0.23	-0.24 ^b	-	-0.58	0.82	1.03
20b•4PF₆	-0.21	-0.22 ^b	-	-0.57	0.82	1.00
23b•6PF₆	-0.17	-0.19 ^b	-	-0.54	0.82	0.96

^aThe potentials could not be accurately determined by CV because of strong adsorption on electrode surface. ^bThe potentials determined by rotating disk voltammetry at 261.66 rad/sec rotational speed. ^cThe number of exchanged electrons per molecule is determined by potential-controlled bulk reductive electrolysis.

The HOMO and LUMO and thus the electrochemical band gaps, $E_g = (E_{\text{LUMO}} - E_{\text{HOMO}})$ were estimated by the relationship:¹⁷²

$$E_{\text{HOMO}} = -[E^{\text{onset ox}} + 4.65] \text{ eV} \quad (3.1)$$

$$E_{\text{LUMO}} = -[E^{\text{onset rd}} + 4.65] \text{ eV} \quad (3.2)$$

$E^{\text{onset ox}}$ and $E^{\text{onset rd}}$ were determined for the second reduction wave according to the usual procedure described in literature.¹⁷³ The electrochemically determined values of LUMO energies does not change or change very little within the two series of rods. The small HOMO-LUMO gap resulted upon electrochemical doping is also confirmed by the electronic absorption spectrum of the radical cation species, where a low energy band at 900-1100 nm (1.37-1.12 eV) is seen (Fig. 3.9).

With increasing length of the oligomers, the reduction potential becomes more positive. The graph of the first reduction peak potentials in the methoxy series vs. $1/N$ (N = number of viologen units) fits a straight line (Fig. 3.5-a).

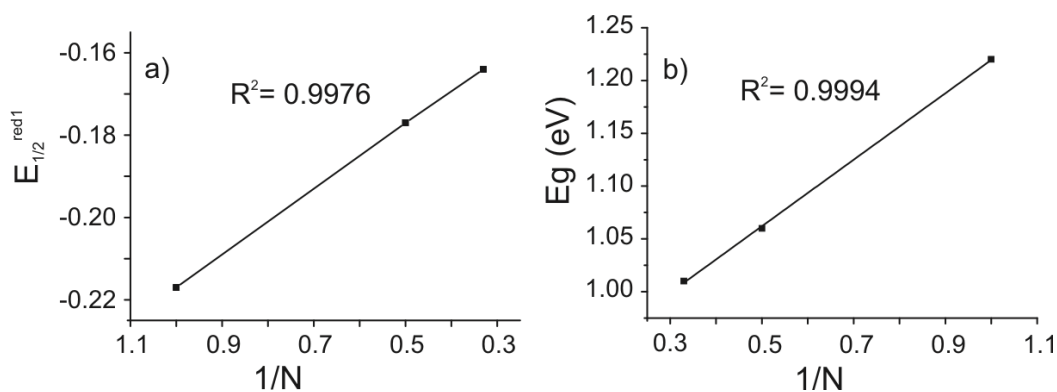


Figure 3.5 a) Plot of the $E_{1/2}^{\text{red } 1}$ of the methoxy-rod series versus $1/N$; b) Plot of the band gap of the methoxy-rod series versus $1/N$. The band gap was calculated with eq. 3.1 and 3.2 and N is equal to the number of viologen units in the oligomers.

The $1/N$ dependence on the reduction potential is not unexpected since the HOMO-LUMO gap of these oligomers also scales with $1/N$, and the reduction potential is related to the energy of the LUMO (Fig. 3.5-b).

Table 3.3 Number of exchanged electrons per molecule measured by preparative electrolysis coulometry.

Rod	Pot.Step (V)	I_{back} (A)	t(s)	Q_{back} (C)	Q_{exp} (C)	Q_{corr} (C)	Q_{theor} (C)	n(e)
20a•4PF₆	0.1 → -0.4	10^{-5}	4453	-0.04	-0.264	-0.224	-0.117	1.91
	-0.4 → 0.1	0	6000	-	0.259	-	0.117	2.21
21a•4PF₆	0.1 → -0.4	10^{-5}	6000	-0.06	-0.495	-0.435	-0.235	1.85
	-0.4 → 0.1	0	7000	-	0.430	-	0.235	1.82
23a•6PF₆	0.1 → -0.4	$2 \cdot 10^{-5}$	6000	-0.12	-0.742	-0.622	-0.187	3.32
	-0.4 → 0.1	0	8000	-	0.528	-	0.187	2.82

3.2.3 Diffusion coefficient investigation of methoxy-rods series

In order to measure the diffusion coefficient of **18a•2PF₆**, **20a•4PF₆** and **23a•6PF₆** several experiments were performed. First, the diffusion of the methoxy-substituted rods was studied in DMF using linear sweep voltammetry at a rotating disk electrode (RDE). For a rotating disk electrode, with area A (cm²) at angular velocity ω (rad x s⁻¹), the limiting current i_{lev} is given by the Levich^{124,174,175} eq.:

$$I_{\text{lev}} = 0.620 n F A D^{2/3} \omega^{1/2} \nu^{-1/6} C_0 \quad (3.3)$$

where n is the number of electrons transferred, F is the Faraday's constant (96485 C•mol⁻¹), D is the solution diffusion coefficient of the electroactive species (cm²s⁻¹), ν is the kinematic viscosity of the electrolyte (for DMF 9.19 *10⁻³ cm²s⁻¹) and C₀ is the concentration of the electroactive species in solution (mol/ml). All RDE measurements were performed in DMF using 0.1M

n-Bu₄NPF₆ as electrolyte at scan rate of 0.005 V/s. As shown in Table 3.4, the monomer's diffusion coefficient is 1.8 fold higher than that of the dimer which in turn is 1.3 times higher than that of the trimer. Considering that **18a•2PF₆** is the simplest rod-shaped viologen which was synthesized, the diffusion of more extended viologen-oligomers should be lower and the values of the diffusion coefficients smaller. As expected in the series of diphenyl-methoxy-viologen oligomers, D decreases from the monomer to the trimer showing that their mobility strongly depends on the viologen-oligomer molecular size. The effect of the viologen-oligomers concentration on the diffusion coefficient was also investigated. It was found that the diffusion coefficient of **23a•6PF₆** varies linearly with the concentration.

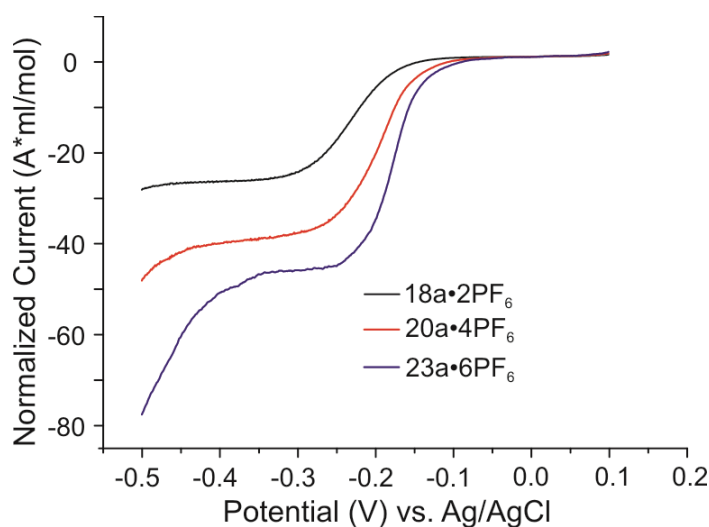


Figure 3.6 Current-potential curves for the reduction of **18a•2PF₆**, **20a•4PF₆** and **23a•6PF₆** with the rotating disk electrode at 314 rad/sec.

As the Fig. 3.7 and Table 3.4 show, a higher concentration is associated with a lower diffusion coefficient, a trend which was observed earlier for some organic and inorganic systems.¹⁷⁶

To cross-check the value of D obtained by the RDE method, the diffusion coefficient measurements were performed also with a gold microelectrode.

The expression of a quasi-steady-state voltammetry at a microdisc electrode has been shown to be:¹⁷⁷

$$I_{lim} = 4nFDcr \quad (3.4)$$

In this expression n denotes the number of electrons transferred per molecule, F is the Faraday constant, c is the concentration, and r is the radius of the electrode. All linear sweep voltammetric measurements at a gold disk microelectrode were performed in DMF using 0.1M $n\text{-Bu}_4\text{NPF}_6$ as electrolyte at a scan rate of 0.005-0.06 V/s.

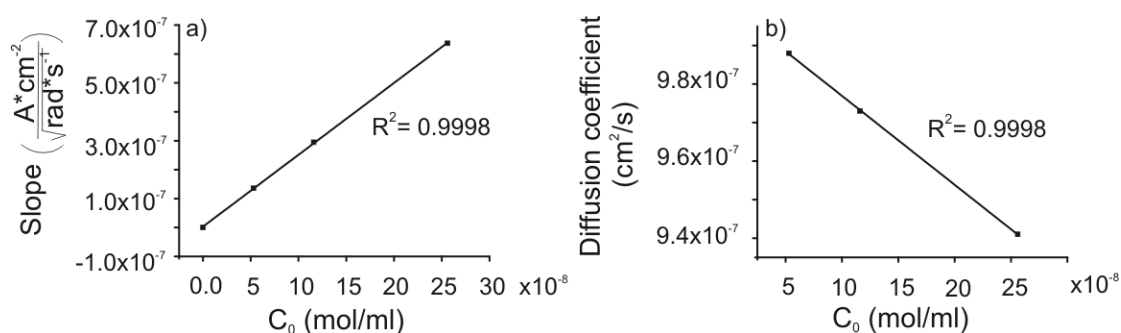


Figure 3.7 a) Slope-concentration dependence of **23a•6PF₆** and b) Diffusion coefficient-concentration dependence of **23a•6PF₆** in DMF-0.1M $n\text{-Bu}_4\text{NPF}_6$.

The diffusion coefficients of **18a•2PF₆**, **20a•4PF₆** and **23a•6PF₆** were calculated from the limiting current at the gold disk microelectrode obtained from reduction of the oligo-viologens at -0.5 V. This method leads to reasonable results. The obtained D values are in the same order of magnitude as determined by RDE (but smaller) showing the same trend.

DOSY is a simple and fast method for the determination of diffusion coefficient, and offers reasonable value with elimination of some factors which affects the precision of electrochemical methods.¹⁷⁸ Generally, ^1H -NMR spectra of the rods showed broad resonances because of the radicals formed as result of their lower reduction potential. To limit the effect of signal

broadening in $^1\text{H-NMR}$, the amino groups in oligo-viologen were protonated by 2 eq. PTSA (p-toluenesulfonic acid) in the NMR tube, and then DOSY measurements were performed. The diffusion coefficients obtained from the NMR experiments in d_6 -DMSO were almost identical to the values measured by RDE and correspond to the protonated molecules (Table 3.5).

Table 3.4 Diffusion coefficient values of **23a•6PF₆** at different concentrations.

Concentration (mol•ml ⁻¹)	D (cm ² s ⁻¹)	Slope (Acm ⁻² /(rads ⁻¹) ^{1/2})	R ²
2.56*10 ⁻⁷	0.941*10 ⁻⁶	6.37*10 ⁻⁷	0.9996
1.16*10 ⁻⁷	0.973*10 ⁻⁶	2.95*10 ⁻⁷	0.9995
0.53*10 ⁻⁷	0.988*10 ⁻⁶	1.36*10 ⁻⁷	0.9984

Table 3.5 Diffusion coefficients (D) of **18a•2PF₆**, **20a•4PF₆** and **23a•6PF₆**.

Compound	RDE	Microelectrode	DOSY	
	D (cm ² s ⁻¹)	D (cm ² s ⁻¹)	Protonated-form	D (cm ² s ⁻¹)
18a•2PF₆	2.29*10 ⁻⁶	1.03*10 ⁻⁶	18a•2PF₆•PTSA	1.73*10 ⁻⁶
20a•4PF₆	1.26*10 ⁻⁶	0.56*10 ⁻⁶	20a•4PF₆•PTSA	1.21*10 ⁻⁶
23a•6PF₆	0.94*10 ⁻⁶	0.44*10 ⁻⁶	23a•6PF₆•PTSA	0.93*10 ⁻⁶

3.2.4 Spectroelectrochemical investigation of π -conjugated rod-like viologens

The absorption spectra of **18a•2PF₆**, **18b•2PF₆**, **20a•4PF₆**, **20b•4PF₆**, **20c•4PF₆**, **21a•4PF₆**, **23a•6PF₆** and **23b•6PF₆** in DMF solution containing 0.1M n-Bu₄NPF₆ at 0.0 V are shown in Fig. 3.8. Viologen oligomers in the oxidized form shows the absorption peaks at ~280 nm and ~320 nm which are characteristic for π - π^* electronic transitions of bipyridinium salts.¹⁷⁹ Obviously, the introduction of new DP-V-DP subunit induced changes in the absorption spectra of viologen oligomers. The viologen monomers show two absorption bands at $\lambda_{\text{max}} = 316$ nm ($\epsilon = 34.8 \times 10^3$) and 485 nm observed for **18a•2PF₆** and at $\lambda_{\text{max}} = 320$ nm ($\epsilon = 40.3 \times 10^3$) and 412 nm for **18b•2PF₆**, respectively. Increasing the monomer length by a new DP-V-DP subunit (**20a-c**, **21a**, and **23a-b**) causes a shift of the absorption maximum to shorter wavelengths. The maximum absorption at ~320 nm becomes a shoulder and new absorption at $\lambda_{\text{max}} = 286$ nm (for **20a•4PF₆**, $\epsilon = 53.3 \times 10^3$), $\lambda_{\text{max}} = 287$ nm (for **21a•4PF₆**, $\epsilon = 49.7 \times 10^3$), $\lambda_{\text{max}} = 290$ nm (for **20b•4PF₆**, $\epsilon = 58.9 \times 10^3$) and $\lambda_{\text{max}} = 287$ nm (for **20c•4PF₆**, $\epsilon = 44.8 \times 10^3$) appeared. The absorption maxima of **23a•6PF₆** ($\lambda_{\text{max}} = 287$ nm, $\epsilon = 72.6 \times 10^3$) and **23b•6PF₆** ($\lambda_{\text{max}} = 287$ nm, $\epsilon = 92 \times 10^3$) are slightly shifted compared to those given by the lower molecular weight analog compound.

As the alkoxy group is changed from methoxy to ethylene oxide and butoxy, the absorption maxima are slightly shifted by 1-4 nm.

After a stepwise increase of the potential up to ~400 mV, viologen radical cations were electrochemically generated (the solution turned deep green). The well-known radical cation of methyl viologen and other alkyl substituted

viologens are blue,¹⁸⁰ while the viologen radical cations of the synthesized rods are deep green (except **18a•2PF₆**). During the reduction process of **18a•2PF₆** a color change from reddish brown to black was observed. The spectrum shows a broad low energy absorption band between 4.1-1.55 eV (302-800 nm) with a maximum of absorption at 1.58 eV (320 nm, $\epsilon = 31.1 \times 10^3$, -0.42 V).

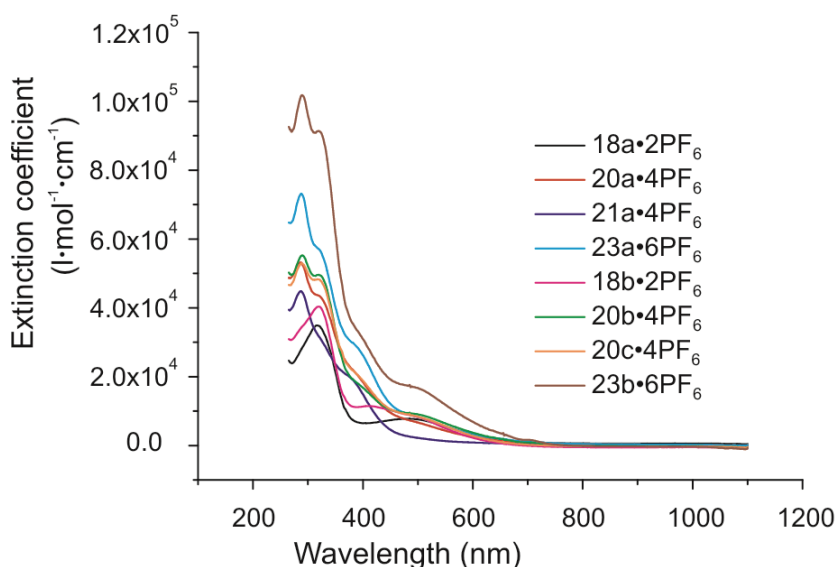


Figure 3.8 Wavelength-dependent extinction coefficients of the **18a-b•2PF₆**, **20a-c•4PF₆**, **21a•4PF₆**, and **23a-b•6PF₆** oligomers at 0.0 V.

The appearance of a shoulder at ca. 2.30 eV (540 nm, $\epsilon = 20 \times 10^3$) in the absorption spectra of $(H_2NDP)_2V^{+•}$ (**18a**) was discussed in terms of a dimer arrangement of bipyridine rings^{181,182} (Fig. 3.9). This absorption was not observed for the other viologen rods in the radical cation state. One explanation for the missing peak, is that the long alkoxy side chains of diphenyl subunits and the increased number of positively-charged nitrogens in one molecule, do not favorise the association of the viologen cations in dimers.¹⁸³ In contrast to the absorption spectrum of **18a**, the spectra of **18b**, **20a-c** and **23a-b** (Fig. 3.9) look similar, exhibiting absorptions in the range 320-800 nm and a maximum which is shifted from $\lambda_{max} = 318$ nm (for

18b•2PF₆, $\epsilon = 34.2 \times 10^3$, -0.34 V to 484 nm (for **23b•6PF₆**, $\epsilon = 67.5 \times 10^3$, -0.38 V).

The absorption band at 605-660 nm is assigned to the viologen radical cations,^{64,181,184} the broad absorption peaks between 708 nm and 1000 nm could not be clarified. It was observed for bis-viologen radical cations (as weak adsorption),¹⁸⁵ or it may originate from CT (charge-transfer) interaction between the electron-accepting viologen subunits and the electron-donating diphenoxy or amino groups¹⁸⁶.

Table 3.6 Extinction coefficient of oligomeric viologen-radical cations.*

Compound	Reduction potential (V)	λ_{\max} (nm)	ϵ (Lmol ⁻¹ cm ⁻¹)
18a•2PF₆	-0.42	320	31.1×10^3
18b•2PF₆	-0.34	318	34.2×10^3
20a•4PF₆	-0.38	441	36.6×10^3
20b•4PF₆	-0.38	658	51.7×10^3
20c•4PF₆	-0.38	457	44.5×10^3
21a•4PF₆	-0.40	451	48.8×10^3
23a•6PF₆	-0.44	463	38.8×10^3
23b•6PF₆	-0.38	484	67.5×10^3

* Extinction coefficients were established from UV-Vis in 0.1M n-Bu₄NPF₆ at the reduction potential with maximum adsorption.

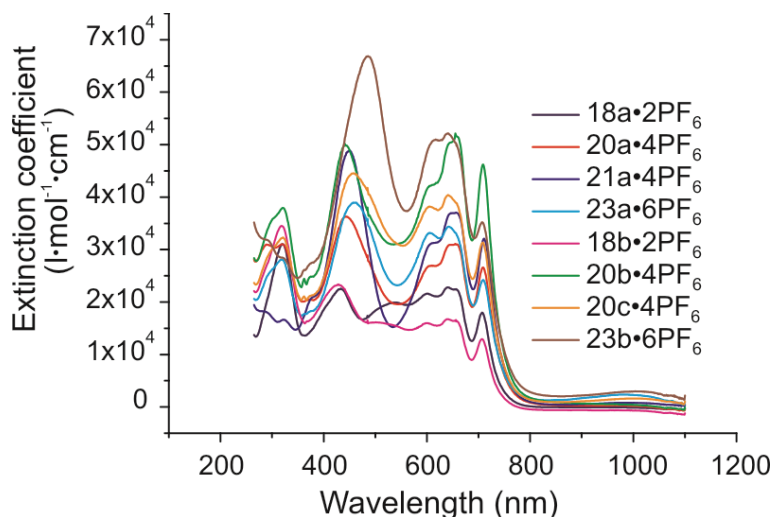


Figure 3.9 Wavelength-dependent extinction coefficients of **18a-b•2PF₆**, **20a-c•4PF₆**, **21a•4PF₆** and **23a-b•6PF₆** oligomers at -0.4 V.

Further reduction up to -0.7 V (vs. ref.) (Fig. 3.10) led to reddish-color solution with a maximum absorption between 390-490 nm (**21a•4PF₆**, **20b•4PF₆**, **20c•4PF₆**, **23a•6PF₆**, **23b•6PF₆**) and 311-319 nm (**18a•2PF₆**, **20a•4PF₆**, **18b•2PF₆**).

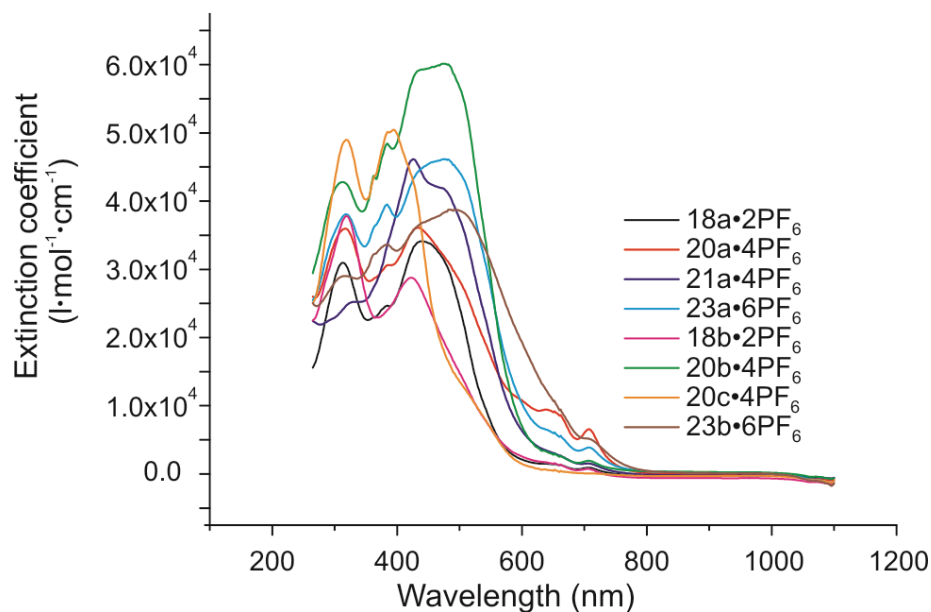


Figure 3.10 Wavelength-dependent extinction coefficients of **18a-b•2PF₆**, **20a-c•4PF₆**, **21a•4PF₆** and **23a-b•6PF₆** at -0.68 V.

The evolution of the peak absorption as a function of the number of viologen units in oxidized state shows a ca. 30 nm shift of the absorption

maximum to the lower wavelengths per viologen subunit addition. This effect has already been observed for other conjugated oligomers.¹⁸⁷ A further increase of the dimer length does not provoke important changes in the absorption maximum of the viologen-trimer, indicating that saturation of electronic delocalization has been achieved.¹⁸⁸

The extinction coefficients of **18a**•2PF₆, **20a**•4PF₆ and **23a**•6PF₆, in oxidized form, increases linearly with the number of viologen units present in molecule (Fig. 3.11). This kind of modification in absorbance was also observed for other conjugated molecules.¹⁸⁹

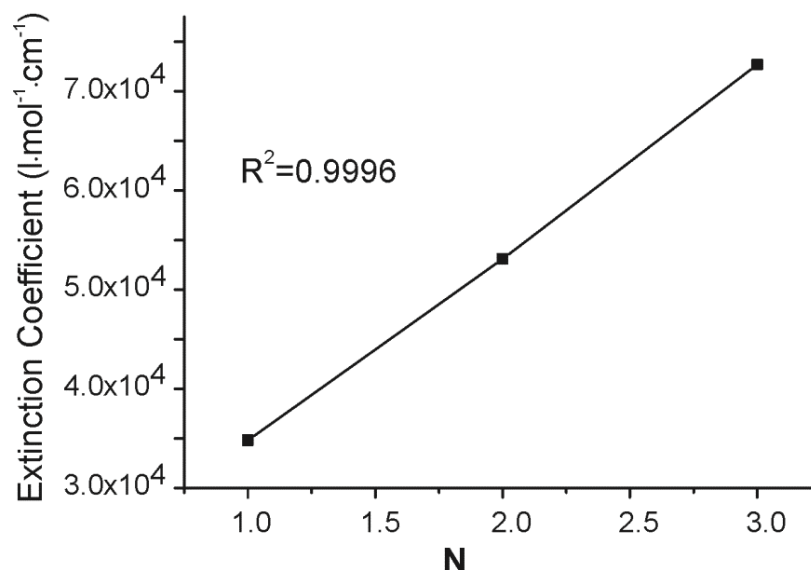


Figure 3.11 Dependence of ϵ (at λ_{\max}) on N (number of viologen subunits) for methoxy-substituted viologen-oligomers in oxidized form.

The predominant feature of the electronic absorption spectra of the viologen-oligomers is a steadily increasing molecular absorption as the number of viologen-diphenyl subunits increases.

3.3 Conclusions

In the present chapter, a series of oligomeric derivatives of alkoxy-diphenyl viologens have been synthesized in order to investigate the effect of

increasing the conjugated length on the optical and electrical properties. The synthesized viologen-oligomers were characterized by ^1H -NMR, ^{13}C -NMR and elemental analysis. It was demonstrated that it is possible to apply the Zincke reaction as a concept to prepare conjugated oligomers containing n-dopable 4,4'-bipyridinium subunits. With the aim of synthesizing highly soluble conjugated oligomers bearing viologen substituents, the alkoxy side groups of the diphenyl subunits were varied. The aniline precursors (**16b-c**) are accessible via benzidine rearrangement. The viologen oligomers bearing ethylene oxide side chains are more soluble as compared to the other series of oligomers. The elongation of the viologen series bearing ethylene oxide side chains was stopped due to the low yield of the benzidine rearrangement reaction.

The formation of other redox states upon electrochemical reduction was not observed for the viologen oligomers as in the case of other conjugated oligomers (oligo-thiophenes).¹⁹⁰ The coulometry experiments indicate that the rods take one electron for each viologen subunit to form radical cations which can be further reduced to neutral viologens. The reduction potential shifts towards more positive values (for about 60 mV) for increasing rod length.

The diffusion coefficients of viologen oligomers bearing methoxy groups were calculated from linear sweep voltammetry at macro and micro disk electrodes. It was found that the diffusion coefficients increase with decreasing molecular weight. The DOSY technique gave reasonable values for the diffusion coefficients for all amino-protonated viologen oligomers investigated.

The evolution of the electronic transitions of the successive redox states (dication, radical cation and neutral) of viologen oligomers with increasing chain length has been analysed and shows saturation after introduction of the second DP-V-DP subunit. The radical cations are characterized by strong adsorption bands in the visible range similar to many viologen radical cations, covering the entire visible spectral range.

3.4 Experimental part

3.4.1 Cyclic voltammetric measurements

N,N-dimethylformamide (DMF, ≥ 99.9), dimethylsulfoxide (DMSO, ≥ 99.9) and n-Bu₄NPF₆ (puriss, electrochemical grade) were purchased from Sigma-Aldrich and used for cyclic voltammetry (CV) and coulometry. CVs were measured as described in Section 2.4.1.

A spectroelectrochemical cell¹³⁰ was used for exhaustive electrolysis in which the two compartments were separated by a fine glass frit. The working electrode consisting of a graphitized carbon felt GFA-5 of ca. 2 cm diameter (from SGL Carbon) and an Ag/AgCl reference electrode (Metrohm, 6.0724.140) (3M KCl aq. solution) were housed in one compartment. The auxiliary electrode was a 2 cm² platinum plate. 0.1M n-Bu₄NPF₆ in DMSO was used as a supporting electrolyte for the experiment.

Connection to the graphitized carbon felt was established via a platinum wire protruding through the top of the compartment containing the compound to be investigated.

3.4.2 Diffusion coefficient studies

The RDE measurements were performed as described in Chapter 2, Section 2.4.1. All measurements were made at RT in a single compartment three-electrode cell with a Pt counter electrode and two different working electrodes: a GC (diameter 0.29 cm diameter, Metrohm, 6.0804.010) and an Au disk microelectrode (CH Instruments, Inc., CHI105, diameter 10 μ m).

DOSY experiments were performed on a Bruker Avance III 500 MHz spectrometer using the Bruker pulse program ledbpgp2s. Diffusion time (D20) was 60 ms, the length of the diffusion gradient was 2500 μ s (P30) and the gradient recovery delays were 200 μ s (D16).

3.4.3 Spectroelectrochemical measurements

The experimental set-up used for the spectroelectrochemical measurements has been mentioned in Chapter 2, Section 2.4.4. The spectroelectrochemical measurements were performed under potentiostatic conditions in the negative range from 0 to -0.8 V using 0.1M n-Bu₄NPF₆ in DMF as electrolyte.

3.4.4 Detailed synthetic procedure

3.4.4.1 Materials and devices

The reagents: 4,4'-bipyridine (Aldrich, 98 %), 1-chloro-2,4-dinitrobenzene (Fluka, \geq 98 %), 2-nitrophenol (Aldrich), brombutyl (Fluka 98 %), [2-(2-(2-chloroethoxy)ethoxy)ethanol] (TCI), o-dianisidine (Sigma), Zn powder (Merck), HCl (Sigma-Aldrich, \geq 37 %), Na₂CO₃ (Merck, \geq 99.9 %), NaOH (Fluka, \geq 98 %), MgSO₄ (Fluka, \geq 97 %), NH₄PF₆ (Fluorochem, \geq 99 %) were used without

further purification. The solvents were distilled following procedures described in the literature.

The apparatus used for measuring ^1H -NMR, ^{13}C -NMR and elemental analysis have been mentioned in Chapter 2, Section 2.4.9.1.

3.4.4.2 Synthesis description

Viologen oligomers: **18a-b**, **19b**, **20b-c** and **22-b** were used for the backbones elongation as Cl^- salts due to the convenient purification of the reaction product and easy removal of excess viologen monomer (**17•2Cl**) and incomplete reaction products on Sephadex LH-20 using MeOH as eluent. ^1H - and ^{13}C -NMR, elemental analysis and CV investigations were performed on **18a-b**, **19b**, **20b-c** and **22-b** as PF_6^- salts that provide satisfactory evaluation of measurements. For this purpose, ca. 0.1 g viologen oligomer was anion exchanged to PF_6^- salt.

General procedure for anion exchange: 0.1 g of viologen oligomer was dissolved in 50 ml water/MeOH mixture and added to 10 ml 3M aq. NH_4PF_6 to afford the PF_6^- salt as a brown precipitate. It was filtered, washed twice with water, and dried under high vacuum (yield 93-96 %).

15b ($\text{C}_{10}\text{H}_{13}\text{NO}_3$): 2-Butoxy-nitrobenzene

20 g (0.14 mol) 2-Nitrophenol, 19.35 g (0.14 mol) anhydrous K_2CO_3 and 17.22 ml (0.16 mol) brombutyl were dissolved in 100 ml dry DMF and stirred with reflux for 3 days under Ar atmosphere. The reaction mixture was filtered, the filtrate collected and the solvent evaporated. The resulted liquid was dissolved in 150 ml ethyl acetate, washed two times with 200 ml aq. 5 % NaOH and 100 ml water. After drying over MgSO_4 , and solvent evaporation, **15b** was obtained as yellow liquid (23.63 g, 84.21 %).

$^1\text{H-NMR}$ (CDCl_3 , 250 MHz) δ : 7.78 (d, J = 1 Hz, 1H); 7.51 (t, J = 7.5 Hz, 1H); 7.07 (d, J = 8.25 Hz, 1H); 6.99 (t, J = 7.5, 1H); 4.10 (t, J = 12.5 Hz, 2H); 1.81 (t, J = 15.2 Hz, 2H); 1.53 (m, J = 30 Hz, 2H); 0.97 (t, J = 15 Hz, 3H).

$^{13}\text{C-NMR}$ (CDCl_3 , 63 MHz) δ : 152.47; 139.92; 134.03; 125.45; 119.96; 114.39; 69.27; 30.97; 19.09; 13.74.

15c ($\text{C}_{12}\text{H}_{17}\text{NO}_6$): 2-{2-[2-(2-Nitrophenoxy)ethoxy]ethoxy}ethanol

15.11 g (0.1 mol) 2-Nitrophenol and 22.11 g (0.16 mol) anhydrous K_2CO_3 were dissolved in 60 ml dry DMF, and heated while stirring at 70°C for 30 minutes under Ar. The solution was cooled to RT and 30 ml (0.19 mol) [2-(2-(2-chloroethoxy)ethoxy)ethanol] was added in portions and stirred at 90°C for 3 days. The reaction mixture was filtered, the filtrate collected and the solvent evaporated. The orange liquid was dissolved in chloroform and washed two times with 200 ml aq. 5% NaOH. The organic layer was collected, dried over MgSO_4 , filtered and the solvent evaporated. After drying in HV, **15c** was obtained as yellow liquid (28.8 g (0.1 mol), 98 %).

$^1\text{H-NMR}$ (CDCl_3 , 250 MHz) δ : 7.83 (d, J = 7.75 Hz, 1H); 7.53 (t, J = 14.75 Hz, 1H); 7.10 (t, J = 12.5 Hz, 1H); 7.03 (d, J = 7.25 Hz, 1H); 4.28 (s, 2H); 3.93 (s, 2H); 3.76 (s, 2H); 3.72 (d, J = 10 Hz, 4H); 3.63 (s, 2H); 2.37 (s, 1H).

$^{13}\text{C-NMR}$ (CDCl_3 , 63 MHz) δ : 152.22; 140.11; 134.11; 125.61; 120.67; 114.92; 72.44; 71.19; 70.45; 69.63; 69.27; 61.78.

16b ($\text{C}_{20}\text{H}_{28}\text{N}_2\text{O}_2$): 3,3'-Butoxy-benzidine

This compound was prepared according to the method described by D. Hinks et al.¹⁹¹ with minor modifications (correction of the number of mol NaOH 50 % required to complete benzidine rearrangement and use of petroleum benzine instead of ligroine as solvent).

20 g (0.102 mol) 2-Butoxy-nitrobenzene (**15b**), dissolved in 50 ml petroleum benzine, was mixed with 27.74 g (0.42 mol) Zn and heated at 70°C. 6.24 ml aq. NaOH (50 %) was added in portions (0.5 ml after every 2 h). The reaction mixture color changed from yellow to orange and colorless. 12 ml (0.66 mol) of water was added and refluxed further for 12 h. The reaction mixture was filtered, mixed with 100 ml aq. HCl (20 %) and stirred for 30 minutes at RT. The solvents were distilled, the residue dissolved in water, neutralized with saturated Na₂CO₃ and extracted three times with chloroform. The organic layer was collected and dried over MgSO₄. After solvent evaporation and drying in HV, **16b** was obtained as brown solid (12.89 g, 76.64 %).

¹H-NMR (CDCl₃, 250 MHz) δ : 6.99 (s, 4H); 6.78 (d, J= 10 Hz, 2H); 4.09 (t, J= 10 Hz, 4H); 3.77 (s, 4H); 1.85 (t, J= 13.75 Hz, 4H); 1.56 (m, J= 21.75 Hz, 4H); 1.02 (t, J= 14.25 Hz, 6H).

¹³C-NMR (CDCl₃, 63 MHz) δ : 146.97; 134.96; 132.62; 119.12; 115.16; 110.20; 68.05; 31.51; 19.40; 13.95.

16c (C₂₄H₃₆N₂O₈): [(4,4'-Diaminobiphenyl-3,3'-oxy)2-ethoxy]2-ethoxy)2-ethanol]

3.43 g (12.67 mmol) 2-{2-[2-(2-Aminophenoxy)ethoxy]ethoxy} ethanol (**15c**) dissolved in 30 ml acetone was mixed with 2.5 g (38.23 mol) Zn and heated to reflux. 3 ml (37.5 mol) aq. NaOH (50 %) was added in portions to the reaction flask. After 24 h the reaction was stopped, the solution filtered and acetone evaporated. The residue was dissolved in 100 ml ethyl acetate, mixed with 1 g (15 mmol) Zn and heated to reflux. Aq. NaOH (50 %) was added in portions until the solution color changed from brown to pale yellow. After 12 h, the

reaction mixture was filtered and the solvent evaporated. The residue was dissolved in 100 ml aq. HCl (20 %) and stirred on an ice bath for 30 minutes. The acid was evaporated and the solid obtained dissolved in water. The pH of this solution was adjusted to 8 by adding saturated Na_2CO_3 . After extraction with chloroform, the organic layer was dried over MgSO_4 , filtered, the solvent evaporated, and the residue purified by column chromatography (elution with ethyl acetate/MeOH (8:2). Yield: 0.66 g (1.37 mmol), 21.69 %.

$^1\text{H-NMR}$ (CDCl_3 , 250 MHz) δ : 6.97 (s, 4H); 6.73 (d, J = 7.5 Hz, 2H); 4.20 (s, 4H); 3.86 (s, 4H); 3.71 (s, 12H); 3.59 (s, 8H).

$^{13}\text{C-NMR}$ (CDCl_3 , 63 MHz) δ : 146.67; 135.46; 132.38; 119.99; 115.89; 111.64; 72.66; 70.71; 70.26; 69.79; 68.43; 61.64.

17•2Cl ($\text{C}_{22}\text{H}_{14}\text{Cl}_2\text{N}_6\text{O}_8$): 1,1'-Bis-(2,4-dinitrophenyl)-4,4'-bipyridinium dichloride

This compound was prepared according to the method described by Nanasawa et al.⁹³ with minor modifications (in order to remove monophenylated 1-(2,4-dinitrophenyl)-4-(4-pyridyl)-pyridinium chloride byproduct, the crude precipitate was washed several times with acetone). A solution of 4,4'-bipyridine (6.4 g, 40 mmol) and 2,4-dinitrochlorobenzene (28.0 g, 140 mmol) in dry MeCN (120 ml) was heated to reflux with stirring for 72 h. The dense yellow precipitate formed was diluted with MeCN (120 ml), filtered and washed several times with MeCN and acetone until a pure (TLC: MeOH: HOAc: H_2O ; 10/4/1) product was obtained (8.0 g, 35 %).

$^1\text{H NMR}$ (D_2O , 250 MHz) δ : 9.41 (d, J = 7.5 Hz, 4H); 9.34 (d, J = 2.5 Hz, 2H); 8.89 (d, J = 4 Hz, 4H); 8.87 (d, J = 5 Hz, 2H); 8.25 (d, J = 10 Hz, 2H).

^{13}C NMR (D_2O , 63 MHz) δ : 152.60; 149.81; 146.82; 142.78; 138.22; 131.13; 130.71; 127.54; 122.76.

$18\text{a}\cdot 2\text{PF}_6$ ($\text{C}_{38}\text{H}_{36}\text{F}_{12}\text{N}_4\text{O}_4\text{P}_2$): 1,1'-Bis-(4,4'-amino-3,3'-methoxy-biphenyl)-4,4'-bipyridinium bis hexafluorophosphate

2g (3.56 mmol) 1,1'-Bis-(2,4-dinitrophenyl)-4,4'-bipyridinium dichloride (**17•2Cl**) was dissolved at 50 °C in 250 ml MeOH/water (80 %, V/V). 2.2 g (9.05 mmol) o-Dianisidine (**16a**) dissolved in 200 ml MeOH/water 80 % (V/V) was added, and the reaction mixture was refluxed for 20 h. The solvents were evaporated and the product precipitated two times with diethyl ether from MeOH. After drying under high vacuum, **18a•2Cl** was obtained as a dark violet solid (1.98 g, 82 %).

$18\text{a}\cdot 2\text{PF}_6$:

^1H NMR (CD_3CN , 250 MHz) δ : 9.12(d, J= 5Hz, 4H); 8.61 (d, J= 7.5 Hz, 4H); 7.65 (d, J= 7.5 Hz, 2H); 7.54 (s, 4H); 7.25 (s, 4H); 6.84 (d, J= 10 Hz, 2H); 4.42 (s, NH_2 , 4H); 4.04 (s, 6H); 3.99 (s, 6H).

^{13}C NMR ($\text{d}_6\text{-DMSO}$, 63 MHz) δ : 152.38; 149.89; 147.93; 147.02; 146.50; 139.45; 129.00; 127.53; 127.10; 126.46; 120.70; 118.76; 114.18; 110.48; 109.84; 57.15; 56.02.

Elemental analysis for $\text{C}_{38}\text{H}_{36}\text{F}_{12}\text{N}_4\text{O}_4\text{P}_2\cdot 4\text{H}_2\text{O}$: C 46.83, H 4.55, N 5.74(calc.), C 46.82, H 4.75, N 5.98 (found).

$18\text{b}\cdot 2\text{PF}_6$ ($\text{C}_{50}\text{H}_{60}\text{F}_{12}\text{N}_4\text{O}_4\text{P}_2$): 1,1'-Bis-(4,4'-amino-3,3'-butoxy-biphenyl)-4,4'-bipyridinium bis hexafluorophosphate

1.5 g (2.68 mmol) 1,1'-Bis-(2,4-dinitrophenyl)-4,4'-bipyridinium dichloride (**17•2Cl**) was dissolved in 250 ml MeOH 80 % (V/V) and heated at 100°C. 3.5 g (10.65 mmol) 3,3'-Butoxy-benzidine (**16b**) was dissolved in 50 ml MeOH

and added to the reaction flask. The reaction mixture was refluxed for 20 h, the solvent evaporated and the residue precipitated two times from MeOH/ethyl acetate. The dark violet precipitate formed was filtered and dried under high vacuum (1.15 g (1.34 mmol), 50.29 %).

18b•2PF₆:

¹H NMR (CD₃CN, 250 MHz) δ : 9.13 (bs, Vio, 4H); 8.63 (bs, Vio, 4 H); 7.63 (bs, CHarom., 2H); 7.51 (bs, CHarom., 4H); 7.22 (bs, CHarom., 4H); 6.83 (bs, CHarom., 2H), 4.42 (bs, H₂N, 4H); 4.29 (bs, O-CH₂, 4H); 4.16 (bs, -O-CH₂, 4H); 1.85 (bs, CH₂, 4H); 1.73 (bs, CH₂, 4H); 1.59 (bs, CH₂, 4H); 1.41 (bs, CH₂, 4H); 1.03 (bs, CH₃, 6H); 0.93 (bs, CH₃, 6H).

¹³C NMR (CD₃CN, 63 MHz) δ : 151.66; 147.24; 147.07; 146.59; 138.81; 128.73; 127.47; 126.68; 126.50; 120.31; 118.79; 114.17; 111.23; 110.38; 69.37 (O-CH₂); 68.18 (O-CH₂); 31.22 (CH₂); 30.57 (CH₂); 19.09 (CH₂); 18.88 (CH₂); 13.20 (CH₃); 13.04 (CH₃).

Elemental analysis for C₅₀H₆₀F₁₂N₄O₄P₂: C56.07, H5.64, N5.23 (calc.), C56.47, H5.47, N5.22 (found).

19a•4PF₆ (C₄₆H₃₄F₂₄N₈O₁₀P₄):

3.6 g (6.41 mmol) of 1,1'-Bis-(2,4-dinitrophenyl)-4,4'-bipyridinium dichloride (**17•2Cl**) was dissolved in 200 ml MeOH/water (1:1), and heated to reflux. o-Dianisidine (**16a**) (0.4 g, 1.63 mmol), dissolved in 30 ml MeOH, was added in portions to the reaction flask. The reaction mixture was refluxed for 48 h, and the solvent was evaporated. Removal of an excess of 1,1'-bis-(2,4-dinitrophenyl)-4,4'-bipyridinium dichloride (**17•2Cl**) was achieved by repetitive precipitation of the residue from MeOH/ethyl acetate (1:2). The purity of the product was checked by TLC on silica gel using: MeOH/H₂O/HOAc (10:4:1).

The product was further dissolved in water/MeOH mixture and added to 10 ml 3M aq. NH_4PF_6 . The resulting brown precipitate was filtered, washed with 40 ml water and dried under high vacuum to yield **19a•4PF₆** (1.06 g, 45.39 %).

¹H NMR (CD₃CN, 250 MHz) δ : 9.25 (s, CHarom., 2H); 9.21 (d, J= 4.25 Hz, Vio, 8H); 8.92 (d, J= 8 Hz, CHarom., 2H); 8.77 (d, J= 6.5 Hz, Vio, 4H); 8.71 (d, J= 6Hz, Vio, 4H); 8.22 (d, J= 8.5 Hz, CHarom., 2H); 7.85 (d, J= 7.5 Hz CHarom., 2H); 7.76 (s, CHarom., 4H); 4.12 (s, O-CH₃, 6H).

¹³C NMR (CD₃CN, 63 MHz) δ : 152.55; 151.30; 147.38; 146.84; 144.42; 131.65; 130.92; 130.57; 127.64; 127.31; 127.21; 127.13; 122.31; 120.62; 112.55; 56.92.

19b•4Cl (C₅₂H₄₆Cl₄N₈O₁₀):

6.76g (12.02 mmol) of 1,1'-Bis-(2,4-dinitrophenyl)-4,4'-bipyridinium dichloride (**17•2Cl**) was dissolved in 200 ml MeOH (80 %). 1.0 g (3 mmol) 3,3'-Butoxy-benzidine (**16c**), dissolved in 50 ml MeOH, was added and allowed to reflux for 4 days. The solvent was evaporated, and the solid dissolved in MeOH. Ethyl acetate was added in portions until a brown precipitate was formed. The product was further purified over Sephadex LH-20 (elution with MeOH). After purification and drying under high vacuum, 0.856 g (0.789 mmol) (25.77 %) product was obtained.

19b•4Cl:

¹H NMR (MeOD, 250 MHz) δ : 9.70 (d, J= 7.5 Hz, Vio (2H) + CHarom. (2H), 4H); 9.57 (bs, Vio, 6H); 9.35 (bs, CHarom., 2H); 9.14 (d, J= 7.5 Hz, Vio, 4H); 9.08 (d, J= 5 Hz, Vio, 4H); 9.02 (d, J= 7.5 Hz, CHarom., 2H); 8.50 (d, J= 8.75 Hz, CHarom., 2H); 8.02 (d, J= 10 Hz, CHarom., 2H); 7.83 (bs, CHarom., 2H);

7.76 (d, J = 8 Hz, CHarom., 2H); 4.43 (bs, O-CH₂, 4H); 1.80 (d, J = 5 Hz, 4H); 1.47 (m, J = 21 Hz, 4H); 0.98 (t, J = 14.25 Hz, 6H).

19b•4PF₆:

¹³C NMR (d₆-DMSO, 63 MHz) δ : 152.58; 151.95; 150.49; 150.02; 147.72; 147.16; 144.86; 143.16; 138.43; 131.42; 131.16; 129.92; 127.14; 126.98; 126.81; 121.89; 120.42; 112.95; 69.60 (O-CH₂); 30.65 (CH₂); 18.86 (CH₂); 12.75 (CH₃).

19c•4Cl (C₅₆H₅₄Cl₄N₈O₁₆):

4.80 g (8.54 mmol) of 1,1'-Bis-(2,4-dinitrophenyl)-4,4'-bipyridinium dichloride (**17•2Cl**) was dissolved in 150 ml MeOH (80 %). 1.0 g (2.12 mmol) 2-(2-{2-[(4,4'-Diamino-biphenyl-3,3'-oxy)ethoxy]ethoxy)-ethanol (**16c**), dissolved in 50 ml MeOH, was added and refluxed for 4 days. The solvent was evaporated and the residue dissolved in MeOH. Ethyl acetate was added in portions, and the precipitate formed was filtered. Further purification was achieved by repetitive column chromatography over Sephadex LH-20 (elution with MeOH). After purification and drying under high vacuum, 0.867 g (0.701 mmol, 33.07 %) product was obtained.

19c•4Cl:

¹H NMR (MeOD, 250 MHz) δ : 9.68 (bs, CHarom. (2H) + Vio (2H), 4H); 9.59 (bs, Vio, 6H); 9.36 (s, CHarom., 2H); 9.12 (bs, Vio, 4H); 9.03 (bs, Vio, 4H); 9.00 (bs, CHarom., 2H); 8.50 (d, J = 8.5 Hz, CHarom., 2H); 8.05 (bs, CHarom., 2H); 7.90 (bs, CHarom., 2H); 7.80 (d, J = 7.5 Hz, 2H); 4.61 (bs, 4H); 3.88 (bs, 4H); 3.70 (bs, 12 H); 3.59 (bs, 4H).

^{13}C NMR (MeOD, 63 MHz) δ : 152.75; 151.76; 150.35; 150.01; 147.84; 147.13; 144.61; 143.15; 138.48; 131.62; 131.45; 129.93; 127.17; 126.98; 121.90; 120.94; 113.91; 72.36; 70.15; 70.06; 69.45; 68.76; 60.69.

$20\text{a}\cdot 4\text{PF}_6$ ($\text{C}_{62}\text{H}_{56}\text{F}_{24}\text{N}_6\text{O}_6\text{P}_4$):

0.35 g (0.24 mmol) (**$19\text{a}\cdot 4\text{PF}_6$**) and 0.31 g (1.28 mmol) of o-dianisidine (**16a**) were dissolved in 100 ml MeCN and refluxed for 48 h. After cooling to RT, 250 ml diethyl ether was added to the reaction mixture, and the formed precipitate was filtered, washed two times with MeOH (2 x 100 ml) and diethyl ether (100 ml). Further purification was achieved by repetitive precipitation of the residue from MeCN/diethyl ether (1:1.5). **$20\text{a}\cdot 4\text{PF}_6$** was obtained as a dark brown powder (0.187 g, 50 %).

^1H NMR (d_6 -DMSO + I_2 , 250 MHz) δ : 9.63 (bs, Vio, 8H); 9.03 (bs, Vio, 8H); 8.00 (bs, CHarom., 4H); 7.83 (bs, CHarom., 8H); 7.62 (bs, CHarom., 2H); 7.36 (bs, CHarom., 2H); 7.02 (bs, CHarom., 2H); 4.06 (bs, O-CH₃, 18H).

^{13}C NMR (d_6 -DMSO + I_2 , 63 MHz) δ : 152.78; 152.35; 151.58; 150.45; 149.84; 147.98; 147.49; 147.08; 146.62; 143.95; 139.50; 131.37; 129.00; 128.12; 127.24; 126.50; 125.78; 122.51; 122.61; 118.77; 114.23; 112.66; 110.57; 109.93; 57.54 (O-CH₃); 57.19 (O-CH₃); 56.07 (O-CH₃).

Elemental analysis for $\text{C}_{62}\text{H}_{56}\text{F}_{24}\text{N}_6\text{O}_6\text{P}_4\cdot 5\text{H}_2\text{O}$: C45.10, H4.02, N 5.09 (calc.), found C45.39, H4.46, and N5.24 (found).

$20\text{b}\cdot 4\text{PF}_6$ ($\text{C}_{80}\text{H}_{92}\text{F}_{24}\text{N}_6\text{O}_6\text{P}_4$):

0.7 g (0.6 mmol) of **$19\text{b}\cdot 4\text{Cl}$** , dissolved in 250 ml MeOH, and 0.9 g (2.74 mmol) of 3,3'-butoxy-benzidine (**16b**), dissolved in 50 ml MeOH, were mixed and refluxed for 3 days. The solvent was evaporated to one-third of the original volume, and ethyl acetate was added in portions until a dark brown

precipitate was formed. The precipitate was filtered and purified over Sephadex LH-20 (elution with methanol). After drying under high vacuum, 0.162 g (0.117 mmol) (24.28 %) product was obtained.

20b•4PF₆:

¹H NMR (d₆-DMSO + I₂, 250 MHz) δ : 9.61 (bs, Vio, 8H); 9.06 (bs, Vio, 8H); 8.00 (d, J= 7.5 Hz, CHarom., 2H); 7.83 (bs, CHarom., 6H); 7.62 (bs, CHarom., 4H); 7.34 (bs, CHarom., 4H); 7.02 (d, J= 8 Hz, CHarom., 2H); 4.34 (t, J= 15.5 Hz, O-CH₂, 8 H); 4.18 (bs, O-CH₂, 4H); 1.80 -1.34 (unresolved coupling, combined integral 24H, CH₂), 0.96 (t, J= 14.5, CH₃, 6H); 0.89 (bs, CH₃, 12H).

¹³C NMR (d₆-DMSO + I₂, 63 MHz) δ : 152.21; 151.96; 150.20; 149.90; 148.02; 143.90; 131.47; 127.99; 127.50; 127.02; 120.60; 120.44; 119.31; 113.37; 112.36; 111.71; 111.44; 69.74; 69.51; 68.51; 31.27; 30.78; 19.18; 19.07; 14.25; 14.09.

20c•4PF₆ (C₉₂H₁₁₆F₂₄N₆O₂₄P₄):

0.67 g (0.54 mmol) **19c•4Cl** in 50 ml MeOH and 0.9 g (2.74 mmol) of **16c** in 50 ml MeOH were refluxed for 3 days. The reaction mixture was allowed to cool to RT, the solvent was evaporated to one-third of the original volume, and ethyl acetate was added in portions until a dark brown precipitate was formed. The precipitate was filtered and purified over Sephadex LH-20 (elution with MeOH). After purification, the solid was dissolved in 20 ml MeOH and added to 15 ml 3M aq. NH₄PF₆. The precipitated PF₆⁻ salt was filtered and washed with water several times to remove an excess of NH₄PF₆. After drying under high vacuum, 0.447 g (0.196 mmol, 36.47 %) product was obtained.

^1H NMR ($\text{d}_6\text{-DMSO} + \text{I}_2$, 250 MHz) δ : 9.60 (bs, Vio, 8H); 9.03 (bs, Vio, 8H); 8.02 (bs, CHarom., 2H); 7.91 (bs, CHarom., 2H); 7.86 (bs, CHarom., 4H); 7.77 (bs, CHarom., 2H); 7.68 (bs, CHarom., 2H); 7.61 (bs, CHarom., 2H); 7.35 (bs, CHarom., 2H); 4.55 (bs, O-CH_2 , 8H); 4.28 (bs, O-CH_2 , 4H); 3.52 (bs, $\text{O}_2\text{C}_2\text{H}_4$, 24H); 3.44 (bs, $\text{O}_2\text{C}_2\text{H}_4$, 24H); 3.41 (bs, $\text{O}_2\text{C}_2\text{H}_4$, 24H).

^{13}C NMR ($\text{d}_6\text{-DMSO} + \text{I}_2$, 63 MHz) δ : 152.04; 151.80; 151.67; 150.30; 150.21; 149.81; 148.07; 145.84; 144.65; 143.66; 139.68; 131.78; 129.11; 128.04; 127.07; 121.06; 120.98; 114.37; 114.28; 72.52 (O-CH_2); 70.38 (O-CH_2); 69.99 (O-CH_2); 69.40 (O-CH_2); 68.84 (O-CH_2); 60.87 (HO-CH_2).

Elemental analysis for $\text{C}_{92}\text{H}_{116}\text{F}_{24}\text{N}_6\text{O}_{24}\text{P}_4$: C48.68, H5.15, N3.70 (calc.), C48.35, H5.14, N3.74 (found).

$21\text{a}\cdot 4\text{PF}_6$ ($\text{C}_{46}\text{H}_{38}\text{F}_{24}\text{N}_4\text{O}_2\text{P}_4$):

0.15 g (0.10 mmol) **$19\text{a}\cdot 4\text{PF}_6$** and 0.10 g (1.09 mmol) aniline were dissolved in 30 ml MeCN and refluxed for 48 h. After cooling to RT, 60 ml diethyl ether was added to the reaction mixture, and the formed precipitate was filtered, washed several times with MeOH and dried under high vacuum. Yield: 0.099 g (73.7 %).

^1H NMR (CD_3CN , 250 MHz) δ : 9.19 (bs, Vio, 8H); 8.69 (bs, Vio, 8H); 7.84 (bs, CHarom., 10H); 7.74 (bs, CHarom., 6H); 4.14 (bs, O-CH_3 , 6H).

^{13}C NMR (CD_3CN , 63 MHz) δ : 152.61; 151.35; 150.89; 147.37; 145.95; 144.41; 132.46; 130.98; 130.76; 127.44; 127.13; 124.44; 120.63; 112.57; 56.92.

Elemental analysis for $\text{C}_{46}\text{H}_{38}\text{F}_{24}\text{N}_4\text{O}_2\text{P}_4\cdot 3\text{H}_2\text{O}$: C42.09, H 3.37, N 4.26 (calc.), C 42.01, H 3.74, N 4.59 (found).

22a•6PF₆ (C₇₀H₅₄F₃₆N₁₀O₁₂P₆):

0.5 g (0.73 mmol) of **18a•2Cl** and 1.7g (3.02 mmol) of 1,1'-bis-(2,4-dinitrophenyl)-4,4'-bipyridinium dichloride (**17•2Cl**) were dissolved in 250 ml MeOH/water 80 % and refluxed for 72 h. The solvent was evaporated, and the crude product was precipitated two times from MeOH/ethyl acetate (1:3). The yellow solid was filtered, dissolved in 200 ml MeOH and added to 10 ml 3M aq. NH₄PF₆. The precipitated solid was filtered and washed twice with water. Further purification was achieved by repetitive precipitation of the residue from MeCN/diethyl ether (1:2). Purity of the product was checked by TLC on silica gel using: MeOH/H₂O/HOAc, 10:4:1. After drying under high vacuum, **22a•6PF₆** was obtained as a dark yellow solid (1.32 g, 86 %).

¹H NMR (CD₃CN, 250 MHz) δ : 9.26 (bs, CHarom., 2H); 9.19 (bs, Vio, 12H); 8.92 (d, J= 10 Hz, CHarom., 2H); 8.73 (d, J= 7.5 Hz, Vio, 12 H); 8.21 (d, J= 7.5 Hz, CHarom., 2H); 7.83 (bs, CHarom., 4H); 7.75 (bs, CHarom., 8H); 4.11 (bs, O-CH₃, 12H).

¹³C NMR (CD₃CN, 126 MHz) δ : 152.18; 152.03; 151.62; 151.33; 148.56; 148.48; 147.96; 147.72; 145.57; 144.49; 139.19; 132.76; 132.07; 131.65; 128.76; 128.43; 128.30; 128.24; 126.83; 123.42; 123.20; 121.76; 113.72; 58.04 (O-CH₃).

Elemental analysis for C₇₀H₅₄F₃₆N₁₀O₁₂P₆•2H₂O: C 39.41, H 2.74, N 6.56 (calc.), C 39.38, H 2.92, N 6.74 (found).

22b•6PF₆ (C₈₂H₇₈F₃₆N₁₀O₁₂P₆):

1 g (1.18 mmol) of **18b•2Cl** in 120 ml MeOH and 2.6 g (4.63 mol) of 1,1'-bis-(2,4-dinitrophenyl)-4,4'-bipyridinium dichloride (**17•2Cl**) in 250 ml MeOH (80 %, V/V) were mixed and refluxed for 4 days. The solvent was evaporated

and the residue dissolved in MeOH. Ethyl acetate was added in portions, the precipitate formed was filtered, and purified over Sephadex LH-20 (elution with MeOH). After purification and drying under high vacuum, 0.4 g (0.24 mmol, 21.02 %) product was obtained.

^1H NMR ($\text{d}_6\text{-DMSO} + \text{I}_2$, 250 MHz) δ : 9.71 (bs, CHarom., 2H); 9.64 (bs, Vio, 12H); 9.18 (bs, CHarom., 2H); 9.07 (bs, Vio, 12H); 8.40, (bs, Charom., 2H); 7.97 (bs, CHarom., 4H); 7.80 (bs, CHarom., 8H); 4.34 (bs, O-CH₂, 8H); 1.67 (bs, CH₂, 8H); 1.33 (unresolved coupling, combined integral 8H); 0.87 (bs, CH₃, 12H).

^{13}C NMR ($\text{d}_6\text{-DMSO} + \text{I}_2$, 63 MHz) δ : 151.55; 150.14; 149.78; 148.06; 147.71; 143.87; 143.41; 138.81; 132.39; 131.48; 130.72; 128.04; 127.13; 122.02; 120.55; 113.37; 69.82; 30.84; 19.06; 14.12.

$23\text{a}\cdot 6\text{PF}_6$ ($\text{C}_{86}\text{H}_{76}\text{F}_{36}\text{N}_8\text{O}_8\text{P}_6$):

0.9 g (0.42 mmol) **$22\text{a}\cdot 6\text{PF}_6$** and 0.55 g (2.25 mmol) o-dianisidine (**16a**) were dissolved in 100 ml MeCN and refluxed for 48 h. After cooling to RT, 250 ml diethyl ether was added to the reaction mixture and the precipitate filtered, washed two times with MeOH (2 x 100 ml) and diethyl ether (100 ml). Further purification was achieved by repetitive precipitation of the residue from MeCN /diethyl ether (1:1.5). After drying under high vacuum, **$23\text{a}\cdot 6\text{PF}_6$** was obtained as a dark colored solid (0.89 g, 93.4 %).

^1H NMR (CD_3CN , 250 MHz) δ : 9.19 (bs, Vio, 12H); 8.69 (bs, Vio, 12H); 7.83 (s, CHarom., 4H); 7.74 (bs, CHarom., 10H); 7.56 (bs, CHarom., 4H); 7.27 (bs, CHarom., 4H); 6.87 (bs, CHarom., 2H); 4.45 (s, NH₂, 4H); 4.11 (s, O-CH₃, 12H); 4.05 (s, O-CH₃, 6H); 4.00 (s, O-CH₃, 6H).

^{13}C NMR ($\text{d}_6\text{-DMSO}$, 63 MHz) δ : 152.77; 152.39; 150.40; 149.87; 148.01; 147.02; 146.55; 143.86; 139.47; 131.36; 128.98; 128.17; 127.53; 127.22; 126.44; 120.62; 118.77; 117.37; 114.17; 112.62; 110.49; 109.85; 108.89; 57.53 (O-CH₃); 57.16 (O-CH₃); 56.01 (O-CH₃).

Elemental analysis for $\text{C}_{86}\text{H}_{76}\text{F}_{36}\text{N}_8\text{O}_8\text{P}_6 \cdot 8\text{H}_2\text{O}$: C43.70, H3.92, N4.74 (calc.), C43.51, H4.269, and N4.94 (found).

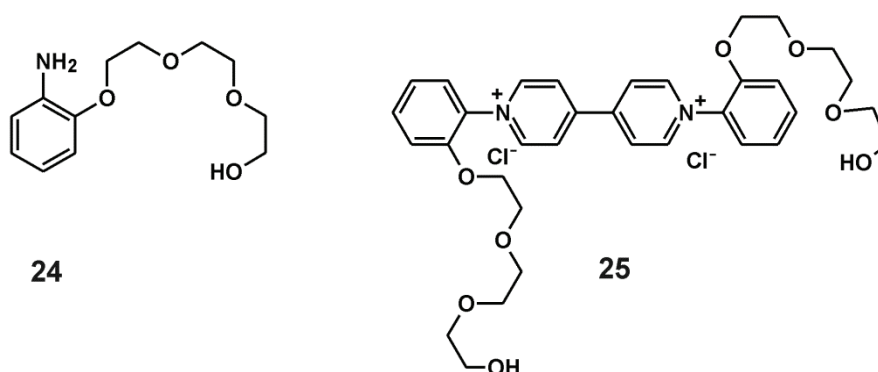
23b•6PF₆ ($\text{C}_{110}\text{H}_{124}\text{F}_{36}\text{N}_8\text{O}_8\text{P}_6$):

0.3 g (0.18 mmol) **22b•6Cl** was dissolved in 200 ml MeOH. To this solution 0.316 g (0.96 mmol) 3,3'-butoxy-benzidine was added and the mixture refluxed for 3 days. The solvent was evaporated, and the residue dissolved in MeOH. Ethyl acetate was added in portions until a brown precipitate was obtained. The formed precipitate was filtered and purified over Sephadex LH-20 (elution with MeOH). After purification, the solid was dissolved in 150 ml MeOH and added to 10 ml 3M aq. NH_4PF_6 in order to perform anion exchange from Cl^- to PF_6^- . After drying under high vacuum, 0.14 g (0.05 mmol, 30 %) product was obtained.

^1H NMR ($\text{d}_6\text{-DMSO} + \text{I}_2$, 250 MHz) δ : 9.63 (bs, Vio, 12H); 9.09 (bs, Vio, 12H); 7.99 (bs, CH_{arom.}, 6H); 7.81 (bs, CH_{arom.}, 12H); 7.55 (bs, CH_{arom.}, 4H); 7.41 (bs, CH_{arom.}, 1H); 7.27 (bs, CH_{arom.}, 1H); 4.35 (bs, O-CH₂, 16H); 1.66 (bs, CH₂, 16H); 1.32 (bs, CH₂, 16H); 0.87 (bs, CH₃, 24 H).

^{13}C NMR ($\text{d}_6\text{-DMSO} + \text{I}_2$, 63 MHz) δ : 152.25; 150.17; 148.33; 143.94; 139.79; 138.87; 136.51; 136.33; 132.87; 131.49; 131.00; 128.02; 127.81; 127.53; 127.14; 120.64; 113.49; 69.66; 30.91; 19.14; 14.30.

Elemental analysis for $\text{C}_{110}\text{H}_{124}\text{F}_{36}\text{N}_8\text{O}_8\text{P}_6 \cdot 7\text{H}_2\text{O}$: C49.26, H5.18, N4.17 (calc.), C48.96, H5.64, and N4.50 (found).

C₁₂H₁₉NO₄: 2-[2-[2-(2-aminophenoxy)ethoxy]ethoxy]ethanol (24)

14.7 g (54.19 mmol) [2-(2-(2-Chloroethoxy)ethoxy)ethanol] and 14.6 g Zn (0.22 mol) were dissolved in 100 ml ethyl acetate and heated to reflux. 24.3 ml aq. NaOH (50 %), (0.3 mol) was added in portions (5 ml every 30 minutes). In a few minutes the solution color changed from orange to reddish brown. After 12 h, 6.4 ml (0.35 mol) water was added, and the mixture was further stirred for 2 days. The reaction mixture was allowed to cool to RT, filtered and washed with 100 ml aq. 1 % HCl. 100 ml of aq. HCl (20 %) were added, and the solution was stirred for 30 minutes at RT. The acid was distilled, and the pH of the solution was adjusted to 8 with saturated NaHCO₃. Further, the aqueous layer was extracted with chloroform. The organic layer was dried over MgSO₄, filtered, the chloroform evaporated, and the residue purified by chromatography (elution first with ethyl acetate and then with MeOH) (7.18g (0.03 mol), 60 %).

¹H NMR (CDCl₃, 250 MHz) δ : 6.70 (m, 4H); 4.08 (s, 2H); 3.91 (s, 4H); 3.79 (d, J= 4 Hz, 2H); 3.65 (s, 2H); 3.56 (s, 2H); 2.12 (d, J= 5 Hz, 1H).

¹³C NMR (CDCl₃, 63 MHz) δ : 146.47; 136.77; 121.85; 118.51; 115.71; 113.03; 72.63; 70.64; 70.23; 69.69; 68.26; 61.54.

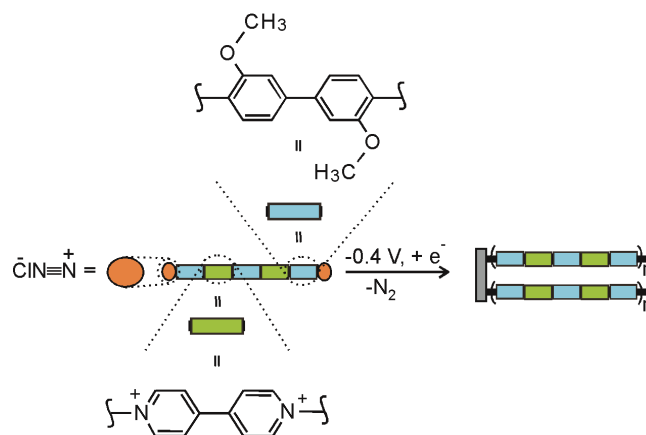
C₃₄H₄₂Cl₂N₂O₈: 1,1'-Bis-(2,2'-biphenoxy-{2-[2-(2-aminophenoxy)ethoxy]ethoxy}ethanol)-4,4'-bipyridinium dichloride (25)

1 g (1.95 mmol) 1,1'-Bis-(2,4-dinitrophenyl)-4,4'-bipyridinium dichloride was dissolved in 200 ml MeOH (80 %) and heated at 130°C. 3 g (6.24 mmol) 2-{2-[2-(2-Aminophenoxy)ethoxy]ethoxy} ethanol was dissolved in 100 ml MeOH, added to the reaction mixture and refluxed for 20 h. The solvent was evaporated, the residue was dissolved in 200 ml ethanol and the solution filtered. The filtrate was collected, the solvent evaporated and the residue dissolved in water. For further purification, the aqueous solution was extracted with chloroform for one week. The water was then evaporated and the solid dried under high vacuum (0.65 g (0.96 mmol), 54 %).

¹H NMR (MeOD, 250 MHz) δ : 9.48 (d, J= 5 Hz, Vio, 4H); 8.95 (d, J= 7.5 Hz, Vio, 4H); 7.79 (d, J= 8.5 Hz, 4H), 7.51 (d, J= 7.25 Hz, 2H), 7.33 (bs, 2H), 4.42 (bs, 4H), 3.79 (bs, 4H), 3.64 (bs, 8H), 3.57 (bs, 4H).

¹³C NMR (MeOD, 63 MHz) δ : 151.21; 150.64; 147.74; 133.40; 131.55; 126.70; 126.27; 121.81; 114.80; 72.33; 70.05; 70.01; 68.86; 68.56; 60.65.

4 Electropolymerization of the viologen rods (18a, 20a and 23a) on conductive substrates



Scheme 4.1 The electropolymerization of viologen oligomers on electrode surface.

4.1 Introduction

Electrodes modified by viologen species have been of increasing interest for electrical, optical, and magnetic performance. Several methods for the modification of electrodes such as the Langmuir-Blodgett (LB) technique,^{192,193} the self-assembly of thio-derivatized viologens^{194,195} (SAM) onto gold electrode surfaces, the layer-by-layer (LBL)^{196,197} assembly, the polycondensation of viologen derivatives of organosilanes,^{198,199} dip coating²⁰⁰ and spin coating^{201,202} of polyviologens or electropolymerization,²⁰³ etc. have been developed to modify electrode surfaces with viologens. The lack of a direct contact between the electrodes and viologens affects the e^- transport at the electrode/molecule interface and limit their practical application in construction of organic electronics. Thus, the direct covalent attachment of organic molecules to the conductive substrate improves the e^- transport that is required for molecular electronic application.

One of the most versatile and facile methods of covalently grafting organic molecules onto conductive²⁰⁴⁻²⁰⁶ and semiconductive²⁰⁷ materials is the reduction of aryl diazonium salts ($\text{Ar-N}\equiv\text{N}^+\text{X}^-$) through either electrochemical or spontaneous reduction with the substrate.^{208,209} Most of the electrode functionalizations described in the literature address the reduction of simple, small diazonium molecules, with some exceptions, e.g. ruthenium complexes, oligo(phenyl-ethynyl)s, diphenylamines, etc.^{210,211} This is the first study on the reduction of long rod-like diazonium compounds (ca. 6 nm).

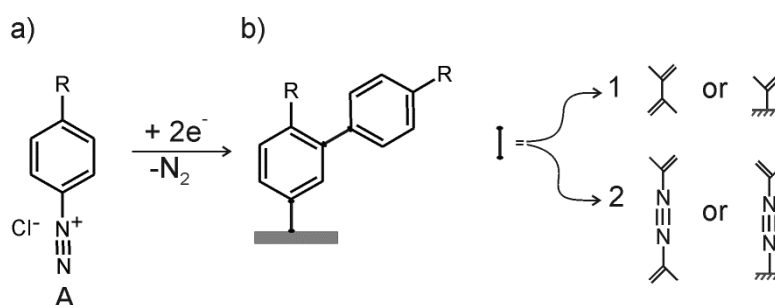
There are two possible polymerization mechanisms of diazonium salts:

a) C-C coupling

In the C-C coupling, the aryl diazonium cation accepts an electron, and aryl radical and N_2 are released. The aryl radical reacts with the electrode surface or with another aryl radical leading to aryl-aryl coupling.^{212,213}

b) azo-bridges coupling (C-N=N-C)

In this reduction process, the aryl diazonium cation accepts an electron from the substrate and generates an aryl radical which attacks another molecule of diazonium salt to form an azo radical-cation. Electrochemical reduction of the formed radical cation yields a neutral azo compound.²¹⁴⁻²¹⁶

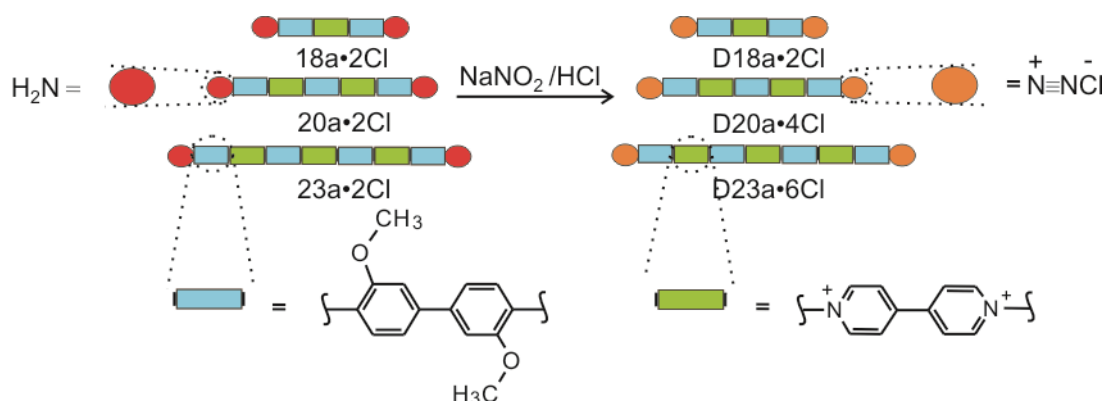


Scheme 4.2 a) Chemical structure of a diazonium molecule A; b) The two possible couplings of diazonium: route 1 (C-C bonds formation) or route 2 (azo-bridges formation). The scheme was adapted from the literature.²¹⁷

4.2 Results and discussion

4.2.1 Reaction of diazotation and coupling

The diazonium species of compounds **18a** (2.4×10^{-3} mM), **20a** (9×10^{-4} mM) and **23a** (6.4×10^{-4} mM) in Cl^- salt form, were prepared in 0.5 M HCl in the electrochemical cell and were not isolated prior to grafting. In order to solubilize **20a**•4Cl and **23a**•6Cl, their solutions were warmed up to 45°C and 3 eq. NaNO_2 was added (color change from green-brown to yellow (Scheme 4.3). The diazonium products were found to be quite stable; their solution was still usable for electrode grafting three weeks after preparation when stored in the refrigerator under Ar.



Scheme 4.3 Synthesis of rod-like viologen diazonium salts.

The electrodes (GC, Au and ITO) were modified by CV and by constant potential reduction of the diazonium salt. The grafted substrate was then thoroughly washed with distilled water to remove any physisorbed molecules and then dried under Ar. The modified surfaces were investigated by CV, UV-Vis, FT-IR, STM and XPS.

a) Electropolymerization of the rod-like viologen diazonium salts (**D18a**, **D20a** and **D23a**) by repetitive cycling

The first scan of a CV obtained for **18a•2Cl** on a bare Au electrode (Fig. 4.1 black line) shows the first viologen reduction peak at -0.27 V. After nitrite addition, the CV shows the classical diazonium electro-reduction feature with an irreversible peak at -0.33 V (Fig. 4.1-a red line). On a second scan, this peak disappeared. The thickness of the film still increases, with the number of potential scans.

In comparison to **18a•2Cl**, compounds **20a•4Cl** and **23a•6Cl** are hardly soluble in aq. HCl and give featureless CV responses (Fig.4.2-a). After nitrite addition, the irreversible reduction peak of the diazonium was observed at -0.14 V. The increase of the peak current observed after repetitive cycling, concomitant with the disappearance of the diazonium peak indicate that the electrode is grafted with each voltammetric cycle. A new reduction peak appears at -0.25 V and is attributed to the first one electron reduction of the oligo-viologen film grafted onto the electrode (Fig. 4.2-a green line).

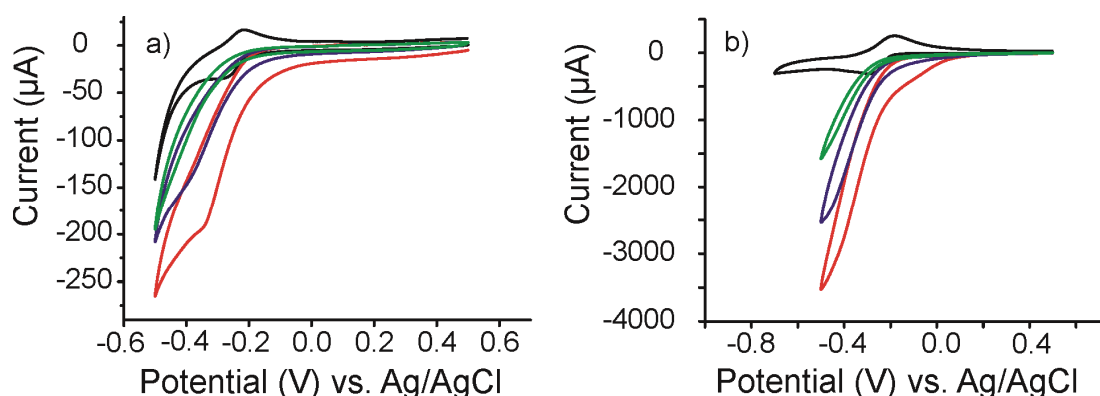


Figure 4.1 CVs of **18a•2Cl** (2.4×10^{-3} mM) in 0.5M HCl on: a) Au and b) ITO electrode (black line). Reduction of in situ formed diazonium salt: 1st cycle red line; 2nd cycle blue line; 10th cycle green line. Scan rate 0.1 V/s.

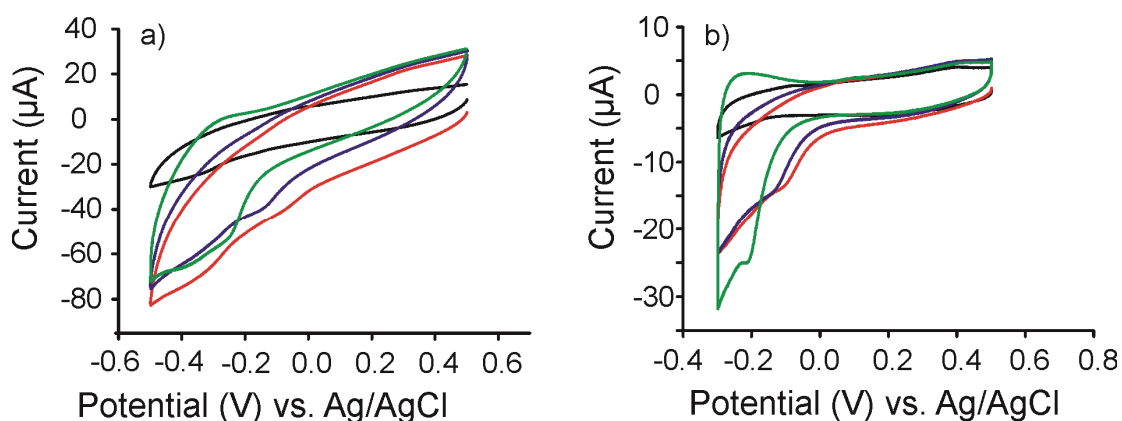


Figure 4.2 CVs of **20a•2Cl** (9×10^{-4} mM) in 0.5M HCl on: a) GC and b) Au electrodes (black lines). Reduction of in situ-formed diazonium salt: 1st cycle red line; 2nd cycle blue line; 10th cycle green line. Scan rate 0.1 V/s.

b) Electropolymerization of the rod-like viologen diazonium salts (**D18a**, **D20a** and **D23a**) by constant potential

The electrodes (GC, Au and ITO) were grafted from solutions of diazonium (**D18a**, **D20a** and **D23a**) in HCl 0.5M. The potential was set at -0.4 V for 250 s. After electrolysis, the electrodes were rinsed thoroughly with water.

4.2.2 Electrochemical characterization of the modified electrodes with the rod-like viologen polymers (Poly-18a, Poly-20a and Poly-23a)

Fig. 4.3 and 4.4 shows CVs recorded in 0.1M aq. KCl for **Poly-18a** and **Poly-20a** on Au, GC and ITO electrodes after cycling for 10 scans.

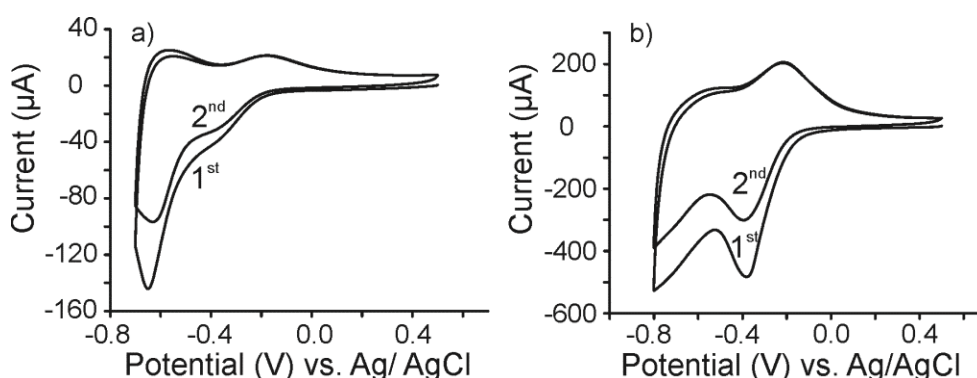


Figure 4.3 CVs of a) Au-**Poly-18a** ($\Gamma = 1.71 \times 10^{-9}$ mol/cm²) and b) ITO- **Poly-18a** ($\Gamma = 4.45 \times 10^{-9}$ mol/cm²) in 0.1M aq. KCl after derivatization in CV mode, scan rate 0.1V/s.

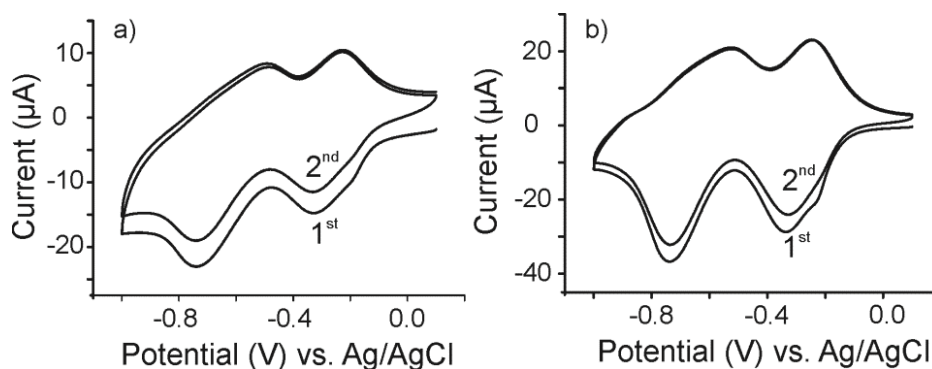


Figure 4.4 CVs of a) GC-**Poly-20a** ($\Gamma = 4.63 \cdot 10^{-9} \text{ mol/cm}^2$) and b) Au-**Poly-20a** ($\Gamma = 9.13 \cdot 10^{-9} \text{ mol/cm}^2$) in 0.1M aq. KCl after derivatization in CV mode, scan rate 50 mV/s.

The cyclic voltammetric responses of the modified electrodes with polyviologens (-0.4 V for 250 s and after cycling for 10 scans) in blank electrolyte shows the $2 e^-$ reduction of the viologen subunits. Obviously, the coupling of a diazonium salt was successful (Fig. 4.5-a, b and Fig. 4.6-a, b).

The voltammograms give rise to reversible reductions corresponding to the reduction of the grafted viologens. The two reversible peaks ascribed to the $V^{2+}/V^{+\cdot}$ and $V^{+\cdot}/V^0$ are cathodically (to more negative potential) and anodically (to more positive potential) shifted upon grafting on ITO glass (Fig. 4.5 and 4.6). This is due to the slow diffusion of counteranions. The thicker the polymer the slower the diffusion.

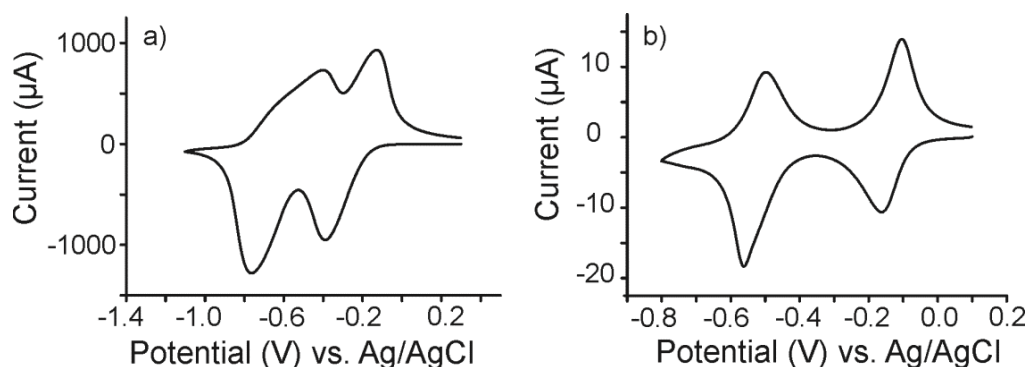


Figure 4.5 CVs of a) ITO-**Poly-18a** electrode ($\Gamma = 5.35 \cdot 10^{-8} \text{ mol/cm}^2$) in 0.1M KCl; b) Au-**Poly-23a** electrode ($\Gamma = 1.50 \cdot 10^{-9} \text{ mol/cm}^2$) in 0.1M DMF- $n\text{-Bu}_4\text{NPF}_6$; scan rate 50 mV/s.

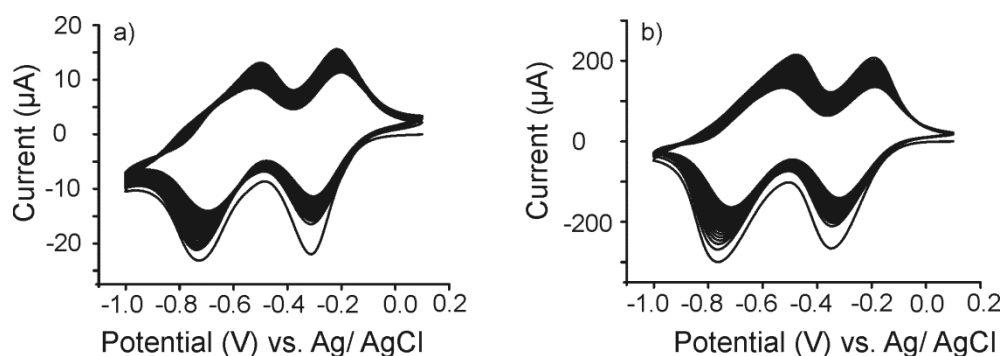


Figure 4.6 CVs (50 scans) of a) GC-**Poly-20a** electrode ($\Gamma = 6.28 \times 10^{-9}$ mol/cm²) and (b) ITO-**Poly-20a** electrode ($\Gamma = 6.47 \times 10^{-9}$ mol/cm²) in 0.1M aq. KCl.

The surface coverage of the attached viologen subunits was evaluated from the area under the reduction peaks. The theoretical surface coverage for a close-packed monolayer was calculated with ArgusLab 4.0.1 based on the van der Waals radii. The area of the methoxy groups bonded at the edge of the phenyl ring is $\sim 7.5 \times 10^{-10}$ mol/cm² for rectangular molecules on the surface. The electrochemical reduction of **D18a**, **D20a** and **D23a** on Au, GC and ITO results in the formation of a multilayer.

4.2.3 FT-IR and XPS characterization of the modified electrodes (Poly-18a-ITO and Poly-20a-ITO)

FT-IR and X-ray photoemission spectroscopy measurements were performed on modified ITO electrodes in order to provide further evidence for the reduction of diazonium groups and polymer growth. In the XPS C1s spectra (Fig. 4.7-a) of the **Poly-20** on ITO, the dominant peak component at 284.7 eV is assigned to the C-C species, the peak at 286 eV correspond to the C-O^{218,219} and C-N species²²⁰ and the shoulder at 289 eV is assigned to carbonyl group (C=O) of oxygen containing hydrocarbons contaminants present in atmosphere, or can result from the C-O bond degradation upon electron bombardement.¹¹⁹ The N1s core level spectra (Fig. 4.7-b) of the

polyviologen grafted film can be fitted with two peaks. The peak at 401.7 eV is assigned to the positively charged nitrogen of viologen, the one at 399.5 eV is attributed to the viologen radical cation formed during X-ray excitation in the analysis chamber.²²¹

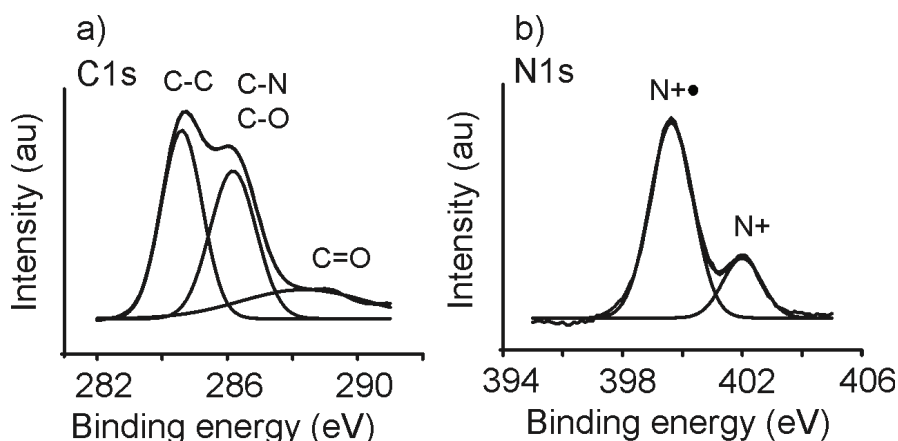


Figure 4.7 C1s a) and N1s b) core level spectra recorded on **Poly-20-ITO** modified electrode. Polymerization time 500 s; $\Gamma_{\text{Poly-20}} = 1.08 \times 10^{-8} \text{ mol/cm}^2$.

The absence of a peak at 403.8 eV in N1s spectra confirms that unreacted diazonium species are not present at the surface.²²² Anyway, the protonated amine or the amine group of viologen precursor can also appear in N1s spectra at ca. 400 and 402 eV.^{223,224} A better analysis of ITO-modified electrode is provided by the FT-IR spectra of the polymer film on ITO.

A comparison of the FT-IR spectra of the original compound **18a·2Cl** and the diazonium salt **D18a** on the surface (Fig. 4.8) of the grafted film (**Poly-18a-ITO**) can be interpreted as follows: the diazonium salt is reduced to phenyl radical (with loss of N_2) and aryl-aryl coupling take place. The FT-IR spectrum of the isolated diazonium salt **D18a** shows that the both amine groups have been diazotized. This is confirmed by the absence of stretching bands for aromatic amines (in-plane N-H bend of at 1525 cm^{-1} and C-N stretch at 1296 cm^{-1} in Fig. 4.8-a) and the presence of $\text{C-N}\equiv\text{N}^+$ stretching

vibration at 2235 cm^{-1} (Fig. 4.8-b). Further, the lack of the band at 2235 cm^{-1} characteristic for diazonium groups in Fig. 4.8-c indicates that the reduction of **D18a** was complete and the polymer grows through aryl-aryl coupling.

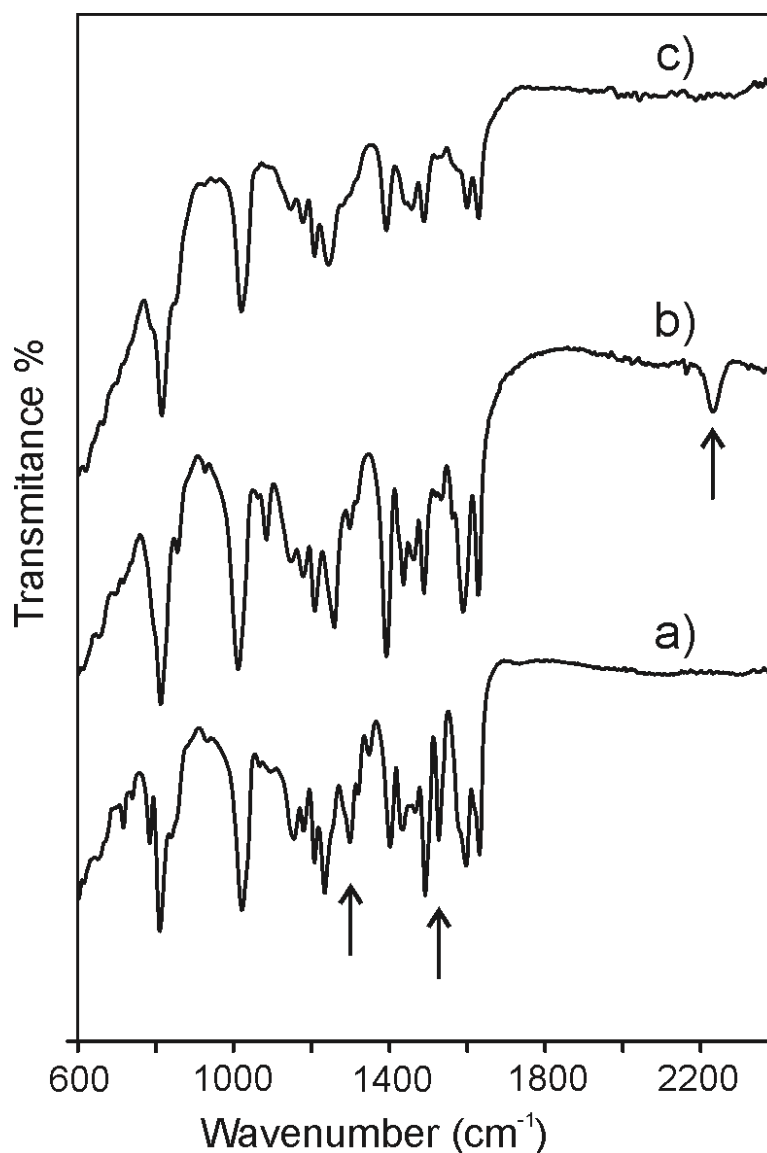


Figure 4.8 FT-IR spectra: a) **18a•2Cl**; b) **D18a•2Cl**; and c) **Poly-18a** on ITO.

4.2.4 Spectroelectrochemical characterization of Poly-18a and Poly-23a on ITO

The UV-Vis spectra of **Poly-18a** and **Poly-23a** on ITO (Fig. 4.9) in oxidized and reduced state, can be considered as a superposition of **18a•2PF₆** and

23a•6PF₆ except some shifts in the absorption maxima in oxidized state and the absence of the peak at 538 nm assigned to a viologen dimer.

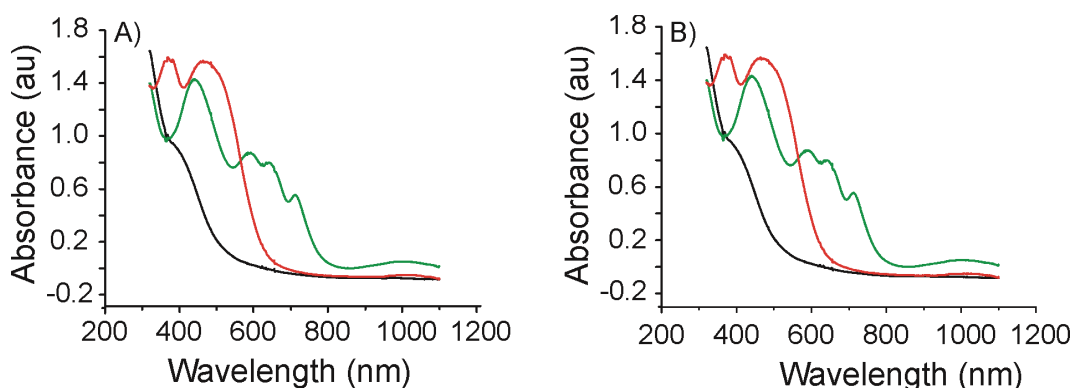


Figure 4.9 UV-Vis spectra of: A) **Poly-18a** and B) **Poly-23a** on ITO. The spectra were registered at different potential steps: 0.0 V (black lines); -0.45 V (green lines) and -1.0 V (red lines).

4.2.5 STM investigation of Poly-18a, Poly-20a and Poly-23a on ITO

A detailed STM analysis of a bare ITO electrode was given in Chapter 2, Section 2.2.7. Fig. 4.10-D is a “far-view” STM image of **Poly-20a** on ITO. The polymer chains appear as rod-like bundles of different lengths.

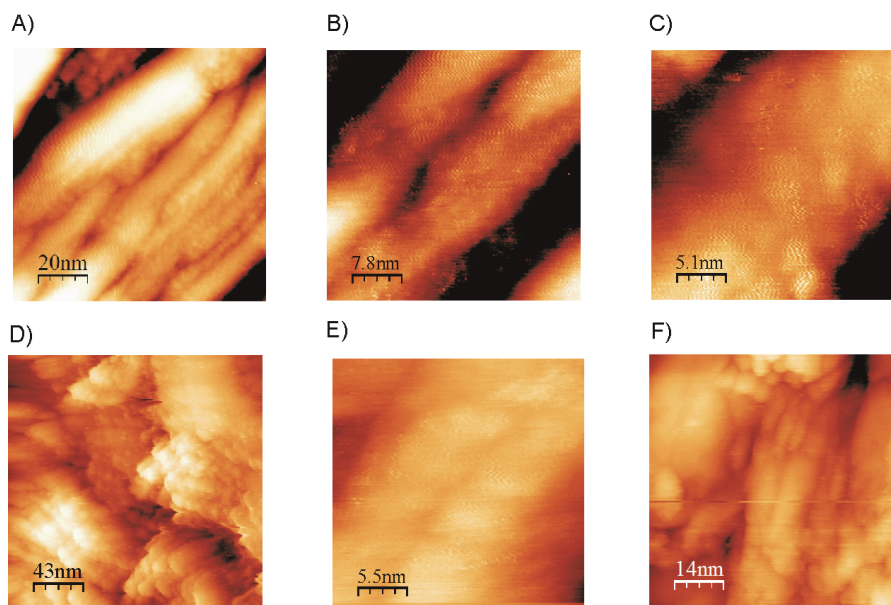


Figure 4.10 STM images ($V_b = 0.050$ V, $I_t = 1.001$ nA) of **Poly-18a** ($\Gamma_{\text{Poly-18a}} = 2 \cdot 10^{-8}$ mol/cm², A-C), **Poly-20a** ($\Gamma_{\text{Poly-20a}} = 1.08 \cdot 10^{-8}$ mol/cm², D-E) and **Poly-23a** ($\Gamma_{\text{Poly-23a}} = 2.5 \cdot 10^{-9}$ mol/cm², F) on ITO: A) 100 x 100 nm, Z range 12.5 nm; B) 45 x 45 nm, Z

range 6.25 nm; C) 25 x 25 nm, Z range 3.13 nm; D) 214 x 214 nm, Z range 25 nm; E) 27 x 27 nm Z range 3.13 nm; F) 72 x 72 nm, Z range 25 nm.

A closer view (Fig. 4.11-B, D) reveals oval-shaped structures whose lateral dimension is ca. 5 nm. Thus, the molecules deposited onto ITO have the size of the monomers involved in formation of a diazonium moiety (model structure on top of the STM image) and is the repetitive units of the polymer.

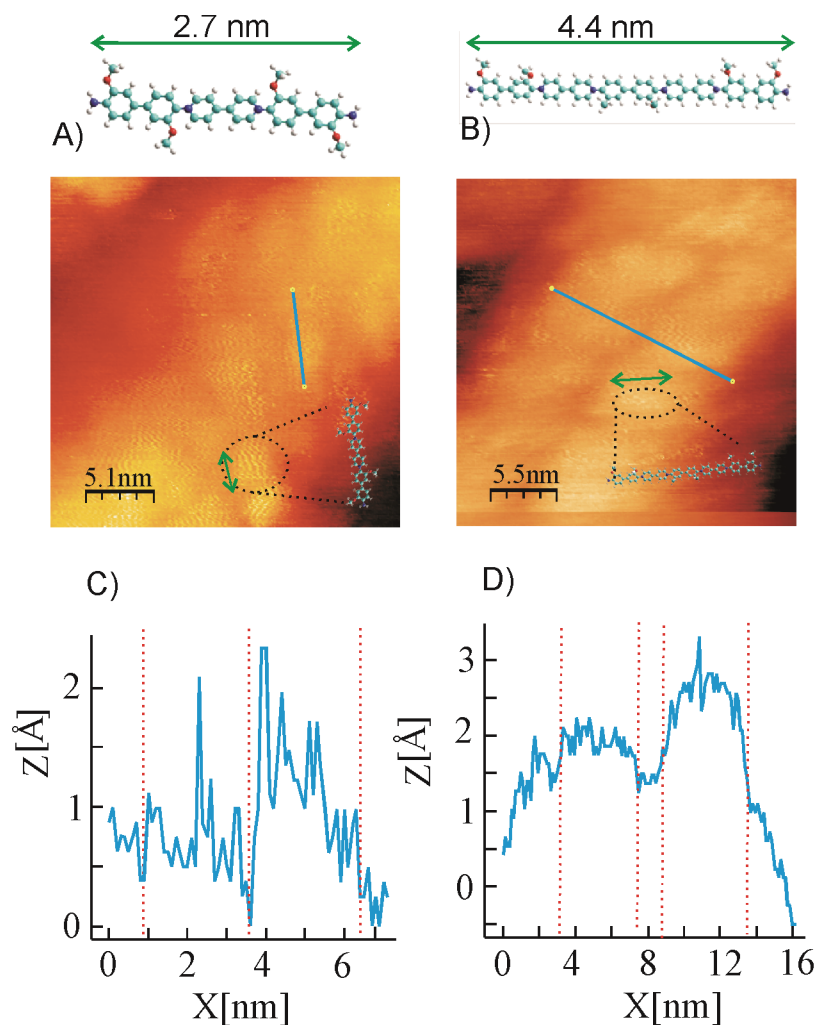


Figure 4.11 STM images ($V_b = 0.050$ V, $I_t = 1.001$ nA) and topographic profiles of **Poly-18a** (A) and **Poly-20a** (B): A) 25 x 25 nm, Z range 3.13 nm; B) 27 x 27 nm, Z range 3.13 nm; C) topographic profile along the blue line in A) and D) topographic profile along the blue line in B).

Similar topographic structures were observed for **Poly-18a** on ITO (Fig. 4.10-A-C). The size of one bright spot (Fig. 4.11-A, C) (around 2.4 nm) is

comparable with the size of a single molecule of **18a** (model structure on top of the STM image). Fig. 4.10-F reveals the rod-like structure of **Poly-23a** of ca. 6 nm width. The polymer multilayer showed disorder, revealing growth in a parallel fashion on the ITO surface. It is not surprising since the length of the monomer used for electropolymerization is 6.1 nm.

4.3 Conclusions

The viologens containing amino groups (**18a•2Cl**, **20a•4Cl** and **23a•6Cl**) were successfully converted into their diazonium salts. The modification of conductive surfaces: GC, Au and ITO on glass, with the rods was observed by electrochemical reduction of "in situ" prepared diazonium salts. The generation of a C-C bond between the 3,3'-methoxy-biphenyl moieties with loss of N₂ was confirmed by FT-IR measurements. The electrochemistry and electrospectroscopic behavior of the polymer is similar to that of the monomer. The polymer thickness is controlled by the reduction time.

STM images of the polymers grafted on ITO (**Poly-18a**, **Poly-20a** and **Poly-23a**) show polymer strips composed of repetitive monomers unit as oval-shaped structures. The monomers (**18a**, **20a** and **23a**) can be distinguished by STM. Applications of the functionalized substrates in electrochemical and electrochromic devices as electron mediators and biosensors are envisioned.

4.4 Experimental

4.4.1 Materials

Acetonitrile (MeCN, Sigma-Aldrich), N,N-dimethylformamide (DMF, Sigma-Aldrich), HCl (37 %, Sigma-Aldrich), NaNO₂ (Alfa Aesar), tetrabutylammonium

hexafluorophosphate ($n\text{-Bu}_4\text{NPF}_6$, Fluka), KCl (Merck). All chemicals were of reagent grade quality and used as received from the supplier.

4.4.2 General procedure of diazotization

The diazonium salts of rod-like viologen-oligomers were generated in situ as follows: **18a** (2.4×10^{-3} mM), **20a** (9×10^{-4} mM) and **23a** (6.4×10^{-4} mM) were dissolved in 0.5 M HCl. 3eq. NaNO_2 were added and the solution bubbled with Ar for 5 minutes. The diazonium salts obtained were electrochemically reduced to modify GC, Au and ITO electrodes.

4.4.3 Cleaning procedure

GC and Au electrodes were polished by alumina slurry on a cloth polishing pad and then ultrasonicated in double distilled water followed by drying under Ar. ITO glass was cleaned after conventional procedure.¹²⁹

4.4.4 Electropolymerization (grafting)

The electrochemical modification was performed with diazonium salts: **D18a**, **D20a** and **D23a**. The modification was followed by CV (potential cycle between 0.5 V and -0.5 V) and by constant potential (-0.4 V). The three-electrode electrochemical cell used for electropolymerization has been described in Chapter 2, Section 2.4.1.

The ITO electrodes used for grafting were of different size: 90 mm² for electrode modification and UV-Vis, 150 mm² for FT-IR and 30 mm² for STM measurements.

4.4.5 Spectroelectrochemistry of Poly-18a and Poly-23a at ITO electrode

The polymer film was grafted on an ITO electrode by electrochemical reduction of the diazonium salt at -0.4 V for 250 s. The equipment used for spectroelectrochemical experiments has been described in detail in Chapter 2, Section 2.4.4. The spectroelectrochemical measurements were performed under potentiostatic conditions in the negative range from 0 to -1.0 V. Spectra were recorded when the absorption was constant, after 200 s.

4.4.6 FT-IR investigation of 18a, D18a and Poly-18a on ITO

The spectra were recorded over the wave number range of 400–4000 cm^{-1} for viologen-oligomer **18a**, its diazonium salt **D18a** and **Poly-18a**-modified ITO electrode. The apparatus used for FT-IR measurements has been mentioned in Chapter 2, Section 2.4.8.

The **Poly-18a**-modified electrodes were obtained by electrochemical reduction of diazonium salts at -0.4 V for 1000 s.

D18a was isolated from solution by precipitation with acetone. The precipitate was filtered, washed with MeOH and dried under high vacuum.

4.4.7 STM investigation of ITO-modified with Poly-18a, Poly-20a and Poly-23a

The experimental set-up used for STM measurements has been described in Chapter 2, Section 2.4.6.

The polymer-coated ITO electrodes were prepared by electrochemical reduction of diazonium salts at constant potential (-0.4 V for 500 s). After modified electrodes were rinsed with water and subjected to STM analysis.

5 Conjugated viologen rods with amide and ester linkage

5.1 Introduction

The synthesis of redox-active π -conjugated systems which present n-type conductivity is a subject of high interest especially for organic photovoltaic technology. The work described in this chapter was motivated by the applications of viologen-based π -conjugated systems as n-type semiconductor systems in organic devices such as field-effect transistors (OFETs),^{225,226} light-emitting diodes (OLEDs),²²⁷ solar cells,²²⁸ and by the formation of supramolecular assemblies that show improved redox and binding properties. The control of the electronic properties of viologen-based π -conjugated systems could be achieved by synthesis of viologen-oligomers. Through chemical tuning of redox-active oligomers it is possible to control molecule's properties like electrochromic properties or reduction potentials.²²⁹ These parameters depend on the levels of the frontier orbital's and their energy gap.^{230,231}

Synthetic approaches were developed to control the HOMO-LUMO gap of conjugated oligomers and hence of the band gap of the new synthesized molecule. The strategy used to design the extended viologen derivatives in the present chapter was the quaternization of 4,4'-bipyridine by conjugated moieties (benzamide or esters).

The synthesis of the molecules described in the current chapter is based on the idea that linking phenyl/thiophene moieties with viologen groups could influence the electronic properties.

Oligo-p-benzamides possess an extended rod-like structure^{232,233} and form self-organized building blocks due to their extended H bonding. The amide linkages of the oligo-p-benzamides are in trans conformation and form hydrogen bonds between polymer chains resulting in helical structures.^{234,235}

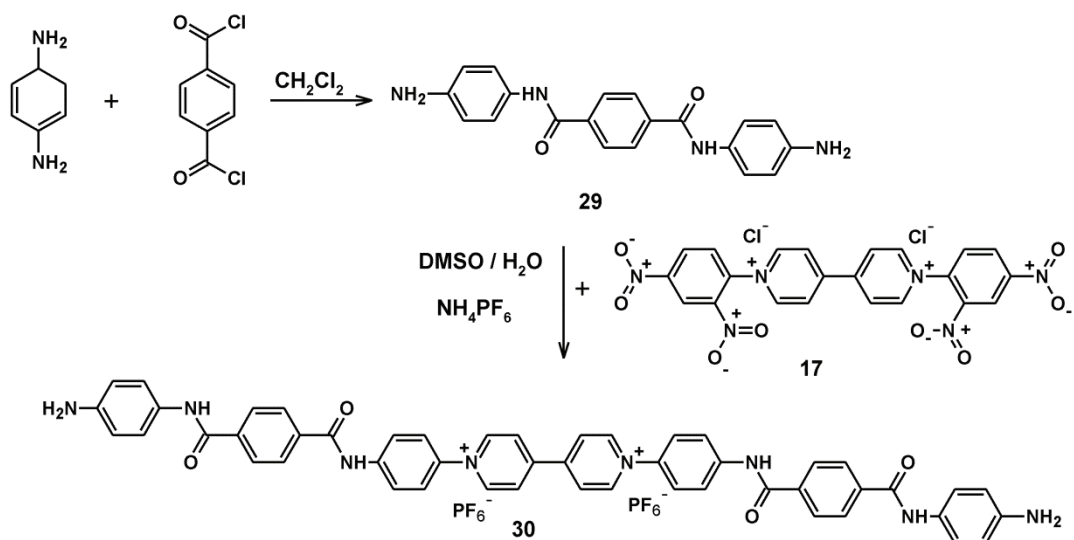
For the synthesis of conjugated viologen-based molecules, it is expected that the introduction of 4,4'-bipyridine into an oligomeric amide backbone provides solubility of the viologen-oligomers in organic solvents and water.

Water-soluble viologen derivatives that have higher oxidation potentials than FAD can mediate electrons efficiently from the FAD centers of glucose oxidase to the electrode substrate.²³⁶ It has already been reported that π -conjugated and heteroaromatic compounds like viologens act as drugs and interact with DNA forming complexes^{237,238} to inhibit gene replication. The supramolecular chemistry of p-benzamides or thiophene-phenylene-esters combined with the redox and electrochromic properties of viologens enable the design of new DNA-targeted drugs which could show improved redox and nucleic acid binding properties. More significantly, in tissue they could be easily fragmented into small molecules by hydrolysis or enzymatic degradation.

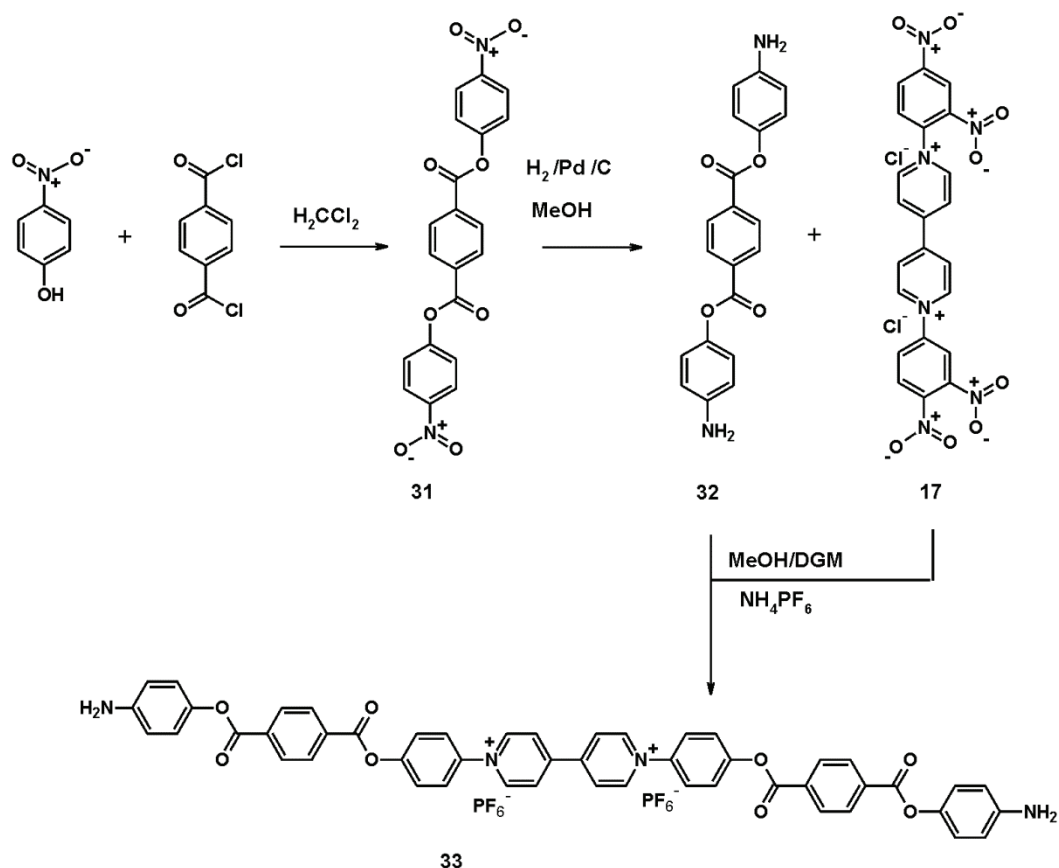
5.2 Results and discussion

5.2.1 Synthesis

A first synthetic trial towards amide based-oligoviologens consists of the combination of two viologen subunits via a benzamide linkage (Scheme 5.1). Bis-1,1'-carboxy-/(amino)-phenyl-bipyridiniums **26** (prepared according to the literature)¹⁴⁹ and **27** (prepared after a procedure described in the literature)^{239,240} were synthesized as monomeric units by the Zincke reaction



Scheme 5.2 Synthesis of bis-1,1'-[N¹,N⁴- bis (4-(amino-phenyl)phenyl) benzene-1,4-dicarboxylate]-4,4'-bipyridinium hexafluorophosphate (**30**).



Scheme 5.3 Synthesis of bis-1,1'-[(4,4'-(amino-phenyl)phenyl)benzene-1,4-dicarboxylate]-4,4'-bipyridinium hexafluorophosphate (**33**).

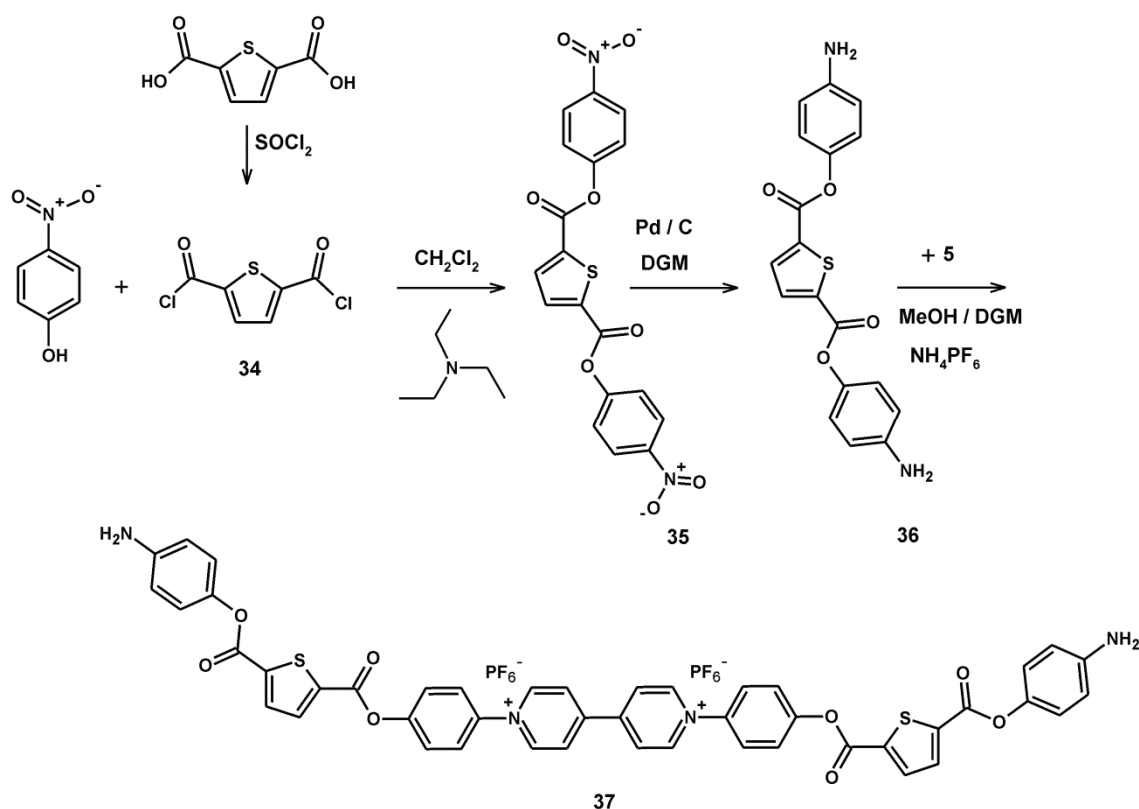
Due to its electron withdrawing character, the 4,4'-bipyridinium subunit increases the acidity of **26**, whereas the basicity of amine **27** is reduced.

The amide formation was finally successful for p-phenylenediamine (PPD) when the reaction was performed with terephthaloyl chloride in dichloromethane (DCM) (Scheme 5.2). The synthesis of **29** was reported by Y. Qian et al.²⁴⁷ and was prepared by reaction of PPD with a series of terephthalic acid esters.

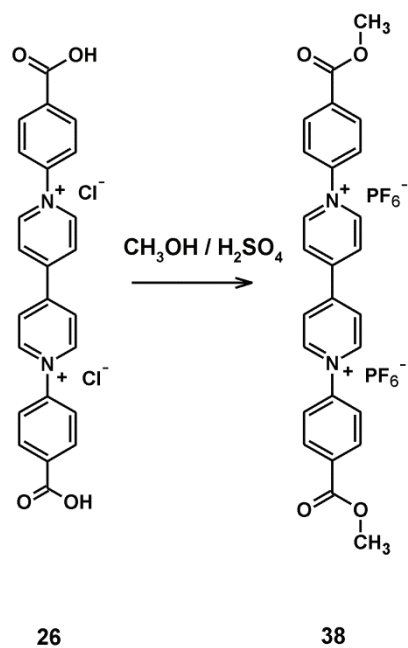
The preparation of the amide **29** from terephthaloyl chloride in dry DCM yielded **29**, a product which could be characterized by NMR spectroscopy. Compound **29** is an amide with additional amino end groups which was reacted with **17** by Zincke reaction in DMSO to afford **30** (Scheme 5.2). Due to its very low solubility in H₂O, MeOH or any other solvent, conversion of **30** into the PF₆⁻ salt was only possible with a poor yield (10.3 %).

In another approach, conjugated viologen rods with ester linkage were synthesized. For this, conjugated dicarboxylates (**32** and **36**) were reacted with **17** by Zincke reaction. **31** was obtained according to Atkins²⁴⁸ with some minor modifications (see detailed experimental procedure) in good yield (87.95 %). The nitro groups were reduced successfully in DGM (diethylene glycol dimethyl ether) to the amine to form **32**.

The viologen rod **33** was obtained by the Zincke reaction of **32** with **17** in high yield (71.57 %). The same reaction scheme was applied to synthesize **37** which is a viologen-thiophene-based conjugated molecule (Scheme 5.4). The synthesis of 2,5-thiophenyldicarbonyl dichloride (**34**) was reported.²⁴⁹



Scheme 5.4 Synthesis of bis-1,1'-[4,4'-(amino-phenyl)phenyl]thiophene-2,5-dicarboxylate-4,4'-bipyridinium hexafluorophosphate (**37**).



Scheme 5.5 Synthesis of bis-1,1'-bis(4-methylbenzoate)-4,4'-bipyridinium bis(hexafluorophosphate) (**38**).

Compound **34** was prepared from 2,5-thiophenyl carboxylic acid with an excess of thionyl chloride (89 %), which further was reacted with p-nitrophenol to afford **35**. The reduction of the two nitro groups proceeded in a similar way as for **32** to form **36** which finally reacts with **17** in MeOH/DGM mixture (1:2) and yields **37** (56.91 %).

The ester **38** (Scheme 5.5) can be obtained by the Zincke reaction of **17** with the methyl-4-aminobenzoate in methanol/water (80 %, V/V). The yield of this reaction was low (20 %). Compound **38** was obtained in good yield (78.62 %) when **26** was esterified with methanol and sulphuric acid.

5.2.3 Cyclic voltammetric characterization of **30** and **38**

Cyclic voltammetric investigation of **30**

Electrochemical studies on **30** were performed at RT. Fig. 5.1 shows the CV of **30**. The first two peaks are characteristic for the reduction of viologen to a viologen radical cation (~ -0.2 V) and a neutral viologen (~ -0.49 V).

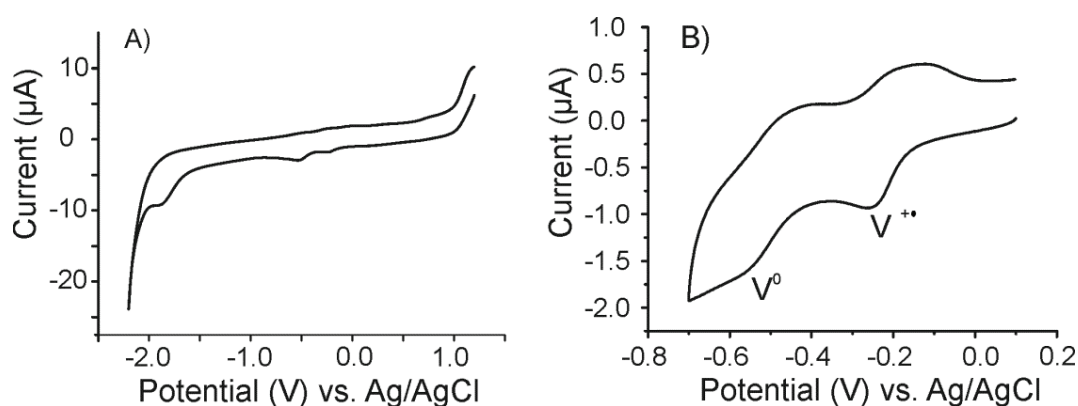


Figure 5.1 Cyclic voltammograms of **30** (0.86×10^{-3} M) in DMSO-0.1M $n\text{-Bu}_4\text{NPF}_6$ at a sweep rate of 100 mVs^{-1} . The potential was swept from: A) +1.2 V and -2.2 V and B) 0.1 V and -0.7 V.

An irreversible cathodic peak shifted to more negative potentials was observed in CV, which was attributed to benzamide reduction. For several

benzamide derivatives this reduction was observed between -2.0 V and -2.5 V.^{250,251}

Cyclic voltammetric investigation of **38**

The presence of viologen subunit was observed when the compound was examined using cyclic voltammetry. One electron reduction of viologen subunit was observed at ~ -0.1 V (Fig. 5.2). The small irreversible reduction peak at -0.37 V (ref. Ag/AgCl) was attributed to the reduction of the benzoate to benzoate radical anion formation which decomposes and forms a benzoate anion (Scheme 5.6).²⁵² It is known that esters which are activated by the presence of an additional electroactive group are easily reduced.²⁵³ The oxidative back peak at +0.78 V observed for **38** was assigned to the oxidation of the benzoate anion, facilitated by the electron-withdrawing bipyridinium ring.²⁵⁴

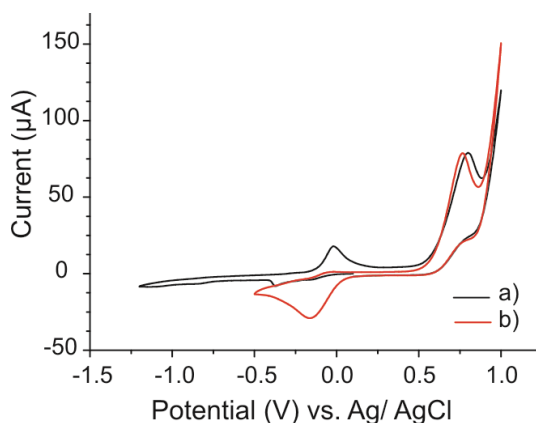
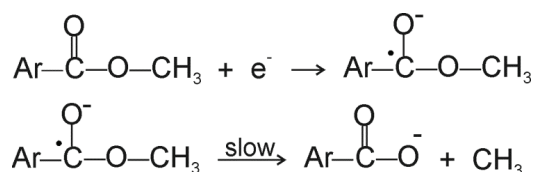


Figure 5.2 Cyclic voltammograms of **38** (1.9×10^{-3} M) in DMF-0.1M n-Bu₄NCl at the scan rate 100 mVs⁻¹. The potential was cycled between: a) +1.0 V and -1.2 V and b) 0.1 V and -0.5 V.



Scheme 5.6 Electrochemistry of benzoate ester at GC electrode.

5.3 Conclusions

In attempts to apply different strategies reported for the preparation of amide bond in general by the connection of **26** with **27** failed. One explanation is the presence of 4,4'-bipyridinium subunit which has an electron withdrawing character and slows down the amide formation reaction.

Molecules **30** and **33** with a viologen subunit consisting of benzene-1,4-dicarboxylates and amide/ester bridge were synthesized using the Zincke reaction. These molecules could find applications in the construction of supramolecules.

A new conjugated molecule (**37**) containing a donor (thiophene unit) and an acceptor (4,4'-bipyridine) moiety have been successfully synthesized. Their molecular structures are confirmed by ^1H -NMR and ^{13}C -NMR. The molecule containing the amide linkage is hardly soluble in DMSO or DMF. By replacing the amide bond with an ester, the solubility in organic solvents DMSO, DMF, MeCN increases. One-electron reduction of benzoates esters is complicated, and results in the formation of radicals that are decomposing and form more complicated products.

5.4 Experimental part

5.4.1 Materials and devices

^1H -NMR and ^{13}C -NMR spectra were recorded on Bruker Avance spectrometer at 250 and 63 MHz, respectively, using the solvent signal as internal standard.

The reagents: p-aminobenzoic acid (PABA) (Fluka, $\geq 98\%$), ammonium hexafluorophosphate (NH_4PF_6) (Fluorochem, $\geq 99\%$), tetrabutylammonium hexafluorophosphate ($n\text{-Bu}_4\text{NPF}_6$) (Sigma-Aldrich, $\geq 99\%$), 1,4-phenylene-

diamine (PPD) (Fluka, $\geq 97\%$), triethylamine (Fluka, $\geq 99.5\%$), terephthaloyl chloride (Sigma-Aldrich, $\geq 99\%$), sodium hydrogen carbonate (NaHCO_3) (Riedel de Haën, 99.7%), p-nitrophenol (Fluka, $\geq 99.5\%$), Pd/C (10% , Fluka), Celite (Fluka), 2,5 thiophenecarboxylic acid (Acros Organics, 96%), sulphuric acid (H_2SO_4) (Sigma-Aldrich, $95\text{--}97\%$), 3-amino-phenol (Aldrich, 98%), 4-aminophenol (Riedel de Haën, 99%) and 1,3-phenylene diamine (TCI, $> 98\%$) were used as purchased.

The organic solvents were purified following procedures described in the literature. All other solvents: diethyl ether (Sigma-Aldrich, $\geq 99\%$), diethylene glycol dimethyl ether (DGM) (Fluka, 99.5%), dimethyl sulfoxide (DMSO) (Sigma-Aldrich, $\geq 99.9\%$) and acetonitrile (MeCN) (Sigma-Aldrich, $\geq 99.9\%$) were used as received.

5.4.2 Cyclic voltammetric investigation of compounds **30 and **38****

The experimental set-up used for the cyclic voltammetric investigation of **30** and **38** has been described in Chapter 2, Section 2.4.1.

The voltammograms were scanned between $+1.2\text{ V}$ and -2.2 V for **30**, and 1.0 V and -1.2 V for **38**, at a scan rate of 100 mVs^{-1} . All solutions were de-aerated by Ar bubbling for 3 minutes prior to the electrochemical experiment. Prior to each electrochemical measurement, the working electrode (GC) was carefully polished with alumina powder on a polishing cloth and then rinsed with distilled water.

5.4.3 Detailed synthetic procedure

26•2PF₆ (C₂₄H₁₈F₁₂N₂O₄P₂): 1,1'-Bis(4-carboxyphenyl)-4,4'-bipyridinium dichloride

To a solution of 2 g (3.5 mmol) 1,1'-bis(2,4-dinitrophenyl)-4,4'-bipyridinium dichloride (**17**) in 200 ml MeOH/water (8:2 V/V) 1.14 g (8.3 mmol) p-aminobenzoic acid (PABA) in 50 ml MEOH/water (8:2 V/V) was added and stirred with reflux for 72 h. While adding PABA, the color of the solution changed immediately from yellow to dark red. After cooling to RT, the product was precipitated by adding 350 ml diethyl ether. The yellow precipitate formed was filtered and washed with diethyl ether. After drying in vacuum, 1.68 g of **26•2Cl** was obtained as yellow powder (yield 69.11 %). Further, **26** was dissolved in MeOH and added to 10 ml 3M aq. NH₄PF₆ to afford the PF₆⁻ salt as a beige precipitate. It was filtered and washed twice with water and dried under high vacuum (**26•2PF₆**: 2.3 g, yield 93.6 %).

¹H-NMR (d₆-DMSO, 250 MHz): 8.11 (s, CH_{arom.}, 4H); 8.31 (s, CH_{arom.}, 4H); 9.10 (s, Vio, 4H); 9.75 (s, Vio, 4H).

¹³C-NMR (d₆-DMSO, 63 MHz): 125.93; 127.15; 131.49; 134.06; 145.46; 146.51; 149.79; 166.58.

29 (C₂₀H₁₈N₄O₂): N¹,N⁴-bis[(4-amino-phenyl)]benzene-1,4-dicarboxylate

To a solution of 5.83 g (53.95 mmol) PPD and 1.1 ml (8 mmol) triethylamine in 100 ml dry DCM, 1.08 g (5.33 mmol) terephthaloyl chloride in 40 ml DCM was added on ice bath in portions over 10 minutes while stirring. Upon addition of terephthaloyl chloride, formation of a yellow precipitate was observed. The solution was further refluxed for 1 h. After cooling to RT, the precipitate was filtered, washed with 150 ml saturated NaHCO₃ solution, 100

ml water and three times with 150 ml acetone. After drying under high vacuum, **4** was obtained as yellow powder (1.62 g, yield 88.18 %).

¹H-NMR (d₆-DMSO, 250 MHz): 4.96 (bs, (NH₂), 4H); 6.55 (bs, CHarom., 4H); 7.38 (bs, CHarom., 4H); 8.01 (bs, CHarom. dicarboxylate ring, 4H); 10.03 (bs, NHamide, 2H).

¹³C-NMR (d₆-DMSO, 63 MHz): 114.14; 122.75; 127.86; 128.31; 137.84; 145.82; 164.44.

30•2PF₆ (C₅₀H₄₀F₁₂N₈O₄P₂): Bis-1,1'-[N¹, N⁴-bis(4-(amino-phenyl)phenyl)benzene-1,4-dicarboxylate]-4,4'-bipyridinium hexafluorophosphate

1g (2.9 mmol) of N¹,N⁴-bis(4-aminophenyl)-terephthalamide (**29**) was dissolved in 80 ml (DMSO/H₂O) mixture (2:1) and heated to reflux. 0.62 g (1.10 mmol) 1,1'-bis(2,4-dinitrophenyl)-4,4'-bipyridinium dichloride (**17**) in 40 ml water was added and stirred for 24 h at 100°C. After cooling to RT, the formed precipitate was filtered. Ethyl acetate was added to the filtrate and the formed precipitate collected by filtration. It was dissolved in H₂O/MeOH mixture and added to 50 ml 3M aq. NH₄PF₆. The formed precipitate (PF₆⁻ salt) was filtered and washed with water. After drying under high vacuum, **30** was obtained as brown powder (0.33 g, yield 10.3 %).

¹H-NMR (d₆-DMSO, 500 MHz): 6.63 (s, CHarom. phenyl ring, 4H); 7.44 (s, CHarom. phenyl ring, 4H); 8.02 (s, CHarom. phenyl ring, 4H); 8.13 (s, CHarom. phenyl ring, 4H); 8.22 (s, CHarom. dicarboxylate ring, 8H); 9.06 (s, Vio, 4H); 9.70 (s, Vio, 4H); 10.83 (s, amide, 2H); 10.89 (s, amide, 2H).

31 (C₂₀H₁₂N₂O₈): 4-(Nitrophenyl)-benzene-1,4-dicarboxylate

To a solution of 5.5 g (39.5 mmol) of p-nitrophenol and 3.5 ml (25.14 mmol) triethylamine in 40 ml DCM at reflux, 2 g (2.85 mmol) terephthaloyl

chloride dissolved in 60 ml DCM was added in portions while stirring and refluxing over about 3 h. The mixture was stirred further for 6 h. The formed precipitate was filtered, washed with 100 ml ethyl acetate and two times with 100 ml hot water. After drying under high vacuum, **31** was obtained as white powder (3.6 g, yield 87.95 %).

¹H-NMR (d₆-DMSO, 250 MHz): 7.67 (d, J= 9.2 Hz, arom. protons of the dicarboxylate ring, 4H); 8.37 (d, J= 7.5 Hz, arom. protons of the phenyl substituted ring, 8H).

¹³C-NMR (d₆-DMSO, 63 MHz): 123.70; 126.05; 130.97; 133.78; 145.82; 155.80; 163.64.

32 (C₂₀H₁₆N₂O₄): Bis(4-aminophenyl)benzene-1,4-dicarboxylate ester

To a solution of 3.18 g (7.8 mmol) of bis(4-nitrophenyl)-benzene-1,4-dicarboxylate (**31**) dissolved in 300 ml diethylene glycol dimethyl ether (DGM) heated to 100°C, 0.5 g Pd/C (10 % Pd) catalyst was added, and the reaction mixture was stirred over night under hydrogen atmosphere. After cooling to RT, the solution was filtered over Celite. The Celite was washed with 50 ml MeOH, the filtrate was evaporated and the yellow residue dried under high vacuum (2.7 g, yield 97.44 %).

¹H-NMR (d₆-DMSO, 250 MHz): 5.14 (s, (NH₂), 4H); 6.60 (d, J= 8.75 Hz, arom. protons of the phenyl ring, 4H); 6.94 (d, J= 8.75 Hz, arom. protons of the phenyl ring, 4H); 8.26 (s, arom. protons of the dicarboxylate ring, 4H).

¹³C-NMR (d₆-DMSO, 63 MHz): 114.51; 122.26; 126.82; 130.46; 134.09; 140.99; 147.27; 164.86.

33•2PF₆ (C₅₀H₃₆F₁₂N₄O₈P₂): Bis-1,1'-[(4,4'-(amino-phenyl)phenyl)benzene-1,4-dicarboxylate]-4,4'-bipyridinium hexafluorophosphate

To a solution of 0.6 g (1.06 mmol) of 1,1'-bis(2,4-dinitrophenyl)-4,4'-bipyridinium dichloride (**17**) in 100 ml MeOH/water (80 %, V/V) heated at reflux, 0.92 g (2.64 mmol) bis (4-aminophenyl)-1,4-benzendicarboxylate ester (**32**) in 100 ml DGM was added. After stirring for 24 h with reflux, MeOH was evaporated, and the precipitate formed was filtered. Further anion exchange to PF₆⁻ was performed by dissolving small portions of the solid in a hot water/MeOH mixture and adding this solution to 10 ml of 3 M aq. NH₄PF₆. The formed precipitate was filtered, washed with 100 ml water and two times with 200 ml hot DGM. After drying under high vacuum, **33•2PF₆** was obtained as brown powder (0.84 g, yield 71.57 %).

¹H-NMR (d₆-DMSO, 250 MHz): 5.23 (bs, (NH₂), 4H); 6.62 (bs, CHarom. phenyl ring, 4H); 6.95 (bs, CHarom. phenyl ring, 4H); 7.86 (bs, CHarom. phenyl ring, 4H); 8.36 (bs, CHarom. dicarboxylate (8H) + CHarom. phenyl ring (4H), 12H); 9.21 (bs, Vio, 4H); 9.94 (bs, Vio, 4H).

¹³C-NMR (d₆-DMSO, 63 MHz): 114.52; 122.32; 124.36; 126.93; 130.51; 130.65; 130.90; 133.22; 134.62; 140.92; 147.38; 164.85.

34 (C₆H₂Cl₂O₂S): 2,5-Thiophenedicarbonyl dichloride

1.5 g (8.63 mmol) of 2,5-thiophenecarboxylic acid was mixed with 25 ml thionyl chloride and stirred for 10 h at 70°C. After cooling to RT, excess thionyl chloride was removed by distillation and the colorless powder dried under high vacuum (1.6 g, yield 89 %).

¹H-NMR (CDCl₃, 250 MHz): 7.99 (s, 2H).

¹³C-NMR (CDCl₃, 63 MHz): 136.50; 145.49; 159.86.

35 (C₁₈H₁₀N₂O₈S): Bis(4-nitrophenyl)benzene-2,5-thiophene-dicarboxylate:

To a solution of 4 g (28.3 mmol) p-nitrophenol and 2.1 ml (15.08 mmol) triethylamine in 40 ml DCM at reflux, 1.5 g (7.17 mmol) terephthaloyl chloride dissolved in 60 ml of DCM, was added in portions while stirring and refluxing over about 30 minutes. The mixture was stirred for further 24 h. The white precipitate formed was filtered, washed with 30 ml DCM and three times with 100 ml hot water. After drying under high vacuum, 2.51 g of **35** was obtained as white powder (yield 84.61 %).

36 (C₁₈H₁₄N₂O₄S): Bis(4-aminophenyl)benzene-2,5-thiophenedicarboxylate:

2 g (4.85 mmol) of bis(4-nitrophenyl)benzene-2,5-thiophenedicarboxylate (**35**) and 0.344 g Pd/C (10% Pd) in 250 ml DGM were stirred at 100°C for 8 h under hydrogen atmosphere. After cooling to RT, the solution was filtered over Celite. The Celite bed was washed with 50 ml MeOH and the brown solid, obtained after filtrate evaporation, was dried under high vacuum (1.53 g, yield 89.35 %).

¹H-NMR (d₆-DMSO, 250 MHz): 5.23 (s, NH₂, 4H); 6.59 (d, J= 7.5 Hz, CHarom. phenyl ring, 4H); 6.94 (d, J= 7.5 Hz, CHarom. phenyl ring, 4H); 8.02 (s, CHarom. thiophene ring, 2H).

¹³C-NMR (d₆-DMSO, 63 MHz): 114.88; 122.25; 135.13; 138.80; 140.54; 147.52; 148.72; 160.54.

Elemental analysis for C₁₈H₁₄N₂O₄S: C61.01, H3.98, N7.90 (calc.), C60.99, H4.15, N7.59 (found).

37•2PF₆ (C₄₇H₃₂F₁₂N₄O₈P₂S₂): Bis-1,1'-[4,4'-(amino-phenyl)phenyl]thiophene-2,5-dicarboxylate]-4,4'-bipyridinium hexafluorophosphate

0.6 g (1 mmol) 1,1'-Bis(2,4-dinitrophenyl)-4,4'-bipyridinium dichloride (**17**) and 0.94 g (2.6 mmol) bis(4-aminophenyl)benzene-2,5-thiophene dicarboxylate (**36**) dissolved in 150 ml (MeOH 80 %-DGM, 1:2) were stirred for 20 h at 100°C. The formed brown precipitate was filtered, dissolved in MeOH/water and added to 50 ml 3M aq. NH₄PF₆. The product (PF₆⁻ salt) was filtered and washed with 100 ml water and 200 ml DGM. After drying under high vacuum, **37•2PF₆** was obtained as brown powder (0.68 g, yield 56.91 %).

¹H-NMR (d₆-DMSO, 250 MHz): 6.59 (s, CH_{arom.} phenyl ring, 4H); 6.94 (s, CH_{arom.} phenyl ring, 4H); 7.81 (s, CH_{arom.} phenyl ring, 4H); 8.08 (s, CH_{arom.} phenyl ring (4H) + CH_{arom.} thiophene ring (4H), 8H); 9.07 (s, Vio, 4H); 9.72 (s, Vio, 4H).

¹³C-NMR (d₆-DMSO, 63 MHz): 114.51; 122.19; 124.18; 127.05; 135.17; 136.08; 137.63; 139.62; 140.59; 146.56; 147.47; 152.56; 159.58; 160.43.

38•2Cl (C₂₆H₂₂N₄Cl₂): 1,1'-Bis(4-methyl-benzoate)-4,4'-bipyridinium dichloride

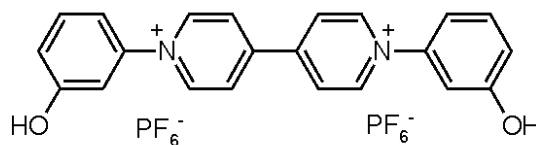
To a solution of 1.12 g (2.39 mmol) 1,1'-bis(4-carboxyphenyl)-4,4'-bipyridinium dichloride (**26**) in 200 ml MeOH, 1.5 ml conc. H₂SO₄ (26 mmol) was added and stirred for 6 h at 80 °C. After cooling to RT, the solvent was evaporated to 100 ml of its volume, and the product was precipitated by addition of diethyl ether. The yellow precipitate was filtered, washed several times with diethyl ether and dried in vacuum.

$^1\text{H-NMR}$ (MeOD, 250 MHz): 3.64 (s, $-\text{OCH}_3$, 6H); 8.11 (d, $J = 7.5$ Hz, CHarom. phenyl ring, 4H); 8.43 (d, $J = 7.5$ Hz, CHarom. phenyl ring, 4H); 8.96 (d, $J = 5$ Hz, Vio, 4H); 8.61 (d, $J = 7.5$ Hz, Vio, 4H).

$^{13}\text{C-NMR}$ (MeOD, 63 MHz): 52.00 ($-\text{OCH}_3$); 124.85; 127.27; 129.96; 131.40; 133.28; 145.61; 145.77; 151.09; 165.40.

The Cl^- salt was further dissolved in water/MeOH (8:2 V/V) and added to 10 ml 3M aq. NH_4PF_6 . The white precipitate (PF_6^- salt) was filtered, washed several times with water and dried under high vacuum (1.12 g, yield 78.62 %). Elemental analysis for $\text{C}_{26}\text{H}_{22}\text{F}_{12}\text{N}_2\text{O}_4\text{P}_2 \cdot 2\text{H}_2\text{O}$: C41.50, H3.48, N3.72 (calc.), C41.10, H3.26, and N4.08 (found).

$39 \cdot 2\text{PF}_6$ ($\text{C}_{22}\text{H}_{18}\text{F}_{12}\text{N}_2\text{O}_2\text{P}_2$): 1,1'-Bis(3-hydroxyphenyl)-4,4'-bipyridinium bis(hexafluorophosphate)

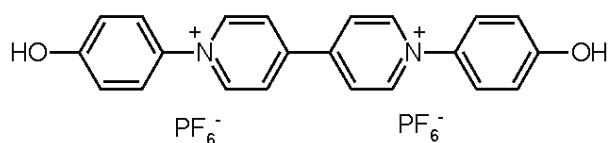


To a solution of 3 g (5.34 mmol) 1,1'-bis(2,4-dinitrophenyl)-4,4'-bipyridinium dichloride (**17**) in 325 ml MeOH/water (8:2 V/V), 1.4 g (12.82 mmol) 3-aminophenol in 60 ml MeOH/water (8:2 V/V) was added and stirred with reflux for 36 h. While adding the amine, the color of the solution changed immediately from yellow to black. After cooling to RT, the product was isolated by adding diethyl ether until an orange precipitate was formed. The precipitate was collected by filtration, dissolved in 150 ml MeOH/water solution and precipitated as PF_6^- salt by addition of 10 ml 3M aq. NH_4PF_6 . The yellow precipitate was filtered, washed with water to remove an excess of NH_4PF_6 and dried under high vacuum (1.97 g, yield 57.17 %).

$^1\text{H-NMR}$ ($\text{d}_6\text{-DMSO}$, 250 MHz): 7.29 (bs, CHarom. of phenyl ring, 6H); 7.55 (bs, CHarom. of phenyl ring, 2H); 8.96 (bs, Vio, 4H); 9.60 (bs, Vio, 4H), 10.46 (bs, OH, 2H).

$^{13}\text{C-NMR}$ ($\text{d}_6\text{-DMSO}$, 63 MHz): 111.73; 115.04; 118.46; 126.62; 133.19; 143.22; 145.72; 149.08; 158.59.

$40 \cdot 2\text{PF}_6$ ($\text{C}_{22}\text{H}_{18}\text{F}_{12}\text{N}_2\text{O}_2\text{P}_2$): 1,1'-Bis(4-hydroxyphenyl)-4,4'-bipyridinium bis (hexafluorophosphate)

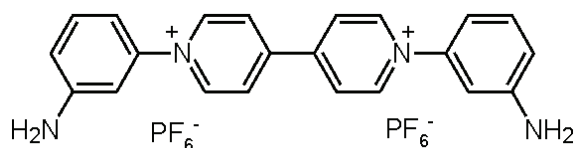


3 g (5.34 mmol) 1,1'-Bis(2,4-dinitrophenyl)-4,4'-bipyridinium dichloride (**17**) in 250 ml of a MeOH/water solution (8:2, V/V) and 1.48 g (13.62 mmol) 4-amino-phenol in 80 ml MeOH/water solution (8:2, V/V) were heated to reflux and stirred for 48 h. After cooling to RT, the product was separated from the reaction mixture by adding 400 ml diethyl ether. The yellow precipitate formed was filtered and washed three times with 100 ml diethyl ether. The precipitate was dissolved in 150 ml MeOH/water and then added to 10 ml 3M aq. NH_4PF_6 . The brown precipitate formed was collected by filtration, washed with water and dried under high vacuum (2.2 g, yield 61.2 %).

$^1\text{H-NMR}$ ($\text{d}_6\text{-DMSO}$, 250 MHz): 7.09 (s, CHarom. phenyl ring, 4H); 7.77 (s, CHarom. phenyl ring, 4H); 8.95 (s, Vio, 4H); 9.55 (s, Vio, 4H); 10.49 (s, OH, 2H).

$^{13}\text{C-NMR}$ ($\text{d}_6\text{-DMSO}$, 63 MHz): 116.94; 126.58; 126.91; 134.43; 145.79; 148.62; 160.71.

41•2PF₆ (C₂₂H₂₀F₁₂N₄P₂): 1,1'-Bis(3-aminophenyl)-4,4'-bipyridinium bis (hexafluorophosphate)



To a solution of 1 g (1.78 mmol) 1,1'-bis(2,4-dinitrophenyl)-4,4'-bipyridinium dichloride (**17**) in 100 ml MeOH/water (8:2 V/V) 1.55 g (14.39 mmol) benzene-1,3-diamine in 20 ml MeOH was added and stirred under reflux for 48 h. While adding the amine, the color of solution changed immediately from yellow to red. After cooling to RT, the solvent was evaporated to dryness, the residue washed three times with 250 ml DCM and ultrasonicated in 150 ml MeOH/ethylacetate mixture (1:2, V/V). The precipitate was collected, dissolved in 50 ml hot water, filtered over filter paper and the filtrate precipitated as PF₆⁻ salt by addition of 10 ml 3M aq. NH₄PF₆. The brown precipitate was collected by filtration, washed with water and dried under high vacuum (0.21 g, yield 18.90 %).

¹H-NMR (CD₃CN, 250 MHz): 4.82 (s, NH₂, 4H); 7.01 (d, J= 12.5 Hz, CHarom. phenyl ring, 6H); 7.44 (d, J= 10 Hz, CHarom. phenyl ring, 2H); 8.60 (d, J= 5 Hz, Vio, 4H); 9.15 (d, J= 5 Hz, Vio, 4H).

¹³C-NMR (CD₃CN, 63 MHz): 108.82; 111.87; 127.06; 131.14; 143.38; 145.22; 150.10.

6 Summary and outlook

The main subject of the thesis is the synthesis of monodisperse rigid viologen oligomers with star and rod conformation, and with an extended π -conjugation system (Fig. 6.1).

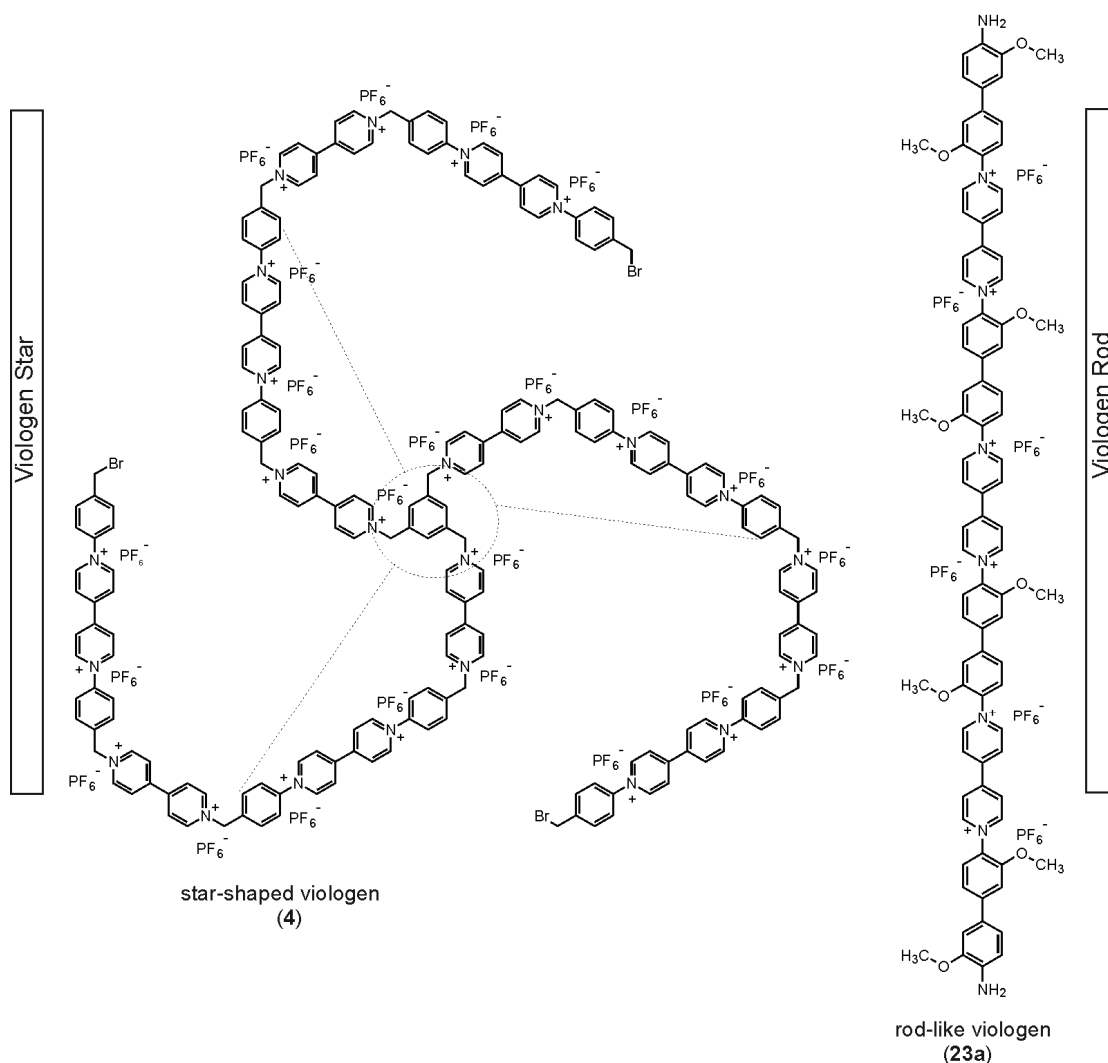


Figure 6.1 Nanometer-sized viologen stars and viologen rods exemplified by compounds **4** and **23a**.

Two approaches were considered for the preparation of the rigid viologen-oligomers: i) consecutive Menshutkin N-alkylations^{255,256} for the synthesis of the star-shaped viologens with three branches consisting of alternating benzyl viologen/phenyl viologen subunits and, ii) consecutive Zincke reactions to

form the rod-like π -conjugated oligomers consisting of alternating alkoxy-diphenyl and 4,4'-bipyridinium subunits. Alkoxy side chains were introduced on the diphenyl subunit to tune the solubility of the oligomers. The end groups of the two types of viologen oligomers (star-shaped and rod-like) are tailored for electropolymerization.

Electrochemistry of the viologen stars shows four redox interdigitated peaks: two for the benzyl viologen subunits and two for the phenyl viologen subunits. The electrochemistry of the viologen rods shows only two waves for the single type of phenyl viologen subunits present in these structures.

Electropolymerization (and Zn^0 induced polymerization) in case of the stars is based on the generation of peripheral benzyl radicals by reduction of the corresponding benzyl bromide.

In case of the rods, polymerization is based on in situ prepared peripheral diazonium salts. The stars and rods are exceptionally large monomers, which can be easily visualized by STM within the polymeric network (Fig. 6.2).

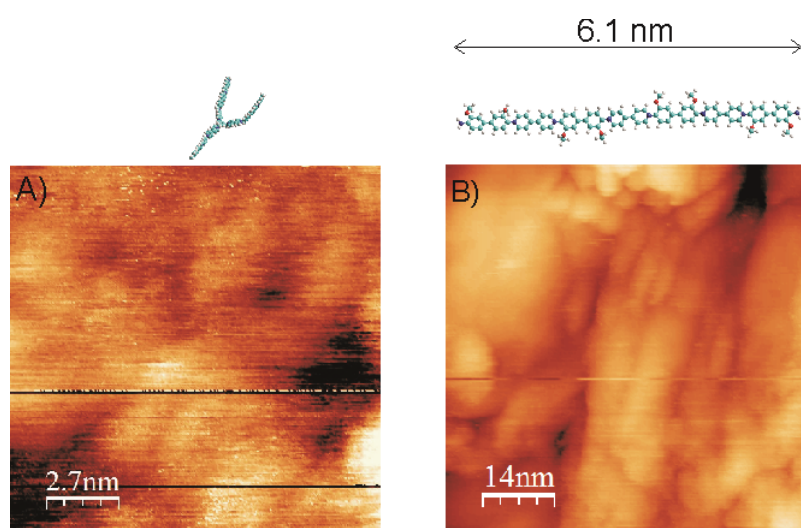


Figure 6.2 STM images ($V_b = 0.050$, $I_t = 1.001$) of polyviologen star (**Poly-4**) and polyviologen rod (**Poly-23a**) on ITO: A) 13.6 x 13.6 nm, Z range 0.781 nm and B) 72 x 72 nm, Z range 25 nm.

Moreover, nanocomposites of polyviologen stars with carbon nanotubes were prepared and visualized by STM.

Outlook:

Organic electronics have recently attracted much academic and commercial interest. Several p-type semiconductors have been found, but n-type semiconductors are less known. The nanometer-sized conjugated viologen presented in this work are ideal candidates for n-doped semiconductors as molecules, as polymer or as polymer composites (e.g. with CNT's).

Future work should, therefore, focus on the conductivity measurements of the rod-like alkoxy-diphenyl/viologen oligomers and polymers.

In analogy to the results of a recent publication,²⁵⁷ SWCNT combined with viologen rods or stars could have interesting transistor behavior (Fig. 6.3).

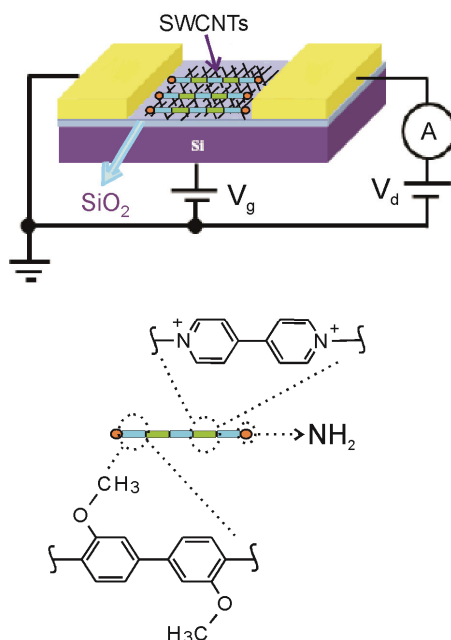


Fig. 6.3 Representation of a CNTs-based field effect transistor doped with the rod-like viologen.

References

- (1) Lightowler, S.; Hird, M. *Chem. Mater.* **2005**, *17*, 5538.
- (2) Davis, W. B.; Svec, W. A.; Ratner, M. A.; Wasielewski, M. R. *Nature (London)* **1998**, *396*, 60.
- (3) Soendergaard, R.; Krebs, F. C. *Polymers (Basel, Switz.)* **2011**, *3*, 545.
- (4) Yang, J.-S.; Yan, J.-L.; Hwang, C.-Y.; Chiou, S.-Y.; Liao, K.-L.; Tsai, H.-H. G.; Lee, G.-H.; Peng, S.-M. *J. Am. Chem. Soc.* **2006**, *128*, 14109.
- (5) Aharoni, S. M. *Macromolecules* **1987**, *20*, 2010.
- (6) Chen, K.-Y.; Chow, T. J.; Chou, P.-T.; Cheng, Y.-M.; Tsai, S.-H. *Tetrahedron Lett.* **2002**, *43*, 8115.
- (7) Bruce, M. I.; Hall, B. C.; Skelton, B. W.; Smith, M. E.; White, A. H. *J. Chem. Soc., Dalton Trans.* **2002**, 995.
- (8) Yam, V. W.-W.; Wong, K. M.-C.; Zhu, N. *Angew. Chem., Int. Ed.* **2003**, *42*, 1400.
- (9) Rappoport, Z.; Liebman, J. F.; Editors *The Chemistry of Cyclobutanes, Part 1*, **2005**.
- (10) Kaszynski, P.; Friedli, A. C.; Michl, J. *J. Am. Chem. Soc.* **1992**, *114*, 601.
- (11) Mehta, G.; Viswanath, M. B.; Kunwar, A. C. *J. Org. Chem.* **1994**, *59*, 6131.
- (12) Semetey, V.; Moustakas, D.; Whitesides, G. M. *Angew. Chem., Int. Ed.* **2006**, *45*, 588.

-
- (13) Hopf, H.; Liebman, J. F.; Perks, H. M. *Chem. Cyclobutanes* **2005**, 2, 1061.
- (14) Campanelli, A. R.; Domenicano, A.; Piacente, G.; Ramondo, F. *J. Phys. Chem. A* **2010**, 114, 5162.
- (15) Ayres, F. D.; Khan, S. I.; Chapman, O. L. *Tetrahedron Lett.* **1994**, 35, 8561.
- (16) Schumm, J. S.; Pearson, D. L.; Jones, L., II; Hara, R.; Tour, J. M. *Nanotechnology* **1996**, 7, 430.
- (17) Binauld, S.; Damiron, D.; Connal, L. A.; Hawker, C. J.; Drockenmuller, E. *Macromol. Rapid Commun.* **2011**, 32, 147.
- (18) Paynter, O. I.; Simmonds, D. J.; Whiting, M. C. *J. Chem. Soc., Chem. Commun.* **1982**, 1165.
- (19) Tour, J. *Molecular Electronics: Commercial Insights, Chemistry, Devices, Architecture and Programming* **2003**, World Scientific Publishing Co.
- (20) Weiss, E. A.; Ahrens, M. J.; Sinks, L. E.; Gusev, A. V.; Ratner, M. A.; Wasielewski, M. R. *J. Am. Chem. Soc.* **2004**, 126, 5577.
- (21) Li, Y.; Zhao, J.; Yin, G. *Comput. Mater. Sci.* **2007**, 39, 775.
- (22) Jones, L., II; Schumm, J. S.; Tour, J. M. *J. Org. Chem.* **1997**, 62, 1388.
- (23) Bai, P.; Li, E.; Collier, P. A.; Chin, W.-S.; Loh, K.-P. *IEEE Conf. Emerging Technol.--Nanoelectron.* **2006**, 173.
- (24) Jestin, I.; Frere, P.; Blanchard, P.; Roncali, J. *Angew. Chem., Int. Ed.* **1998**, 37, 942.

- (25) Jones, L., II; Pearson, D. L.; Schumm, J. S.; Tour, J. M. *Pure Appl. Chem.* **1996**, 68, 145.
- (26) Kong, J.; Franklin, N. R.; Zhou, C.; Chapline, M. G.; Peng, S.; Cho, K.; Daitl, H. *Science (Washington, D. C.)* **2000**, 287, 622.
- (27) Reimers, J. R.; Lu, T. X.; Crossley, M. J.; Hush, N. S. *Nanotechnology* **1996**, 7, 424.
- (28) Anderson, H. L. *Chem. Commun. (Cambridge)* **1999**, 2323.
- (29) Javey, A.; Kim, H.; Brink, M.; Wang, Q.; Ural, A.; Guo, J.; McIntyre, P.; McEuen, P.; Lundstrom, M.; Dai, H. *Nat. Mater.* **2002**, 1, 241.
- (30) Bahr, J. L.; Mickelson, E. T.; Bronikowski, M. J.; Smalley, R. E.; Tour, J. M. *Chem. Commun. (Cambridge)* **2001**, 193.
- (31) Zhu, Y.; Bakis, C. E. *Tech. Conf. Am. Soc. Compos., 25th, US-Jpn. Conf. Compos. Mater., 14th* **2010**, 1, 776.
- (32) Lau, C. H.; Cervini, R.; Clarke, S. R.; Markovic, M. G.; Matisons, J. G.; Hawkins, S. C.; Huynh, C. P.; Simon, G. P. *J. Nanopart. Res.* **2008**, 10, 77.
- (33) Bunten, K. A.; Kakkar, A. K. *J. Mater. Chem.* **1995**, 5, 2041.
- (34) Miyamae, T.; Yoshimura, D.; Ishii, H.; Ouchi, Y.; Miyazaki, T.; Koike, T.; Yamamoto, T.; Seki, K. *J. Electron Spectrosc. Relat. Phenom.* **1996**, 78, 399.
- (35) Valasek, M.; Pecka, J.; Jindrich, J.; Calleja, G.; Craig Peter, R.; Michl, J. *J. Org. Chem.* **2005**, 70, 405.

- (36) Gutov, A. V.; Rusanov, E. B.; Chepeleva, L. V.; Garasevich, S. G.; Ryabitskii, A. B.; Chernega, A. N. *Russ. J. Gen. Chem.* **2009**, *79*, 1513.
- (37) Zimmerman, H. E.; Goldman, T. D.; Hirzel, T. K.; Schmidt, S. P. *J. Org. Chem.* **1980**, *45*, 3933.
- (38) Simbrunner, C.; Nabok, D.; Hernandez-Sosa, G.; Oehzelt, M.; Djuric, T.; Resel, R.; Romaner, L.; Puschnig, P.; Ambrosch-Draxl, C.; Salzmann, I.; Schwabegger, G.; Watzinger, I.; Sitter, H. *J. Am. Chem. Soc.* **2011**, *133*, 3056.
- (39) <http://www.cryscade.com/technology.htm>.
- (40) Matile, S. *Chem. Rec. (New York, N.Y.)* **2001**, *1*, 162.
- (41) Sakai, N.; Mareda, J.; Matile, S. *Acc. Chem. Res.* **2005**, *38*, 79.
- (42) Ni, C.; Matile, S. *Chem. Commun. (Cambridge)* **1998**, 755.
- (43) Weiss, L. A.; Sakai, N.; Ghebremariam, B.; Ni, C.; Matile, S. *J. Am. Chem. Soc.* **1997**, *119*, 12142.
- (44) Sakai, N.; Ni, C.; Bezrukov, S. M.; Matile, S. *Bioorg. Med. Chem. Lett.* **1998**, *8*, 2743.
- (45) Chaieb, A.; Vignau, L.; Brown, R.; Wantz, G.; Huby, N.; Francois, J.; Dagron-Lartigau, C. *Opt. Mater. (Amsterdam, Netherlands)* **2008**, *31*, 68.
- (46) Ervithayasuporn, V.; Abe, J.; Wang, X.; Matsushima, T.; Murata, H.; Kawakami, Y. *Tetrahedron* **2010**, *66*, 9348.
- (47) Wallace, J. U.; Chen, S. H. *Adv. Polym. Sci.* **2008**, *212*, 145.

- (48) Maillou, T.; Le Moigne, J.; Geffroy, B.; Lorin, A.; Rosilio, A.; Dumarcher, V.; Rocha, L.; Denis, C.; Fiorini, C.; Nunzi, J. M. *Synth. Met.* **2001**, *124*, 87.
- (49) Larios-Lopez, L.; Navarro-Rodriguez, D.; Arias-Marin, E. M.; Moggio, I.; Reyes-Castaneda, C. V.; Donnio, B.; Lemoigne, J.; Guillon, D. *Liq. Cryst.* **2003**, *30*, 423.
- (50) Liu, P.; Zhang, Y.; Feng, G.; Hu, J.; Zhou, X.; Zhao, Q.; Xu, Y.; Tong, Z.; Deng, W. *Tetrahedron* **2004**, *60*, 5259.
- (51) Pisula, W.; Tomovic, Z.; Wegner, M.; Graf, R.; Pouderoijen, M. J.; Meijer, E. W.; Schenning, A. P. H. J. *J. Mater. Chem.* **2008**, *18*, 2968.
- (52) Tschierske, C. *Nature (London, U. K.)* **2002**, *419*, 681.
- (53) Kreger, K.; Baete, M.; Neuber, C.; Schmidt, H.-W.; Strohmriegl, P. *Adv. Funct. Mater.* **2007**, *17*, 3456.
- (54) Sonoda, T.; Rahmat, H.; Ozaki, M.; Yoshino, K.; Schneider, W.; Lee, K. K.; Naka, A.; Ishikawa, M. *Appl. Phys. Lett.* **1999**, *75*, 2193.
- (55) Wang, J.; Tian, L.; Argenti, A.; Uhrich, K. E. *J. Bioact. Compat. Polym.* **2006**, *21*, 297.
- (56) Jelinkova, M.; Strohalm, J.; Etrych, T.; Ulbrich, K.; Rihova, B. *Pharm. Res.* **2003**, *20*, 1558.
- (57) Ronconi, C. M.; Stoddart, J. F.; Balzani, V.; Baroncini, M.; Ceroni, P.; Giansante, C.; Venturi, M. *Chem.--A Eur. J.* **2008**, *14*, 8365.
- (58) Bhattacharya, P.; Kaifer, A. E. *J. Org. Chem.* **2008**, *73*, 5693.
- (59) Heinen, S.; Walder, L. *Angew. Chem., Int. Ed.* **2000**, *39*, 806.

- (60) Gattuso, G.; Gargiulli, C.; Parisi, M. F. *Int. J. Mol. Sci.* **2007**, *8*, 1052.
- (61) Marangoci, N.; Fifere, A.; Farcas, A.; Harabagiu, V.; Pinteala, M.; Simionescu, B. C.; Perichaud, A. *High Perform. Polym.* **2008**, *20*, 553.
- (62) Sun, X. W.; Wang, J. X. *Nano Lett.* **2008**, *8*, 1884.
- (63) Li, J. J. *Name Reactions in Heterocyclic Chemistry*, John Wiley & Sons, **2004**.
- (64) Kim, C. S.; Lee, S.; Tinker, L. L.; Bernhard, S.; Loo, Y.-L. *Chem. Mater.* **2009**, *21*, 4583.
- (65) Santa-Nokki, H.; Kallioinen, J.; Korppi-Tommola, J. *Photochem. Photobiol. Sci.* **2007**, *6*, 63.
- (66) Kim, Y.; Malliaras, G. G.; Ober, C. K.; Kim, E. J. *Nanosci. Nanotechnol.* **2010**, *10*, 6869.
- (67) Sharrett, Z.; Gamsey, S.; Hirayama, L.; Vilozy, B.; Suri, J. T.; Wessling, R. A.; Singaram, B. *Org. Biomol. Chem.* **2009**, *7*, 1461.
- (68) Jain, V.; Khiterer, M.; Montazami, R.; Yochum, H. M.; Shea, K. J.; Heflin, J. R. *ACS Appl. Mater. Interfaces* **2009**, *1*, 83.
- (69) Kim, H. J.; Seo, J. K.; Kim, Y. J.; Jeong, H. K.; Lim, G. I.; Choi, Y. S.; Lee, W. I. *Sol. Energy Mater. Sol. Cells* **2009**, *93*, 2108.
- (70) Cha, S. H.; Oh, M. S.; Lee, K. H.; Im, S.; Lee, B. H.; Sung, M. M. *Appl. Phys. Lett.* **2008**, *92*, 023506/1.
- (71) Bongard, D.; Moeller, M.; Rao, S. N.; Corr, D.; Walder, L. *Helv. Chim. Acta* **2005**, *88*, 3200.

- (72) Liu, X.; Neoh, K. G.; Zhao, L.; Kang, E. T. *Langmuir* **2002**, *18*, 2914.
- (73) Ferreyra, N. F.; Coche-Guerente, L.; Labbe, P.; Calvo, E. J.; Solis, V. M. *Langmuir* **2003**, *19*, 3864.
- (74) Creager, S. E.; Fox, M. A. *J. Electroanal. Chem. Interfacial Electrochem.* **1989**, *258*, 431.
- (75) Chang, H. C.; Osawa, M.; Matsue, T.; Uchida, I. *J. Chem. Soc., Chem. Commun.* **1991**, 611.
- (76) Cosnier, S.; Dawod, M.; Gorgy, K.; Da Silva, S. *Microchim. Acta* **2003**, *143*, 139.
- (77) Deronzier, A.; Essakalli, M. *J. Chem. Soc., Chem. Commun.* **1990**, 242.
- (78) Zhao, W. Y.; Marfurt, J.; Walder, L. *Helv. Chim. Acta* **1994**, *77*, 351.
- (79) Marfurt, J.; Zhao, W. Y.; Walder, L. *J. Chem. Soc., Chem. Commun.* **1994**, 51.
- (80) Kwon, Y. S.; Lee, N. S.; Choi, W. S.; Shin, H. K.; Qian, D. J. *Ultramicroscopy* **2008**, *108*, 1101.
- (81) Kamata, K.; Suzuki, T.; Kawai, T.; Iyoda, T. *J. Electroanal. Chem.* **1999**, *473*, 145.
- (82) Kamata, K.; Kawai, T.; Iyoda, T. *Langmuir* **2001**, *17*, 155.
- (83) Kolivoska, V.; Gal, M.; Pospisil, L.; Valášek, M.; Hromadova, M. *Phys. Chem. Chem. Phys.* **2011**, *13*, 11422.
- (84) Valášek, M.; Pecka, J.; Jindrich, J.; Calleja, G.; Craig, P. R.; Michl, J. *J. Org. Chem.* **2005**, *70*, 405.

- (85) Hromadova, M.; Kolivoska, V.; Sokolova, R.; Gal, M.; Pospisil, L.; Valášek, M. *Langmuir* **2010**, *26*, 17232.
- (86) Takahashi, K. *Pure Appl. Chem.* **1993**, *65*, 127.
- (87) Albers, W. M. *Bioelectrochem. Bioenerg.* **1997**, *42*, 25.
- (88) Kathiresan, M.; Walder, L. *Macromolecules (Washington, DC, United States)* **2010**, *43*, 9248.
- (89) Braunschweig, A. B.; Ronconi, C. M.; Han, J.-Y.; Arico, F.; Cantrill, S. J.; Stoddart, J. F.; Khan, S. I.; White, A. J. P.; Williams, D. J. *Eur. J. Org. Chem.* **2006**, 1857.
- (90) Trabolsi, A.; Khashab, N.; Fahrenbach, A. C.; Friedman, D. C.; Colvin, M. T.; Coti, K. K.; Benitez, D.; Tkatchouk, E.; Olsen, J.-C.; Belowich, M. E.; Carmielli, R.; Khatib, H. A.; Goddard, W. A., III; Wasielewski, M. R.; Stoddart, J. F. *Nat. Chem.* **2010**, *2*, 42.
- (91) Leventis, N.; Yang, J.; Fabrizio, E. F.; Rawashdeh, A.-M. M.; Oh, W. S.; Sotiriou-Leventis, C. *J. Am. Chem. Soc.* **2004**, *126*, 4094.
- (92) Hui, F.; Noel, J.-M.; Poizot, P.; Hapiot, P.; Simonet, J. *Langmuir* **2011**, *27*, 5119.
- (93) Nanasawa, M.; Miwa, M.; Hirai, M.; Kuwabara, T. *J. Org. Chem.* **2000**, *65*, 593.
- (94) Amabilino, D. B.; Ashton, P. R.; Belohradsky, M.; Raymo, F. M.; Stoddart, J. F. *J. Chem. Soc., Chem. Commun.* **1995**, 751.
- (95) Papadakis, R.; Tsolomitis, A. *J. Phys. Org. Chem.* **2009**, *22*, 515.
- (96) Freitag, M.; Galoppini, E. *Langmuir* **2010**, *26*, 8262.

- (97) Heinen, S. *Elektroactive Dendrimere mit Viologengerüst* **1999**, Diss., Universität Osnabrück.
- (98) Asaftei, S.; De Clercq, E. *J. Med. Chem.* **2010**, *53*, 5895.
- (99) Porter, W. W., III; Vaid, T. P. *J. Org. Chem.* **2005**, *70*, 5028.
- (100) Dupuis, B.; Michaut, C.; Jouanin, I.; Delaire, J.; Robin, P.; Feneyrou, P.; Dentan, V. *Chem. Phys. Lett.* **1999**, *300*, 169.
- (101) Sato, H.; Tamamura, T. *J. Appl. Polym. Sci.* **1979**, *24*, 2075.
- (102) Lee, C.; Lee, Y. M.; Moon, M. S.; Park, S. H.; Park, J. W.; Kim, K. G.; Jeon, S.-J. *J. Electroanal. Chem.* **1996**, *416*, 139.
- (103) Chidichimo, G.; Imbardelli, D.; De Simone, B. C.; Barone, P.; Barberio, M.; Bonanno, A.; Camarca, M.; Oliva, A. *J. Phys. Chem. C* **2010**, *114*, 16700.
- (104) James, M. *MOPAC 2009*, <http://OpenMopac.net>
- (105) Belanger, D.; Lyskawa, J. *Chem. Mater.* **2006**, *18*, 4755.
- (106) Isse, A. A.; De Giusti, A.; Gennaro, A. *Tetrahedron Lett.* **2006**, *47*, 7735.
- (107) Ohsaka, T.; Nakanishi, M.; Hatozaki, O.; Oyama, N. *Electrochim. Acta* **1990**, *35*, 63.
- (108) Dalton, E. F.; Murray, R. W. *J. Phys. Chem.* **1991**, *95*, 6383.
- (109) Ng, H. T.; Fang, A.; Huang, L.; Li, S. F. Y. *Langmuir* **2002**, *18*, 6324.
- (110) Zhou, L.; Ho, P. K. H.; Zhang, P. C.; Li, S. F. Y.; Xu, G. Q. *Appl. Phys. A: Mater. Sci. Process.* **1998**, *66*, S643.
- (111) HyperChem(TM), I., Professional 8.0.8, Hypercube, Inc., 1115 NW 4th Street, Gainesville, Florida 32601, USA.

- (112) Kirchner, B.; Pham, D. T.; Gentz, K.; Zorlein, C.; Hai, N. T. M.; Tsay, S. L.; Kossmann, S.; Wandelt, K.; Broekmann, P. *New J. Chem.* **2006**, *30*, 1439.
- (113) Tsay, J. S.; Tsay, S. L.; Fu, T. Y.; Broekmann, P.; Sagara, T.; Wandelt, K. *Phys. Chem. Chem. Phys.* **2010**, *12*, 14950.
- (114) Noh, J.; Hyung, K. H.; Lee, W.; Han, S. H. *J. Phys. Chem. C* **2008**, *112*, 18178.
- (115) Xu, F. J.; Yuan, S. J.; Pehkonen, S. O.; Kang, E. T.; Neoh, K. G. *NanoBiotechnology* **2006**, *2*, 123.
- (116) Yang, R.; Yang, X. R.; Evans, D. F.; Hendrickson, W. A.; Baker, J. *J. Phys. Chem.* **1990**, *94*, 6123.
- (117) Kusanagi, H.; Chatani, Y.; Tadokoro, H. *Polymer* **1994**, *35*, 2028.
- (118) Boettcher, C.; Schade, B.; Ecker, C.; Rabe, J. P.; Shu, L.; Schlueter, A. D. *Chem.--A Eur. J.* **2005**, *11*, 2923.
- (119) Crispin, X.; Marciniak, S.; Osikowicz, W.; Zotti, G.; Denier Van Der Gon, A. W.; Louwet, F.; Fahlman, M.; Groenendaal, L.; De Schryver, F.; Salaneck, W. R. *J. Polym. Sci., Part B: Polym. Phys.* **2003**, *41*, 2561.
- (120) Liu, X.; Neoh, K. G.; Kang, E. T. *Langmuir* **2002**, *18*, 9041.
- (121) Deng, J.; Zhou, C.; Song, N. *Macromolecules (Washington, DC, United States)* **2009**, *42*, 6865.
- (122) Sharma, S. K.; Pandey, R. K.; Sharma, M.; Sharma, A. B.; Rao, K. N.; Mohan, S.; Reddy, D. S. *J. Optoelectron. Adv. Mater.* **2008**, *10*, 442.

- (123) Andrews, R.; Weisenberger, M. C. *Curr. Opin. Solid State Mater. Sci.* **2004**, 8, 31.
- (124) Wang, J. *Analytical Electrochemistry*, **3rd ed.**, New York: John Wiley & Sons, **2006**.
- (125) Heinen, S.; Meyer, W.; Walder, L. *J. Electroanal. Chem.* **2001**, 498, 34.
- (126) Zhou, D.-L.; Carrero, H.; Rusling, J. F. *Langmuir* **1996**, 12, 3067.
- (127) Shimakoshi, H.; Ninomiya, W.; Hisaeda, Y. *J. Chem. Soc., Dalton Trans.* **2001**, 1971.
- (128) Parker, F. S. *Applications of Infrared, Raman, and Resonance Raman Spectroscopy in Biochemistry*, **1983**.
- (129) Kang, E.-H.; Liu, X.; Sun, J.; Shen, J. *Langmuir* **2006**, 22, 7894.
- (130) Steiger, B.; Walder, L. *Helv. Chim. Acta* **1992**, 75, 90.
- (131) Allouche, A.-R. *J. Comput. Chem.* **2011**, 32, 174.
- (132) Stewart, J. **MOPAC2009**, *Computational Chemistry*, web: <http://openmopac.net>.
- (133) Volke, J.; Volkova, V. *Collect. Czech. Chem. Commun.* **1969**, 34, 2037.
- (134) Bauer, H.; Stier, F.; Petry, C.; Knorr, A.; Stadler, C.; Staab, H. A. *Eur. J. Org. Chem.* **2001**, 3255.
- (135) Xiao, Y.; Chu, L.; Sanakis, Y.; Liu, P. *J. Am. Chem. Soc.* **2009**, 131, 9931.
- (136) Saotome, Y.; Endo, T.; Okawara, M. *Macromolecules* **1983**, 16, 881.

- (137) De Sa, A. C. P. F.; Pontes, G. M. A.; Dos Anjos, J. A. L.; Santana, S. R.; Bieber, L. W.; Malvestiti, I. J. *Braz. Chem. Soc.* **2003**, *14*, 429.
- (138) Trofimov, B. A.; Mal'kina, A. G.; Dorofeev, I. A.; Myachina, G. F.; Rodionova, I. V.; Vakul'skaya, T. I.; Sinegovskaya, L. M.; Skotheim, T. A. *Dokl. Chem.* **2007**, *414*, 125.
- (139) Inoue, Y.; Tokito, S.; Ito, K.; Suzuki, T. *J. Appl. Phys.* **2004**, *95*, 5795.
- (140) Drolet, N.; Morin, J.-F.; Leclerc, N.; Wakim, S.; Tao, Y.; Leclerc, M. *Adv. Funct. Mater.* **2005**, *15*, 1671.
- (141) Zhen, C.-G.; Chen, Z.-K.; Liu, Q.-D.; Dai, Y.-F.; Shin, R. Y. C.; Chang, S.-Y.; Kieffer, J. *Adv. Mater. (Weinheim, Germany)* **2009**, *21*, 2425.
- (142) Chen, F.-P.; Xu, B.; Zhao, Z.-J.; Tian, W.-J.; Lu, P.; Im, C. *Chin. Phys. B*, **2010**, *19*, 037801/1.
- (143) Gebhardt, V.; Bacher, A.; Thelakkat, M.; Stalmach, U.; Meier, H.; Schmidt, H. W.; Haarer, D. *Synth. Met.* **1997**, *90*, 123.
- (144) Camaioni, N.; Ridolfi, G.; Fattori, V.; Favaretto, L.; Barbarella, G. *J. Mater. Chem.* **2005**, *15*, 2220.
- (145) Newman, C. R.; Frisbie, C. D.; da Silva Filho, D. A.; Bredas, J.-L.; Ewbank, P. C.; Mann, K. R. *Chem. Mater.* **2004**, *16*, 4436.
- (146) Shankar, K.; Mor, G. K.; Paulose, M.; Varghese, O. K.; Grimes, C. A. *J. Non-Cryst. Solids* **2008**, *354*, 2767.
- (147) Yang, C.; Cho, S.; Heeger, A. J.; Wudl, F. *Angew. Chem., Int. Ed.* **2009**, *48*, 1592.

- (148) Monk, P. The Viologens, *John Wiley & Sons, Chichester (UK)* **1998**.
- (149) Gutov, A. V.; Rusanov, E. B.; Ryabitskii, A. B.; Tsimbal, I. F.; Chernega, A. N. *Russ. J. Gen. Chem.* **2009**, 79, 1910.
- (150) Albers, W. M.; Lekkala, J. O.; Jeuken, L.; Canters, G. W.; Turner, A. P. F. *Bioelectrochem. Bioenerg.* **1997**, 42, 25.
- (151) Takahashi, K.; Nihira, T.; Akiyama, K.; Ikegami, Y.; Fukuyo, E. *J. Chem. Soc., Chem. Commun.* **1992**, 620.
- (152) Porter, W. W., III; Vaid, T. P.; Rheingold, A. L. *J. Am. Chem. Soc.* **2005**, 127, 16559.
- (153) Akhtaruzzaman, M.; Tomura, M.; Zaman, M. B.; Nishida, J.-i.; Yamashita, Y. *J. Org. Chem.* **2002**, 67, 7813.
- (154) Pospisil, L.; Hromadova, M.; Fanelli, N.; Valášek, M.; Kolivoska, V.; Gal, M. *Phys. Chem. Chem. Phys.* **2011**, 13, 4365.
- (155) Hromadova, M.; Kolivoska, V.; Sokolova, R.; Gal, M.; Pospisil, L.; Valášek, M. *Langmuir* **2010**, 26, 17232.
- (156) Funston, A.; Kirby, J. P.; Miller, J. R.; Pospisil, L.; Fiedler, J.; Hromadova, M.; Gal, M.; Pecka, J.; Valášek, M.; Zawada, Z.; Rempala, P.; Michl, J. *J. Phys. Chem. A* **2005**, 109, 10862.
- (157) Iyoda, T.; Matsushita, M. M.; Kawai, T. *Pure Appl. Chem.* **1999**, 71, 2079.
- (158) Matsushita, M. M.; Tachikawa, T.; Suzuki, T.; Kawai, T.; Iyoda, T. *Mol. Cryst. Liq. Cryst. Sci. Technol., Sect. A* **1999**, 334, 149.
- (159) Kanbara, T.; Yamamoto, T. *Macromolecules* **1993**, 26, 1975.
- (160) Izuhara, D.; Swager, T. M. *J. Mater. Chem.*, **2011**, 21, 3579.

- (161) Genisson, Y.; Marazano, C.; Mehmandoust, M.; Gnecco, D.; Das, B. C. *Synlett* **1992**, 431.
- (162) Colquhoun, H. M.; Greenland, B. W.; Zhu, Z.; Shaw, J. S.; Cardin, C. J.; Burattini, S.; Elliott, J. M.; Basu, S.; Gasa, T. B.; Stoddart, J. F. *Org. Lett.* **2009**, *11*, 5238.
- (163) Lamy-Pitara, E.; N'Zemba, B.; Barbier, J.; Barbot, F.; Miginiac, L. *J. Mol. Catal. A: Chem.* **1999**, *142*, 39.
- (164) Ghigo, G.; Osella, S.; Maranzana, A.; Tonachini, G. *European J. Org. Chem.* **2011**, 2326.
- (165) Shine, H. J.; Zmuda, H.; Park, K. H.; Kwart, H.; Horgan, A. G.; Collins, C.; Maxwell, B. E. *J. Am. Chem. Soc.* **1981**, *103*, 955.
- (166) Cheng, J.-D.; Shine, H. J. *J. Org. Chem.* **1975**, *40*, 703.
- (167) Ludden, J. *Synthese von Viologen-Stäbchen* **2010**, *Masterarbeit*, Universität Osnabrück.
- (168) Porter William, W., 3rd; Vaid Thomas, P. *J. Org. Chem.* **2005**, *70*, 5028.
- (169) Hertl, P.; Rieker, A.; Speiser, B. *J. Electroanal. Chem. Interfacial Electrochem.* **1986**, *200*, 147.
- (170) Macias-Ruvalcaba, N. A.; Evans, D. H. *J. Phys. Chem. C* **2007**, *111*, 5805.
- (171) Ronlan, A.; Coleman, J.; Hammerich, O.; Parker, V. D. *J. Amer. Chem. Soc.* **1974**, *96*, 845.
- (172) Tang, Z.-M.; Lei, T.; Wang, J.-L.; Ma, Y.; Pei, J. *J. Org. Chem.* **2010**, *75*, 3644.

- (173) Misra, A.; Kumar, P.; Srivastava, R.; Dhawan, S. K.; Kamalasanan, M. N.; Chandra, S. *Indian J. Pure Appl. Phys.* **2005**, *43*, 921.
- (174) Kachoosangi, R. T.; Wildgoose, G. G.; Compton, R. G. *Electroanalysis* **2007**, *19*, 1483.
- (175) Hatozaki, O.; Anson, F. C. *J. Phys. Chem.* **1996**, *100*, 8448.
- (176) Gurjar, V. G.; Sharma, I. M. *J. Appl. Electrochem.* **1989**, *19*, 113.
- (177) Jacob, S. R.; Hong, Q.; Coles, B. A.; Compton, R. G. *J. Phys. Chem. B* **1999**, *103*, 2963.
- (178) Suarez-Gustave, S.; Greenbaum, S.; Chung, S. H.; Peled, E.; Duvdevani, T.; Aharon, A.; Melman, A. *Prepr. Symp. - Am. Chem. Soc., Div. Fuel Chem.* **2002**, *47*, 370.
- (179) Li, L. S.; Jan, D.; Jia, Q. X.; Li, A. D. Q. *Abstracts of Papers, 221st ACS National Meeting, San Diego, CA, United States, April 1-5, 2001* **2001**, COLL.
- (180) Chidichimo, G.; Imbardelli, D.; De Simone, B. C.; Barone, P.; Barberio, M.; Bonanno, A.; Camarca, M.; Oliva, A. *J. Phys. Chem. C* **2010**, *114*, 16700.
- (181) Miyama, H.; Nosaka, Y.; Kobayashi, T.; Kuwabara, A. *J. Polym. Sci., Polym. Lett. Ed.* **1983**, *21*, 945.
- (182) Bordyuh, A. B.; Polyshchuk, A. P.; Polyshchuk, I. Y.; Klimusheva, G. V.; Mirnaya, T. A.; Yaremchuk, G. G.; Koval'chuk, A. V. *Ukr J. Phys.* **2004**, *49*, 1095.
- (183) Sassoon, R. E.; Gershuni, S.; Rabani, J. *J. Phys. Chem.* **1985**, *89*, 1937.

- (184) Park, J. Y.; Lee, S. B.; Park, Y. S.; Park, Y. W.; Lee, C. H.; Lee, J. I.; Shim, H. K. *Appl. Phys. Lett.* **1998**, *72*, 2871.
- (185) Park, Y. S.; Lee, K.; Lee, C.; Yoon, K. B. *Langmuir* **2000**, *16*, 4470.
- (186) Ronconi, C. M.; Stoddart, J. F.; Balzani, V.; Baroncini, M.; Ceroni, P.; Giansante, C.; Venturi, M. *Chem.--A Eur. J.* **2008**, *14*, 8365.
- (187) Zhao, Y.; Slepko, A. D.; Akoto, C. O.; McDonald, R.; Hegmann, F. A.; Tykwinski, R. R. *Chem.--A Eur. J.* **2005**, *11*, 321.
- (188) Zhao, Y.; Tykwinski, R. R. *J. Am. Chem. Soc.* **1999**, *121*, 458.
- (189) Humphrey, J. L.; Lott, K. M.; Wright, M. E.; Kuciauskas, D. *J. Phys. Chem. B* **2005**, *109*, 21496.
- (190) Casado, J.; Ortiz, R. P.; Delgado, M. C. R.; Azumi, R.; Oakley, R. T.; Hernandez, V.; Navarrete, J. T. L. *J. Phys. Chem. B* **2005**, *109*, 10115.
- (191) Hinks, D.; Freeman, H. S.; Nakpathom, M.; Sokolowska, J. *Dyes Pigm.* **2000**, *44*, 199.
- (192) Shimomura, M.; Kasuga, K.; Tsukada, T. *Thin Solid Films* **1992**, *210-211*, 375.
- (193) Martin, S.; Cea, P.; Gascon, I.; Lopez, M. C.; Royo, F. M. *J. Electrochem. Soc.* **2002**, *149*, E402.
- (194) Gittins, D. I.; Bethell, D.; Nichols, R. J.; Schiffrin, D. J. *J. Mater. Chem.* **2000**, *10*, 79.
- (195) Haiss, W.; Albrecht, T.; van Zalinge, H.; Higgins, S. J.; Bethell, D.; Hoebeinreich, H.; Schiffrin, D. J.; Nichols, R. J.; Kuznetsov, A. M.; Zhang, J.; Chi, Q.; Ulstrup, J. *J. Phys. Chem. B* **2007**, *111*, 6703.

- (196) DeLongchamp, D. M.; Kastantin, M.; Hammond, P. T. *Chem. Mater.* **2003**, *15*, 1575.
- (197) Terzi, F.; Zanardi, C.; Zanfognini, B.; Pigani, L.; Seeber, R.; Lukkari, J.; Aaritalo, T.; Kankare, J. *J. Phys. Chem. C* **2009**, *113*, 4868.
- (198) Dominey, R. N.; Lewis, T. J.; Wrighton, M. S. *J. Phys. Chem.* **1983**, *87*, 5345.
- (199) Bookbinder, D. C.; Wrighton, M. S. *J. Am. Chem. Soc.* **1980**, *102*, 5123.
- (200) Mortimer, R. J.; Warren, C. P. *J. Electroanal. Chem.* **1999**, *460*, 263.
- (201) Barroso-Fernandez, B.; Theresa Lee-Alvarez, M.; Seliskar, C. J.; Heineman, W. R. *Anal. Chim. Acta* **1998**, *370*, 221.
- (202) Akahoshi, H.; Toshima, S.; Itaya, K. *J. Phys. Chem.* **1981**, *85*, 818.
- (203) Cheng, K.-C.; Chen, P.-Y. *Electroanalysis* **2008**, *20*, 207.
- (204) Liu, G.; Boecking, T.; Gooding, J. J. *J. Electroanal. Chem.* **2007**, *600*, 335.
- (205) Maldonado, S.; Smith, T. J.; Williams, R. D.; Morin, S.; Barton, E.; Stevenson, K. J. *Langmuir* **2006**, *22*, 2884.
- (206) Covaci, O. I.; Bucur, B.; Bucur, M. P.; Radu, G. L. *Microchim. Acta* **2010**, *169*, 335.
- (207) de Villeneuve, C. H.; Pinson, J.; Bernard, M. C.; Allongue, P. *J. Phys. Chem. B* **1997**, *101*, 2415.
- (208) Bahr, J. L.; Yang, J.; Kosynkin, D. V.; Bronikowski, M. J.; Smalley, R. E.; Tour, J. M. *J. Am. Chem. Soc.* **2001**, *123*, 6536.

- (209) Adenier, A.; Combellas, C.; Kanoufi, F.; Pinson, J.; Podvorica, F. *I. Chem. Mater.* **2006**, *18*, 2021.
- (210) Tsukahara, Y.; Wada, T.; Tanaka, K. *Chem. Lett.* **2010**, *39*, 1134.
- (211) Mahouche-Chergui, S.; Gam-Derouich, S.; Mangeney, C.; Chehimi, M. M. *Chem. Soc. Rev.* **2011**, *40*, 4143.
- (212) Anariba, F.; DuVall, S. H.; McCreery, R. L. *Anal. Chem.* **2003**, *75*, 3837.
- (213) Kariuki, J. K.; McDermott, M. T. *Langmuir* **2001**, *17*, 5947.
- (214) Lyskawa, J.; Belanger, D. *Chem. Mater.* **2006**, *18*, 4755.
- (215) Mevellec, V.; Roussel, S.; Tessier, L.; Chancolon, J.; Mayne-L'Hermite, M.; Deniau, G.; Viel, P.; Palacin, S. *Chem. Mater.* **2007**, *19*, 6323.
- (216) LeStrat, F.; Murphy, J. A.; Hughes, M. *Org. Lett.* **2002**, *4*, 2735.
- (217) Agnes, C.; Arnault, J.-C.; Omnes, F.; Joussetme, B.; Billon, M.; Bidan, G.; Mailley, P. *Phys. Chem. Chem. Phys.* **2009**, *11*, 11647.
- (218) Ng, S. W.; Neoh, K. G.; Wong, Y. T.; Sampanthar, J. T.; Kang, E. T.; Tan, K. L. *Langmuir* **2001**, *17*, 1766.
- (219) Zhao, L.; Neoh, K. G.; Kang, E. T. *Chem. Mater.* **2002**, *14*, 1098.
- (220) Lee, C.-Y.; Harbers, G. M.; Grainger, D. W.; Gamble, L. J.; Castner, D. G. *J. Am. Chem. Soc.* **2007**, *129*, 9429.
- (221) Alvaro, M.; Garcia, H.; Garcia, S.; Marquez, F.; Scaiano, J. C. *J. Phys. Chem. B* **1997**, *101*, 3043.
- (222) Laforgue, A.; Addou, T.; Belanger, D. *Langmuir* **2005**, *21*, 6855.

- (223) Buttry, D. A.; Peng, J. C. M.; Donnet, J.-B.; Rebouillat, S. *Carbon* **1999**, 37, 1929.
- (224) Rannou, P.; Rouchon, D.; Nicolau, Y. F.; Nechtschein, M.; Ermolieff, A. *Synth. Met.* **1999**, 101, 823.
- (225) Liang, Z.; Tang, Q.; Liu, J.; Li, J.; Yan, F.; Miao, Q. *Chem. Mater.* **2010**, 22, 6438.
- (226) Chua, L.-L.; Zaumseil, J.; Chang, J.-F.; Ou Eric, C. W.; Ho Peter, K. H.; Sirringhaus, H.; Friend Richard, H. *Nature* **2005**, 434, 194.
- (227) Tonzola, C. J.; Alam, M. M.; Kaminsky, W.; Jenekhe, S. A. *J. Am. Chem. Soc.* **2003**, 125, 13548.
- (228) Rand, B. P.; Genoe, J.; Heremans, P.; Poortmans, J. *Prog. Photovoltaics* **2007**, 15, 659.
- (229) Blanchard, P.; Verlhac, P.; Michaux, L.; Frere, P.; Roncali, J. *Chem.--Eur. J.* **2006**, 12, 1244.
- (230) Kuhn, H. *J. Chem. Phys.* **1949**, 17, 1198.
- (231) Zade, S. S.; Bendikov, M. *Org. Lett.* **2006**, 8, 5243.
- (232) Abbel, R.; Schleuss, T. W.; Frey, H.; Kilbinger, A. F. M. *Macromol. Chem. Phys.* **2005**, 206, 2067.
- (233) Plante, J.; Campbell, F.; Malkova, B.; Kilner, C.; Warriner, S. L.; Wilson, A. J. *Org. Biomol. Chem.* **2008**, 6, 138.
- (234) Tanatani, A.; Yokoyama, A.; Azumaya, I.; Takakura, Y.; Mitsui, C.; Shiro, M.; Uchiyama, M.; Muranaka, A.; Kobayashi, N.; Yokozawa, T. *J. Am. Chem. Soc.* **2005**, 127, 8553.
- (235) Saraogi, I.; Incarvito, C. D.; Hamilton, A. D. *Angew. Chem., Int. Ed.* **2008**, 47, 9691.

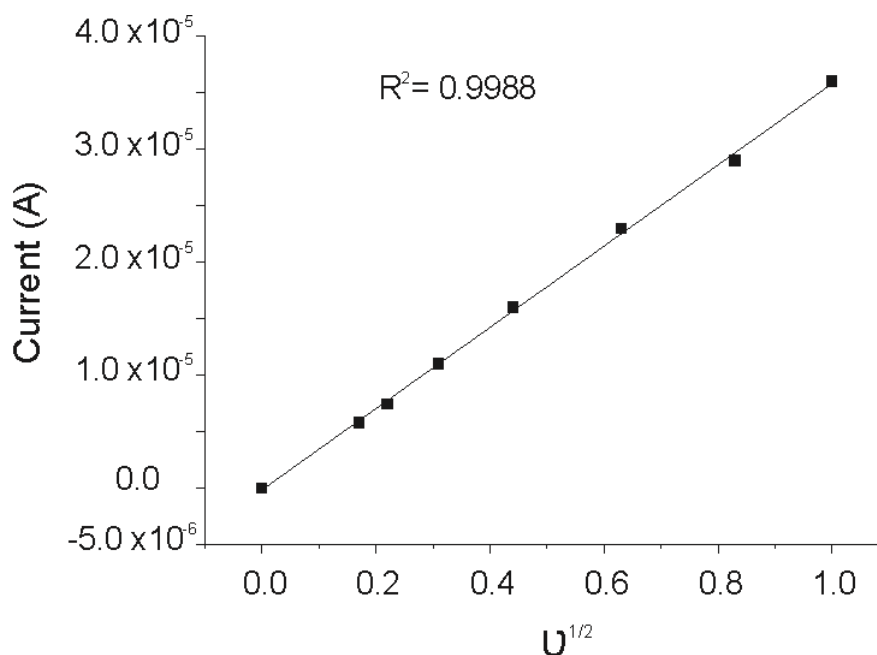
- (236) Gorton, L.; Editor *Comprehensive Analytical Chemistry Volume XLIV: Biosensors and Modern Biospecific Analytical Techniques*, **2005**.
- (237) Kakibe, T.; Ohno, H. *Chem. Commun. (Cambridge, U. K.)* **2008**, 377.
- (238) Li, J. H.; Cheng, G. J.; Dong, S. J. *Electroanalysis* **1997**, 9, 834.
- (239) Rosseinsky, D. R.; Monk, P. M. S. *J. Chem. Soc., Faraday Trans.* **1993**, 89, 219.
- (240) Asaftei, C. S. *Synthesis of redox units and modification of mesoporous surfaces by covalent cascade reactions* **2006**, Diss., Universität Osnabrück.
- (241) Mas, T.; Pardo, C.; Elguero, J. *ARKIVOC (Gainesville, FL, U. S.)* **2004**, 86.
- (242) Amma, A.; Mallouk, T. E. *Tetrahedron Lett.* **2004**, 45, 1151.
- (243) Nefzi, A.; Ong, N. A.; Houghten, R. A. *Tetrahedron Lett.* **2000**, 41, 5441.
- (244) Tang, P. *Org. Synth.* **2005**, 81, No pp given.
- (245) Mylavarapu, R. K.; Gcm, K.; Kolla, N.; Veeramalla, R.; Koilkonda, P.; Bhattacharya, A.; Bandichhor, R. *Org. Process Res. Dev.* **2007**, 11, 1065.
- (246) Higashi, F.; Nishi, T. *J. Polym. Sci., Part A: Polym. Chem.* **1986**, 24, 701.
- (247) Qian, Y.; Zhang, S.-j.; Sang, X.-y.; Chen, S.-l.; Hou, H.-q. *Huaxue Shiji* **2005**, 27, 739.
- (248) Atkins, K. M.; Lopez, D.; Knight, D. K.; Mequanint, K.; Gillies, E. R. *J. Polym. Sci., Part A: Polym. Chem.* **2009**, 47, 3757.

- (249) Gao, M. Z.; Reibenspies, J. H.; Wang, B.; Xu, Z. L.; Zingaro, R. A. *J. Heterocycl. Chem.* **2004**, *41*, 899.
- (250) Benedetti, L.; Borsari, M.; Dallari, D.; Fontanesi, C.; Grandi, G.; Gavioli, G. *Electrochim. Acta* **1994**, *39*, 2723.
- (251) Jorge, S. M. A.; De Campos, P. M.; Stradiotto, N. R. *J. Braz. Chem. Soc.* **1999**, *10*, 176.
- (252) Pletcher, D.; Slevin, L. *J. Chem. Soc., Perkin Trans. 2* **1996**, 217.
- (253) Vincent, M. L.; Peters, D. G. *J. Electroanal. Chem.* **1992**, 327, 121.
- (254) Silvester, D. S.; He, W.; Aldous, L.; Hardacre, C.; Compton, R. G. *J. Phys. Chem. C* **2008**, *112*, 12966.
- (255) Menshutkin, N., Z. *Phys. Chem.* **1890**, *5*, 589.
- (256) Bhowmik, P. K.; Han, H.; Nedeltchev, I. K. *J. Polym. Sci., Part A: Polym. Chem.* **2002**, *40*, 2015.
- (257) Kim, S. M.; Jang, J. H.; Kim, K. K.; Park, H. K.; Bae, J. J.; Yu, W. J.; Lee, I. H.; Kim, G.; Loc, D. D.; Kim, U. J.; Lee, E.-H.; Shin, H.-J.; Choi, J.-Y.; Lee, Y. H. *J. Am. Chem. Soc.* **2009**, *131*, 327.

Appendix

A.1 Cyclic voltammetry of **4**

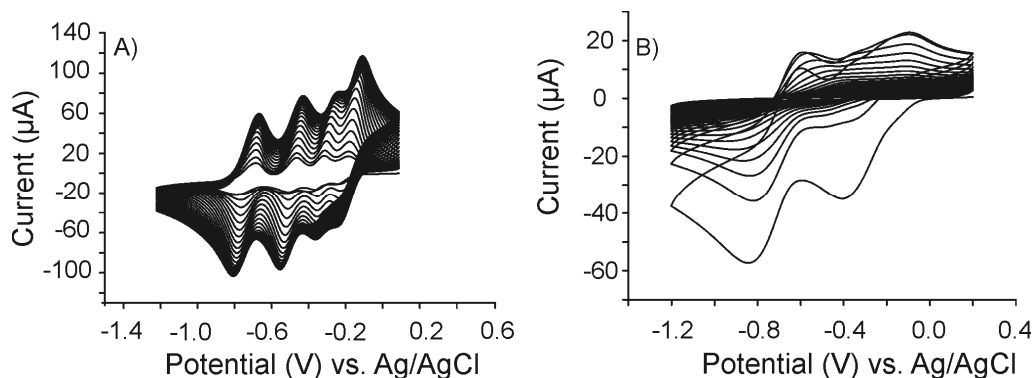
The peak current of the first reduction of **4** linearly increased with the square root of the scan rate in the range 0.03-1.0 Vs⁻¹, indicating that **4** follows diffusional process under experimental conditions.



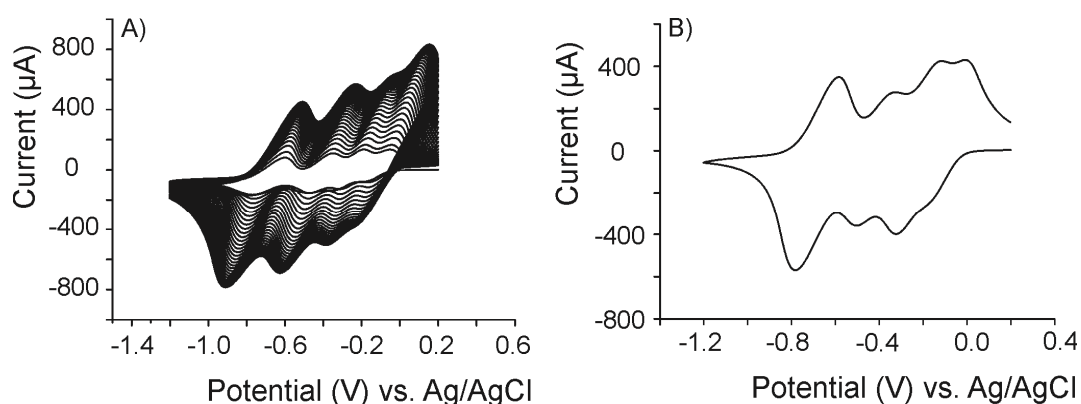
A.1 Dependence of the peak current (i_p) on the square root of the scan rate (V).

A.2 Electropolymerization of **4** and **7** at GC, Au and ITO electrodes

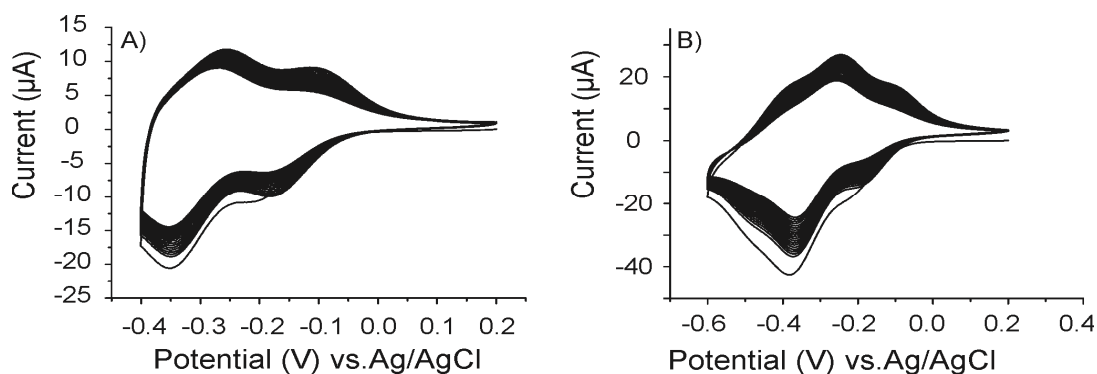
Polymer films were deposited on GC, gold and ITO from monomer solutions in 0.1M n-Bu₄NPF₆/DMF by scanning the potential between 0.2 V and -1.2 V vs. Ag/AgCl at 100 mVs⁻¹. The sweep was stopped after 60 cycles and the modified electrode was rinsed with acetone prior to further experiments.



A.2 A) The electropolymerization of **4** (4.9 × 10⁻⁴ M). B) CVs of **Poly-4** on Au. CVs were measured in 0.1 M n-Bu₄NPF₆ at a scan rate of 100 mV/s.



A.3 A) The electropolymerization of **4** (4.9 × 10⁻⁴ M). B) CVs of **Poly-4** on ITO. CVs were measured in 0.1 M n-Bu₄NPF₆ at a scan rate of 100 mV/s.



A.4 CVs of **Poly-4** on GC in 0.1 M n-Bu₄NPF₆ and scan rate 100 mVs⁻¹: A) potential range 0.2 → -0.4 V and B) potential range 0.2 → -0.6 V. GC was modified from 4.9 × 10⁻⁴ M of **4** during 20 scans at U = 100 mVs⁻¹ and potential range: 0.2 V → -1.2 V.

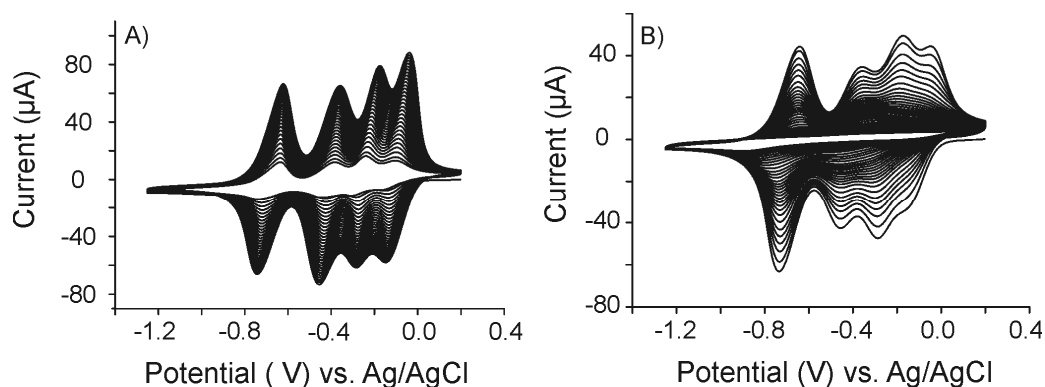
As Fig. A.4 clearly show, the modified GC electrode is more stable while scanning the potential only over the first three viologen reduction waves.

$$\text{Polymer stability: } (QME_{20}/QME_1) \times 100 \quad (A1)$$

$$(3.11 \times 10^{-5} / 4.64 \times 10^{-5}) \times 100 = 67.22 \% \text{ potential scan } 0.2 \text{ V} \rightarrow -0.4 \text{ V.}$$

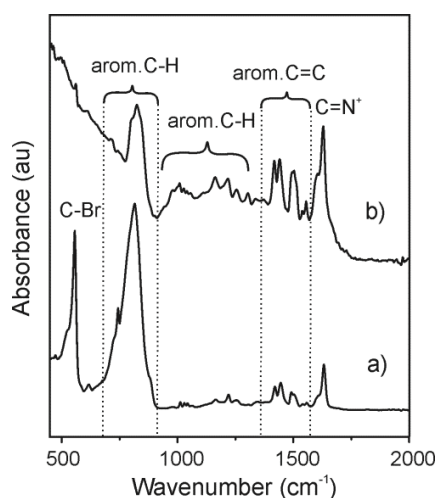
$$(11.51 \times 10^{-6} / 10.65 \times 10^{-5}) \times 100 = 10.78 \% \text{ potential scan } 0.2 \text{ V} \rightarrow -1.2 \text{ V.}$$

QME_1 and QME_{20} are the charge calculated from CV of modified GC after integration over the whole scan region. ME_1 is the first scan and ME_{20} is the 20th scan.



A.5 A) The electropolymerization on ITO of **7** ($1.76 \times 10^{-4} \text{ M}$). B) CVs of **Poly-7** on ITO. CVs were measured in 0.1M $n\text{-Bu}_4\text{NPF}_6$ at a scan rate of 100 mV/s.

A.3 FT-IR characterization of Poly-4 (chemical polymerization)



A.6 FT-IR spectra of **4** (a) and **Poly-4** (b).

List of abbreviations

aq.	aqueous
AcOH	acetic acid
BnV	dibenzyl viologen
BnV ^{•+}	dibenzyl viologen radical cation
n-Bu ₄ NPF ₆	tetrabutylammonium hexafluorophosphate
bs	broad singlet
bd	broad doublet
CH _{arom.}	aromatic proton(s)
¹³ C-NMR	carbon nuclear magnetic resonance spectroscopy
CV	cyclic voltammogram
CVs	cyclic voltammograms
D	diffusion coefficient
DCM	dichloromethane
DGM	diethylene glycol dimethyl ether
DMF	dimethylformamide
DMSO	dimethyl sulfoxide
E ^{0'}	formal reduction potential

ΔE_p	potential difference between the anodic and cathodic peak potentials
eV	electron volt
Fc	ferrocene
$[\text{Fe}(\text{CN})_6]^{3-}$	potassium ferricyanide
GC	glassy carbon
h	hour
HEV	1,1'-bis-2-hydroxyethyl-4,4'-bipyridinium dibromide
$^1\text{H-NMR}$	proton nuclear magnetic resonance spectroscopy
i_{abs}	absolute peak current
i_p	peak current
i_t	tunneling current
ITO	indium tin oxide
NH_4PF_6	ammonium hexafluorophosphate
M	molar concentration
MeCN	acetonitrile
MeOH	methanol
MeV	methylviologen

rad	radian
RT	room temperature
PABA	p-aminobenzoic acid
PhV	diphenyl viologen
PHV ^{•+}	diphenyl viologen radical cation
PPD	p-phenylenediamine
PTSA	p-toluenesulfonic acid
RDE	rotating disk electrode
rpm	revolutions per minute
Ru(bpy) ₃	tris(2,2'-bipyridyl) dichlororuthenium (II) hexahydrate
Γ	surface coverage
UV-VIS	ultraviolet-visible spectroscopy
ν	scan rate
V _b	bias voltage
Vio	protons of 4,4'-bipyridinium ring
vs.	versus
TBACl	tetrabutylammonium chloride

Curriculum Vitae

Personal Information

Name: Constantin Veronica-Alina

Date and place of birth: 6th October, Tulcea (Romania)

Marital status: single

Nationality: Romanian

Work Experience

Since November 2006 Research assistant and PhD. student at the Department of Molecular Electrochemistry, Institute of Chemistry, University of Osnabrück, Germany.

Key aspects of research: Synthesis and electrochemical investigation of π -conjugated viologens.

2005-2006 Research assistant at the National Institute of Research & Development for Technical Physics, Iași, Romania.

Key aspects of research: Fabrication of metallic nanowires by electrodeposition into nonporous alumina membranes.

2004-2005 Internship abroad research through the University of Martin-Luther, Halle, Germany.

Key aspects of research: Isolation of natural products.

Education and Training

Since February 2007 PhD student at the Department of Molecular Electrochemistry, Institute of Chemistry, University of Osnabrück, Germany.

September 2006 Masters degree in Enzymology and Biotechnology

at the University of Al. I. Cuza, Faculty of Chemistry, Iași, Romania.

June 2004 License degree in Technological Biochemistry at the University of Al. I. Cuza, Faculty of Chemistry, Iași, Romania.

30.06/12.07.2003 French summer school in Biochemistry: “Biologie et Pathologie moléculaires. Biotechnologies”, Iași, Romania.

Conferences

1. Poster presentation: “Synthesis and Electrochemistry of Rod-like Oligo-Viologens”, Veronica-Alina Constantin, Lorenz Walder, Electrochemistry in Interfacial Nanoscience, 6th ECHEMS Meeting, June 20-23, **2010**, Sandbjerg, Denmark.

2. Talk: “A Dendrimer with Multiple Switchable Radical Centers. Synthesis and Characterization”, Veronica-Alina Constantin, Workshop: “Magnetism in solids and molecules”, November 21, **2007**, Osnabrück, Germany.

3. Poster presentation: “Synthesis and Magnetic Properties of Fe-Ni and Cu-Ni Composite Coatings”, Horia Chiriac, Anca Moga, Veronica-Alina Constantin, III Joint European Magnetic Symposia, June 26-30, **2006**, San Sebastian, Spain.

4. Poster presentation: “Preparation and Magnetic Properties of Fe-Ni and Cu-Ni Composite Coatings”, Horia Chiriac, Anca Moga, Veronica-Alina Constantin, International Edition of Romanian Conference on Advanced Material, September 11-14, **2006**, Bucharest-Măgurele, Romania.

Publications

1. “Triple-Branched Viologen Stars: Synthesis and Polymerization via Peripheral Benzyl Coupling”, Veronica-Alina Constantin, Dirk Bongard,

Lorenz Walder, DOI: 10.1002/ejoc.201101586, Eur. J. Org. Chem.

2. "Synthesis and electrochemical Investigations of π -conjugated Viologen Oligomers", Veronica-Alina Constantin, Johannes Ludden, Lorenz Walder, manuscript in preparation.

3. "Star-shaped Viologen-CNTs Composites: Synthesis and STM Characterization", Veronica-Alina Constantin, Shamaila Sadaf, Lorenz Walder, manuscript in preparation.

Erklärung

Ich erkläre an Eides statt, dass ich die vorliegende Arbeit selbstständig, und keine anderen als die angegebenen Hilfsmittel verwendet habe. Alle Stellen, die dem Wort oder Sinn nach anderen Arbeiten entnommen sind, habe ich in jedem einzelnen Fall, unter genauer Angabe der Quelle kenntlich gemacht.

Ein früherer Promotionsversuch hat nicht stattgefunden.

Osnabrück, Februar 2012

Veronica-Alina Constantin